ЖУРНАЛ
ПРИКЛАДНОЙ ХИМИИ

JOURNAL OF
APPLIED CHEMISTRY
OF THE USSR

(ZHURNAL PRIKLADNOI KHIMY)

IN ENGLISH TRANSLATION

VOL. 30 NO. 11

CONSULTANTS BUREAU, INC.
227 WEST 17TH STREET, NEW YORK 11, N. Y.
an agency for the interpretation of international knowledge

Consultants Bureau Complete Subscription
TRANSLATIONS of SOVIET JOURNALS for 1958

Price quoted covers complete translation of all issues, plus comprehensive index.

BIOLOGY and MEDICINE

	per year
Biochemistry (Biokhimiia. 6 issues per year)	$ 20.00
Bulletin of Experimental Biology and Medicine (12 issues per year)	20.00
Pharmacol. and Toxicol. (6 issues per year)	25.00

CHEMISTRY, PURE and APPLIED

Journal of General Chemistry of the USSR (Obshchei Khimii. 12 issues, 3600 pp.)	90.00*
Journal of Analytical Chemistry of the USSR (6 issues)	80.00
Journal of Applied Chemistry of the USSR (Prikladnoi. 12 issues)	60.00*
Bulletin of the Acad. Sci. USSR, Div. Chem. Sci. (Izvestiia. 12 issues)	45.00*
Chemistry Sections of Proc. Acad. Sci. USSR (Doklady, 36 issues per year, to be published in 6 issues)	
Chemistry Section	110.00
Chemical Technology Section	25.00
Agrochemistry Section	15.00
Geochemistry Section	25.00
All four sections of Proc. Acad. Sci. cited above may be purchased as a unit for only	135.00
Physical Chemistry Section of Proc. Acad. Sci. USSR (Doklady, 36 issues, to be published in 6 issues)	160.00

* Write for special low prices for libraries of non-profit academic institutions.

PHYSICS

The Soviet Journal of Atomic Energy (12 issues per year)	75.00
Supplements to J. Atomic Energy—prices to be announced.	

MISCELLANEOUS

Colloid Journal (J. Expt. and Theoretical Physics and Chemistry of Colloids. 6 issues)	80.00
Geological Sciences Section, Proc. Acad. Sci. USSR (Doklady, 36 issues, to be published in 6 issues)	200.00
Metallurgist (12 issues)	95.00

These complete Consultants Bureau translations, by scientists for scientists, include all tabular material and diagrams integral with the text. Each issue of each translation is mailed to subscribers upon publication.

C/b CONSULTANTS BUREAU, INC.
227 W. 17th St., NEW YORK 11, N.Y.

JOURNAL OF APPLIED CHEMISTRY OF THE USSR

(ZHURNAL PRIKLADNOI KHIMII)

Volume 30, No. 11

November, 1957

(A Publication of the Academy of Sciences of the U.S.S.R.)

IN ENGLISH TRANSLATION

Copyright, 1958

CONSULTANTS BUREAU, INC.
227 West 17th Street
New York 11, N. Y.

Printed in the United States

	Domestic	Foreign
Annual Subscription	$60.00	$65.00
Annual Subscription for libraries of non-profit academic institutions	20.00	25.00
Single Issue	7.50	

Note: The sale of photostatic copies of any portion of this copyright translation is expressly prohibited by the copyright owners.

SIGNIFICANCE OF ABBREVIATIONS MOST FREQUENTLY ENCOUNTERED IN SOVIET PERIODICALS

FIAN	Phys. Inst. Acad. Sci. USSR.
GDI	Water Power Inst.
GITI	State Sci.-Tech. Press
GITTL	State Tech. and Theor. Lit. Press
GONTI	State United Sci.-Tech. Press
Gosenergoizdat	State Power Press
Goskhimizdat	State Chem. Press
GOST	All-Union State Standard
GTTI	State Tech. and Theor. Lit. Press
IL	Foreign Lit. Press
ISN (Izd. Sov. Nauk)	Soviet Science Press
Izd. AN SSSR	Acad. Sci. USSR Press
Izd. MGU	Moscow State Univ. Press
LEIIZhT	Leningrad Power Inst. of Railroad Engineering
LET	Leningrad Elec. Engr. School
LETI	Leningrad Electrotechnical Inst.
LETIIZhT	Leningrad Electrical Engineering Research Inst. of Railroad Engr.
Mashgiz	State Sci.-Tech. Press for Machine Construction Lit.
MEP	Ministry of Electrical Industry
MES	Ministry of Electrical Power Plants
MESEP	Ministry of Electrical Power Plants and the Electrical Industry
MGU	Moscow State Univ.
MKhTI	Moscow Inst. Chem. Tech.
MOPI	Moscow Regional Pedagogical Inst.
MSP	Ministry of Industrial Construction
NII ZVUKSZAPIOI	Scientific Research Inst. of Sound Recording
NIKFI	Sci. Inst. of Modern Motion Picture Photography
ONTI	United Sci.-Tech. Press
OTI	Division of Technical Information
OTN	Div. Tech. Sci.
Stroiizdat	Construction Press
TOE	Association of Power Engineers
TsKTI	Central Research Inst. for Boilers and Turbines
TsNIEL	Central Scientific Research Elec. Engr. Lab.
TsNIEL-MES	Central Scientific Research Elec. Engr. Lab.—Ministry of Electric Power Plants
TsVTI	Central Office of Economic Information
UF	Ural Branch
VIESKh	All-Union Inst. of Rural Elec. Power Stations
VNIIM	All-Union Scientific Research Inst. of Meteorology
VNIIZhDT	All-Union Scientific Research Inst. of Railroad Engineering
VTI	All-Union Thermotech. Inst.
VZEI	All-Union Power Correspondence Inst.

Note: Abbreviations not on this list and not explained in the translation have been transliterated, no further information about their significance being available to us. — Publisher.

JOURNAL OF APPLIED CHEMISTRY OF THE USSR IN ENGLISH TRANSLATION

November, 1957

TABLE OF CONTENTS

	Page	Russ. Page
The 80th Birthday of A. E. Arbuzov	1639	1573
Reactions of Sulfur Dioxide with Metal Oxides in an Oxidizing Atmosphere. V. V. Pechkovsky	1643	1580
Investigation of the Resistance to Oxidation of Alloys of Titanium and Niobium Borides. V. S. Neshpor and G. V. Samsonov	1648	1584
Regeneration of Oxythioarsenate Solutions. N. I. Brodskaya, M. I. Gerber, V. P. Teodorovich, and A. D. Shusharina	1653	1588
Investigation of the Oxidation of Alloys Containing the Intermetallic Compound NiAl. E. I. Mozhukhin, L. Kh. Pivovarov, and Ya. S. Umansky	1658	1593
Kinetics of the Reaction of Sodium Aluminate Solution with Lime. B. V. Drozdov and M. F. Malyshev	1664	1600
General Laws of Absorption Processes in High-Speed Rotary Absorbers. S. N. Ganz	1668	1604
The Voltage "Peak" of Copper Oxide Cells. V. N. Flerov	1677	1614
Mechanism of Corrosion of Metals in Molten Chlorides. N. D. Tomashov and N. I. Tugarinov	1681	1619
Investigation of the Corrosion of Zinc, Iron, Aluminum, and Magnesium in Aqueous Dioxane Solutions of Certain Electrolytes. Yu. B. Kletenik	1688	1626
Mineral Pigments for Leather Coating Colors. A. L. Zaides and R. A. Metlitskaya	1694	1633
Method for the Preparation of Water-repellent, Oil-resistant, and Weather-resistant Organosilicon Drying Oils. A. P. Antykov	1702	1641
Investigation of Bituminous Liptobioliths from Tkibuli, for Preparation of an Oil Varnish. P. N. Dzhaparidze, L. A. Drakin and L. R. Tvaradze	1709	1647
Causes of the Gumming of Diesel Fuels During Storage. S. R. Sergienko and P. N. Galich	1714	1653
Influence of Hexamethylenetetramine on the Conversion of Polyvinyl Chloride into a Space Polymer. G. S. Petrov and V. F. Prosvirkina	1721	1660
The "Limiting" Degree of Polymerization of Cellulose. V. I. Sharkov, I. I. Korolkov, and E. N. Garmanova	1728	1668
Preparation of Aminocarbanilides. V. N. Klyuev, A. A. Spryskov and S. N. Solodushenkov	1733	1672
Glycerol-diphenic Acid Polyesters. A. I. Kogan and M. M. Kitaigorodsky	1738	1677
BRIEF COMMUNICATIONS		
Reaction of Calcium Sulfate with Aluminates at 1200°. T. A. Ragozina	1742	1682

(continued)

TABLE OF CONTENTS (continued)

	Page	Russ. Page
Germanium in Coke Oven Wastes. N. P. Diev and V. I. Davydov	1746	1685
Thermodynamics of the Interaction of Fused $CaCl_2$ with Alkali Metal Chloride Melts. M. V. Smirnov, S. F. Palguev, L. A. Lyapina, and Yu. N. Krasnov	1749	1687
The Preparation of Pure Silica. O. N. Nikitina	1752	1690
The Dynamic Activity of Adsorbents. I. V. Lyubinov and N. I. Smirnov	1754	1691
Phase Diagram of the System $Na_3AlF_6 - Li_3AlF_6 - Al_2O_3$. V. P. Mashovets and V. I. Petrov	1758	1695
Equation for Calculation of Flooding Velocities in Packed Columns. V. V. Kafarov and Yu. I. Dytnersky	1761	1698
Throwing Power in Electroforming. A. M. Ginberg and Yu. A. Klyachko	1765	1701
Corrosion of Steel in the Atmosphere of a Steel Mill. A. V. Shreider and A. I. Sokolikov	1770	1706
Electrically Calibrated Ice Calorimeter. M. V. Kniga and K. P. Mishchenko	1773	1708
Effect of Raney Nickel on Hydrocarbons under Conditions of Prolonged Contact. A. A. Balandin and S. E. Raik	1776	1711
Synthesis of Lepidine Bases from Acetanilines and Oxo Compounds. B. I. Ardashev and B. A. Tertov	1781	1715
The Analysis of Phthalic Anhydride. E. E. Shkolman and N. M. Voroshilova	1783	1716
The Synthesis of Toluene. I. L. Kotlyarevsky and A. S. Zanina	1787	1719
BOOK REVIEW		
W. Hübner and A. Schiltknecht, Die Praxis der Anodischen Oxydation des Aluminiums. Düsseldorf, 1956, pp. 355.	1791	1723

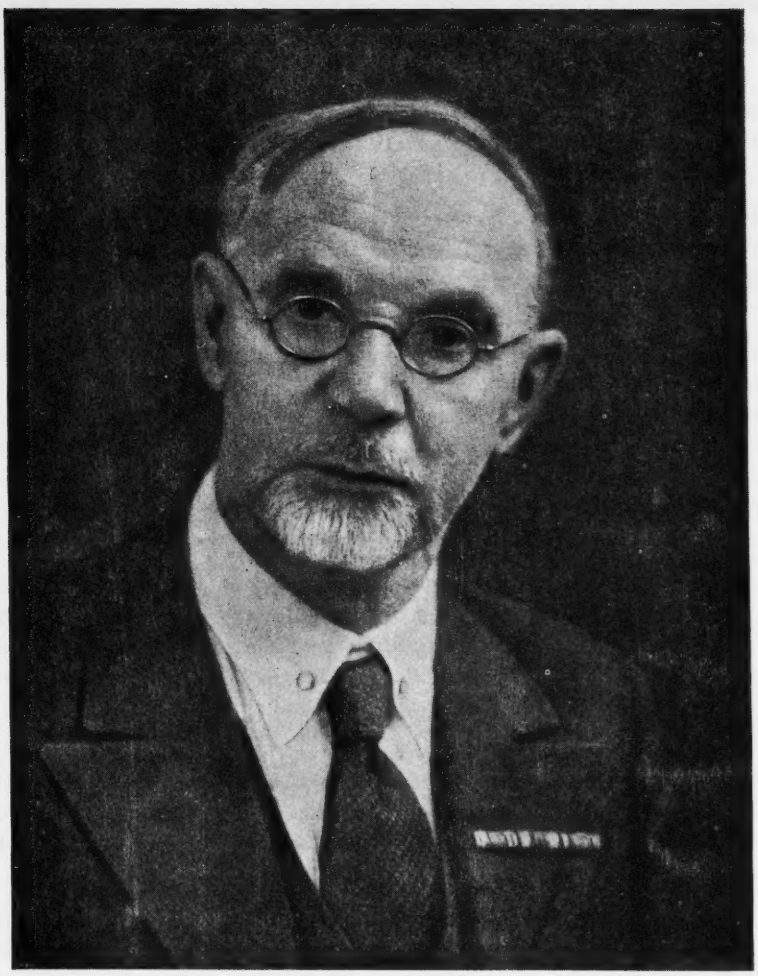

A. E. Arbuzov

THE 80th BIRTHDAY OF A. E. ARBUZOV

Aleksandr Erminingeldovich Arbuzov is a direct successor of the noted Russian chemists, N. N. Zinin, A. M. Butlerov, and the other Kazan chemists who founded the well-known Kazan school of chemistry. The representatives of this school have carried out investigations not only in pure, but in applied chemistry, especially in the technology of organic synthesis.

In a competition in 1911 A. E. Arbuzov was chosen as Assistant Professor of organic chemistry by the physicomathematical faculty and the Senate of Kazan University. It was in this laboratory that A. E. Arbuzov showed his great talent as a research chemist.

Like the classical Russian chemists, Arbuzov has given and still gives much effort to the study of natural resources for the synthesis of organic compounds. While his predecessors and contemporary members of the Butlerov school have studied Russian petroleum, Arbuzov has devoted himself to the study of the composition of galipot and turpentine from different conifers, especially the ordinary pine (Pinus sylvestris).

Before the October Revolution, rosin and turpentine from pine resin taken from the so-called turpentine pine were imported from abroad, in spite of the abundance of pine wood in Russia. It was believed that the turpentine pine would be unprofitable because of the severe Russian climate. In 1924 the Higher Soviet of National Ecohomy raised the question of the possibility of developing the turpentine pine in various parts of the Soviet Union. A. E. Arbuzov offered his services and from 1924-1926 under his direction experiments were carried out in the Raifsk forest near Kazan in an area of one hectare to show the possibility of a turpentine industry in the Volga provinces and to work out the best methods for obtaining rosin.

After many forestry experiments, A. E. Arbuzov disproved the opinion of the foreign specialists of the impossibility of a rosin-galipot industry in central Russia and showed the economic feasibility of the turpentine industry in the Tatarsk and Mariisk Autonomous Republics and other regions along the Volga. This work of Arbuzov furnished the needed impulse for the initiation and rapid development of a new branch of forestry. It is enough to say that as early as 1940 our country occupied second position in the world in the production of rosin and turpentine.

As a result of his studies, Arbuzov was the first to discover the presence in the resin system of a high pressure (the manometer showed 2-3 atmospheres); he established a series of rules for obtaining the resin, and he worked out methods for isolating galipot in pure and stable form.

These purely scientific studies had a greater interest because they were directly related to the basic problems of turpentine economy, and the method which he worked out for obtaining galipot with a minimum of evaporation and oxidation permitted its exact analysis and that of the turpentine obtained from it.

Further studies of the composition of turpentine using the physicochemical (optical) methods of Darmoir--Dupont* first showed the true composition and nature of the native turpentine; this was very valuable for its chemical treatment in industry. Studies in this field were carried on very actively for many years by the student and close colleague of A. E. Arbuzov, B. A. Arbuzov.

Arbuzov is an excellent glass blower. He has designed many pieces of original apparatus for chemical research. From the small Arbuzov pycnometers to complex two-meter fractionating columns, from various accurate aerometers to factory thermometers which measure temperatures to 400°, from water pumps to complicated glass apparatus, all have been built by Arbuzov. His skill in glass blowing is one link which connects him with all the chemical factories and research institutes of Kazan. Many research workers, engineers, physicians, physicists and other scientists have expressed their thanks to Arbuzov for the help he has given them in their fields.

*Transliterated from Russian.

Arbuzov published in 1912 a practical handbook of glass blowing, which was later reprinted by the State Technical Press. In my opinion, this handbook is a reference not only for an organic research chemist, but also for an industrial glass blower. Arbuzov has been constantly in close touch with our glass factories which turn out apparatus. In recent years the workers in the "Triumph of Labor" factory have often consulted Arbuzov on questions of Soviet pyrex glass and new chemical apparatus.

At the beginning of the first world war Russia was cut off from her usual foreign sources of drugs and a serious shortage occurred, especially in the group of salicylates. This situation was aggravated by the great increase in demand for drugs under wartime conditions and presented many Russian chemists with the problem of organizing the independent production of pharmaceuticals. Chemical preparation of drugs began in many of the great cities of Russia – St. Petersburg, Moscow, Kiev, Tomsk and others.

The young Kazan University professor A. E. Arbuzov set himself the wider purpose of establishing in Kazan a Phenol-Salicylic Acid factory which would not only produce drugs, but would train a group of young technologists, chemists and technicians, needed to organize a native pharmaceutical industry.

Even in its initial stage this important endeavor met a great and unexpected difficulty; it had to overcome the dominant opinion that it was impossible under Russian conditions to prepare such a wide range of drugs as salycylic acid, sodium salicylate, aspirin, salol and others. This difficulty was overcome by the energy and persistance of the scholarly patriot; in 1915, 15,000 rubles were assigned for construction of the factory and work went forward rapidly.

While the Phenol-Salicylic Acid Factory was being built, the laboratory workers trained by Arbuzov were undertaking a detailed study of each reaction in the technology of producing the drugs. A. A. Ivanov studied the sulfanation of benzene in an autoclave with a stirrer which was made from an ammonia cylinder. L. N. Parfentyev investigated in detail the alkali fusion of sodium benzenesulfonate.

The experimental Phenol-Salicylic Acid Factory was set up in the old Kazan factory of the Krestovnikov Brothers (now named for M. N. Bakhitov). In distinction from many other preparations of a similar nature, the salicylates were prepared in the Kazan factory not from coal-tar benzene, but from petroleum benzene, a by-product of the Kazan gas works which used petroleum. All the other substances needed for the syntheses, such as carbonic acid and acetic anhydride, were prepared in the factory itself. Arbuzov always took an active part in the construction of all the factory equipment and its mounting.

After production of phenol was started, the manufacture of salicylic acid, sodium salicylate, aspirin, and salol was organized. Salicylic acid was obtained by the Kolbe process as perfected by Schmidt; heating sodium phenolate in an autoclave with carbon dioxide at 130°. The first experiments on the preparation of salicylic acid gave low yields because of poor absorption of carbon dioxide by sodium phenolate. Then Arbuzov recommended the use of a method causing the swelling-up of the phenolate under vacuum, which he had successfully used in the synthesis of alcoholates. This method proved satisfactory. Saturation of the phenolate by carbon dioxide proceeded quickly and smoothly and the yield rose sharply.

Arbuzov and his assistant, A. A. Dunin, found another method for obtaining acetic anhydride. Due to Arbuzov's persistance and the accuracy of his experiments, acetic anhydride was obtained in 98% yield. Studies on the synthesis of acetic anhydride had been made in other places up to 1922, but the results were not successful.

During the period of its greatest activity, the Phenol-Salicylic Acid Factory (in which there was not one qualified worker) produced daily up to 16 kg of aspirin which was not inferior in chemical and pharmaceutical properties to the well-known patented German Bayer aspirin.

We can add that the plans of the Soviet scientist were justified and the experiment of gathering all the technical personnel of the factory was so successful that A. E. Arbuzov later gave advice on the construction and operation of the salicylic autoclave in the large Zemgor Factory, the commercial manufacture of acetic anhydride in the Moscow Chemicopharmaceutical Factory and other processes.

In 1921 under Arbuzov's direction, a small scale production of saccharin and lacto-saccharin was organized in the Kazan State University laboratory or organic chemistry. Under the name of "Arbuzov saccharin" this was popular in the markets of Kazan and other cities along the Volga.

A method was worked out, also under Arbuzov's direction, for obtaining creosote from birch tar, and with the pharmacist A. I. Brening a process was perfected for obtaining terpene hydrate. A method was also developed

in Arbuzov's laboratory for the technical preparation of salvarsan. All these studies showed the close connection of Arbuzov's laboratory with the demands of the pharmaceutical industry.

In 1926 A. E. Arbuzov became head of a group of chemists and engineers who were building a small factory to manufacture water-soluble nigrosine which was badly needed by the local tanning industry. The factory was established and began to produce a high quality nigrosine.

All the starting materials — nitrobenzene, nitrophenol, aniline, etc. — were prepared in the factory itself. The factory did not exist very long. From the first, Arbuzov's nigrosine met strong competition in the market from foreign firms. These firms partly succeeded in their object. The nigrosine was difficult to distribute; it seemed that only the "Spartak" Factory was willing to use it. After an explosion of an autoclave in the factory there was a fire, and the factory then ceased to operate.

In 1934 Arbuzov and the engineer B. P. Lugovkin worked out an original method for obtaining furfural from agricultural wastes — straw, oat hulls, etc. This method was distinctive in that phosphoric acid was used as a catalyst, and not sulfuric or hydrochloric. The yield of high quality furfural obtained in this way was greater than in the other processes but the cellulose was hardly changed; for example, the straw changed color only slightly and even kept its mechanical properties. This was evidently the best of the existing methods for preparing furfural.

It was found that American chemists also tried to use phosphoric acid as a catalyst, but with negative results.

A. E. Arbuzov was for a long time consultant to the M. N. Bakhitov Soap Factory in Kazan. He also took part in the plans of the Lenin Factory, where the workers in gratitude elected him an honorary workman.

In the Great War of 1941-1945, on an assignment of the State Committee of Defense, Arbuzov and his co-workers, G. Kh. Kamai and A. I. Razumov produced γ-phenylpropyl alcohol from ethyl cinnamate by a new process which he worked out and perfected. The yield of high quality γ-phenylpropyl alcohol reached 94%. In these years Arbuzov synthesized a considerable amount of γ,γ-dipyridyl and some important dyes for the needs of the front.

Beginning in 1947, Arbuzov and the workers in the organic chemistry laboratory of the Chemical Institute of the Kazan Branch of the Academy of Sciences, USSR, have devoted and still devote much attention to developing industrial methods for preparing ethyl pyrophosphate. This compound was first isolated in pure form by A. E. and B. A. Arbuzov in 1932. In the same year they first synthesized other esters of pyrophosphoric and monothiopyrophosphoric acids and studied them in detail.

Soon after this in Germany the chemists of the I.G. Farbenindustrie noticed the strong myotic activity and then the insecticidal power of these compounds. As a result of such investigations in European countries — Germany, England, and then the U.S.A. — there developed a large industry for insecticides to combat organisms harmful to farms and orchards.

In 1948 a group of chemists of the Kazan Branch of the Academy of Sciences of the USSR under the direction of A. E. Arbuzov synthesized a large number of organophosphorus compounds.

The most useful and promising insecticides among hundreds of such compounds are tetraethyl pyrophosphate (TEPP), tetraethyl monothiopyrophosphate (pyrophos) tetraethyl dithiopyrophosphate (dithiophos), and finally, octamethyl tetramidopyrophosphate (octamethyl). From all the studies of these four compounds made in the Scientific Institute for Fertilizers and Insectofungicides by E. A. Pokrovsky and under field conditions at 35 points in our country, we can say that they are now among the most effective substances used to combat agricultural pests. A. E. Arbuzov worked out a very simple, one-step method for obtaining TEPP at the Kazan Branch. An obstacle to its wide use is its strong toxic action on warm-blooded animals.

Five variant syntheses have been developed for pyrophos, of which two in particular are suitable for industrial application. However, since our industry at the present time is manufacturing another organophosphorus compound with similar properties, called thiophos, the introduction of pyrophos is still held back.

Tetraethyl dithiopyrophosphate (dithiophos) is a very interesting and promising insecticide. Several laboratory methods for its synthesis have been worked out and its action on insects and warm-blooded animals has been carefully studied.

Dithiophos was studied and showed positive results on pests of grains (wheat, corn) including wireworms. It

has great value for citrus and subtropical fruit culture. It can be used against Japanese wax scale which is not attacked by other preparations.

Very hopeful results have also been obtained with dithiophos as a means of destroying mosquito larvae in cisterns, ticks in pastures, and flukes on mollusks. The synthesis of dithiophos is very simple and adaptable to factory methods. It can be synthesized in good yield by the action of water on diethyldithiophosphoric acid chloride. At the beginning of last year one factory prepared 200 kg and it was used during the summer and autumn in different parts of the country.

Octamethyl tetramidopyrophosphoric acid is also an interesting insecticide.

Octamethyl was prepared a number of times in the laboratory under Arbuzov's direction in lots of several kilograms, and, as field studies showed in more than 30 research centers in the Soviet Union, it was a very valuable insecticide with so-called systemic action.

Octamethyl is effective against harmful Pentastomidae, cotton spiders and fruit flies. It is very effective against red and silver citrus flies, since it rids the trees of insects and at the same time prevents further infestation for from 3 weeks to 4 months. It has a high toxicity for aphids, Psyllidae, mealy bugs, citrus and tea borers, Japanese scale, and also for cereal mites (on wheat, barley, and corn), apple aphids, etc. Octamethyl attacks pests but does not injure the animals which eat the pests; this permits a combination of chemical and biological methods for combating the pests.

Preliminary studies in the Kazan Branch of the Academy of Sciences of the USSR showed that, in addition to its insecticidal action, octamethyl has a stimulating action on the growth and harvest of peas and corn if the seeds are soaked before sowing, or are sprinkled. The manufacturing process for octamethyl is sufficiently developed for its wide introduction.

The Ministry for Chemical Industry has decided to produce octamethyl in large amounts in 1957.

Equally interesting are the investigations, increasing in number each year, which concern the action of organophosphorus compounds, especially pyrophosphates, monothiopyrophosphates and dithiophosphates, on animals, beginning with the simplest and ending with warm-blooded animals, including humans.

The most characteristic property of these organophosphorus compounds is their strong anticholinesterase activity. This property is most interesting to physiologists and physicians. The organophosphorus compounds have already been studied and partly introduced into practice for treating such human diseases as glaucoma, muscular atrophy and myasthenia. New fields for their use will be obstetrics, psychiatry, etc.

Tetraethyl monothiopyrophosphate was studied in detail in the Eye Clinic of the First Moscow Medical Institute by Prof. V. N. Arkhangelsky and in the Kiev Medical Institute by Assistant Ustimenko. Their studies showed that this preparation (with the shortened name "phosarbin") is an excellent drug for treating glaucoma. Phosarbin has a better action than foreign drugs, including pilocarpine. The Ministry of Health of the USSR has decided to introduce phosarbin into medical practice. In 1957 this preparation will be produced on a mass scale by our industry and will be sufficient for use in a wide network of medical institutions.

Such is the short list of work in the field of applied chemistry of A. E. Arbuzov. This work is particularly closely connected with the chemicopharmaceutical industry.

We wish to the man who continues the work of the notable Kazan school of chemistry many more years of productive work in his favorite field for the advantage of our country.

Gilm Kamai

REACTIONS OF SULFUR DIOXIDE WITH METAL OXIDES IN AN OXIDIZING ATMOSPHERE

V. V. Pechkovsky

The A. M. Gorky State Institute, Perm

The problem of utilization of gases containing sulfur dioxide has attracted the attention of research workers for a long time [1]. Among the numerous means for possible utilization of sulfur dioxide in such gases, considerable importance attaches to methods whereby various sulfates, such as those of potassium, aluminum, magnesium, zinc, manganese and calcium, are formed by the reaction of the gas with powdered solids at 300-700° [1-4]. This does not exhaust the importance of the interaction of sulfurous waste gases with metal oxides. The effects which accompany these reactions are also of interest in studies of certain aspects of oxidative and sulfating roasting of sulfide ores, and of the catalytic oxidation of sulfur dioxide [5-7].

These facts prompted the present study of the interaction of sulfur dioxide with solid powdered metal oxides in an oxidizing atmosphere in the 400-1000° range.

The object of the investigation was to study the degree of conversion of various metal oxides into the corresponding sulfides in relation to the temperature, time, physicochemical properties of the mixture and products, and the sulfur dioxide content of the gas.

EXPERIMENTAL

Pure metal oxides in powder form were taken for the experiments.

The metal oxides and their mixtures were kept at the required temperatures for definite times (up to 1 hour) in a stream of the dry gas in a tubular furnace. The gas consisted of a mixture of air and of sulfur dioxide from a cylinder. Gas mixtures with the following average contents of sulfur dioxide (in volume %) were used: 2.5, 5.0, 7.5, 10.0 and 20.0.

TABLE 1

Effect of Temperature on the Degree of Conversion of Fe_2O_3, CuO and MnO (τ* = 15 min) (5% SO_2 in the original gas)

Oxide	% conversion of oxide at temperature (°C)					
	400	500	600	700	800	900
Fe_2O_3	11.6	19.9	24.3	6.0	0.6	0.0
CuO	3.1	10.8	17.1	17.0	14.4	0.5
Mn_2O_3	34.5	39.7	45.4	50.3	52.8	53.3

* Here and subsequently τ = duration of the experiment (in minutes).

It was found in preliminary qualitative experiments that treatment of metal oxides with mixtures of sulfur dioxide and air in the 400-1000° range converts the oxides into the corresponding sulfates. In the case of calcium

oxide, treatment with a mixture of air and sulfur dioxide yields calcium sulfide and sulfite together with the sulfate. It was also found that pure zinc oxide is not converted to the sulfate at all.

When magnesium oxide containing up to 16% of the oxides of iron and copper is treated, the sulfates of iron and copper are not found in the products. When magnesium oxide containing cobalt and manganese oxides was treated, a certain amount of cobalt and manganese sulfates was found in the products. Data on the degree of conversion of various metal oxides into the sulfates are given in Tables 1-7.

TABLE 2

Effect of SO_2 Content of the Original Gas in the Degree of Conversion of MgO, CaO and Co_2O_3 (τ = 15 min)

SO_2 content (vol. %)	% conversion of oxide at temperature (°C)											
	600			700			800			900		
	MgO	CaO	Co_2O_3	MgO	CaO	Co_2O_3	MgO	CaO	Co_2O_3	MgO	CaO	Co_2O_3
2.5	1.7	8.4	21.6	2.5	10.4	24.1	3.4	12.0	24.8	4.3	13.8	12.6
5.0	2.0	25.3	27.7	3.2	40.5	30.3	4.1	41.6	32.1	5.2	49.2	30.0
7.5	2.4	31.1	28.8	3.6	43.8	30.6	4.6	45.0	33.0	7.0	54.5	31.2

TABLE 3

Effects of Temperature and Nature of Catalyst on the Degree of Conversion of MgO (τ = 15 min)

(9% catalyst in mixture; 5% sulfur dioxide in original gas)

Catalyst	% conversion of MgO at temperature (°C)						
	400	500	600	700	800	900	1000
Cr_2O_3	9.6	22.8	32.1	35.3	35.0	35.9	32.6
Fe_2O_3	7.1	21.6	27.2	30.4	31.0	30.8	28.8
CuO	4.3	11.2	19.6	30.0	28.2	29.6	26.2
Co_2O_3	2.5	14.0	31.3	35.1	34.8	35.0	31.1
Mn_2O_3	4.0	7.3	20.0	32.2	33.0	34.2	30.9

TABLE 4

Effect of Contents of Fe_2O_3 Catalyst in the Mixture on the Degree of Conversion of MgO (τ = 15 min)

(5% SO_2 in the original gas)

Temperature (°C)	% conversion of MgO with different % contents of Fe_2O_3 in mixture						
	1.0	2.0	3.5	6.0	9.0	16.0	30.0
500	9.7	15.1	19.5	21.3	21.6	20.8	21.7
800	25.5	28.4	30.7	30.0	31.0	30.2	31.3

TABLE 5

Effects of Temperature and SO_2 Content of of the Original Gas on the Degree of Conversion of MgO (τ = 15 min)

(9% Fe_2O_3 in the mixture)

Temperature (°C)	% conversion of MgO with different SO_2 contents (in vol. %) in gas			
	2.5	7.5	10.0	20.0
500	16.0	28.7	45.5	67.7
600	16.8	33.6	51.0	75.8
700	17.1	39.2	56.6	86.1
800	17.1	38.6	54.9	85.6

Examination of the experimental data leads to the conclusion that the formation of sulfates in the interaction of metal oxides with sulfur dioxide in an oxidizing atmosphere may predominantly occur by two routes.

TABLE 6

Effect of Time on the Degree of Conversion of MgO and Co_2O_3

(5% SO_2 in the original gas)

τ	% conversion of oxide at temperature (°C)					
	Co_2O_3			MgO		
	600	700	800	600	700	800
5	17.1	22.2	27.3	—	—	—
10	24.5	28.0	31.8	1.2	2.6	3.0
30	28.5	31.8	32.3	2.3	4.1	6.3
45	29.1	32.0	33.1	3.6	5.9	8.0
60	30.0	32.2	33.8	5.0	7.4	11.3

TABLE 7

Effect of Time on the Degree of Conversion of MgO
(temperature 600°)
(9.0% Fe_2O_3 in the mixture)

τ	% conversion of MgO with different SO_2 contents (in vol. %) in gas			
	2.5	5.0	7.5	10.0
15	16.8	27.2	33.6	51.0
30	27.2	51.4	66.6	91.0
45	40.6	78.6	91.6	93.5
60	54.5	93.6	95.5	96.1

The first route may be schematically represented by the reactions:

$$SO_2 + \frac{1}{2} O_2 \rightleftarrows SO_3, \quad (1)$$

$$MeO + SO_3 \rightleftarrows MeSO_4. \quad (2)$$

The second route of sulfate formation in these conditions may be schematically represented by the reactions:

$$MeO + SO_2 \rightleftarrows MeSO_3, \quad (3)$$

$$MeSO_3 + \frac{1}{2} O_2 \rightarrow MeSO_4. \quad (4)$$

The relative proportions of the sulfates formed by the two routes are determined by the rates of Reactions (1-4) under particular conditions.

The results given in Tables 1-7 indicate that the degree of conversion of metal oxides into the corresponding sulfates depends on numerous factors, the most important of which are the physicochemical properties of the sulfates formed, the presence of catalysts in the reaction zone, temperature, time and the sulfur dioxide content of the original gas.

It follows from the data in Tables 1-3 that the general form of the relationship between the temperature and the degree of conversion of metal oxides and their mixtures is in the form of a curve with a maximum.

The reason for the existence of the maximum is that the rates of Reactions (1-3) increase with temperature, but the equilibrium in these reactions is shifted to the left with increase of temperature.

The position of the maximum on the temperature—conversion curve depends on the physicochemical properties of the sulfates formed and on the presence of catalysts in the reaction zone. The degree of conversion also depends strongly on these factors.

Tables 1-3 show that under equal conditions the degree of conversion of an oxide increases with increasing affinity of this oxide for sulfur trioxide, i.e., with increasing thermal stability of the sulfate formed.

A measure of the affinity of a metal oxide for sulfur trioxide is the equilibrium pressure of SO_3 over the corresponding sulfate.

At a given temperature, the sulfates of certain metals can be arranged in the following sequence, representing decreasing equilibrium dissociation pressures:

$$FeSO_4 > CuSO_4 > ZnSO_4 > CoSO_4 > MnSO_4 > MgSO_4 > CaSO_4.$$

In other words, the affinity of, say, calcium oxide for sulfur trioxide is less than that of iron oxide.

Comparison of the positions of sulfates in this series with the degrees of conversion of the corresponding oxides suggests at first sight that there is no direct relationship between the thermal stability of the sulfate formed and the degree of conversion. In fact, at temperatures up to 600° the degree of conversion of, say, iron oxide is higher than that of calcium oxide. However, this merely shows that catalytic processes play an enormous role in the sulfation of metal oxides.

If the sulfation of metal oxides which do and do not catalyze Reaction (1) is considered separately, a relationship between the degree of conversion of a given oxide and the thermal stability of the sulfate formed is clearly seen.

Thus, the catalytically inactive oxides form the following sequence in increasing degree of conversion at a given temperature: $ZnO < MgO < CaO$, while the catalytically active oxides form the following sequence at temperatures above 600°: $Fe_2O_3 < CuO < Co_2O_3 < Mn_2O_3$.

Thus, there is a connection between the degree of conversion and the thermal stability of the sulfate formed.

The role of catalysts of Reaction (1) in the sulfation of oxides by sulfur dioxide is illustrated very clearly by the sulfation of magnesium oxide in presence of various catalysts.

It follows from the data in Tables 6 and 7 that at 600°, in experiments lasting 60 minutes, the degree of conversion of pure magnesium oxide and of magnesium oxide with an added catalyst (ferric oxide) is 5.0 and 93.6% respectively.

Examination of the data in Tables 3 and 4 shows that the degree of conversion of magnesium oxide in presence of catalytically active additives depends on the kind of additive and only a little on the amount added.

It may be concluded from the data in Table 4 that the degree of conversion of magnesium oxide increases in presence of small amounts of catalytically active substances. Thus, at 800° in experiments of 15 minutes' duration the degree of conversion of magnesium oxide with 2% Fe_2O_3 added is 28.4%, and remains almost constant with increase of the amount of the additive.

With regard to the nature of the catalytically active additive, it follows from the data in Table 3 that the additives tested can be arranged in the following series in order of catalytic activity in the sulfation of magnesium oxide: $Cr_2O_3 > Fe_2O_3 > CuO$. This sequence is in complete harmony with the known catalytic activity of these oxides in Reaction (1) [5,6].

Further, the results in Tables 2, 5 and 7 show that the degree of conversion both of pure metal oxides and of mixtures increases with increasing content of sulfur dioxide in the gas mixture. It must be emphasized, however, that the sulfation of magnesium oxide in presence of catalysts is very rapid even when the gas mixture contains only 2.5% SO_2.

Data on the effect of duration of the experiment on the degree of conversion of metal oxides are of interest. The results in Tables 6 and 7 show that the degree of conversion – time curves for magnesium and cobalt oxides differ somewhat. In the sulfation of cobalt oxide the process is very rapid during the first 5-10 minutes, after which it slows down sharply, whereas the rate of sulfation of magnesium oxides changes relatively little with time.

This cannot be ascribed merely to differences in the resistance of the films of magnesium sulfate and cobalt sulfate to diffusion. It is probable that the rate of the process is decreased as the result of formation of catalytically inactive cobalt sulfate on the grains of catalytically active cobalt oxide. In the case of sulfation of magnesium oxide in presence of catalytically active ferric oxide, it follows from the data in Table 3 that the rate of the process does not decrease sharply with time. The reason is that in presence of magnesium oxide the film of iron sulfate is continuously removed from the ferric oxide surface, and the latter therefore retains its catalytic activity.

LITERATURE CITED

[1] Z. P. Rozenknop, Extraction of Sulfur Dioxide From Gases (Goskhimizdat, 1952).*

[2] S. I. Volfkovich and F. G. Margolis, Bull. Acad. Sci. USSR, Div. Chem. Sci. 5, 322 (1942).

[3] F. G. Margolis, Z. N. Lunskaya and S. I. Volfkovich, J. Appl. Chem. 28, 453 (1955).**

* In Russian.
** Original Russian pagination. See C. B. translation.

[4] M. E. Pozin, The Technology of Mineral Salts (Goskhimizdat, 1949). *

[5] G. K. Boreskov, Catalysis in the Production of Sulfuric Acid (Goskhimizdat, 1954).*

[6] G. M. Zhabrova, Progr. Chem. 24, 598 (1955).

[7] V. I. Smirnov, Oxidative Roasting of Copper Ores and Concentrates (ONTI, 1938).*

Received March 9, 1956

* In Russian.

INVESTIGATION OF THE RESISTANCE TO OXIDATION OF ALLOYS OF TITANIUM AND NIOBIUM BORIDES

V. S. Neshpor and G. V. Samsonov

Studies of the oxidation resistance of metal-like compounds of the transition metals at high temperatures are of considerable interest. These compounds have stable interatomic bonds and retain their hardness at high temperatures (up to 1500-2000°), which makes them potentially useful components for heat-resisting materials and alloys for use in high-speed cutting tools.

However, these materials are oxidized at high temperatures by the action of atmospheric oxygen. It was shown earlier [1] that the oxidation resistance of titanium carbide increases in presence of additions of boron and silicon owing to the formation of a protective film of borosilicate glass on the surface of the material. The increase in weight of a specimen of titanium carbide containing additions of 17% silicon and 9.5% boron, as the result of surface oxide formation during exposure of 200 hours at about 1100°, did not exceed 0.07%.

Silicides of the transition metals also show considerable resistance to oxidation [2, 3].

Study of the corrosion resistance of borides of the transition metals is of interest in relation to the possible formation of surface glassy oxide films, preventing free access of oxygen.

The oxidation resistance of the borides of titanium and niobium and their alloys, which form a continuous series of solid solutions [4], was studied in the present investigation. The x-ray densities of the original borides were $\rho_{TiB_2} = 4.53$ and $\rho_{NbB_2} = 7.08$ g/cc, which are close to the published densities [5] of these compounds. The lattice constants of titanium and niobium borides respectively were a = 3.028 A, c = 3.224 A and a = 3.082 A, c = 3.278 A.

The specimens were made by sintering and hot pressing of the powdered components in graphite molds, followed by high-temperature annealing in a graphite tubular furnace in a hydrogen atmosphere and slow cooling of the specimens in the furnace after the annealing.

The residual porosity, determined from the values of the hydrostatic and additive densities of the sintered and annealed specimens, did not exceed 5-8% for most of the alloys (Table 1). The porosity values given in Table 1 are approximate only, as the true density of a solid solution in general differs from the additive value.

It is seen that the density of the specimens, both the original components and their alloys, decreases after annealing. The probable explanation is that, owing to the large interatomic bond forces in these compounds, shrinkage and recrystallization during annealing take place with difficulty [4], and decay of internal stresses, leading to some volume increase, prevails.

The specimens were heated in air in a tubular resistance furnace to oxidize them. The rate of oxidation was found from the change in weight of the specimens after exposure at a definite temperature.

It must be pointed out that, in general, determination of the resistance to oxidation from the change in weight after heating is not a reliable method owing to the possibility of partial volatilization of the oxidation products; the depth of the corroded layer rather than the change in weight should be used [1]. In the present instance, however, the change in weight can be used fairly reliably for comparison of the oxidation resistance of alloys of the system TiB_2—NbB_2 with different contents of the components, as the borides of titanium and niobium are similar in chemical nature and form a continuous series of solid solutions.

TABLE 1

Densities of Specimens of TiB_2–NbB_2 Alloys

Composition of alloys				Additive calculated density (g/cc)	Hydrostatic measured density (g/cc)		Porosity (%)	
molar %		wt.%			before annealing	after annealing	before annealing	after annealing
TiB_2	NbB_2	TiB_2	NbB_2					
0	100	0	100	7.08	7.03	6.98	0.6	1.4
20	80	13.3	86.7	6.59	6.60	6.53	0.0	0.7
30	70	20.7	79.3	6.34	6.21	6.00	2.0	5.2
40	60	28.5	71.5	6.10	6.10	6.05	0.0	0.7
50	50	37.8	62.2	5.84	5.62	5.55	3.7	5.0
60	40	47.6	52.4	5.58	5.42	4.41	2.7	20.8
70	30	58.3	41.7	5.33	4.57	4.88	15.2	8.4
80	20	70.9	29.1	5.10	5.04	4.44	1.4	13.0
90	10	84.6	15.4	4.79	4.58	4.60	4.0	3.7
100	0	100	0	4.53	4.48	4.45	1.2	1.6

The specimens were heated at 450, 500, 550, 600, 700, 800, 900 and 1000°. The time of exposure at each temperature was 1 hour. After the heating, the specimens were cooled and weighed. The weight changes of the specimens for different oxidation temperatures are given in Table 2 and Fig. 1. It is seen that the specimens increased in weight over almost the entire temperature range. This indicates that formation of nonvolatile oxygen compounds on the specimen surface greatly predominates over any possible volatilization of boric anhydride or other oxides of boron.

TABLE 2

Weight Increase of Specimens of Alloys of the System TiB_2–NbB_2 on Oxidation in Air

Composition of alloy (molar %)		Weight increase (in $g/cm^2 \cdot 10^{-4}$) at oxidation temperature (°C)							
TiB_2	NbB_2	450	500	550	600	700	800	900	1000
0	100	0.248	0.99	1.736	1.86	4.99	16.2	28.6	32.5
20	80	—	0.221	0.663	0.774	1.55	3.54	11.6	16.5
30	70	—	—	1.39	2.93	0.76	8.01	10.5	13.9
40	60	0.151	0.670	1.34	1.67	1.78	4.35	8.97	—
50	50	—	0.494	1.09	0.998	1.28	3.09	5.73	10.4
60	40	0.243	0.885	5.92	0.774	1.15	3.21	6.25	14
70	30	—	—	3.55	4.65	6.87	12.9	20.3	90.1
80	20	—	0.623	0.830	1.35	2.39	3.95	8.06	13.0
90	10	0	0.505	1.21	1.60	2.69	4.85	9.90	20.1
100	0	0.420	0.630	0.630	1.78	2.00	7.36	20.4	12.0

The specimens became coated with thin glassy oxide films on oxidation. Since boron and both the metallic components — titanium and niobium — are glass formers [6], it is possible that the film consists of complex vitreous boron–niobium and boron–titanium salts of pyroboric acid, which is the most stable of the boric acids at high temperatures.

The presence of $B_4O_7^{n}$ ions was detected qualitatively [7] in the products of high-temperature oxidation of other metal-like compounds containing boron. A formula for the average chemical composition of the glass may be tentatively derived, by analogy with complex aluminosilicates, from the formulas of titanium pyroborate $Ti(B_4O_7)_2$ and niobium pyroborate $Nb_2(B_4O_7)_5$, the amounts of these components in the glass being assumed proportional to the molecular contents of titanium and niobium borides in the corresponding alloys.

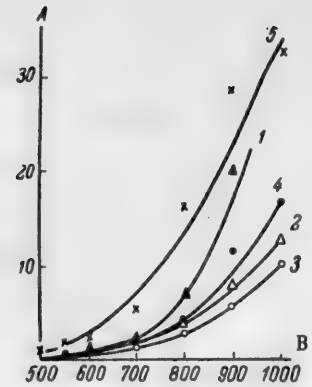

Fig. 1. Effect of oxidation temperature on the weight increase of the specimens.
A) Weight increase per unit surface area (in g/ $cm^2 \cdot 10^{-4}$);
B) temperature (in °C). Respective contents of TiB_2 and NbB_2 in the alloys (in molar %): 1) 100 and 0; 2) 80 and 20; 3) 50 and 50; 4) 20 and 80; 5) 0 and 100.

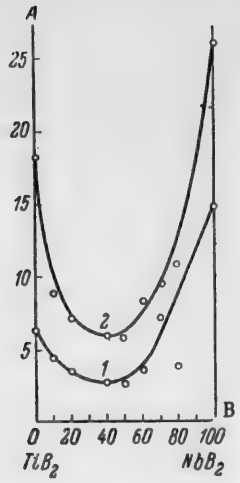

Fig. 2. Effect of alloy composition on the thickness of the oxide film.
A) Film thickness (in μ); B) content of TiB_2 and NbB_2 (molar %). Temperature (in °C): 1) 800; 2) 900.

Fig. 2 shows the approximate film thicknesses calculated from the weight increases of the specimens due to oxygen absorbed from the air, on the assumption that the composition of the film is as given above, with any slight volatilization of boron oxides disregarded.

It follows from Fig. 2 that the film thickness and therefore the resistance to oxidation are continuous functions of the composition of the alloys, with a minimum at equimolar proportions of the components, similar to that found for the oxidation of metal alloys [8]. A similar relationship was found in a study of the oxidation resistance of alloys of the system TiB_2—TiN [9].

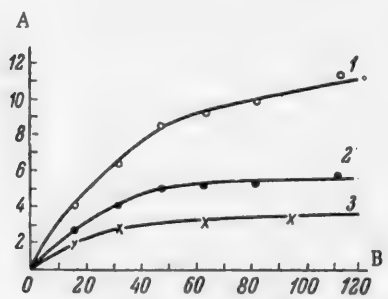

Fig. 3. Oxidation isotherms of the alloys at 800°.
A) Weight increase (in g/ $cm^2 \cdot 10^{-4}$);
B) time (minutes).
1) Pure niobium boride; 2) pure titanium boride; 3) alloy of 50 molar % TiB_2 and 50 molar % NbB_2.

The data in Table 2 and Fig. 2 indicate that the alloy with the highest resistance to high-temperature oxidation in air has the composition 50 molar % (37.8 wt. %) of TiB_2 and 50 molar % (62.2 wt. %) of NbB_2. The cause of this is probably the denser packing of the atoms of the components of the oxidized surface layer in the network structure of the glassy film and the smaller dimensions of the cells of the atomic network [6], in comparison with oxides of other compositions.

The form of the oxidation isotherms (Fig. 3) suggests that the oxidation rate of boride alloys, like the oxidation rate of many metallic alloys, is determined by the rate of diffusion of oxygen atoms to the groups of atoms of the boride alloys through the oxide film formed on the specimen surface. The dense, vitreous nature of this film makes the boride alloys very resistant to oxidation by atmospheric oxygen; this is analogous to the oxidation resistance of titanium silicide and carbide with additions of silicon and boron [1-3].

Analysis of the weight increase—oxidation temperature curves (Fig. 1) shows that this is an exponential relationship; in Fig. 4 the weight increase—oxidation temperature relationship is plotted in semilogarithmic coordinates, the plots being straight lines with breaks at about 650°, above which the oxidation is more rapid. Such instances have been described in the literature [10], and were attributed to changes of structure and interatomic

bond forces in the oxide films. It is probable that above 650° the angular vibrations of the atoms in the networks of the vitreous oxide films become intense enough for effective increase of the cells of the atomic network of the glass, facilitating diffusion of oxygen through the oxide film and decreasing the true activation energy of the oxidation process, although the apparent activation energy, determined from the slope of the semilogarithmic plot, increases above the inflection point, as has been demonstrated theoretically [10].

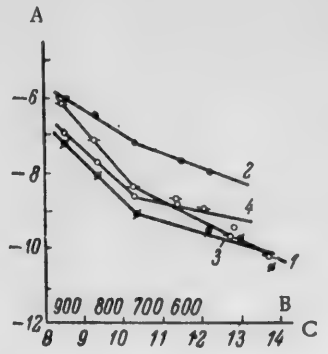

Fig. 4. Weight increase—oxidation temperature relationship plotted in semilogarithmic coordinates.
A) Value of $\ln(\Delta p)$; B) temperature (in °C); C) value of $\frac{1}{T} \cdot 10^{-4}$.
Respective contents of TiB_2 and NbB_2 in alloys (in molar %):
1) pure titanium boride; 2) 70 and 30; 3) 60 and 40; 4) 40 and 60.

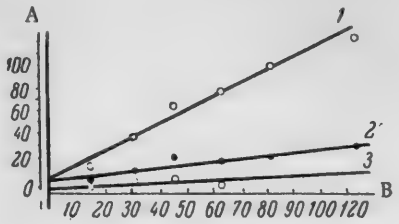

Fig. 5. Weight increase of specimens as a function of time; $\left(\frac{\Delta g}{s}\right)^2 = k\tau$.
A) Weight increase $\left(\frac{\Delta g}{s}\right)^2 \cdot 10^{-3}$;
B) time (minutes).
1) Pure niobium boride; 2) pure titanium boride; 3) alloy of 50 molar % TiB_2 and 50 molar % NbB_2.

An investigation of the time variation of the weight increase of specimens of titanium and niobium borides and of an alloy containing 50 molar % TiB_2 and 50 molar % NbB_2, in oxidation at 800°, revealed the existence of a parabolic relationship (Fig. 5), represented by the equation:

$$(\Delta p)^2 = k\tau,$$

where Δp is the weight increase per unit area (in g/cm^2); τ is the oxidation time (minutes) and k is the rate constant of the oxidation reaction (in $g/cm^2 \cdot$ minute).

Calculation gave the following values for the oxidation-rate constant: for pure niobium boride, $12.9 \cdot 10^{-9}$, for pure titanium boride, $2 \cdot 10^{-9}$ and for an alloy containing 50 molar % TiB_2 and 50 molar % NbB_2, $0.5 \cdot 10^{-9}$ $g/cm^2 \cdot$ minutes. Thus, an alloy containing 50 molar % TiB_2 and 50 molar % NbB_2 is oxidized much more slowly than the pure titanium and niobium borides.

The results obtained in this investigation are in satisfactory agreement with data on the oxidation of titanium boride [7] and confirm that the oxidation of solid solutions of borides conforms to laws characteristic for carbides, nitrides and metallic alloys.

LITERATURE CITED

[1] O. Accountis, H. Sisler, T. Shevlin and G. Bole, J. Am. Ceram. Soc. 37, 173 (1954).

[2] R. Kieffer, F. Benesovsky, H. Nowotny and H. Schachner, Z. Metallkunde, 43, 284 (1952).

[3] R. Kieffer and F. Benesovsky Symposium on Powder Metallurgy, Iron and Steel Inst Prepr. Gr. IV, 40 (1954).

[4] G. V. Samsonov and V. S. Neshpor, J. Phys. Chem. 29, 839 (1955).

[5] P. Shwarzkopf and R. Kieffer, Refractory Hard Metals (N.Y., 1953).

[6] W. Zachariasen, J. Am. Chem. Soc. 54, 3841 (1932).

[7] G. V. Samsonov and N. K. Golubeva, J. Phys. Chem. 30, 1258 (1956).

[8] O. Kubaschewski and B. Hopkins, Oxidation of Metals and Alloys (Russian translation) (IL, 1955).

[9] G. V. Samsonov and E. V. Petrash, Metal Science and Treatment 4, 19 (1955).

[10] V. I. Arkharov, J. Tech. Phys. 24, 100 (1954).

Received May 12, 1956

REGENERATION OF OXYTHIOARSENATE SOLUTIONS*

N. I. Brodskaya, M. I. Gerber, V. P. Teodorovich, and A. D. Shusharina

The Leningrad Scientific Research Institute of Petroleum Processing and Production of Synthetic Liquid Fuel

The previous communication [1] contained the results of experiments on the regeneration of arsenical soda solutions similar in composition to the liquors used in industrial practice.

However, in view of the fact that these solutions contain arsenic compounds differing in the degree of substitution of oxygen by sulfur, analytical methods for which have not yet been developed, we synthesized individual sodium thio- and oxythioarsenate, of the compositions $Na_3AsS_4 \cdot 8H_2O$ and $Na_3AsS_3O \cdot 11H_2O$.

Synthesis of sodium thio- and oxythioarsenate [2]. The individual thio- and oxythioarsenate compounds were prepared as follows. Sodium thioarsenate $Na_3AsS_4 \cdot 8H_2O$ was prepared from arsenious trisulfide by the reaction with sodium sulfide and sulfur

$$As_2S_3 + 3Na_2S + 2S = 2Na_3AsS_4 .$$

A ground mixture of arsenious trisulfide and sulfur was boiled with a solution of sodium sulfide until the As_2S_3 and S were completely dissolved.

After evaporation, the hot solution was filtered; crystals of $Na_3AsS_4 \cdot 8H_2O$ deposited on cooling. These crystals were separated on a Buchner funnel, washed with 50% alcohol solution, and recrystallized from boiling water. The $Na_3AsS_4 \cdot 8H_2O$ consisted of white crystals with a faint greenish tinge, readily soluble in water. Analytical data for the substance are given in Table 1.

TABLE 1

Compound	g-atoms Na / g-atoms As	g-atoms S / g-atoms As	pH of 0.05 molar solution	pH at which arsenious sulfide is precipitated
$Na_3AsS_4 \cdot 8H_2O$	—	3.97	9.6	5.7
$Na_3AsS_4 \cdot 8H_2O$, recrystallized from water	—	4.02	9.25	5.7
$Na_3AsS_3O \cdot 11H_2O$	—	2.98	~11	6.0
$Na_3AsS_3O \cdot 11H_2O$, recrystallized from water	3.0	2.92	~11	6.5

*Communication II in the series on the oxidation of oxythioarsenates in aqueous solutions.

This work was carried out under the guidance of V. V. Ipatyev and reported at the Conference on Sulfur Recovery held at the State Institute of the Nitrogen Industry, June 18-20, 1952.

Sodium oxythioarsenate $Na_3AsS_3O \cdot 11H_2O$ was prepared from the thioarsenate described above by reaction with caustic soda.

$$Na_3AsS_4 + 2NaOH = Na_3AsS_3O + Na_2S + H_2O.$$

Warm caustic soda solution was added to a boiling solution of sodium thioarsenate, the mixture was boiled for 30-40 minutes, and alcohol was added to precipitate crystals of $Na_3AsS_3O \cdot 11H_2O$. The crystals were filtered off on a Buchner funnel, washed with 50% alcohol, and dried.

$Na_3AsS_3O \cdot 11H_2O$ consists of very small white crystals. Analytical data for the substance are given in Table 1.

As the pH of industrial arsenical soda liquors varies between 6.5 and 9.5, the solutions were acidified with sulfuric acid to different pH values. The temperature of the experiments was 20°.

Regeneration of oxythioarsenate solutions. The results obtained are given in Tables 2 and 3 and in Fig. 1.

The experimental results show that 0.05 molar* solutions of Na_3AsS_4 and Na_3AsS_3O have pH about 10-11, and their regeneration rate is very low, so that sulfur is precipitated only after several hours and in small amounts.

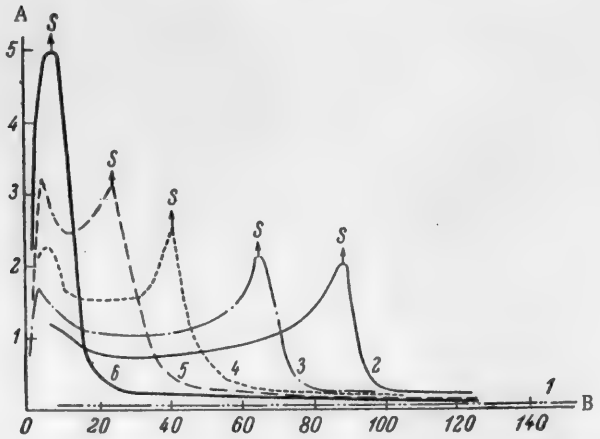

Fig. 1. Rate of absorption of oxygen by 0.05 molar Na_3AsS_4 solutions acidified to different pH values.

A) Rate of oxygen absorption (ml/minute), B) time (minutes). Solutions of Na_3AsS_4 acidified to pH values: 1) original ~10; 2) 8.3; 3) 7.8; 4) 7.5; 5) 7.3; 6) 6.55.

After acidification of these solutions with acid, the regeneration rate increases considerably, and greater amounts of elemental sulfur are liberated. When solutions of Na_3AsS_4 and Na_3AsS_3O were acidified with sulfuric acid to the stoichiometric composition Na_2HAsS_4 and Na_2HAsS_3O, the pH of the former solution was ~6, and of the latter, ~7.

The form of the curves in Fig. 1 confirms the results obtained in experiments with industrial arsenical soda liquors [1]: the maxima on the regeneration curves are shifted to the right with increase of pH.

Change of solution pH during regeneration. For elucidation of the mechanism of the process, the variations of pH during regeneration are of interest. Therefore, together with the determinations of the oxygen-absorption rate, the solution pH was measured by means of the glass electrode. The glass electrode was placed in the solution inside the laboratory regenerator, so that the pH could be measured throughout the oxidation process.

The curves in Fig. 2 show variations of pH in the course of regeneration in certain experiments on the oxidation of Na_3AsS_4 and Na_3AsS_3O solutions oxidized with sulfuric acid. The pH curves have well-defined maxima,

* 0.05 molar solutions were used because the liquors used in works conditions are close to 0.05 molar with respect to arsenic.

at times corresponding to the maximum rates of oxygen absorption and to the start of sulfur liberation.

The existence of maxima on the pH–time curves suggests the occurrence of two superposed processes. For interpretation of this experimental fact, solutions of sodium hydrosulfide of different pH were oxidized.

TABLE 2

Oxidation of Na_3AsS_4 Solutions Acidified with Sulfuric Acid to Different pH Values

Solution used					Regeneration data					
amount (in ml)							amount of sulfur formed			
0.106 molar Na_3AsS_4	0.1 N H_2SO_4	H_2O	g-atoms S / g-atoms As	pH value	ml of oxygen used for regeneration of 100 ml of solution.	start of sulfur deposition (min)	in g/liter	$\frac{S_{el}}{S_{el}+S_{thio}} \cdot 100$*	g-atoms Sel / g-atoms As	g-atoms S** / g-atoms As in solution after regeneration
50	0	50	~4.0	~10.0	137.8	413	0.367	18	0.21	2.85
50	2	48	3.85***	8.3	136.8	87	0.280	14	0.16	2.7
50	4	46	3.87	7.8	135.6	65	0.341	17	0.20	2.7
50	6	44	3.89	7.5	131.5	42	0.458	23	0.27	2.7
50	8	42	3.84	7.4	128.0	34	0.454	23	0.27	2.8
50	10	40	3.86	7.3	132.0	25	0.583	28	0.34	2.6
50	12	38	3.81	7.2	121.5	15	0.584	30	0.34	2.6
50	25	25	3.68	6.8	108.2	8	0.946	49	0.56	2.5
50	30	20	3.64	6.7	103.8	7	1.087	56	0.64	2.5
50	40	10	3.49	6.55	104.0	6	1.393	67	0.79	2.3
50	50	0	3.48	6.25	94.2	5	1.815	84	1.03	2.3

TABLE 3

Oxidation of Na_3AsS_3O Solutions Acidified with Sulfuric Acid to Different pH Values

Solution used					Regeneration data					
amount (in ml)							amount of sulfur formed			
0.094 molar Na_3AsS_3O	0.1 N H_2SO_4	H_2O	g-atoms S / g-atoms As	pH value	ml of oxygen used for regeneration of 100 ml of solution	start of sulfur deposition (min)	in g/liter	$\frac{S_{el}}{S_{el}+S_{thio}} \cdot 100$*	g-atoms Sel / g-atoms As	g-atoms S** / g-atoms As in solution after regeneration
50	30	20	2.92***	9.15	43.5	130	0.149	23	0.10	2.5
50	44.4	5.6	2.96	7.9	30.8	4	0.255	47	0.17	2.6
50	50	0	2.85	7.6	25.8	2	0.368	70	0.23	2.5
50	50	0	2.80	7.4	27.7	2	0.468	77	0.30	2.4
50	50	0	2.82	7.2	28.7	1	0.750	100	0.50	

Curves for the variation of the oxidation rates of sodium hydrosulfide solutions with time and the pH of these solutions are given in Fig. 3. Here again the curves for pH and the oxidation rate have maxima at points corresponding to sulfur liberation.

* This column gives the yield of elemental sulfur as % of the total sulfur, both liberated as elemental sulfur (S_{el}) and converted into thiosulfate (S_{thio}), on the assumption that the absorbed oxygen was all used for liberation of sulfur and formation of thiosulfate.

** Less the thiosulfate sulfur.

*** The decrease of the sulfur–arsenic ratio was caused by partial liberation of hydrogen sulfide on acidification of the solution.

The following reactions can probably occur in the oxidation of sodium hydrosulfide:

$$NaSH + \frac{1}{2}O_2 = NaOH + S, \quad (1)$$

$$2NaSH + 2O_2 = Na_2S_2O_3 + H_2O.$$

At relatively low pH values (pH < 7.5) these reactions in all probability occur simultaneously, as both thiosulfate formation and sulfur liberation were observed in the oxidation of hydrosulfide. The solution pH rises as Reaction (1) proceeds, whereas in Reaction (2) the pH falls. These reactions evidently proceed at different rates.

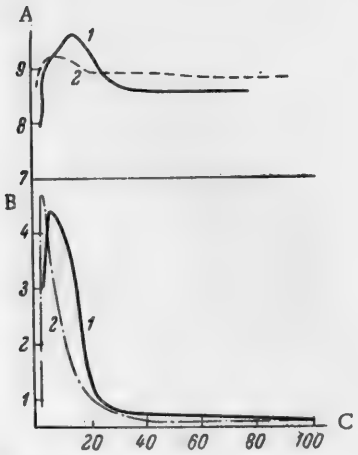

Fig. 2. Variations of pH during oxidation of solutions.
A) pH; B) rate of oxygen absorption (in ml/ minute);
C) time (minutes).
Solutions acidified with sulfuric acid: 1) Na_3AsS_4; 2) Na_3AsS_3O.
Curves for the regeneration of these solutions are given in the lower part of the diagram.

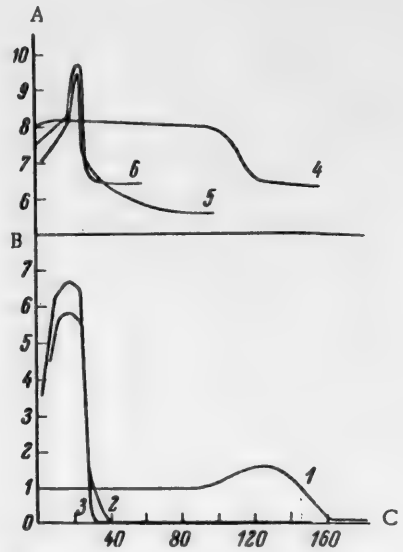

Fig. 3. Curves for the oxidation rates of sodium hydrosulfide solutions (1, 2, 3) acidified to different pH values, and variations of pH during regeneration (4, 5, 6).
A) pH, B) rate of oxygen absorption (in ml/ minute); C) time (minutes).
pH values: 1) 4-7.8; 2) 5-7.0; 3) 6-6.7.

It is quite probable that oxidation of sodium thioarsenates is accompanied by oxidation of the sodium hydrosulfide formed by hydrolysis of these salts.

DISCUSSION OF RESULTS

The results of experiments performed with individual synthesized compounds of the compositions $Na_3AsS_4 \cdot 8H_2O$ and $Na_3AsS_3O \cdot 11H_2O$ confirmed the results obtained in the oxidation of works arsenical soda liquors, leading to the conclusion that for improvement of the regeneration process both in regard to the rate and to the sulfur yield the process should be carried out at a low ratio of nominal soda [3] to arsenious anhydride, and at low pH.

The laboratory results were confirmed under works conditions. On the basis of these investigations, the nominal soda content of the liquor used in the Ishimbai petroleum refinery was reduced in 1949; this improved the purification process considerably, decreased the soda consumption and raised the yield of elemental sulfur. The optimum weight ratio of nominal soda to arsenious anhydride was found to be 1.1-1.3, which approximately corresponds to the formula Na_2HAsS_4. Operational experience in plants where the gas contains considerable amounts of carbon dioxide (the shale-processing combine in Kokhtla-Yarve and the shale-gas works in Slantsy) showed that

the best performance is obtained with the same ratio of nominal soda to arsenious anhydride.

The weight ratio of soda to arsenious anhydride was reduced to 1.07 at the Moscow coke-oven works in 1955 [4]; this also gave favorable results.

SUMMARY

It is shown that for improvement of the regeneration process, in regard both to sulfur yield and to the rate of the process, the regeneration must be carried out with a low ratio of nominal soda to arsenious anhydride and at low pH.

LITERATURE CITED

[1] N. I. Brodskaya, M. I. Gerber and V. P. Teodorovich, J. Appl. Chem. 30, 10, 1510 (1957).*

[2] J. W. Mellor, Comprehensive Treatise on Inorganic and Theoretical Chemistry, IX, 143, 153, 316, 330 (1933).

[3] M. I. Gerber, S. S. Iordan and V. P. Teodorovich, Factory Labs. 7, 823 (1954).

[4] Information Bull. State Inst. for Planning of Gas Purification Plants 115 (1955).**

Received July 17, 1956

* Original Russian pagination. See C. B. translation.

** In Russian.

INVESTIGATION OF THE OXIDATION OF ALLOYS CONTAINING THE INTERMETALLIC COMPOUND NiAl

E. I. Mozhukhin, L. Kh. Pivovarov and Ya. S. Umansky

The Moscow Steel Institute

The phase diagram for the system nickel–aluminum shows several chemical compounds: Ni_3Al, Ni_2Al, $NiAl_3$ [1]. The compound NiAl is homogeneous over a considerable concentration range, has the highest melting point (1638°) of all the alloys in the system nickel–aluminum and is of definite importance in relation to its use in heat-resisting alloys [2,3].

The heat resistance of one-phase alloys consisting of the compound NiAl only, and of the two-phase alloy NiAl + Ni_3Al was studied in the present investigation. For comparison, the heat resistance of electrolytic nickel and the one-phase cobalt–aluminum alloy containing the compound CoAl was also determined. The compound CoAl is analogous to the compound NiAl [4].

The one-phase alloys were made by fusion in an induction furnace, in a magnesite crucible. The two-phase alloys were made by the methods of powder metallurgy. The chemical compositions of the alloys studied are given in Table 1.

TABLE 1

Chemical Composition of the Materials Studied

Alloy	Chemical composition (in wt. %)								
	Ni	Al	Fe	Si	S	C	Mn	P	Co
Cast alloy 1	64.44	34.40	Traces	Traces	0.007	0.10	–	–	–
Cast alloy 2	73.47	25.86	0.64	0.05	0.012	0.037	0.35	–	–
Sintered alloy 3*	81	19.00	–	–	–	–	–	–	–
Cast alloy 4	–	33.84	0.30	0.07	0.010	Absent	Absent	Traces	63.89
Electrolytic nickel	99.95	–	0.004	Traces	0.0006	0.004	0.0005	0.001	–

Alloys 1 and 4 have the same composition (in atomic %): about 46.5 of nickel or cobalt, and 53.5 of aluminum. These alloys are one-phase solid solutions of aluminum in the compounds NiAl and CoAl. Alloy 2 is a one-phase substitutional alloy, consisting of a solution of nickel in the compound NiAl; its composition (in atomic %) is: 57 Ni, 43 Al.

Alloy 1 was brittle in the cast state and contained a certain amount of pores. Specimens of Alloy 1 were prepared by treatment of individual pieces of the castings on a grinding wheel. Specimens of regular geometric shape could not be formed by this method, and specimens in the form of plane-faced polyhedrons had to be used. Specimens with few surface pores were chosen for the experiments.

Specimens of Alloy 2 were made by anodic–mechanical cutting of castings.

For measurement of the surface area of specimens of irregular shape, paper imprints of every face were

* Composition of the original charge.

weighed on an analytical balance. The results of parallel determinations of the surface area of a single specimen did not differ by more than 0.1 cm^2. Similar deviations were found between the specimen areas calculated from the geometric dimensions of the specimens and the areas determined as described above.

In addition to the experiments on the oxidation of these specimens, experiments on the oxidation of powdered Alloys 1 and 2 were carried out.

The course of oxidation was studied by means of continuous weighing. Specimens with platinum wire attached (or powders in platinum crucibles) were placed in a vertical tubular electric furnace heated to the temperature of the experiment, and suspended from the pan of an analytical balance situated over the furnace. The furnace tube was open above and below during the experiment, allowing free access of air to the specimen. The furnace temperature was automatically regulated by means of an electronic thermoregulator. The thermocouple of the regulator was placed in the immediate proximity of the specimen. The temperature was regulated to the nearest ±10°. In addition, the furnace temperature was checked by means of another thermocouple.

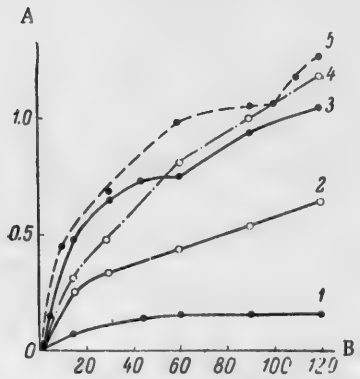

Fig. 1. Oxidation curves of Alloy 1, Alloy 4, and Ni at various temperatures.
A) Weight increase (in mg/cm^2);
B) time (minutes).
Curves: 1, 2, 3) Alloy 1; 4) Alloy 4; 5) nickel.
Temperature (in °C): 1) 870; 2, 4, 5) 1000, 3) 1150.

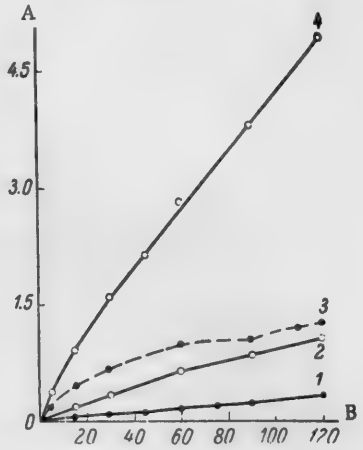

Fig. 2. Oxidation curves of Alloy 2 at various temperatures and of nickel at 1000°.
A) Weight increase (in mg/cm^2);
B) time (minutes).
Curves: 1, 2, 4) Alloy 2; 3) nickel.
Temperature (in °C): 1) 870; 2,3) 1000; 4) 1150.

The first weighing was performed 5 minutes after insertion of the specimen into the furnace, and subsequent weighings were made at 5, 10, or 15-minute intervals (according to the weight increase). By this method it was possible to follow the growth of the oxide film as soon as a thin layer of oxides was formed on the specimen surface. If the weight increases were small, the displacement of the balance pointer from the zero position on a previously calibrated scale was recorded; a rider and weights were used for large increases in weight.

The oxidation curves of the alloys and nickel are given in Figs. 1-3.

Oxide films, adhering firmly to the specimen surfaces, were formed on all the alloys during oxidation. The films on nickel were yellow, on Ni–Al alloys they were gray, and on Co–Al alloy, blue.

Comparison of the oxidation curves for 1000° (Figs. 1 and 2) shows that Ni–Al alloys are more heat-resistant than pure Ni; the oxidation of Alloy 1 even at 1150° is less than that of Ni at 1000° (Fig. 1). It also follows from the curves (Fig. 1) that the compound NiAl (Alloy 1) is oxidized much more slowly than the compound CoAl (Alloy 4).

The oxidation curves of nickel and Alloy 2 (at 1150°) show breaks, indicating breakdown in the continuity of the films owing to cracking caused by internal stresses.

The open porosity of specimens of Alloy 3, formed by sintering, had a considerable influence on the magnitude of the weight increase per unit surface area of the specimens (the porosity of the specimens was determined by the oil-impregnation method).

Specimens with few pores (less than 3%) are oxidized less than nickel, whereas specimens of higher porosity (10-30%) are oxidized considerably more (Fig. 3).

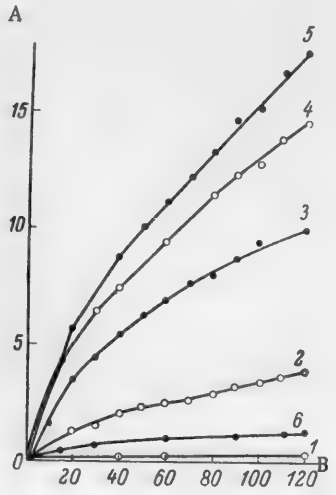

Fig. 3. Oxidation curves of Alloy 3 specimens of different porosity, and of nickel, at 1000°.
A) Weight increase (in mg/cm²);
B) time (minutes).
Porosity of alloy (in %): 1) 3;
2) 10.7; 3) 198; 4) 30.9; 5) 31.2;
Curve 6) nickel.

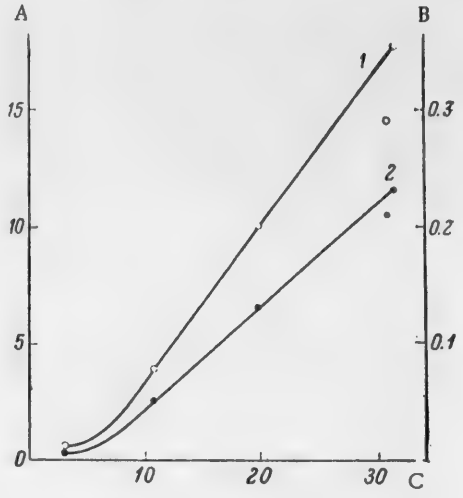

Fig. 4. Influence of porosity on the oxidation of Alloy 3.
A) Weight increase in 2 hours (in mg/cm²);
B) value of constant K; C) open;
porosity (%).
1) Weight increase in 2 hours;
2) constant K.

For determination of the oxidation laws, oxidation curves were plotted in log weight increase–log time coordinates. The plots obtained for all the alloys studied were linear, and therefore the oxidation processes may be represented by equations of the type

$$G^A = Kt$$

where G is the weight increase per unit surface area of the specimen, t is the time, and A and K are constants.

The constants A and K, determined graphically, are given in Table 2. For the calculations, the weight increase (G) was in mg/cm² and the time (t) in minutes.

As is known, the value of A depends on the nature of the oxidation process. When A = 1, the oxidation rate is determined by the rate of the reaction on the specimen surface, and in this case the oxide film does not protect the alloy against oxidation. When A = 2, the oxidation rate is determined by the rate of ion diffusion through the oxide film.

The values of A given in Table 2 show that the oxidation rate of Alloy 2 is determined mainly by the rate of the reaction at the metal–oxide film interface. Therefore the oxide film on Alloy 2 has almost no protective properties. The value of K, which represents the weight increase per unit time, greatly increases with temperature (by a factor of about 23 in the case of Alloy 2 when the temperature is increased from 870 to 1150°). The value of A is almost unchanged with temperature, indicating that the nature of the oxidation of the alloy is the same at different temperatures.

The values of A for Alloy 1 are greater than 2.0, and therefore the rate of the reaction at the metal surface is not the determining factor of the oxidation process. The oxidation rate cannot be determined only by the diffusion of ions through the film, since A is greater than 2.0.

Additional factors, which retard diffusion, operate in this instance.

For specimens of Alloy 3, made by sintering, the values of A do not change with variation of the open porosity of the specimens from 10 to 30%; the open porosity has a significant influence on values of K only. The fact that the open porosity has no influence on the value of A indicates that the oxidation of the open-pore surfaces does not depend on the porosity, and the processes involved do not differ from the processes occurring in the oxidation of the external surface, because the state of the open-pore surfaces does not depend on the porosity and does not differ from the state of the external surface.

TABLE 2

Values of the Constants A and K in Equation of the Type $G^A = Kt$

Material	Oxidation temperature (°C)	A	K
Cast Alloy 1	870	2.2	0.0014
	1000	2.3	0.0040
	1150	2.3	0.0068
Powder of Alloy 1 fraction −0125 +0085. layer 1 mm thick	1000	2.3	0.00035
Cast Alloy 2	870	1.0	0.0025
	1000	1.2	0.015
	1150	1.2	0.058
Powder of Alloy 2 fraction −0125 + 0085, layer 1 mm thick	1000	2.9	0.00018
Sintered Alloy 3, with porosity			
31.2%	1000	1.5	0.23
30.9%	1000	1.6	0.19
19.8%	1000	1.6	0.13
10.7%	1000	1.6	0.049
2.7%	1000	1.6	0.001
Cast Alloy 4	1000	1.7	0.013
Nickel	1000	2.0	0.013

The effects of open porosity on the value of K and the weight increase per 1 cm^2 of the external specimen surface in 2 hours of oxidation are shown graphically in Fig. 4. The explanation for the linear course of the relationships between 30 and 10% porosity is that the individual open pores are of the same size in specimens differing in porosity; the higher the porosity, the more individual pores are present in the specimen. The total pore volume is in this case directly proportional to the pore surface.

In the oxidation of powders of the −0125 + 0085 fraction of Alloy 1 at 1000° (see Table 2), the value of A for the powdered alloy was equal to the value of A for the compact specimens (for calculation of the weight increase per 1 cm^2, the specific surface of the powder was determined by the air-permeability method). The relatively low value of K for the powdered alloy (K = 0.00035) may be attributed to the difficult access of air to internal layers of the powder, resulting in less oxidation per unit surface.

The situation was quite different in the oxidation of powders of the −0125 + 0085 fraction of Alloy 2 at 1000°. The value of A for the powder was 2.9, whereas for the compact alloy at the same temperature A was 1.2.

This large difference in the oxidation behavior of powdered Alloys 1 and 2 is due to the different nature of the oxidation processes in these alloys.

Compact specimens of Alloy 1 become coated with a strong film of oxides, as is shown by the high value of A, in excess of 2. A similar film is evidently formed on the powder particles. This film, which adheres firmly to the particle surfaces, prevents surface migration of the atoms and thereby hinders the processes which decrease the surface roughness of the powder particles, and which usually take place during the sintering of metallic powders [5].

Dense surface oxide films are not formed on compact specimens of Alloy 2. Evidently, no films adhering closely to the surface are formed on the surface of the powder particles either. The films formed do not prevent surface migration of atoms, so that the total surface area of the particles decreases, leading to a decrease of the rate of weight increase calculated per unit original surface area of the powder.

For elucidation of the structure of the oxide films, x-ray patterns were obtained for the surfaces of specimens oxidized for 10 hours at 1200°. These conditions were used so that oxide films of sufficient thickness could be formed. The results are given below:

Alloy	Phases present
Alloy 1	NiAl, $NiO \cdot Al_2O_3$
Alloy 2	NiAl, $NiO \cdot Al_2O_3$, α-Al_2O_3
Alloy 3	Ni_3Al, $NiO \cdot Al_2O_3$

The x-ray patterns of the oxidized specimens of Alloys 1 and 2 contain lines of the original structure (NiAl), while the patterns for Alloy 3 had only Ni_3Al lines, NiAl lines being absent. In addition to the lines of the original structure, all the x-ray patterns contained lines of a phase with a cubic face-centered lattice, the lattice parameter being 8.00 A. The lattice and parameter of this phase correspond to the compound $NiO \cdot Al_2O_3$.

The x-ray pattern of the oxidized specimen on Alloy 2 also contained Ni_3Al lines, not present in the pattern of the original structure, and lines of the phase α-Al_2O_3.

The oxidized specimens of Alloy 4 were covered with a blue film. It is known that the spinel $CoO \cdot Al_2O_3$ has this color.

Thus, there is no doubt about the presence of a spinel in the oxide films formed on the surfaces of the compounds NiAl and CoAl.

The structural mechanism of the oxidation of the alloys studied can be deduced from the results of phase analysis of the oxide films.

The formation of a layer of new phase must take place with minimum deformation of the lattice of the new phase. Growth of the phase $NiO_3 \cdot Al_2O_3$ on NiAl fully satisfies this condition. The $NiO \cdot Al_2O_3$ lattice may be close to the NiAl lattice structurally and dimensionally if we assume orientation of the same type as exists between α-Fe and γ-Fe_2O_3 [6]:

$$(001)_{NiO \cdot Al_2O_3} \parallel (001)_{NiAl}$$
$$[010]_{NiO \cdot Al_2O_3} \parallel [110]_{NiAl}$$

The differences in the interatomic distances in the [110] direction of the NiAl lattice and in the [010] direction for the spinel $NiO \cdot Al_2O_3$ depend on the composition of NiAl, since the lattice constant of NiAl varies with the composition of this compound. For a compound corresponding to the formula NiAl the difference between the interatomic distances in these two directions is 1.4%, while for a solid solution of nickel in the compound NiAl, with 60 atomic % of nickel present, this difference is only 0.5%.

There are twice as many aluminum atoms as nickel atoms in the spinel lattice, while the alloy contains approximately equal numbers of nickel and aluminum atoms; therefore growth of the spinel film requires directed diffusion of aluminum atoms to the specimen surface.

In Alloy 1, close to the compound NiAl in composition, decrease of the aluminum content in the surface layer does not lead to formation of a second phase, Ni_3Al. The oxide film adheres closely to the surface of Alloy 1.

In surface layers of Alloy 2, near the boundary of the homogeneous region of NiAl, the compound Ni_3Al appears with decrease of the aluminum content during formation of the spinel; this breaks down the continuity of the oxide film and decreases the heat resistance of the alloy. The value of A for this alloy is close to unity. The presence of the compound Ni_3Al, the lattice of which is analogous to the nickel lattice, in the surface layers is confirmed by x-ray analysis.

The presence of α-Al_2O_3 in the film of Alloy 2 can probably also be attributed to breakdown on the oxide film during formation of Ni_3Al in the surface layers of the alloy.

An interesting fact is that the cobalt–aluminum alloy (Alloy 4) is oxidized more rapidly than the nickel–aluminum alloy of analogous composition (Alloy 1), although the oxide film on Alloy 4 also consists of a spinel. It is possible that when Alloy 4 is oxidized a second phase which breaks down the spinel film, is formed in the surface layer, since the compound CoAl has a somewhat narrower region of homogeneity.

In oxidation of the two-phase Alloy 3, a structurally bound film of the spinel $NiO \cdot Al_2O_3$ can be formed only on NiAl grains and only if there are cracks in the film. A film with such structural correspondence cannot exist on Ni_3Al grains. If the continuity of the film is disrupted, the values of A in the equation to the oxidation curve should be between 1 and 2. According to our results, for Alloy 3, $A = 1.6$.

SUMMARY

1. The processes in the oxidation of the compound NiAl depend on its composition. In presence of excess Al atoms a dense oxide film is formed. In presence of excess Ni atoms the continuity of the film is disrupted by separation of the Ni_3Al phase, with acceleration of the oxidation processes.

2. Powders of the compound NiAl, which forms dense oxide films, conform to the same oxidation law as the compact compound. When the continuity of the oxide film breaks down, the oxidation rate of the powders decreases rapidly with time owing to the decrease of the surface area of the powder particles.

3. The compound CoAl is oxidized more than the compound NiAl of corresponding composition.

LITERATURE CITED

[1] I. Schram, Z. Metallkunde, 33, 377 (1941).

[2] R. Wachtell, U.S. Atomic Energy Commission Publ. (1952); through Metallurgical Abstracts 22, 1, 33 (1954).

[3] R. A. Long, Metal Progress, 68, 3, 123-128 (1955).

[4] A. Radley, G. Seager, J. Institute of Metals, 64, 1, 81-88 (1939).

[5] V. Ivensen, J. Tech. Phys. 22, 4, 677-685 (1952).

[6] V. Arkharov, Oxidation of Metals (Metallurgy Press, 1945).*

Received June 8, 1956

*In Russian.

KINETICS OF THE REACTION OF SODIUM ALUMINATE SOLUTION WITH LIME

B. V. Drozdov and M. F. Malyshev

Department of Inorganic and Analytical Chemistry of the Leningrad Technological Institute, and the All-Union Aluminum–Magnesium Institute

Interaction of sodium aluminate solutions with lime is one of the reactions taking place in the production of alumina by the sinter process, both from bauxites and from nephelines. The kinetics of this reaction has been studied very little, partly because of the peculiar course of this reaction, and partly because of the difficulties involved in its study, as aluminate solutions are unstable systems which tend to decompose under the influence of various factors.

This is a heterogeneous reaction, which may be schematically represented by the following over-all equation:

$$nCa(OH)_2 + Na_2O \cdot Al_2O_3 + xH_2O = nCaO \cdot Al_2O_3 \cdot xH_2O + 2NaOH \qquad (1)$$

Stainless-steel beakers, 120 ml in capacity, were used for the kinetic experiments. The liquids were agitated mechanically by a stirrer rotating at 17-18 r.p.m. The required temperature was maintained in an air thermostat to the nearest ±1° by means of a thermoregulator.

For preparation of the lime, marble was roasted, ground and sifted through a No.03 sieve. The active calcium oxide was determined by titration with 0.5 N hydrochloric acid in presence of phenolphthalein. The substance was found to contain 97% of active calcium oxide.

For preparation of sodium aluminate solutions, aluminum hydroxide was dissolved in caustic soda solutions. The effects of CaO and Al_2O_3 contents and of the caustic ratio* were studied.

The amount of lime taken in all the experiments was in excess of its solubility. It could then be assumed that the amount of lime had no significant influence on the rate of reaction. In fact, it follows from the data given below that the decisive factor is the amount of lime in the pulp, and especially the $\frac{CaO}{Al_2O_3}$ ratio in it.

The results obtained in the interaction of sodium aluminate solution with lime, with 218 g CaO per liter, initial $\alpha_k = 2$, at 70° are given below.

Initial Al_2O_3 concentration (in g/liter)	293.5	202.0	103.0	50.0	10.3
Amount of Al_2O_3 reacted (in % after 1 minute)	16.9	24.5	68.0	87.6	99.1
Half-life of sodium aluminate	2 days	14 minutes	44 sec	34.2 sec	25 sec

The effect of variations of the CaO content of the pulp on the rate of reaction of the lime with aluminate solution, initially containing 283.3 g Al_2O_3 per liter, initial $\alpha_k = 2$, at 70° is shown by the following data:

CaO content (g/liter)	218	366	436
Half-life (minutes)**	67	39	26

* The caustic ratio α_k is the molecular ratio $Na_2O : Al_2O_3$.

** The time required for half the sodium aluminate to react.

All attempts to apply kinetic equations for 1st, 2nd and 3rd order reactions to the experimental data proved unsuccessful,* and kinetic equations for reversible reactions also proved inapplicable.

Experiments on the reaction kinetics were carried out at constant $\frac{CaO}{Al_2O_3}$ ratio, 1.65 by weight and 3 molar, with initial $\alpha_k = 2$, at 70°.

The results are given below.

Initial Al_2O_3 concentration (g/liter)	195.5	97.5	50.66	10.0
Half-life (seconds).	44	46.5	54	52

It follows from these results that despite 20-fold variations of the Al_2O_3 and CaO contents in the solution, the half-life remains constant within the limits of experimental error. This suggests that the kinetics of Reaction (1) at constant $\frac{CaO}{Al_2O_3}$ ratio in the pulp can be formally described by the equation for a 1st order reaction.

Despite the fact that the half-life is constant, detailed calculations showed that the experimental data do not fit the kinetic equation for a 1st order reaction (Tables 1-4), nor is the equation for a reversible reaction applicable. The calculations show that as the reaction proceeds, it is retarded to an increasing extent in comparison with a 1st order reaction. Gradual self-retardation of the reaction takes place.

The kinetics of the interaction of sodium aluminate solution with lime may be explained on the following considerations.

The reaction between sodium aluminate solution and lime evidently occurs mainly at the surface of the lime particles. During the first instant of interaction at the free surface of the particles the reaction rate is high and is determined by chemical factors. During this period the kinetics may be formally represented by a 1st order equation.

The solid reaction product, calcium aluminate, is not removed from the surface of the lime particles, but forms a porous film on it. The reaction proceeds further by diffusion of sodium aluminate through the porous film of calcium aluminate, which gradually grows. The caustic soda formed in the reaction diffuses in the opposite direction. Therefore, as the reaction proceeds it is slowed down increasingly as the result of a decrease in the surface area of the lime particles, growth of the calcium aluminate film, and clogging of the film pores with caustic soda.

These views on the reaction mechanism are confirmed by comparison of the reaction rates when the porous film of calcium aluminate is continuously removed from the lime particles by agitation with steel balls. The influence of agitation with steel balls on the interaction of aluminate solution with lime, with initial Al_2O_3 concentration 306 g/liter, CaO content 218 g/liter, initial $\alpha_k = 2$, at 70°, is shown by the data below.

	With balls	Without balls
30% Al_2O_3 reaction after (minutes)	8	80
Amount of Al_2O_3 reacted after 1 hour (%)	55	29.8

These results show that with continuous destruction of the forming calcium aluminate film the reaction rate is considerably higher than in experiments with which the porous film is allowed to grow without hindrance on the particle surfaces. It appears, however, that the steel balls do not destroy the film completely, and a film gradually grows as the reaction proceeds; this is shown by the fact that the difference between the experiments with and without the use of balls gradually diminishes.

For studies of the kinetics of self-retarding reactions, Drozdov's equation [1], which has been successfully applied by a number of authors [2-5], is useful:

$$M = \frac{1}{t} \log \frac{a}{a-x} - \beta \frac{x}{t}, \qquad (2)$$

here a is the initial concentration of the reacting substance; x is the amount reacted at time t; M is the overall

* This is confirmed in the present paper by the data given below; it will be seen that the rate constant for a 1st order reaction decreases rapidly and continuously.

rate constant of the reaction; β is the coefficient of retardation of the reaction.

This equation is applicable if the experimental data plotted in $\frac{1}{t}\log\frac{a}{a-x}$ and $\frac{x}{t}$ coordinates give a straight line.

TABLE 1

Reaction of Sodium Aluminate Solution with Lime (initial Al_2O_3 concentration 293.5 g/liter, CaO content 218 g/liter, $\alpha_k = 2.0$, temperature 70°)

Time (min)	$a-x$	$\frac{1}{t}\log\frac{a}{a-x}$	$\frac{x}{t}$
1	244 0	0.0792	49.5
5	231.0	0.0207	12.5
10	221.0	0.0121	7.25
30	212.5	0.0047	2.70
60	206.0	0.0026	1.45
180	203.0	0.0009	0.505

TABLE 2

Reaction of Sodium Aluminate Solution with Lime (initial Al_2O_3 concentration 202 g/liter, CaO content 218 g/liter, $\alpha_k = 1.98$, temperature 70°)

Time (min)	$a-x$	$\frac{1}{t}\log\frac{a}{a-x}$	$\frac{x}{t}$
1	152.5	0.1239	49.5
5	115.3	0.0485	17.3
10	103.5	0.0292	9.9
30	92.8	0.0113	3.64
60	83 2	0.0064	1.98
180	81.0	0.0014	0.67

TABLE 3

Reaction of Sodium Aluminate Solution with Lime (initial Al_2O_3 concentration 100.5 g/liter, CaO content 218 g/liter, Na_2CO_3 content 175 g/liter, $\alpha_k = 19.6$, temperature 70°)

Time (min)	$a-x$	$\frac{1}{t}\log\frac{a}{a-x}$	$\frac{x}{t}$
1	47.5	0.322	53
5	24.1	0.124	17.3
10	19.9	0.070	8.06
30	11.3	0.032	2.97
60	8.5	0.0178	1.54
180	6.9	0.0065	0.52

TABLE 4

Reaction of Sodium Aluminate Solution with Lime (contents (in g/liter): Al_2O_3 103.4, Na_2CO_3 180, CaO 58.7; $\alpha_k = 1.90$, temperature 70°)

Time (min)	$a-x$	$\frac{1}{t}\log\frac{a}{a-x}$	$\frac{x}{t}$
1	82.9	0.0969	20.5
5	81.5	0.0208	4.4
10	77.7	0.0124	2.6
30	76.6	0.0043	0.895
60	73.4	0.0029	0.50

In fact, the experimental results gave good agreement with the equation in a number of cases, proving the applicability of Equation (2) to the reaction under consideration.

The applicability of the equation is demonstrated particularly clearly if the retardation begins from the start of the reaction. In some cases, when the retardation is not great, a 1st order equation is applicable at the start of the reaction, which later conforms to Equation (2).

In the experiments the results of which are given in Tables 1 and 2, the cause of the retardation was deficiency of CaO in the solution.

The applicability of Equation (2) is illustrated by Curves 1 and 2 in the Figure, and by the data in Table 2.

Retardation of the reaction may also be caused by the presence of a considerable amount of soluble carbonate in solution, resulting in the formation of a film of insoluble calcium carbonate on the active surface of the lime particles, according to Equations (3) and (4). In practice, sodium aluminate solutions always contain some sodium carbonate.

$$Ca(OH)_2 + Na_2CO_3 = CaCO_3 + 2NaOH \quad (3)$$

$$nCaO \cdot Al_2O_3 \cdot xH_2O + nNa_2CO_3 = nCaCO_3 + \\ + Na_2O \cdot Al_2O_3 + 2(n-1)NaOH + xH_2O \quad (4)$$

An example of retardation caused by Reactions (3) and (4) is provided by the experimental data in Table 3.

The data in Table 3 and Curve 3 in the Figure show that despite the high $\frac{CaO}{Al_2O_3}$ ratio the reaction is nevertheless retarded owing to the presence of a high concentration of sodium carbonate in the solution.

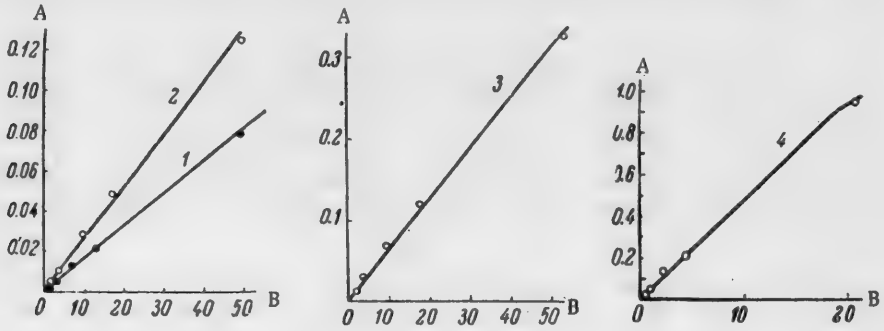

Graphic verification of Equation (2).

A) $\log \frac{a}{a-x}$, B) $\frac{x}{t}$.

The curves are explained in the text.

The retardation is still greater if the $\frac{CaO}{Al_2O_3}$ ratio is inadequate and the solution also has a high content of sodium carbonate. This is illustrated by the data in Table 4 and Curve 4 in the Figure.

This investigation does not exhaust all the factors which influence the rate of reaction of sodium aluminate solutions with lime. The results show, however, that even if Reaction (1) may be regarded as reversible, in the conditions studied the equilibrium is shifted very far to the right.

SUMMARY

In a study of the mechanism of the reaction between sodium aluminate solution and lime it was shown that if lime is deficient, or sodium carbonate is present in excess, or both, the experimental data conform satisfactorily to the kinetic equation for a self-retarding reaction:

$$M = \frac{1}{t} \log \frac{a}{a-x} - \beta \frac{x}{t}.$$

LITERATURE CITED

[1] B. V. Drozdov, Proc. 2nd All-Union Conf. on Theoretical and Applied Electrochemistry (Kiev, 1949) p. 106.*

[2] E. K. Mankash and A. B. Pakshver, J. Phys. Chem. 25, 4, 468 (1952); Colloid J. 14, 2, 112 (1952);** Proc. 7th Conf. on High-Molecular Compounds (Izd. AN SSSR, 1952).*

[3] A. L. Rotinyan, J. Appl. Chem. 21, 807 (1948); J. Gen. Chem. 19, 498 (1949).**

[4] B. V. Drozdov and A. L.Rotinyan, J. Gen. Chem. 19, 1848 (1949).**

[5] A. L.Rotinyan, B. V. Drozdov and R. M. Kogan, J. Appl. Chem. 21, 810 (1948).

Received September 29, 1956

* In Russian.

** Original Russian pagination. See C. B. Translation.

GENERAL LAWS OF ABSORPTION PROCESSES IN HIGH-SPEED ROTARY ABSORBERS

S. N. Ganz

The Dnepropetrovsk Institute of Chemical Technology

Numerous investigations have demonstrated in recent years that the most effective way of accelerating mass-transfer processes between gases and liquids in direct contact is by increasing the turbulence of the gas–liquid system as much as possible.

This follows from the work of Pozin et al. [1-4], who studied mass-transfer processes in foam equipment, of Kuzminykh [5], Shabalin et al. [6], and others, who studied absorption processes in bubbling equipment, Kishinevsky et al. [7, 8, 9], who studied absorption processes in conditions of vigorous agitation in stirred vessels, etc.

Our investigations of mass-transfer processes in rotary high-speed absorbers [10-16] made it possible to establish the general laws governing absorption in such equipment and to determine the optimum process conditions.

Single-compartment and multicompartment horizontal high-speed rotary absorbers were used for our investigations. The design of the single-compartment absorbers is clear from our earlier papers [10-16]. The design of the multicompartment absorbers is shown diagrammatically in Fig. 1 (a and b).

In Fig. 1, a the absorbers are arranged consecutively in one line. In this case the motion of the liquid and gas is linear. In Fig. 1, b the absorber compartments are arranged in parallel and are separated by partitions with passages for the gas at the end walls. This arrangement gives a zigzag motion of the gas and liquid. The partitions between the compartments are equipped with overflow weirs at their lower ends, so that the required liquid level is maintained in each compartment. The compartments contain horizontal shafts with disks attached. Multicompartment absorbers were used for absorption processes accompanied by reversible reactions.

The design characteristics of the equipment and its operating conditions determine definite relationships which apply to all systems.

These relationships depend on the peripheral disk speed, the design of the disks and their arrangement on the shaft, the linear velocity of the gas, the amount of liquid in the apparatus, etc. These relationships are briefly considered below.

Influence of peripheral disk speed on the rate of absorption. The investigations showed that increase of the peripheral disk speed up to a certain limit results in a considerable increase of the absorption rate in all cases. This follows from the empirical formulas found for different systems, given below.

a) For absorption of N_2O_3 by $Ca(OH)_2$ solution:

$$K_d = (1490 - 241x^{-1}) \cdot V_d^{0.333} + (590 \cdot x^{-1} - 3080). \quad (1)$$

b) In absorption of N_2O_3 by sulfuric acid, the absorption coefficients are found from the equation

$$K_d = K_0 \cdot e^{0.18 \cdot V_d}, \quad (2)$$

where K_0 depends on the NO + NO_2 concentrations in the gas and the H_2SO_4 concentration in the solution.

c) For absorption of NO by $FeSO_4$ solution:

$$K_d = 276 \cdot V_d^{0.82}. \quad (3)$$

d) for absorption of nitrogen oxides (with 80-85% oxidation of NO) by 20% HNO_3 solution:

$$K_d = (29x + 494) \cdot \log V_d + (5.6x - 73). \quad (4)$$

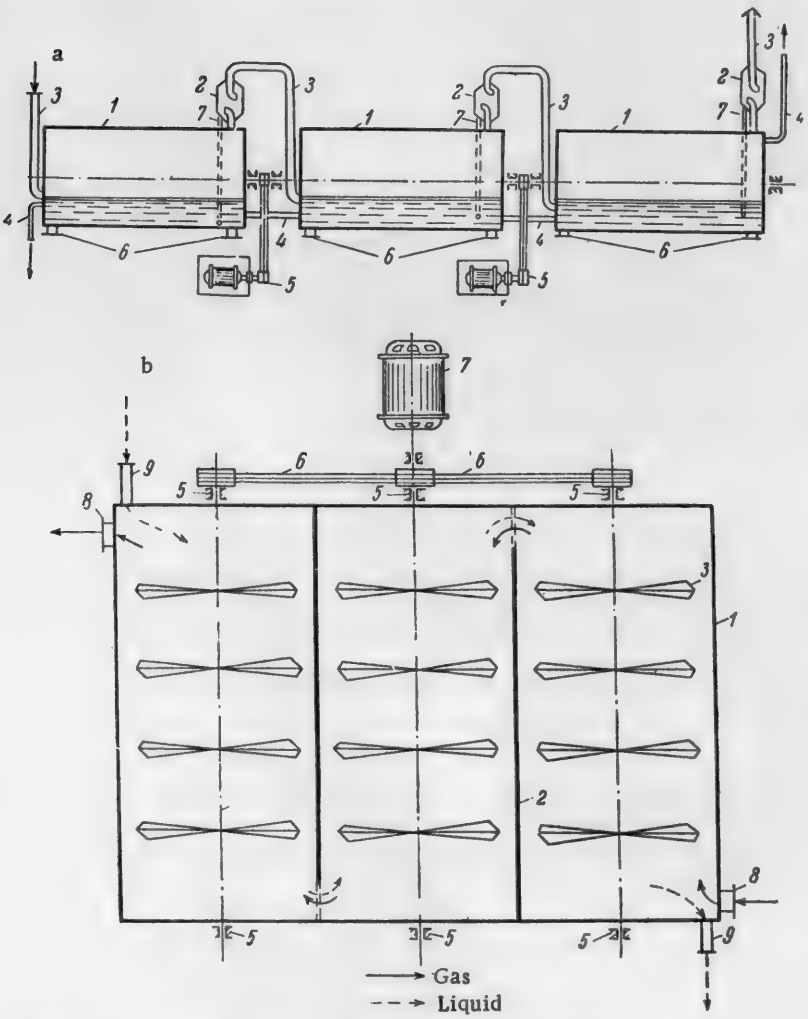

Fig. 1. Schematic design of multicompartment absorbers.
a .1) Absorbers; 2) separators; 3) gas ducts ; 4) pipes ; 5) drives; 6) overflow pipes; 7) circulation pipes; b. 1) absorber shell; 2) partitions; 3) disks; 4) shafts ; 5) bearings; 6) driving belts ; 7) motor; 8) gas pipes; 9) liquid pipes.

e) In absorption of H_2S by arsenical soda solution, the absorption coefficient is found from the equation

$$K_d^n = 1.05 \cdot n, \text{ or } K_d^v = 244.6 \cdot V_d. \quad (5)$$

f) The absorption coefficients also increase with increase of the peripheral disk speed in the absorption of a soluble gas, NH_3, by water.

For a gas containing 7-10% NH_3, at a gas rate of 500-600 m^3 gas/ m^3 abs. hour, absorption of NH_3 is complete at peripheral disk speeds up to 0.8 m/ sec. Below this peripheral speed

$$K_d^n = 15 \cdot n + 1600, \text{ or } K_d^v = 5100 \cdot V + 1600. \quad (6)$$

g) For absorption of CO_2 by aqueous ammonia solutions (containing 7-8% NH_3) the absorption coefficients are given by the equation

$$K_d^n = 25.75(\log n - 1.912), \text{ or } \quad K_d^V = 2575(\log V_d + 0.62). \tag{7}$$

The following notation is used in Equations (1-7): K_d is the coefficient of absorption (in kg/ m^3 · hour · atm), V_d is the peripheral disk speed (in m/ second), x is the concentration of the component being absorbed (in %), n is the number of revolutions of the shaft of the laboratory absorber per minute.

It follows from the above equations that increase of the peripheral disk speed is an important factor in increasing the rate of absorption. This acceleration of the process is caused by increased turbulence of the gas–liquid system and the consequent acceleration of convective diffusion.

Scale trials of the absorption process in absorbers of different diameters gave the best results with the following relative proportions of peripheral speeds and absorber dimensions:

Diameter of absorber (in m)	0.072	0.142	0.285	0.57	0.88
Disk diameter = 0.9 of the absorber diameter (in m) . . .	0.065	0.130	0.260	0.520	0.8
Optimum peripheral disk speed (in m/ second)	5-6	7-9	10-12	15-16	20-22

Analysis of the experimental data showed that the condition for equal hydrodynamic regimes in absorbers of different diameters is represented by the equation

$$n_{pr} = n_{lab}\left(\frac{d_{lab}}{D_{pr}}\right)^{0.52}, \tag{8}$$

where n_{pr} and D_{pr} are the r.p.m. and diameter of the disks of the projected absorber, and n_{lab} and d_{lab} are the r.p.m. and disk diameter of the laboratory absorber used for determination of the absorption coefficients given by Equations (1-7).

Variations of the absorption rate with the hydrodynamic conditions may be represented by the curves in Fig. 2.

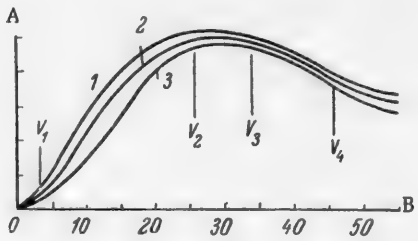

Fig. 2. General variations of the absorption rate with the hydrodynamic conditions and concentration of the absorbed component. A) Degree of absorption (%); B) peripheral disk speed (m/second). Concentration of component being absorbed: 1) α_{max}; 2) α_{mod}; 3) α_{min}.

The relationship illustrated in Fig. 2 is characteristic of any absorption process in horizontal high-speed rotary absorbers. The curves may be displaced in either direction according to the specific characteristics of a given system, but retain their characteristic curvature. It follows from Fig. 2 that with increase of the peripheral disk speed from V_0 to V_2 the absorption rate rises rapidly at first; the process is then stabilized over the region $V_2 - V_3$, and on further increase of the disk speed from V_3 to V_4 the absorption rate begins to fall. When $V_d > V_4$ the curves again tend to become parallel to the abscissa axis. Over the region V_0 to V_1 the liquid is stirred. As the peripheral disk speed increases from V_1 to V_2 the liquid undergoes vigorous spraying, and a considerable layer of foam is formed. A gas–liquid mixture is formed over the region $V_2 - V_3$.

These conditions correspond to the highest degree of absorption, as the area of phase contact is most highly developed and resistance to diffusion is at a minimum. Further increase of the peripheral disk speed leads to a decrease of the rate of absorption. The explanation is that, according to the laws of Thomson [17] and Laplace, the dispersed particles of liquid collide with each other in the movement of the gas–liquid mixture and, owing to the excess pressure,* form larger aggregates which fall out of the main stream. These large drops coalesce with the film and form a liquid ring at the cylinder walls. In this case a gas poor in liquid moves along the axis of the absorber, the foam structure breaks down, phase contact deteriorates, and the absorption rate falls. With further increase of the peripheral disk speed the process becomes

*Set up by the centrifugal force of the disks.

stabilized, as equilibrium becomes established at the boundary between the liquid film and the gas–liquid mixture; the amount of liquid deposited on the film surface becomes equal to the amount removed by aeration and dispersion. In consequence, the concentration of liquid in the gas–liquid mixture becomes constant, and the absorption process is thereby stabilized.

A similar effect was observed by Skryabin [18] in his study of the hydraulic resistance of a gas–liquid mixture.

It follows from Fig. 2 that in conditions of low turbulence (V_d = 1-5 m/second) the rate of absorption depends both on the concentration of the gas and the concentration of the absorbent. At lower disk speeds K_d predominantly depends on the concentration of the absorbent. The turbulence of the liquid and gas increases with increasing disk speed. Hydrodynamic mass transfer then becomes immeasurably greater than mass transfer by molecular diffusion. At intermediate disk speeds the absorption rate is determined mainly by the physical solubility of the gas, in agreement with Kishinevsky's findings.

In the $V_2 - V_3$ range, both the liquid and the gas are in a state of high turbulence, and therefore the partial pressure of the gas has less relative effect on the absorption rate than it has in conditions of low turbulence. This situation is characterized by the convergence of the curves in the $V_2 - V_3$ region in Fig. 2.

It may be noted that the curves in Fig. 2 are analogous to the curves representing power consumption in rotation of the shaft. It follows from our investigations [19] and from analysis of the data by means of the similarity theory that the power of drives for similar absorbers is given by the following equation (for disks with vanes set at 15° relative to each other):

$$N_{start} = 90 \cdot \alpha \cdot \beta \cdot z \cdot \rho^{0.02} \cdot \mu^{0.98} \cdot d^{3.4} \cdot n_s^{2.02} \text{ horsepower} \qquad (9)$$

where α is a correction factor = 1.02-1.07; β is the overload factor in starting = 1.4-1.7; z is the number of disks; d is the disk diameter (in m), n_s is the number of disk revolutions per second; ρ is the density of the liquid (in kg · sec ^{2}/m^4); μ is the absolute viscosity of the liquid (in kg · sec./m^2).

Consequently, up to the maximum absorption rates, in the range $V_0 - V_3$, $K_d = f(N)$.

It follows from all this that the peripheral disk speed is a powerful independent factor which determines the absorption rate.

Characteristics of the individual process factors. In high-speed rotary absorbers, drop, bubbling, and film absorption occurs simultaneously. The last is a consequence of the renewal of the disk surface. The magnitude of the renewed disk surface increases rapidly with increasing angular velocity of the shaft. For example, if the disk diameter d = 1.5 m, z = 4, and n = 300 r.p.m, the renewed disk surface is $F = \left(\frac{\pi \cdot d^2}{4} \cdot 2\right) \cdot z \cdot n \cdot 60 \cdot = \left(\frac{3.14 \cdot 1.5^2}{4} \cdot 2\right) \cdot 4 \cdot 300 \cdot 60 = 64000$ m^2/hr.

With increasing disk speed the renewed disk surface increases linearly, as is seen in Fig. 3. The relationship plotted here was calculated for an absorbed with 4 disks 1 m in diameter.

Absorption in drops is also important in mechanical absorbers. Each disk acts as a centrifugal sprayer; at constant viscosities and densities of the liquid and gas the drop diameter depends on the peripheral disk speed, as is shown by the following equation [20]:

$$d_{dr} = 98.5 \cdot \frac{1}{n} \sqrt{\frac{2a}{D \cdot \gamma}}, \qquad (10)$$

where d_{dr} is the diameter of a drop (in m), γ is the density of the liquid (in kg/m^3), n is the number of revolutions of the disk per minute, D is the disk diameter (in m), and a is the surface tension (in kg/m).

The average drop diameter in laboratory absorbers varied from 0.1 to 2 mm. Drops which become detached from the disks forcibly strike the absorber walls or the liquid surface and break up into smaller drops. The surface area of the drops may, in the first approximation, be calculated by means of the equation

$$f_{dr} = \left(\frac{6 \cdot Q}{d_{dr}} \cdot 2\right) \cdot z_d, \qquad (11)$$

where f_{dr} is the surface area of 1 m^3 of the drops (in m^2), Q is the amount of liquid sprayed per second (in m^3/sec), d_{dr} is the drop diameter (in m), z_d is the number of disks.

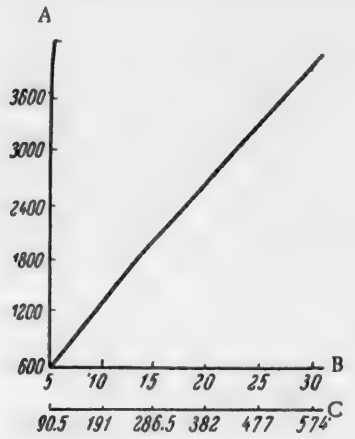

Fig. 3. Effect of peripheral disk speed on the phase-contact renewal area (d_{disk} = 1 m, z = 4). A) Phase-contact renewal area (in m^2/minutes); B) peripheral disk speed (in m/second), C) shaft speed in r.p.m.

For d_{dr} = 0.1 mm, Q = 0.00478 m^3/second, and z_d = 4 (the fact that both sides of each disk act is taken into account), the constant surface area of the drops in a pilot-scale absorber is $f_{dr} = \frac{6 \cdot 0.00478}{0.0001} \cdot 2 \cdot 4 \approx 3120\ m^2$.

It has been noted by Shabalin [21] and others that the impact effect of the drops is of great significance in the absorption process. In a rotary absorber the drops are detached from the disks at a high velocity, which is transformed into impact force. Bombardment of the absorber walls by a continuous stream of drops sets up an increased pressure on the walls. As an example, we calculated the impact force of a drop on the wall of an absorber 0.23 m in diameter.

The weight of a drop of d_{dr} = 3 mm is $m = \frac{4}{3} \pi \cdot r^2 \cdot \gamma$, m = 0.000014 kg.

The disk diameter in this case is 0.21 m. If the disks rotate at 600 r.p.m., the specific pressure of the drops is given by the equation:

$$G = \frac{p}{f} = \frac{m \cdot V}{\tau \cdot f} = \frac{0.000014 \cdot 6.6}{0.785 \cdot 0.003^2 \cdot 0.0045} = 286\ \text{kg/m}^2,$$

where V is the peripheral disk speed, 6.6 m/second, f is the projection area of a drop with d = 3 mm, τ is the impact time of a drop = 0.0045 second, P is the impact force of a drop $\frac{m \cdot V}{\tau} = \frac{0.000014 \cdot 6.6}{0.0045} = 0.002$ kg.

In works absorbers with disk diameter $\simeq$ 2 m and V_d = 35-40 m/second the impact force of the drops is considerably greater. This factor also favors acceleration of absorption.

In high-speed rotary absorbers there is intensive friction between the gas and the liquid, which increases the turbulence of the system and accelerates absorption.

The absolute values of the friction between the gas and liquid are impossible to determine, but this factor can be estimated by determination of the frictional force between the liquid and the rotating disks.

In calculation of the friction between the disk and the liquid it may be assumed that the liquid is stationary relative to the disk, and that the distribution of the static pressure on the disk surface can be represented by the usual triangle of forces.

The total pressure on the part of the disk immersed in the liquid can be found from the equation[22]

$$P = \frac{b}{3 \cdot h} \{a (0.75 \cdot D_d^2 - a^2) - 0.75 \cdot D_d^2 (0.5D - h) \varphi\}, \qquad (12)$$

where h = 250 mm = 0.25 m—depth of immersion of the disk; γ = 1000 kg/m^3—the density of water; b = h · γ = = 0.25 · 1000 = 250, D_d = 1m—the external diameter of the disk; φ = arc · cos $\left(1 - \frac{2 \cdot h}{D_d}\right)$ = arc · cos · $\left(1 - \frac{2 \cdot 0.25}{1}\right)$ = = 60° = 1.05 rad. $a = \frac{D_d}{2} \cdot \sin \varphi = 0.5 \cdot \sin 60° = 0.435$ m.

Substitution of the relevant dimensions gives:

$$P = \frac{250}{3 \cdot 0.25} \{0.435 (0.75 \cdot 1^2 - 0.435^2) - 0.75 \cdot 1^2 (0.5 \cdot 1 - 0.25) \cdot 1.05\} =$$

= 16 kg on one side of the disk, or 32 kg on both sides.

From the equation for the frictional moment

$$M_{fr} = P \cdot f \cdot \rho, \tag{13}$$

where ρ is the radius of rotation of the point of application (barycenter) of the frictional force $= \frac{D_d}{2} - \frac{h}{3} =$ $= 0.417$ m, and f is the coefficient of friction ≈ 0.03,
and from the formula for the power required to overcome friction

$$N_{fr} = M_{fr} \frac{\omega}{75} = M_{fr} \frac{\pi \cdot n^*}{30 \cdot 75}, \tag{14}$$

we find that in this case the power required for 4 disks is 1.34 horsepower.

The calculated data plotted in Fig. 4 show that the power consumption is a linear function of the angular velocity of the disks. It follows that the frictional forces which accelerate absorption increase in proportion to the shaft speed.

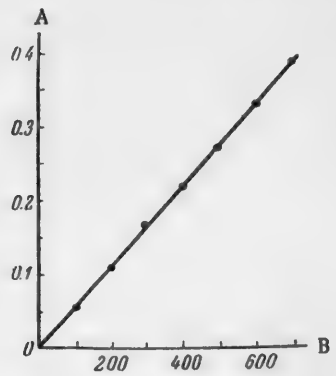

Fig. 4. Effect of shaft speed on the power required to overcome friction (d_{disk} = 1 m).
A) Power consumption (in horsepower), B) shaft speed in r.p.m.

Owing to the intensive agitation of the gas and liquid, bubbling absorption is an important factor in high-speed rotary absorbers. The rotating disks continuously submerge the gas and give rise to intensive bubbling, which results in the formation of a considerable and constant layer of foam. The amount of foam increases with the shaft speed. The density of the foam is found from the formula

$$\gamma_f = \frac{Q \cdot \gamma_L}{H \cdot F}, \tag{15}$$

where γ is the density of the foam (in kg/m^3), Q is the amount of liquid in the absorber (in m^3), H is the height of the foam layer, γ_L is the density of the liquid (in kg/m^3), and F is the cross section of the absorber at the liquid level (in m^2).

The height and density of the foam layer are an indirect measure of the contact area between the liquid and gas phases, which determines the absorption rate to a considerable extent.

Effect of design characteristics on the absorption rate. It follows from the foregoing that the absorption rate depends to a considerable extent on the hydrodynamic conditions in the absorber. These conditions are determined not only by the peripheral disk speed, but also by the design characteristics of the absorber; the most important of these are the number of disks, their design, arrangement of the disks on the shaft, ratio of the diameter of the absorber to its length, and the relative volume of liquid in the absorber.

Each rapidly-rotating disk retains near itself a certain amount of liquid in the form of a suspension and foam. In this case stepwise absorption occurs in the absorber, and the action of each disk is analogous to the action of a plate of definite efficiency in a bubble tower. Therefore it is evident that the degree of absorption increases with the number of disks in the absorber. However, it follows from Equation (9) that the power consumption is proportional to the number of disks. Therefore increase of the number of disks results in increased power consumption. Numerous investigations have shown that the number of disks can be calculated by means of the formula:

$$\frac{C_1}{C_2} = \left(\frac{100}{100 - x}\right)^n, \tag{16}$$

where n is the number of disks, x is the % absorption with one disk, and C_1 and C_2 are the concentrations (in %) of the gas being absorbed, at the entry and exit respectively.

* n = 600 r.p.m.

As a rule, the greatest absorption with the lowest expenditure of energy is obtained with the use of four disks fixed at distances of 0.6-0.7 disk diameter along the shaft.

The disk design is very important. Disks with vanes cut around the circumference, as shown in Fig. 5, are the simplest and most reliable. In Fig. 5, a, all the vanes are bent in one direction, in Fig. 5, b, the vanes are bent alternately in the same direction, and in Fig. 5, c, the vanes are all bent toward each other, and the disks are set on the shaft so that the vane openings face each other. Experiments showed that the best results are obtained with arrangement 5, c; this is illustrated in Fig. 6 by data on the absorption of H_2S by arsenical soda solution. The curves in this figure represent the degree of absorption of H_2S at different peripheral disk speeds. The corresponding absorption coefficients are plotted in Fig. 7.

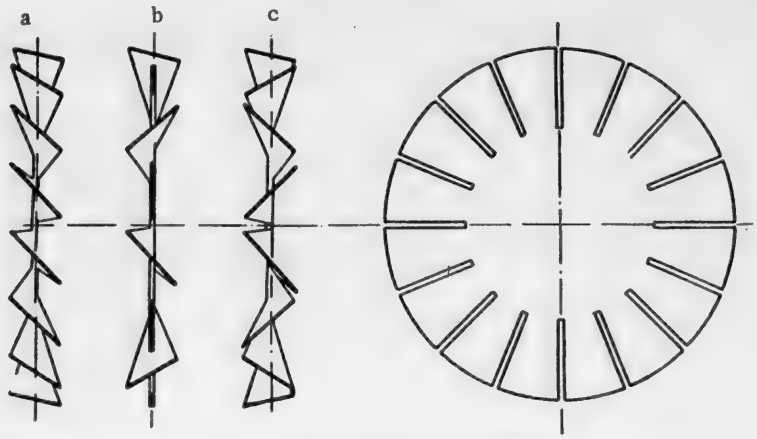

Fig. 5. Disk design. Vanes set at 15-16°; a) in the same direction; b) alternately toward each other; c) all toward each other.

The upper curve (Fig. 6) represents absorption of H_2S with the use of type c disks. It is clearly seen that under otherwise equal conditions the disk design has a very important influence on the degree of absorption and the coefficient of the absorption rate.

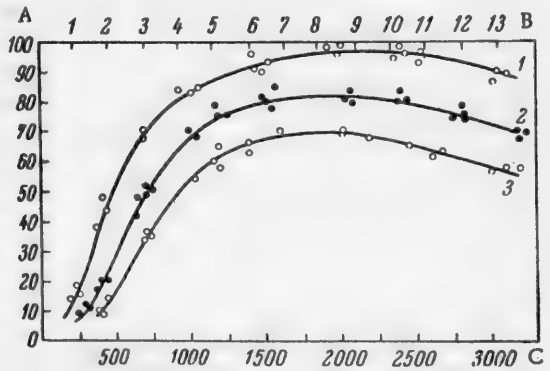

Fig. 6. Effects of vane design and shaft speed on the degree of absorption of H_2S by arsenical soda solution. A) Degree of absorption (%); B) peripheral disk speed (m/second); C)shaft speed (r.p.m.). Disk designs: 1) a ; 2) b ; 3) c (see Fig. 5).

When type c disks are used, rapid rotation creates continuous regions of foam and liquid droplets between the disks; the best hydrodynamic conditions are obtained at peripheral speeds corresponding to the maxima on the curves. The best results were obtained with vanes set at 15-17°, the vane width being $\frac{1}{10} - \frac{1}{14} \cdot \pi \cdot D_d$.

Determination of the ratio of absorber length (L) to its diameter (D) is a very difficult problem, as design and power considerations are contrary to the technological requirements. An analysis of the structural features of the equipment at different L : D ratios was carried out in a special investigation [23]. It was found that at constant volume of the absorber, v_a and constant peripheral disk speed, V_d, the power consumption increases when the diameter of the absorber is increased and its length decreased simultaneously. The weight of the absorber is least at L : D ≃ 1.4.

Hydrodynamic investigations showed that the linear velocity of the gas in the absorber is an important factor in turbulence. It was found that the optimum linear velocities lie in the range 0.7-2.5 m/second.

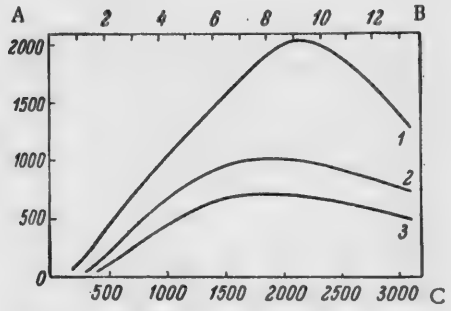

Fig. 7. Coefficients of absorption of H_2S by arsenical soda solution.
A) Absorption coefficients (in kg/m^3 × × hour × atm.); B) peripheral disk speed (m/second); C) shaft speed (r.p.m.). Disk designs: 1) a ; 2) b; 3) c (see Fig. 5).

In view of the fact that from the technological aspect the most suitable gas rates are in the range 400-500 m^3 gas/m^3 absorber per hour, the optimum L : D ratio is 2.2-3.

The absorption rate also depends to a considerable extent on the volume of liquid in the absorber. With a small amount of liquid its concentration in the gas is low, and it produces less turbulence in the system. If too much liquid is present the open cross section of absorber decreases the linear velocity of the gas increases and the gas breaks through in large streams, the foam regime breaks down, and the liquid drops become much larger.

In either case the degree and rate of absorption are diminished. It was found in investigations of various systems that the optimum volume of liquid in the absorber should be 20-25% of the absorber volume, and the liquid level should be at a height equivalent to 0.23-0.26 of the absorber diameter.

The horizontal velocity of the liquid in the absorber has no significant influence on the hydrodynamic conditions, as the velocity of the liquid carried by the disks at right angles to the gas stream is thousands of times as great as the horizontal velocity.

SUMMARY

1. The results of experimental investigations were used to establish the general laws governing absorption processes in high-speed rotary absorbers in relation to design characteristics and operating conditions.

2. It is shown that the most favorable hydrodynamic conditions for maximum acceleration of absorption processes are obtained in high-speed rotary absorbers. These conditions include: extensive area of phase contact, impact effect of the drops, intensive friction between the gas and the liquid, and rapid hydrodynamic transfer of the interacting components.

3. The most suitable design characteristics of rotary absorbers, and the hydrodynamic conditions in them, have been determined.

LITERATURE CITED

[1] M. E. Pozin and I. P. Mukhlenov, Proc. Acad. Sci. USSR 92, 293 (1953).

[2] M. E. Pozin, I. P. Mukhlenov, E. S. Tumarkina and E. Ya. Tarat, J. Appl. Chem. 27, 12 (1954).*

[3] M. E. Pozin, I. P. Mukhlenov and E. Ya. Tarat, The Foam Method for Removal of Dust, Smoke and Mist from Gases (Goskhimizdat, 1953).**

[4] M. E. Pozin, Author's Certif. 80468 (1949).

[5] I. N. Kuzminykh, J. Chem. Ind. 8, 229 (1950).

[6] K. N. Shabalin, S. F. Krylov and V. I. Oborin, J. Chem. Ind. 16, 10 (1939).

*See C. B. Translation.
**In Russian.

[7] M. Kh. Kishinevsky and A. V. Panfilov, J. Appl. Chem. 22, 1 (1949).

[8] M. Kh. Kishinevsky and M. A. Kerdivarenko, J. Appl. Chem. 24 (1951).*

[9] M. Kh. Kishinevsky, J. Appl. Chem. 24, 5 (1951). *

[10] S. N. Ganz and S. B. Kravchinskaya, J. Appl. Chem. 28, 2 (1955).*

[11] S. N. Ganz and S. I. Kapturova, J. Appl. Chem. 28, 6 (1955).*

[12] S. N. Ganz, J. Appl. Chem. 28, 10 (1955).*

[13] S. N. Ganz, J. Appl. Chem. 29, 7, 1018 (1956).*

[14] S. N. Ganz and L. I. Mamon, J. Appl. Chem. 30, 4 (1957).*

[15] S. N. Ganz and M. A. Lokshin, J. Appl. Chem. 30, 10, 1525 (1957).*

[16] S. N. Ganz, J. Appl. Chem. 30, 9, 1311 (1957).*

[17] Thomson, Phil. Mag. (4), 17, 61 (1859) and 42, 448 (1881).

[18] A. K. Skryabin, Sci. Res. Inst. Chem. Machine Constr. 9 (Mashgiz, 1951).

[19] S. N. Ganz and M. A. Lokshin, Trans. Dnepropetrovsk Inst. Chem. Tech. 5 (1956).**

[20] M. E. Lurye, Drying (Gosenergoizdat, Moscow-Leningrad, 1948).**

[21] K. N. Shabalin, Friction Between Gas and Liquid in Absorption Technology (Metallurgy Press, 1948).**

[22] Machine-Building Encyclopedia, 2 (1951).**

[23] S. N. Ganz and M. A. Lokshin, Trans. Dnepropetrovsk Inst. Chem. Tech. 5 (1956).**

Received May 7, 1956

---

* See C. B. Translation.
** In Russian.

THE VOLTAGE "PEAK" OF COPPER OXIDE CELLS

V. N. Flerov

The A. A. Zhdanov Polytechnic Institute, Gorky

One of the advantages of the copper oxide cell is a smooth discharge curve. In continuous discharge under normal conditions, the voltage of the cell decreases by only 10-12% after discharge of the nominal capacity. This important advantage is, however, to some extent lost if the cell operates intermittently. When a "rested" cell is put on discharge, it operates for some time at 0.9-0.8 v, and only after it has discharged some of its capacity does the voltage drop to the normal value of 0.7-0.5 v. The region of higher voltage is known in practice as the "voltage peak." The existence of a voltage "peak" leads to overloading of instruments supplied for copper oxide cells. On the other hand, it is tempting to use the "peak" region as the operating voltage of cells used in intermittent discharge. For this it is necessary to understand the nature of the voltage "peak" and the influence of operating conditions on it.

Relatively few papers deal with the action of copper oxide cells.

Johnson [1] reported the existence of two horizontal voltage plateaus on the discharge curve of the copper oxide cell. In Johnson's opinion, during the first horizontal discharge stage CuO is reduced to Cu_2O. Before the total disappearance of CuO from the electrode, Cu_2O begins to be discharged owing to polarization of the first process. During the second horizontal stage, reduction of CuO and Cu_2O occurs simultaneously. Allmand [2] studied the electrode potentials of various oxygen compounds of copper: CuO, $Cu(OH)_2$, Cu_2O. He noted that copper hydroxide and freshly prepared copper oxide were unstable in alkali solution, so that the electrode potentials changed with time. Okatov [3] denied the possibility of two-stage discharge of copper oxide electrodes, and confirmed this view by calculations.

In our opinion, detailed studies of the voltage "peak" observed after "rest" of the cell should help to elucidate the discharge mechanism of copper oxide electrodes.

The object of the present work was a study of the influence of a number of factors on the duration of the voltage "peak" of copper oxide cells.

EXPERIMENTAL

Laboratory-type copper oxide cells, each consisting of one positive and two negative electrodes, were used. The cells were filled with 100 ml of NaOH solution, sp. gr. 1.19, i.e., the calculated capacity was about 10 amp.-hrs. Electrodes made with a combustible binder by a method described earlier [4] were used for most of the experiments.

In each experiment fresh electrolyte was used, in which the cell was first discharged by 0.5-0.6 amp.-hr. The electrolyte surface was covered with a thin layer of vaseline oil to prevent access of carbon dioxide. The experiments were carried out in thermostats with the temperature regulated to the nearest ± 0.1°.

The cause of the voltage "peak" in the copper oxide cell is the copper oxide electrode. The polarization of the zinc electrode as such is relatively small and reaches its maximum value during the first few minutes of discharge. On the other hand, the discharge curve of the copper oxide electrode has two distinct regions (Fig. 1). When the cell is put on discharge, the potential of the copper oxide electrode falls rapidly to 0.88 v (a zinc reference electrode was used), and then decreases gradually to about 0.82 v. After the discharge has continued for

some time the potential drops abruptly to 0.67-0.68 v, and the electrode is discharged at this potential under continuous discharge conditions.

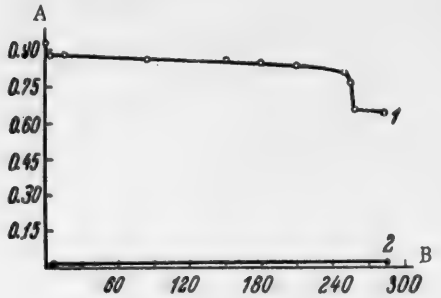

Fig. 1. Variation of the potentials of the electrodes of the copper oxide cell during discharge.
$D_{c,a}$ = 2.0 ma/cm², t = +20°, "rest" time, 3 days.
A) Potential against a zinc reference electrode (in v); B) discharge time (minutes).
1) Copper oxide electrode; 2) zinc electrode.

Effect of "resting time" of the cells. Increase of the "resting time" of the cells lengthens the "peak" voltage region (Fig. 2). However, the cell performance deteriorates after very long resting times. The "peak" plateau of such cells is relatively small or vanishes completely; after the "peak" period the voltage is considerably below the usual operating voltage, and the cell comes back to normal only gradually. This behavior is found in cells after more than 1 or 2 months' rest.

Effect of temperature. The duration of the voltage "peak" is increased by increase of temperature during "rest" of the cells (Fig. 3). The temperature during discharge of the cell also has a considerable influence. A cell rested at room temperature and cooled before discharge gives no "peak" plateau at all. On the contrary, such cells have an initial region of decreased voltage. The same cell, rapidly warmed to room temperature, gives up the same capacity at the voltage "peak" as a standard comparison cell. When the cell is discharged for a long time at subzero temperatures, it gives a "peak", although this is not large.

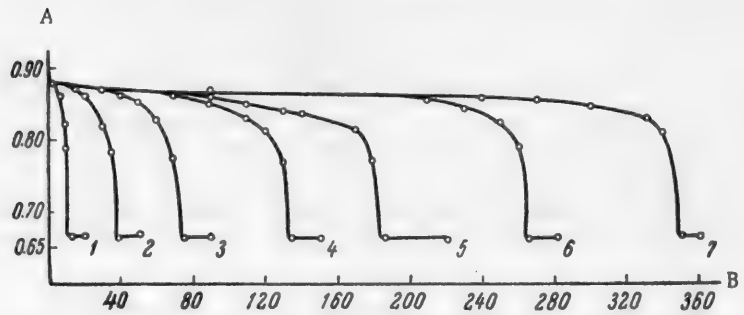

Fig. 2. Voltage variations of copper oxide cells during discharge.
D_c = 2.0 ma/cm², t = +20°.
A) Voltage (in v); B) discharge time (minutes).
"Resting time" of cells: 1) 2 hour; 2) 3 hours; 3) 6 hours; 4) 12 hours; 5) 24 hours; 6) 3 days; 7) 7 days.

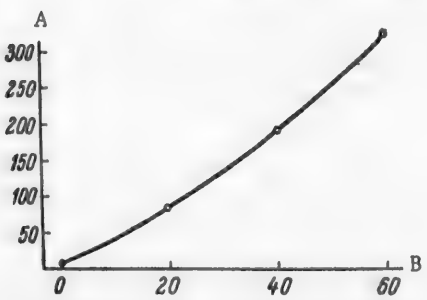

Fig. 3. Effect of temperature during "rest" on the duration of the voltage "peak of a copper oxide cell.
D_c = 2.0 ma/cm², "rest" of 24 hours.
A) Duration of "peak" (minutes); B) temperature °C

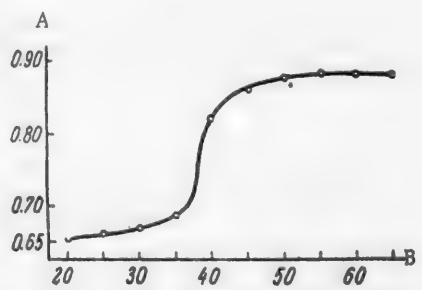

Fig. 4. Variation of the operating voltage of a copper oxide cell with increase of temperature during discharge.
D_c = 4.0 ma/cm².
A) voltage (in v); B) temperature °C.

Increase of temperature during discharge leads to an abrupt increase of voltage (Fig. 4). The temperature at which the voltage increases depends on the current strength, the degree of discharge of the cell and the previous discharge conditions. Depending on these conditions, the voltage jumps were observed both at +30 and +60°. However, it was not possible to make the cells operate for a long time at the "peak" and at elevated temperatures. After a few hours of operation the voltage of such cells fell to the normal level.

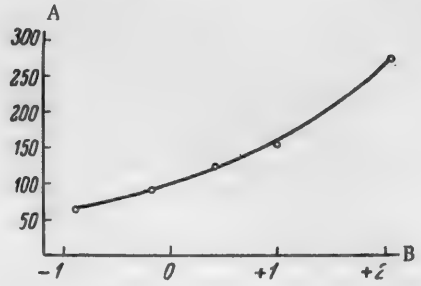

Fig. 5. Effect of the current strength in preliminary discharge on the duration of the "peak" of a copper oxide cell.
D_c = 2.0 ma/cm², "rest" of 2 days.
A) Duration of "peak" (minutes);
B) log D_c^{prelim} (D_c in ma/cm²).

Effect of discharge conditions. The duration of the voltage "peak" greatly depends on the previous discharge conditions. A cell discharged under more severe conditions before "rest" has a considerably longer "peak" period (Fig. 5). High current loads for brief periods result in appreciable activation of the positive electrode. After a cell which is being discharged under normal conditions is short-circuited, its operating voltage rises to the "peak" value (Fig. 6). The duration of the "peak" increases with the duration of the high load.

In the case of a cell which has been discharged to a considerable extent, all the preceding discharge conditions have a considerable effect. After equal "rest" periods, cells discharged continuously have peaks of considerably longer duration than cells discharged intermittently.

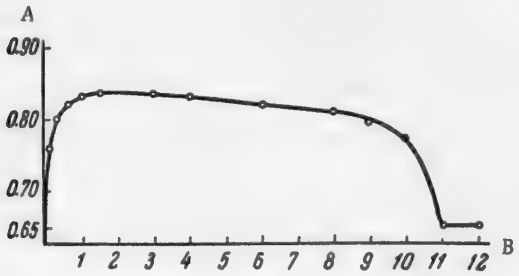

Fig. 6. Variation of the voltage of an operating copper oxide cell after short-circuiting of the cell for 2 minutes.
(D_c^{short} = 150 ma/cm²).
D_c = 2.0 ma/cm².
A) Voltage (in v); B) discharge time (minutes).

The cells give up more of their capacity at the voltage "peak" at lower current strengths. For example, a freshly made cell charged with NaOH (sp.gr. 1.19) and put, after 20 minutes, on discharge at 4 ma (D_c = 0.16 ma/cm²), gave up 0.6 amp.-hr. at the peak. A similar cell put on discharge at 50 ma, gave up only 0.02 amp.-hr. at the peak.

Effect of the nature of the electrolyte. The duration of the "peak" decreases with progressive discharge of the cell. An exhausted cell has a "voltage" peak $^1/_2$ - $^1/_4$ of the duration of the peak of a cell which has not been discharged much. The rise of the cell e.m.f. to the equilibrium value after it is placed on open circuit is retarded with increasing discharge of the cell (Fig. 7). The nature of the electrolyte has a considerable influence on the "peak". The "peak" is longer in cells with potash electrolyte than in cells with caustic soda. The duration of the "peak" is increased with increasing concentration of caustic potash in the cell. Thus, freshly made cells with KOH of sp.gr. 1.40 have a peak of about twice the duration of "peaks" in cells with NaOH (sp.gr. 1.19).

Effect of silicate binder. A mixture of water glass and sugar solution is used in practice as a binder in the formation of copper oxide electrodes. The pressed electrodes are baked and subjected to surface reduction. Such electrodes contain about 4% SiO_2. The nature of the voltage "peak" in copper oxide cells with these electrodes was investigated.

The general laws mentioned above for cells with "silicate-free" electrodes hold true also for cells with electrodes containing silicate. However, certain differences are present.

The voltage falls more smoothly from the "peak" to the operating value in cells with electrodes containing silicate. The electrolyte concentration has a much greater influence on the "peak". Freshly charged cells have almost no "peak" even after a considerable holding period. The e. m. f. of such cells rises more slowly when they are placed on open circuit, especially in the case of exhausted cells, when the e.m.f. does not reach its equilibrium value even after 12 hours.

After renewal of the electrolyte in discharged cells which operated under continuous normal discharge conditions, a prolonged "peak" was given by these cells after a "rest" period. For example, a cell type MOE-250, which had yielded 243 amp.-hrs. in continuous discharge at 0.5 amp., operated for 26 hours at the "peak" after renewal of the electrolyte and 4 days of "rest."

DISCUSSION OF RESULTS

The distinct plateau on the discharge curve of the copper oxide electrode (Fig. 1) shows that the voltage "peak" after "rest" of the cell is caused by the presence of a substance with a high positive potential in the electrode. This substance is not present in the electrode of an uncharged cell. It appears only after more or less prolonged action of the electrolyte on the electrode, and it is formed only at the boundary between CuO and the discharged part of the electrode, and not throughout the whole mass of the electrode (Fig. 2). The formation of this substance is accelerated by increase of temperature or electrolyte activity, and by increase of current density during the previous discharge (Figs. 3, 5, 6). It is probable that this substance may be formed either in the idle cell or during discharge. This is confirmed by the greater quantity of electricity given up by the cell at the voltage "peak" during slow discharge, and by the increase of the voltage of the working cell to the "peak" value on increase of temperature (Fig. 4).

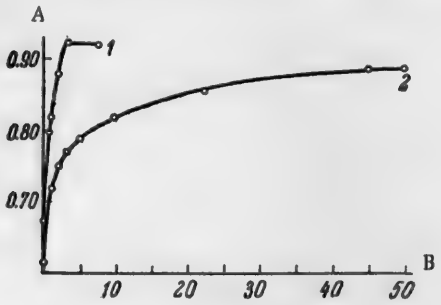

Fig. 7. Change of cell e.m.f. when placed on open circuit.
A) e.m.f. (in v), B) time (minutes).
Degree of discharge of cells (%): 1) 5, 2) 90.

The differences in the nature of the "peak" in copper oxide cells with electrodes containing silicate binder, and cells with silicate-free electrodes, are probably caused by the presence of cupric and cuprous silicates in the electrodes [5]. These compounds decompose only slowly under the action of alkali.

A special investigation is required to determine the nature of the substance which causes the voltage "peak" in copper oxide cells. However, it may already be claimed that the mechanism proposed by Johnson [1] for the discharge of a copper oxide electrode is hardly quite trustworthy. It is imposible to account for all the effects associated with the voltage "peak" on the basis of this mechanism.

SUMMARY

It was shown in a study of the effects of operating conditions on the voltage "peak" of copper oxide cells that the duration of the voltage "peak" increases with the temperature and current strength of the previous discharge, and with increasing "rest" time.

LITERATURE CITED

[1] Johnson, Trans. Am. Electroch. Soc. 1, 187 (1902).

[2] A. J. Allmand, J. Chem. Soc. 95, 2151 (1909); 97, 603 (1910).

[3] A. P. Okatov, Chemical Sources of Current (Goskhimizdat, 1948).*

[4] V. N. Flerov, J. Appl. Chem. 30, 9, 1326 (1957).**

[5] H. O. Hofman, Metallurgy of Copper (Russian translation) (Metallurgy Press, 1934).

Received May 7, 1956

* In Russian.

** Original Russian pagination. See C. B. Translation.

MECHANISM OF CORROSION OF METALS IN MOLTEN CHLORIDES

N. D. Tomashov and N. I. Tugarinov

Molten metals have found extensive applications in industry; however, their wider use is hampered by their intense corrosive activity; the mechanism of corrosion of metals in molten salts has not been clarified up to now and the investigations devoted to this problem do not make use of modern concepts of the theory of corrosion of metals.

At the present time, students of the theory of corrosion have at their disposal an enormous amount of experimental data and a sufficiently substantiated theoretical and methodological basis, especially in the area of electrochemical corrosion [1-3]. Nevertheless, the majority of workers in this field [4-8] approach the problem of corrosion of metals in molten salts from the purely chemical point of view.

Since molten salts are conductors of second order [9] (i.e., they are characterized by ionic conductivity in the same way as the aqueous salt solutions), and since the electrochemical field has a significant effect on corrosion, we possess a solid foundation for the assumption that corrosion in molten salts is an electrochemical process. In fact, total protection of assembly parts in contact with heated molten salts was achieved by Ryabchenkov and Abramov by cathodic protection with a current density of 3 amp / cm^2 [10].

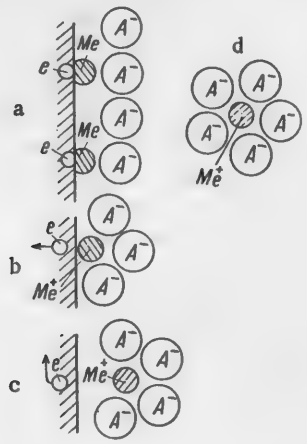

Fig. 1. Diagram of the mechanism by which the atoms of metal pass into the molten salt. (a, b, c, d — states of the process).

The object of the present work was to study the mechanism of corrosion of metals in molten salts by applying the modern theories and methods of investigation of electrochemical corrosion of metals, worked out and applied earlier for the case of corrosion in aqueous solutions.

Surface heterogeneities of metals immersed in molten salts. The electrochemical corrosion of metals immersed in a molten salt can be represented in general by the following scheme: 1) At the anodic areas the metal in ionic state passes into the molten salt where it is dissolved by the anions of the molten salt [11] (Fig. 1). 2) The electrons migrate from the anodic to the cathodic areas. 3) At the cathodic areas the depolarizer is regenerated by the incoming electrons.

The electrochemical heterogeneity of the surface, even of a single-phase metal or alloy, can be explained by the presence of stresses at the peripheries of the grains and by the presence of intragranular segregations. Therefore, as can be seen in Fig. 2, the corrosion proceeds essentially at the anodic areas — at the grain boundaries (after a sufficient time), remains intercrystalline and has a penetration rate of about 0.1 mm/hr.

By studying the distribution of the anodic areas and by measuring the depth of penetration of the corrosion pits, one can calculate the loss of weight corresponding only to the corrosion along the grain boundaries. This loss of weight can be legitimately considered to be the result of the corrosion of microcells "grain—boundary." If one compares these values with those corresponding to total corrosion, determined directly by the change of

weight, one can deduce the relative share of electrochemical corrosion of iron in molten chlorides, and also the general corrosion activity of a given molten salt.

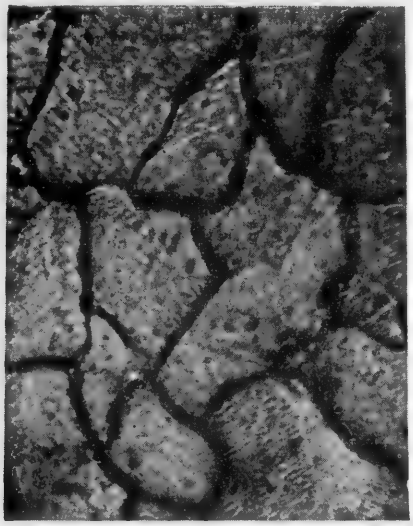

Fig. 2. Sample of Armco iron after 30 minutes in NaCl at 900°C.

The general corrosion activity of chlorides (most important salts for practical purposes) with respect to iron increases in the order: NaCl, KCl, $CaCl_2$, while the share of the attack due to electrochemical corrosion remains almost constant and equal to about 70% for all these salts.

Electrochemical Investigations. By analogy with aqueous solutions the process taking place at the anodic areas during the corrosion of metals in molten salts can be thought of as the passage of the metal atom into the molten salt in the state of ion.

$$Me \rightarrow Me^{++} + 2\ominus.$$

The cathodic process of assimilation (by the depolarizer) of electrons migrating from the anodic areas can be represented in a general way by the following reaction:

$$D + \ominus \rightarrow [D\ominus],$$

where the role of the cathodic depolarizer (D) can be played not only by the gases dissolved in the molten salts but also by additional elements contained in the molten electrolyte.

As is well known, the anodic as well as the cathodic process is responsible for the slowing down of the corrosion process because of overpotential, polarization and slowing down of the diffusion process. Therefore, study of the kinetics of the anodic and cathodic processes can provide a general picture of the corrosion rate of metals in molten salts. The most used and the most fruitful method of study of electrochemical processes taking place on anodic and cathodic areas during corrosion in electrolytes is the method consisting of drawing polarization curves under different conditions.

For the study of the electrochemical processes in molten salts one can use as the reference electrode a chlorine-carbon electrode, which answers all the requirements of a reference electrode – it is reversible, it cannot be polarized, and no complex formation takes place . However, such an electrode is very difficult to prepare. We prepared a chlorine-carbon electrode in the form of a carbon tube through which we continually passed pure dry chlorine obtained by electrolysis. The electrode was separated from the electrolyte by a quartz tube of a special form, provided with a little nozzle and filled with quartz, which served as a diaphragm (Fig. 3, 3).

The curves of anodic and cathodic polarization were made using the quartz cell (Fig. 3). The kinetics of the anodic and cathodic processes and the magnitude of the limit diffusion current can be determined from the polarization curves drawn in the system of coordinates potential – current density. If we translate the polarization curves into the so-called corrosion polarization diagram, i.e., we represent the anode and the cathode potentials as the function of the corrosion current, we can determine the character of the control of the corrosion process under given conditions [1-2]. The activation energy corresponding to different values of the potential can be calculated from the curves of anodic and cathodic polarization obtained at different temperatures (Fig. 4). The variation of the activation energy as the function of potential (Fig. 5) showed that the slowing down of the cathodic process is determined by the occurrence of at least two plateaux. For the values of the potential below −2.1 volts, the activation energy of the cathodic process is 18,000 cal/mole while activation energy for the viscosity of sodium chloride, according to Dantum [10], is 13,000 cal/mole. The similarity of these values indicates that when the potential is of the order of −1.9 to −2.1 volts the cathodic process is controlled by diffusion and depends to a great extent on the viscosity. For potentials above −2.4 volts the activation energy is 40,000 cal/mole apparently representing the activation energy of the cathodic deposition of sodium.

It is well known that the depolarization process can be divided into a number of successive elementary steps. In the case of the cathodic process of ionization of oxygen in molten salts these steps can be considered to be: 1) diffusion of the depolarizer (atoms or cations) toward the cathode; 2) assimilation of electrons, resulting

from the ionization of oxygen dissolved in the molten salt, $O_2 - 4\ominus \rightarrow 2O^{--}$.*

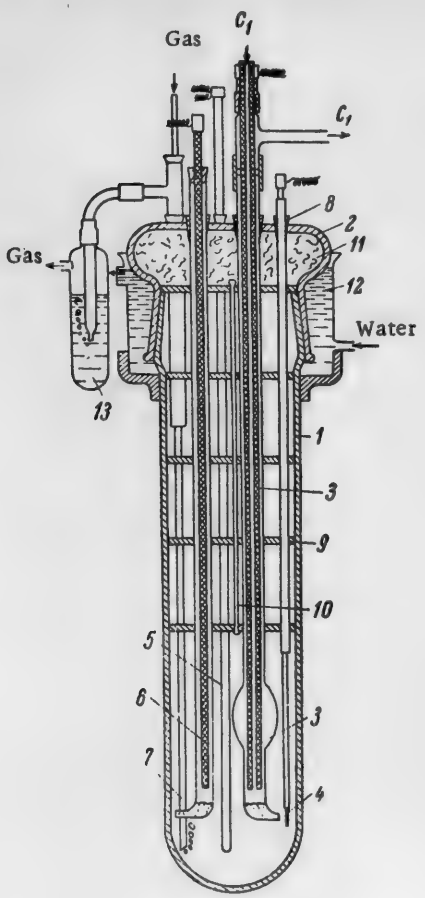

Fig. 3. Cell used to obtain polarization curves.
1) Quartz cell, 2) ground cover, 3) carbon tube of the chlorine reference electrode, 4) sample (wire one mm in diameter), 5) thermocouple in a quartz jacket, 6) additional (polarizing) electrode, 7) tube (quartz or porcelain) for the supply of gas to the molten salt, 8) little rubber bushings, 9) porcelein screens, 10) hooks for the suspension of screens, 11) asbestos filling, 12) water-cooling jacket, 13) control washing bottle.

When sufficiently negative potential of the cathode is reached, cathodic depolarization processes other than the ionization of oxygen can take place; thus, for example, one may have a change in the charge of some metal ions:

$$Fe^{+++} + \ominus \rightarrow Fe^{++}$$

or even discharge of alkaline or alkaline earth cations of the salt on the cathode, as for example:

$$Na^{+} + \ominus \rightarrow Na.$$

The polarization curves obtained for the iron electrode in molten NaCl (Fig. 6) do not show clearly the section of the curve corresponding to the first step of the cathodic process – ionization of oxygen (section $V_X - a$ of the curves 1, 2, 3) – because of the deformation of the initial section by the process of solution of the cathode and because of the low magnitude of the overpotential of ionization of oxygen on the scale used for the figure.

The cathodic depolarization proceeds with overpotentials, and the overpotential is proportional to the logarithm of the current density according to Tafel's formula $\eta = a + b \cdot \ln i$. Therefore, when one draws polarization curves of anodic and cathodic polarization in potential – logarithm of current density coordinates, (the steps of the cathodic process proceeding with overpotential) one obtains for rectilinear sections on the curve of the variation of the potential as the function of the logarithm of current density. In fact, in these coordinates curves 4, 5 and 6 of Fig. 6, corresponding to the cathodic polarization, have three distinct sections: 1) $X - K$ linear section corresponding to the process of depolarization of oxygen by ionization, i.e., when the cathodic process is controlled essentially by the rate of the reaction $O_2 + 4\ominus \rightarrow 2O^{--}$; 2) section $K - B$, corresponding to the diffusion of the depolarizer to the cathode; 3) section $B - G$, corresponding to a new process, in the present case to the cathodic deposition of sodium cations.

The polarization curves drawn in semilogarithmic coordinates, i.e., the cathode curves $X - G - 4$, 5 and 6 and the anode curves $X - A$, allow us to determine the magnitude of the corrosion current ($i_X = 0.0015$ amp/cm^2) and the value of the corrosion potential ($v_X = 1.73$ volt) on the basis of the electrochemical mechanism of corrosion [3], by prolonging the linear sections up to their intersection point X. The experimental value of the current (solution current) calculated according to Faraday's law from the loss of weight of Armco iron in the molten salt is somewhat smaller, of the order of 0.0004 amp/cm^2. Apparently this difference can be explained by the fact that in reality the corrosion process in molten salts is determined not by a homogeneous electrochemical mechanism but by a heterogenous electrochemical mechanism [2], when the anodic and cathodic processes are not distributed regularly over the whole surface but are localized, as we have shown; the anodic process occurring essentially along the grain boundary and the cathodic within the body of the grain. However, the similarity between the cal-

*This process in turn is the result of a series of consecutive more elementary stages [2].

culated and experimentally obtained values of corrosion current substantiate the fact that the corrosion of metals in molten salts is an electrochemical mechanism and that the method of polarization curves can be applied to the study of processes taking place during the corrosion of metals in molten salts.

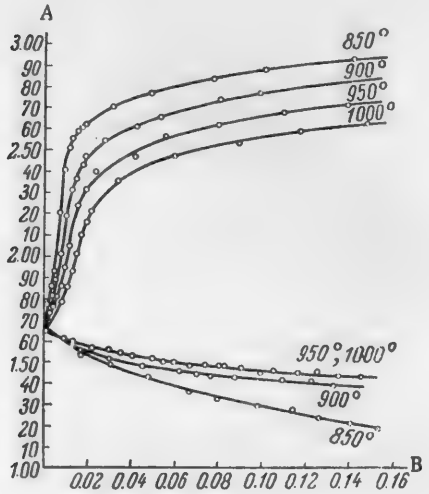

Fig. 4. Curves of anodic and cathodic polarization of Fe in molten NaCl at different temperatures.
A) Negative values of the potential (in volts); B) density of corrosion current (in amp/cm).

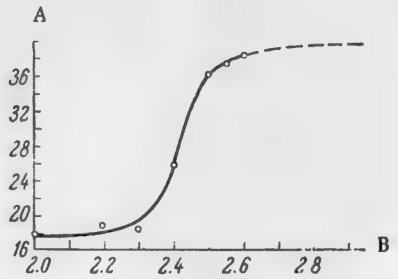

Fig. 5. Variation of the activation energy of the cathodic process as the function of the potential during cathodic polarization of Fe in NaCl.
A) Activation energy Q (in kcal/mole · 10^3);
B) negative values of the potential (in volts).

The results show that the corrosion of iron in molten sodium chloride is under cathodic control; no significant slowing down of the reaction by anodic process can be observed (Fig. 4, 6).

We have studied the effect of different depolarizers – gases (oxygen, carbon dioxide, water vapor) and salts (sulfates, nitrates, nitrites) – on the cathodic process and on the corrosion of iron in molten sodium chloride. Without presenting all the polarization curves obtained we may summarize the reactions of cathodic polarization as follows:

$$O_2 + 4\ominus \rightarrow 2O^{--}; \quad (1)$$

$$CO_2 \rightleftarrows CO + O; \quad O + 2\ominus \rightarrow O^{--}; \quad (2)$$

$$H_2O \rightarrow H^+ + OH^-; \quad H^+ + \ominus \rightarrow \frac{1}{2} H_2; \quad (3)$$

$$SO_4^{--} + 8\ominus \rightarrow S^{--} + 4O^{--}; \quad (4)$$

$$NaNO_3 + 6\ominus \rightarrow Na_2O + 2NO + 3O^{--}; \quad (5)$$

$$NaNO_2 + 2\ominus \rightarrow Na_2O + 2NO + O^{--}. \quad (6)$$

From the polarization curves we determined the limit diffusion current and the polarization capacity of the cathode; when the anodic process is slowed down very slightly they represent a semiquantitative measure of the corrosion activity of sodium chloride containing different additional elements. The date obtained as the result of analysis of the polarization curves are in good agreement with the data obtained by the loss of weight of iron in molten sodium chloride containing the same additional elements.

The greater corrosion activity of calcium chloride with respect to sodium and potassium chlorides (Fig. 7) was investigated with the same method and is explained in an analogous way. In fact, the curves represented in Fig. 8 show that in calcium chloride (Curve 3) an appreciable slowing down of the cathodic process can be observed, the calcium ion itself becoming the depolarizer by absorbing two electrons according to the reaction:

$$Ca^{++} + 2\ominus \rightarrow Ca.$$

The formation of metallic calcium is easily observable by small explosions on the surface of the molten salt and by the presence of calcium, revealed by chemical and metallographic analysis, in the corroded sample.

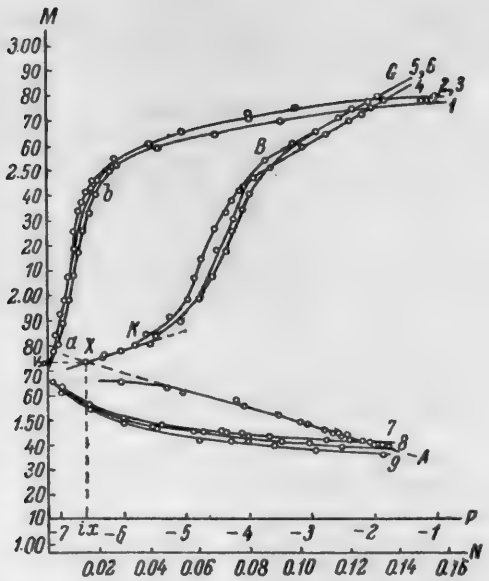

Fig. 6. Reproducibility of anodic (7, 8, 9) and cathodic (1, 2, 3) polarization curves of Fe in NaCl at 900° in potential (M in volts) – current density (N in amp/cm^2) and in potential (M) – logarithm of current density (P) coordinates – curves 4, 5, 6 and X – A.

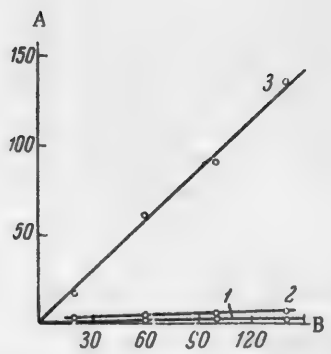

Fig. 7. Corrosion of Fe in different chlorides at temperatures 70°C above the melting point of the chloride.
A) Corrosion activity K (in g/m^2),
B) time τ (in minutes).
Curves: 1) NaCl; 2) KCl; 3) $CaCl_2$.

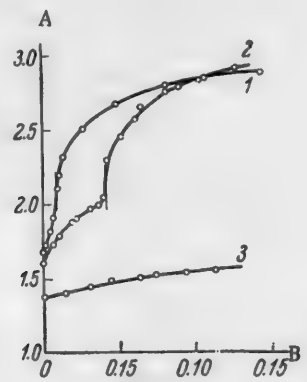

Fig. 8. Curves of cathodic polarization of Fe at 900°C in different molten chlorides.
1) NaCl; 2) NaCl + 1% $CaCl_2$; 3) $CaCl_2$.
A) Negative values of the potential (in volts); B) Current density (in amp/cm^2).

It can be seen that the addition of 1% calcium chloride to sodium chloride decreases the polarization and increases the intensity of diffusion currents $i_2 \approx 3i_1$ (Fig. 8, curves 1 and 2), thus increasing the corrosion activity of sodium chloride.

SUMMARY

1. The investigation of the structure of polished surfaces of Armco iron etched in molten salts at high temperature showed that the activity of the salt increases in the order NaCl, KCl, and $CaCl_2$. In all cases the etching of the surface is heterogeneous. It was shown that about 70% of the surface corrosion is concentrated around the boundaries of the grains (anodic zone).

2. Activation energies for different potentials of the iron electrode were calculated on the basis of the data provided by the curves of anodic and catodic polarization, obtained at different temperatures in molten sodium chloride. The results obtained lead to the conclusion that for values of the potential of the iron cathode up to −1.8 volts (with respect to the chlorine-carbon electrode) the cathodic process is fundamentally controlled by the ionization of oxygen (overpotential); from −1.9 to −2.1 volts it is controlled by the diffusion of the depolarizer (oxygen) to the cathode and for values of the potential more negative than −2.4 volts, the cathodic process is determined by the deposition of metallic sodium on the electrode.

3. If air, oxygen, carbon dioxide, or water vapor is passed through the molten salts the density of the limit cathode diffusion current increases considerably. It was shown that carbonic acid and water introduced in the molten salts are deposited as cathodic depolarizers of the corrosion process and are reduced to carbon monoxide and to hydrogen respectively during the process.

4. Sulfate ions, carbonate ions, nitrate ions and nitrite ions are active cathodic depolarizers in molten chlorides. This explains the increased activity (with respect to iron) of molten chlorides containing these anions.

5. The results of the investigation show that the corrosion of metals in molten salts is of electrochemical nature. The method of polarization curves allows one to learn the mechanism of cathodic and anodic processes taking place during the corrosion of metal in molten chlorides.

Corrosion of metal in molten salts can be briefly described as follows: a) anodic process − passage of metal ions into the molten salt under the effect of anions of the salt:

$$Me - \ominus \rightarrow Me^{+};$$

b) migration of electrons from the anodic area to the cathodic area;

c) cathodic process − assimilation of electrons by the depolarizer (O_2, H_2O, CO_2, Ca^{++} etc.).

6. The investigation allows us to indicate the fundamental measures to be taken for the prevention of corrosion in molten salts: a) convection current, inducing the increase of the limit diffusion current, must be decreased to a minimum by insulating the surface of the salt bath. As is well known, the heat losses by radiation from the surface of open salt baths reach 30-35%; b) Calcium chloride, either pure or in the eutectic form with another chloride, must not be used as heating medium or heat carrier; c) the method of cathodic protection insuring complete protection of the metal against corrosion by molten salts must be improved and used; d) the presence of active cathodic depolarizers (oxygen, carbon, dioxide, humidity and a number of oxidizing anions) in the molten bath must be eliminated and the probability of their introduction into the bath decreased.

LITERATURE CITED

[1] G. V. Akimov, Foundations of the Study of Corrosion and Protection of Metals, Metallurgy Press (1946).*

[2] N. D. Tomashov, Theory of Metal Corrosion, Metallurgy Press (1952).*

[3] A. N. Frumkin, V. S. Bagotsky, Z. A. Iofa and B. N. Kabanov, Kinetics of Electrode Processes, Moscow State University Press (1952).*

[4] E. Zing, P. Obergoffer and Piwowarski, Stahl and Eisen, 10 (1929).

[5] A. Soite, Decarburisation of Carbon Steels in Salt Baths (in German) (1931).

[6] I. F. Afonsky and A. A. Kroshkin, Salt Baths for Heat Treatments of Steels, State Scientific−Technical Press for Machine Construction Literature (1934).*

[7] E. I. Gurovich, J. Appl. Chem. (USSR) 28, 4 (1954).**

[8] V. P. Kochergin and G. I. Stolyarova, J. Appl. Chem. (USSR) 5 (1956).**

[9] P. F. Antipin, A. F. Alabyshev, B. P. Artamonov, N. A. Belozersky and V. P. Barzakovsky, Electrochemistry of Molten Salts, United Scientific and Technical Press (1937).*

---

* In Russian.

** See C. B. Translation.

[10] A. V. Ryabchenkov and V. F. Abramova, Collection of Reports of the Central Scientific Institute of Machine Technology, 11, (1948).

[11] P. S. Titov, Equlibrium Potentials of Liquid Molten Metals. State United Scientific and Technical Press (1938).*

Received August 8, 1956

* In Russian.

INVESTIGATION OF THE CORROSION OF ZINC, IRON, ALUMINUM AND MAGNESIUM IN AQUEOUS DIOXANE SOLUTIONS OF CERTAIN ELECTROLYTES

Yu. B. Kletenik

The State University, Rostov-on-Don

The convenient method discovered by Favorsky [1] for preparation of dioxane has made the practical use of this substance possible. Dioxane is now finding increasing use as a solvent, both in the pure state and in aqueous solutions in a wide range of concentrations, in a number of industries [2, 3]. Some dioxane complexes are used as valuable agents for sulfonation, nitrosation and other reactions in organic synthesis [4].

In this connection, investigations of the corrosion resistance of metals in aqueous dioxane solutions of electrolytes are of considerable practical interest. Moreover, results of theoretical interest may be expected in this field owing to the high tendency of dioxane to form complexes [1, 3-6].

We did not find any significant information on this question in the available literature.

The principal method used was the plotting of graphs for the corrosion rates of metals in aqueous dioxane solutions of different electrolytes as functions of the solvent composition, i.e., of the water and dioxane contents of the solvents. This made it possible to compare corrosion in aqueous dioxane media with corrosion in aqueous media, which has been studied most fully. Further, it was possible to compare the effects of the solvent composition on the corrosion of different metals.

The corrosion resistance of metals is a property which cannot be quantitatively determined with accuracy, as the corrosion process is influenced by many factors [7, 8]. Great caution is necessary in comparisons of the results obtained for the corrosion of different metals in the same medium, and even more so if one solvent is progressively replaced by another. However, because of the sharp differences between the solvent composition – corrosion rate curves for different metals, with consistent reproducibility of these characteristics for one metal, and the same comparisons of the curves obtained in our experiments and conclusions drawn from such comparisons are justified.

The corrosion of zinc, iron and aluminum in aqueous dioxane solutions of sulfuric and hydrochloric acids, the corrosion of magnesium in aqueous dioxane solutions of acetic acid and in water–dioxane mixtures without electrolytes, and corrosion of iron and aluminum in aqueous dioxane solutions of chlorides was studied.

EXPERIMENTAL

Dioxane of "pure" grade was purified by distillation and tested for absence of peroxide (by the titanium sulfate test). This dioxane contained about 1 wt.% of water,* which was taken into account in preparation of the solutions. For experiments with anhydrous solutions the dioxane was dried over metallic sodium, frozen out at 6-7°, and distilled over metallic sodium in the 101.1-101.2° range. This dioxane had m.p. 11.6°. All the other reagents were of "chemically pure" grade. Lithium chloride was used as the crystalline hydrate (the water of crystallization being taken into account in preparation of the solutions), or dehydrated by heat in a current of hydrogen chloride.

* The water content was determined cryoscopically.

Spectroscopically pure zinc was cast in the form of cylindrical specimens 6 mm in diameter 25 mm long. Spectroscopically pure aluminum was cut in the form of circular specimens 17 mm in diameter and 3 mm thick. Technical iron was used, of "steel 45" grade, in the form of specimens 30 × 20 × 3 mm. Technical (electrolytic) magnesium was used, the specimens being 20 × 15 × 4 mm in size. All the metals except zinc were treated mechanically in the following sequence: emery paper, polishing paper, carefully elutriated glass powder. The polished specimens were washed with alcohol, rinsed with water and placed in the corrosive solution. The zinc was cleaned with emery paper, etched for 10 minutes in 15% H_2SO_4, washed with water and placed at once in the corrosive solution. The reason for the different treatment used for zinc was that the corrosion rate of a polished zinc surface increases for a long time and only becomes more or less constant after well-defined crystals appear on the surface.

All the corrosion experiments were carried out at 21 ± 1°.

Corrosion in aqueous dioxane solutions of acids. The corrosion rate in aqueous dioxane solutions of acids was determined volumetrically, from the amount of hydrogen evolved. The conductivity of these solutions was used as the measure of changes in the activity of the corrosive acid.

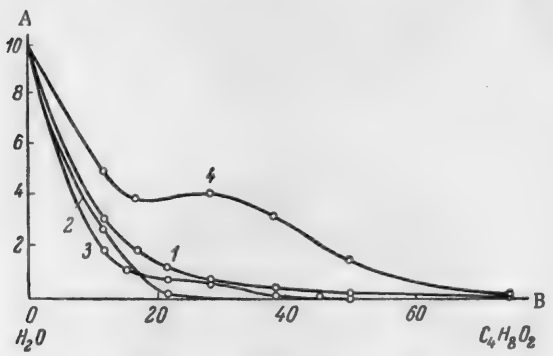

Fig. 1. Corrosion in sulfuric acid solution. A) Corrosion rate (in arbitrary units); B) contents of $C_4H_8O_2$ and H_2O (in molar %). 1) Conductivity; 2) zinc; 3) steel 45; 4) aluminum.

When the corrosion rate – solution composition curves were plotted, the corrosion rate in aqueous solution was arbitrarily taken as 10 in all cases. This figure was also used for the conductivity of the corresponding aqueous acid solution. The period during which the corrosion rate became more or less constant was determined for each metal and each series of solutions* from the corrosion rate – time curves. The value of the corrosion rate which was reached after the specimen remained in the solution for this period was used for plotting of the corrosion rate – solution composition curves for the given metal. Each point on these curves represents the mean value of the results obtained with several specimens.

The results so obtained for zinc, iron and aluminum in sulfuric acid solutions containing 1 mole of sulfuric acid per 6 moles of solvent are plotted in Fig. 1. 6 specimens were used in the corrosion tests on zinc, and 4 specimens each in the tests on iron and aluminum. The corrosion rate in aqueous solution, nominally taken as 10 in Fig. 1, is 4 ml of hydrogen per 1 cm^2 per minute for zinc, 2 ml of hydrogen per 1 cm^2 per hour for iron and 0.25 ml of hydrogen per 1 cm^2 per hour for aluminum.

In this series of solutions, starting from 12 molar % of dioxane in the solvent, zinc exhibits clearly defined passivation. The rate of corrosion of a pickled specimen (either moist after washing or dried) falls sharply during the first few seconds after immersion in the solution. The zinc surface becomes covered with a slight dull film, which rapidly dissolves in acid solution free from dioxane. The attack on the surface is irregular. Punctate corrosion (Fig. 2, b and c) passes into deep pitting (Fig. 2, d). A photograph of a zinc surface corroded in dioxane-free acid solution (Fig. 2, a) is shown for comparison. The number and depth of the pits increase with time. Iron is also passivated in sulfuric acid solutions, but to a much smaller extent than zinc. Punctate corrosion becomes most prominent in a solution with 28 molar % of dioxane in the solvent. The punctate corrosion does not pass into pitting corrosion, but merely makes the corroded surface uneven, which leads to some increase of the corrosion rate. Punctate corrosion does not develop in solutions with considerably higher dioxane contents.

In the case of aluminum the appearance of the corroded surface is the same in all the solutions of this series.

No evolution of hydrogen on zinc, iron, or aluminum was observed in anhydrous dioxane solutions of sulfuric acid of different concentrations.

Figure 3 shows the effect of solvent composition in solutions containing 1 mole of hydrogen chloride per

* A series of solutions means all the solutions with the same concentration of a given electrolyte and different proportions of water and dioxane.

30 moles of solvent, on the corrosion rates of zinc, iron and aluminum. The curves break off because of the phase separation which occurs on further increase of the dioxane content. 5 specimens of zinc and 4 specimens of iron and aluminum were used for determinations of each point. The corresponding corrosion rates in aqueous solution are 2 ml of hydrogen per 1 cm^2 per minute, 0.4 ml per 1 cm^2 per hour, and 3.3 ml per 1 cm^2 per hour; respectively.

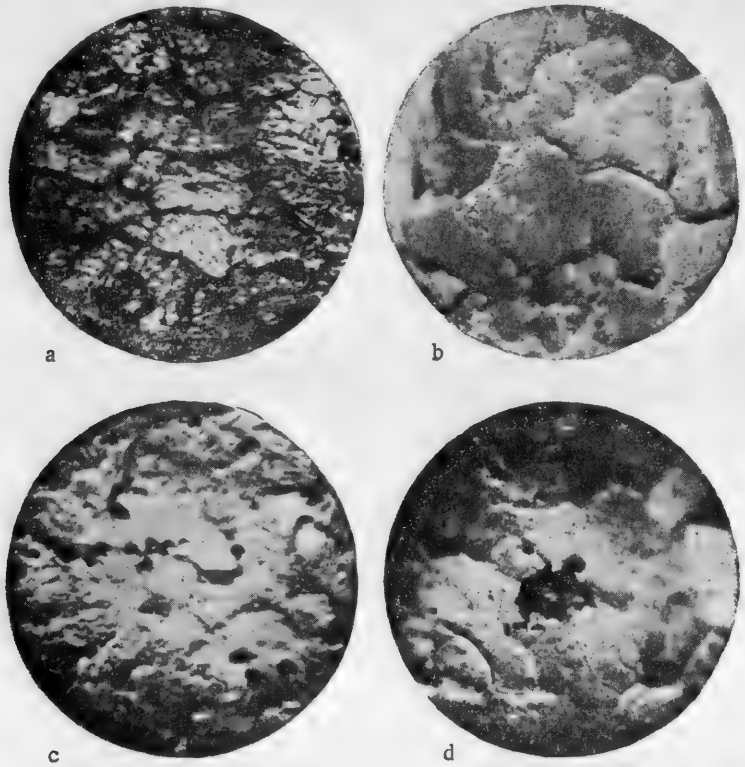

Fig. 2. Corrosion of zinc in aqueous dioxane solutions of sulfuric acid. a) Aqueous solution (after 30 minutes in solution); b) 80 molar % of water (1 hour in solution); c) 70 molar % of water (3 hours in solution); d) 50 molar % of water (24 hours in solution).

The corrosion rate of aluminum in solutions of this series only reaches more or less constant values after 1.5-2 hours of exposure to the corrosive solution. During this time the specimen surfaces acquire the appearance of well-defined crystals. The appearance of the corroded surfaces of all three metals does not change with variations of the dioxane content in the solution.

The corrosion of magnesium was studied in aqueous dioxane solutions containing 0.5 wt. % of acetic acid.* The results (each point was determined for 4 specimens) are plotted in Fig. 4 (Curve 2). The corrosion rate in aqueous solution was equivalent to 5 ml of hydrogen per 1 cm^2 per hour. The conductivities of the solutions of this series are plotted on the same diagram (Curve 1). Hydrogen is not liberated on magnesium in anhydrous dioxane solutions of acetic acid.

The above experimental results suggested that dioxane may have a loosening effect on the passivating films on the metals. To test this suggestion, we determined the corrosion rate of magnesium in aqueous dioxane without electrolytes, the corrosive agent being one of the solvents – water. The reciprocal of the time required for liberation of the first ml of hydrogen from 12 dm^2 of the specimen surface was taken as the measure of corrosion. Each point was determined for 4 specimens. The results are plotted in Fig. 4 (Curve 3). The corrosion rate in water was taken as 1.

* The acid concentrations in sulfuric and hydrochloric acid solutions were expressed in mole fractions because of the hypothesis, which proved unjustified, that there may be a connection between complex formation in solution and the corrosion rate.

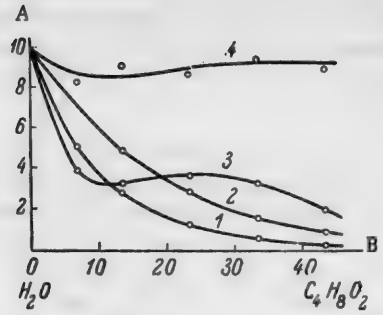

Fig. 3. Corrosion in hydrochloric acid solutions.
A) Corrosion rate (in arbitrary units);
B) $C_4H_8O_2$ content (molar %).
1) Conductivity; 2) zinc; 3) steel 45; 4) aluminum.

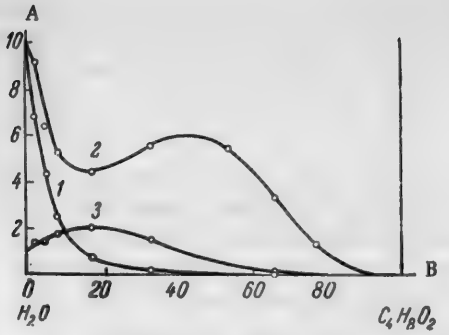

Fig. 4. Corrosion of magnesium.
A) Corrosion rate (in arbitrary units);
B) contents of $C_4H_8O_2$ and H_2O (in molar %).
Explanations of the curves are given in the text.

Corrosion in aqueous dioxane solutions of chlorides. On the hypothesis that dioxane has a loosening action on the protective films on the metals, interesting results could be expected in experiments on corrosion in neutral aqueous dioxane solutions of chlorides, where, first, the loosening effects of dioxane and Cl ions should be superposed, and second, the protective film on iron plays a very important part in its corrosive behavior. The corrosive effects of aqueous dioxane solution of chlorides on iron and aluminum were studied.

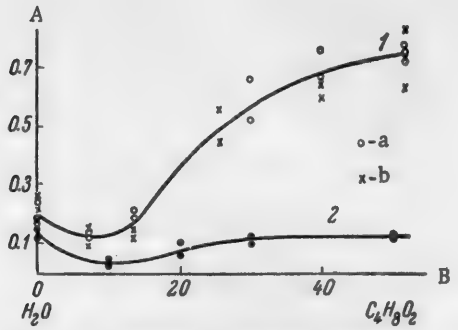

Fig. 5. Corrosion in chloride solutions.
A) Corrosion rate (in mg/ cm^2 · day);
B) contents of $C_4H_8O_2$ and H_2O (in molar %).
1) Steel 45 (a – 1% LiCl, b – 0.16% KCl);
2) aluminum.

The iron specimens were set vertically on glass supports in beakers with even upper edges. The beakers were covered with flat pieces of glass in such a way as to leave a gap of 0.5 mm between the edge of the beaker and the glass to allow free access of oxygen to the surface of the solution. The specimens were left 4 days in the corrosive solutions. The corrosion of the metal was calculated from the weight loss of the specimens (residual corrosion products were dissolved by treatment of the specimens with ammoniacal solutions of ammonium citrate). The results are plotted in Fig. 5. Each point represents a result obtained for one specimen. The circles correspond to aqueous dioxane solutions containing 1 wt.% of lithium chloride. The crosses correspond to aqueous dioxane solutions containing 0.15 wt. % of potassium chloride. The curves for both series of solutions coincide within the reproducibility limits of the experiments.

Curve 1 (for LiCl) breaks off as the result of the phase separation which occurs on further increase of the mole fraction of dioxane in the solution. Curve 2 (for KCl) breaks off in consequence of the limited solubility of potassium chloride in aqueous dioxane solutions. In the same mixtures, but with higher contents of dioxane saturated with potassium chloride (its solubility in such mixtures is very low) the corrosion of iron is fairly rapid down to water contents of not less than 10-15 molar %. The corrosion in such solution is not uniform over the entire surface, but occurs in isolated patches. In dry dioxane saturated with anhydrous lithium chloride* polished iron specimens did not lose their initial luster during 20 days. No changes in weight detectable on the analytical balance were found.

The corrosion of aluminum in 1% solutions of lithium chloride was also studied by the gravimetric method.

* To eliminate the risk of access of moisture from the air, the beakers, loosely covered with glass, were placed in a large desiccator over anhydrous calcium chloride.

The specimens were put in jars with ground-glass stoppers provided with small holes for access of air and kept in the corrosive solutions for 60 days. The results are plotted in Fig. 5 (Curve 2). Each point corresponds to a result obtained for one specimen. The scale of the corrosion rate is increased 20-fold for this curve.

DISCUSSION OF RESULTS

Two facts stand out in an examination of the results obtained in the corrosion studies on iron, zinc and aluminum in aqueous dioxane solutions of sulfuric acid. The first is the passivation effect, which is most pronounced in the case of zinc and less so in the case of iron. Since passivation does not occur in hydrochloric acid solutions, dioxane cannot be the passivating agent. The only other alternative is caused by adsorption of homopolar molecules of sulfuric acid or of a dioxane–sulfuric acid complex. The fact that analogous passivation of zinc does not occur in concentrated solutions of sulfuric acid, which undoubtedly contain large numbers of undissociated molecules, is convincing evidence in favor of the latter hypothesis.

The second fact, seen quite distinctly for both sulfuric and hydrochloric acid solutions, is the sharp difference in the position of the corrosion curves for zinc and aluminum, respectively. The curve for magnesium in acetic acid solutions is quite analogous to the curve for aluminum in sulfuric acid solutions (it must be taken into account that when the mole fraction of sulfuric acid is constant, its volume concentration in solution decreases with increasing dioxane content). The difference in the positions of the curves for passivated and nonpassivated metals is readily explained if it is assumed that dioxane, in virtue of its great tendency to complex formation, loosens the protective films on the metals by forming surface compounds with the films.

The loosening effect of dioxane is partially masked in hydrochloric acid solutions by the well-known loosening effect of the Cl ion. The volume concentration of hydrogen chloride in such solutions decreases with increase of the dioxane concentration. Evidently the activity of the Cl ions decreases to an even greater extent owing to the decrease of the dielectric constant of the medium, with a consequent decrease of the degree of dissociation of the electrolyte. Despite this, the corrosion curve for aluminum is almost horizontal over a region in which the conductivity of the solutions decreases 40-fold. A similar region is found on the curve for iron. All this leads to the conclusion that the simultaneous presence of dioxane and Cl ions results in a mutually intensifying action exerted by them on the protective films. This conclusion is confirmed by the results obtained in studies of the corrosion of iron and aluminum in neutral solutions of chlorides.

The hypothesis that the increase of the corrosion rate of iron in neutral aqueous dioxane solutions is accounted for by easier diffusion of oxygen to the specimen surface is refuted by the following facts: the solubility of oxygen is lower in water–dioxane mixtures than in pure water (according to our results, mixtures of oxygen-saturated water and freshly boiled dioxane are supersaturated with respect to the gas dissolved in them). The suggestion that dioxane peroxide may act as a carrier of oxygen is also unjustified. According to literature data [9], which we confirmed for the solutions used in our work, the rate of peroxide formation on contact of dioxane with atmospheric oxygen is negligible relative to the corrosion rate.

The solubility of the oxides of iron and aluminum in dioxane and in water–dioxane mixtures is negligible. The weight of the residue after evaporation of 10 ml of a solution saturated with Fe_2O_3, $Fe(OH)_3$ or Al_2O_3 (anhydrous dioxane or mixtures of two volumes of dioxane with one volume of water were saturated) and after subsequent filtration could not be detected on an analytical balance. Therefore the protective films cannot be dissolved by neutral solutions, as the latter would be soon saturated with the oxides. The most likely hypothesis remains that of the loosening effect of dioxane on the protective films.

It is possible that the observed combined influence of dioxane and Cl ions on the corrosion of passivated metals may be accounted for by the surface formation of complexes of the metal chlorides with dioxane. This suggestion is supported by the following fact. Aluminum dissolves rapidly in anhydrous concentrated solutions of hydrogen chloride in dioxane, with vigorous evolution of hydrogen and heat. When the solution is cooled, crystals of the complex $AlCl_3 \cdot 2C_4H_8O_2$ are deposited.

In conclusion, it must be pointed out that the significance of these facts is not confined to aqueous dioxane media with high contents of water. They should be correlated with the tendency of water–dioxane mixtures to separate into layers when various electrolytes are dissolved in them. In this connection we may refer to the work of Kobe and Strong [10], who found that out of 31 salts tested, 16 caused phase separation of water–dioxane mixtures.

Some strongly hydrated electrolytes such as HCl and LiCl cause phase separation – the formation of a small lower layer – even when the water content in the dioxane is very low. This layer is an aqueous dioxane solution of the electrolyte; our experiments showed that this may be highly corrosive. The formation of such layers in chemical equipment may cause intense corrosion, especially at the boundary with the main dioxane solution.

SUMMARY

1. The corrosion of zinc, iron, and aluminum in aqueous dioxane solutions of sulfuric and hydrochloric acids, the corrosion of magnesium in aqueous dioxane solutions of acetic acid and in water–dioxane mixtures without electrolyte, and the corrosion of iron and aluminum in aqueous dioxane solutions of chlorides was studied. It was found that in sulfuric acid solutions passivation of the metals takes place; it is most pronounced in the case of zinc and is probably caused by adsorption of a dioxane–sulfuric acid complex.

2. A sharp distinction was found between corrosion-rate curves for metals which are strongly passivated in acid media (aluminum, magnesium) and the curves for metals which are weakly passivated in these media (iron) or are not passivated at all (zinc).

3. The joint influence of Cl ions and dioxane on the corrosion rate of passivated metals (aluminum, iron) is one of mutual intensification, which is most pronounced in the case of iron in aqueous dioxane solutions of chlorides.

4. It is suggested that dioxane has a loosening effect on the passivating films.

The author thanks O. A. Osipov for suggesting the subject of this investigation.

LITERATURE CITED

[1] A. Favorsky, J. Russ. Phys.-Chem. Soc. 38, 4, 741 (1906).

[2] C. Ellis, Chemistry of Petroleum Derivatives, I (Russian translation) (ONTI, 1936).

[3] Ya. F. Mezhennyi, "Physicochemical Investigations of Solutions in Dioxane and Aqueous Dioxane," Author's Summary of Dissertation (Kiev, 1954).*

[4] A. P. Terentyev and L. A. Kazitsyna, Reactions and Investigation Methods of Organic Compounds (Goskhimizdat, 1952).*

[5] Ya. F. Mezhennyi, J. Gen. Chem. 16, 3, 447 (1946).

[6] Ya. K. Syrkin and K. M. Anisimov, Proc. Acad. Sci. USSR 59, 8, 1457 (1948).

[7] G. V. Akimov, Theory and Methods of Investigation of Metal Corrosion (Izd. AN SSSR, 1945).*

[8] N. D. Tomashov, Theory of Metal Corrosion (Metallurgy Press, 1952).*

[9] K. Hess and H. Frahm, Ber. 71, 2627 (1938).

[10] K. A. Kobe and J. P. Strong, J. phys. Chem. 44, 629 (1940).

Received September 17, 1956

* In Russian.

MINERAL PIGMENTS FOR LEATHER COATING COLORS

A. L. Zaides and R. A. Metlitskaya

Mineral pigments (iron oxide, lead chromate, titanium dioxide) are generally used as the coloring components of leather finishes. The properties of these pigments (color, covering power, etc.) depend on the method used for their preparation.

Of the iron oxide pigments, the orange-red ferric oxide made by heating ferrous sulfate at 700-900° is commonly used. Either ordinary or the finely dispersed chrome yellow is used; these differ in the conditions (temperature) used in their production. Paint-grade titanium dioxide is generally used as a white pigment in leather finishes, as the finer grade used for viscose has a yellowish tinge.

Samples of these pigments of domestic and foreign origin, differing in their behavior in leather finishes, were available for our investigations.

The objects of the investigation were to study the properties of the pigments by different methods and to find the causes of the differences in their behavior in leather finishes.

EXPERIMENTAL

Iron oxide pigments. Samples of red iron oxide made in different factories were used. They were studied by several methods: the chemical composition was determined, the structure was established by x-ray analysis and electron microscopy, and the covering power and color were studied.

The x-ray photographs were taken in a cylindrical camera by the Debye method with sealed iron tubes at 10 ma and 37 kv, the camera diameter being 57.3 mm. The exposure was 3-4 hours.

The EM-100 electron microscope was used for the electron microscope studies at 12000 magnification, by two methods: 1) direct observations of the pigment dispersed in a casein sol, and 2) the use of replicas of films containing the pigments. In the second method the pigment was first ground together with high-viscosity nitrocellulose. The mixture was diluted (1 : 1) with a solvent (acetone or butyl acetate) and poured onto degreased glass to form a uniform film. The film was allowed to dry and then stripped from the glass; the external side of this film was coated with quartz dust under vacuum to form the replica; the film was then cut into small pieces and the nitrocellulose was dissolved in acetone. The quartz replicas so obtained were placed on the specimen holder for the electron microscope investigations. At many points the pigment particles adhered to the quartz film, making it possible to observe the pigment replica and the pigment itself simultaneously. In direct observations of a pigment under the electron microscope there is a risk that when the sol is diluted (which is necessary in order to reduce the pigment concentration to a level suitable for electron-microscopic observation) particles of different size become distributed in such a way that the heavier particles sink to the bottom and do not enter the drop of solution used for examination. The second method is free of this disadvantage. The particles are distributed in the same way as in the film on leather. The replica together with adherent particles of pigment can be observed simultaneously.

The covering power was determined by the chessboard method used in the paint industry. The color, brightness, and purity of shade were determined visually from trial paintings on chalk paper.

Analytical data for the samples of ferric oxide pigments tested are given in Table 1.

The covering power of paints made from these pigments, and sedimentation from water were also investigated. As is seen in Table 2, the sedimentation was determined gravimetrically.

All the samples gave the same x-ray pattern (Fig. 1).

Electron microscope investigations showed that the ferric oxide pigments differ in particle size and particle-size distribution.

TABLE 1

Analytical Data for Ferric Oxide Pigments

Composition and properties	Sample 1*	Sample 2**	Sample 3***	Sample 4****
Fe_2O_3 (in %)	96	98	97-98	92-97
SO_3 (in %)	—	Traces	0.3	0.3
Residue insoluble in HCl	0.47	1.8	2.54	0.7 to 2.5%
Residue on sieve of 4900/ mm^2 mesh (%).	—	0.65	0.8	0.2-3.0
Covering power of dry pigment (in g/ m^2)	3.5-4	4.8	4-5	5-6
Color	Bright orange-red	Dull yellowish red	Dull violet-red	Dingy dull violet-red

TABLE 2

Comparative Characteristics of Paints Made with Different Pigments

Properties	Sample 1	Sample 2	Sample 3
Covering power (in g/ m^2)	7.2	10.6	10.9
Sedimentation in 3 hours (%)	10	24	20

Electron micrographs of these pigments, showing the most characteristic distinctions between them, are given in Figs. 2-4.

TABLE 3

Covering Power of Paints Made from Sample 4

Pigment	Covering power (in g/ m^2)
Before purification	8.1
After purification	6.4

The polydisperse ferric oxide pigments were separated into two layers by wet separation in presence of casein as a protective colloid: an upper yellow-red paler layer, and a lower red-violet darker layer. Both layers were investigated under the electron microscope; the covering power of the paints made from these pigments was determined (Table 3).

Chrome yellows. 4 samples of chrome yellow were studied: 2 imported, 1 highly disperse and 1 ordinary. Their properties are given in Table 4.

All the samples of chrome yellow gave the same x-ray pattern. The electron micrographs are given in Figs. 5-7.

Titanium dioxide. 5 samples of titanium dioxide used in leather finishes were studied. All these samples differed in their properties (Table 5).

Electron microscope investigations showed that the titanium dioxide samples differed in degree of homogeneity and in particle size.

Electron micrographs of these pigments, showing the most characteristic distinctions between them, are given in Figs. 8-12.

* Imported, from Lvov Paint Works.

** From Leningrad Chemical Works.

*** From Dulevo Paint Works.

**** From Rostov Magnesia and Ultramarine Works.

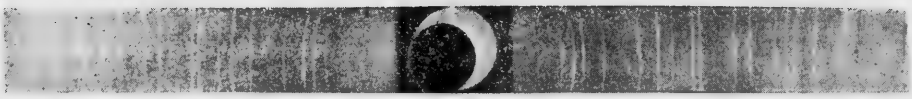

Fig. 1. x-Ray pattern of red ferric oxide pigments.

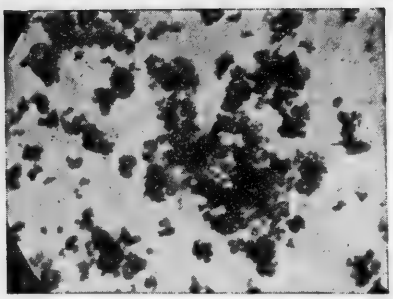

Fig. 2. Electron micrograph of imported ferric oxide pigment.

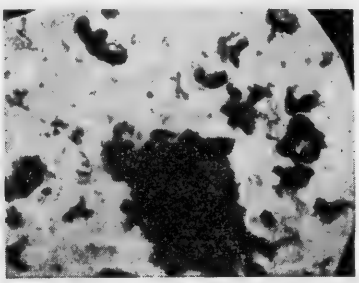

Fig. 3. Electron micrograph of ferric oxide pigment from the Leningrad Works.

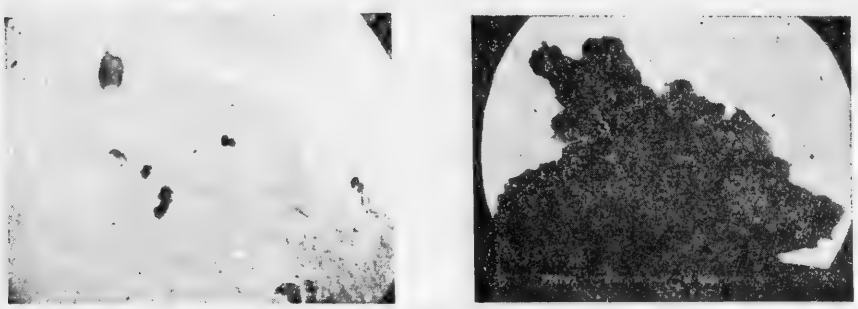

Fig. 4. Electron micrographs of ferric oxide pigment from the Rostov Works. Left – upper layer; right – lower layer.

TABLE 4

Properties of Chrome Yellows

Properties	Sample 1*	Sample 2**	Sample 3***	Sample 4****
Covering power, g/m^2	29	30	40	50
Color	Bright lemon-yellow		Somewhat purer than the ordinary	Yellow with dingy tinge

TABLE 5

Properties of Titanium Dioxide Samples

Properties	Sample 1****	Sample 2*****	Sample 3******	Sample 4*******	Sample 5********
TiO_2 content (%)	99.3	97.5	98.7	99	—
Covering power (in g/m^2)	30.8	59.3	51.0	44.0	24.8
Covering power in film form (in g/m^2)	66.2	80.0	80.0	77.6	75.0
Water-soluble salts	0.2	0.5	0.7	0.6	—
Oil absorption	46.5	55.8	53.8	38.0	—
Residue on 4900/cm^2 sieve	0.00	0.00	0.15	0.15	0.00

DISCUSSION OF RESULTS

The results obtained for red ferric oxide pigments showed that the samples differed mainly in size uniformity and particle size. Their ferric oxide contents varied from 92 to 98 % (Table 1). Despite these variations, the x-ray patterns of the pigments were all alike. The x-ray studies showed that the finished pigments are not individual oxides; in other words, they do not consist of, say, only FeO_3 or Fe_3O_4, but are mixtures of different oxides; this is shown by the fact that the interplanar spacings calculated for these pigments do not coincide with data given in reference tables for the individual oxides. All the iron oxide pigments studied contained the same oxides, and only the relative proportions of these oxides could be different in different pigments. This accounts for the different ferric oxide contents of different samples. For example, if one pigment should contain more Fe_2O_3 or FeO, and another more Fe_3O_4, the former contains less iron than the second when the compositions are calculated as Fe_2O_3. This is also why the ferric oxide content of a pigment does not characterize its properties. For example, Sample 1 is qualitatively better than Sample 3, although the former contains 96% and the latter up to 98% of ferric oxide. Similarly, there is no direct relationship between the ferric oxide content and the covering power of a pigment. The color, brightness and covering power of a pigment depend both on the composition and on the particle size.

The electron micrographs clearly reveal the differences between the pigment samples. Sample 1 consists of more or less uniform particles about 0.3 μ in size. If the particles are close to each other, they do not coalesce but form a sort of lace pattern in which the individual crystal faces are visible (Fig. 2).

* Imported.

** Highly disperse (domestic).

*** Ordinary (domestic).

**** For viscose, 1948 production.

***** For paint, 1951 production.

****** For paint, 1954 production.

******* For paint, 1955 production.

******** Imported.

Fig. 5. Electron micrographs of imported chrome yellows.
Left – from England, right – from Austria.

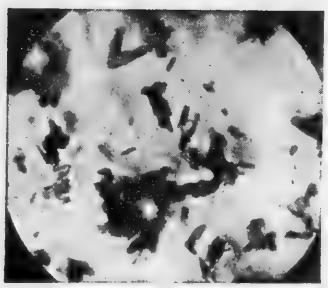

Fig. 6. Electron micrograph of highly disperse chrome yellow from the Yaroslavl Works.

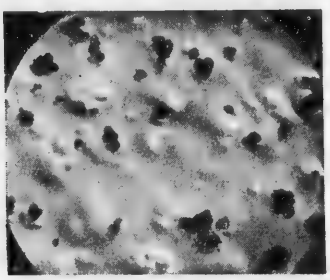

Fig. 7. Electron micrograph of ordinary chrome yellow from the Yaroslavl Works.

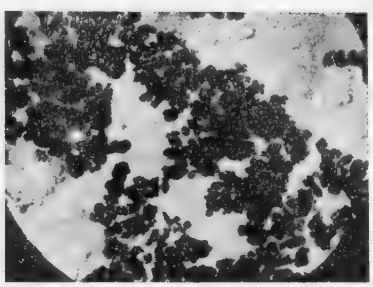

Fig. 8. Electron micrograph of titanium dioxide for viscose, 1948 production.

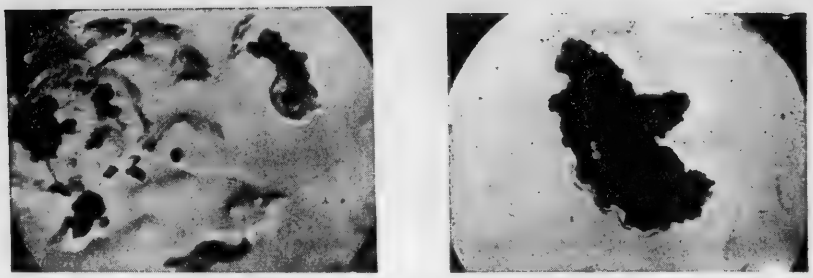

Fig. 9. Electron micrographs of titanium dioxide for paints, 1951 production.

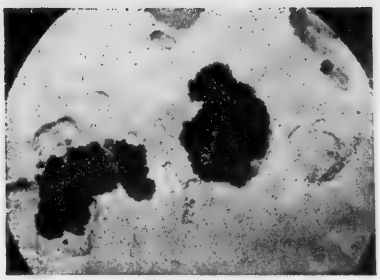

Fig. 10. Electron micrograph of titanium dioxide for paints, 1954 production.

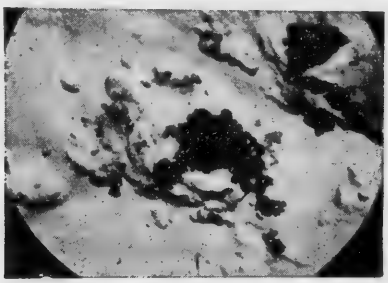

Fig. 11. Electron micrograph of titanium dioxide for paints, 1955 production.

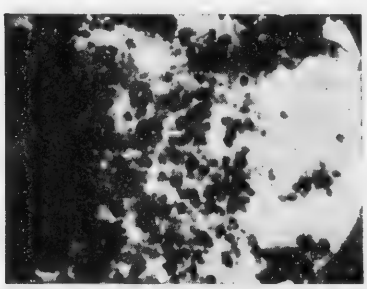

Fig. 12. Electron micrograph of imported titanium dioxide from Austria.

Sample 2 is polydisperse, with particles between 0.1 and 3-4 μ. This pigment is rather similar to Sample 1 in the nature of the particle distribution in the film (Fig. 3).

Sample 3 and 4 are very polydisperse. Particles occupying several fields of vision occur, together with the fine particles. According to electron microscope data, the maximum particle size in Sample 3 reaches 12μ, and in Sample 4, as much as 18μ (Fig. 4, right), in presence of particles of the order of 0.1-0.5μ (Fig. 4, left).

The homogeneity of the pigments may also be estimated indirectly by sedimentation of the pigment in paints. Sample 1 gave the best results here also.

The homogeneity of a pigment has a decisive influence on the quality of the films. Films containing fine homogeneous particles are even, smooth, glossy, and have a higher abrasion resistance. Films made with pigment Sample 1 have these properties. The other pigments are heterogeneous, the greatest heterogeneity being found in Sample 4.

One method for increasing homogeneity is by wet separation. Electron micrographs showed that the particles in the upper layer are more uniform in size, although there are occasional particles up to 3μ in size. The number of large particles in the lower layer is much greater; this is seen particularly clearly in quartz replicas. Purification of the pigment improves the covering power of paints, and makes it possible to obtain thinner films on leather.

The polydispersity of ferric oxide pigments can probably be attributed to the conditions of their production. Wet separation improves the pigment by removal of the largest particles.

As in the case of the ferric oxide pigments, the results showed that the main differences between the different samples of titanium dioxide pigments depend on the particle size and particle uniformity of these pigments.

The electron micrograph of an imported sample of titanium dioxide (from Austria) shows that the particles are small, uniform, separate from each other, and are distributed regularly over almost the entire field of vision. This distribution of the pigment particles in the electron micrograph corresponds to their distribution in the coating on leather.

The particle distribution of Sample 1 (viscose) in the film is similar to that of the imported pigment (Fig. 8). The particles are fine, do not coalesce, and are distributed regularly over the film. Some aggregation of the particles is seen in Samples 2 and 3 (Figs. 9 and 10). It is seen in the electron micrographs that the individual fine particles form clusters. This makes their distribution in the film irregular.

In Sample 4 (Fig. 11) the distribution of the particles in the film is as nonuniform as in the previous two samples, but the particles are separate, and individual fine particles can be clearly distinguished in the clusters seen in the electron micrograph.

The differences in the microstructure of these samples of titanium dioxide influence their properties. The covering power of the pigment itself, and of paint made with it, is best for Sample 1 (viscose). This is followed by Sample 4; Samples 2 and 3 have the worst covering power. These results also agree with data on the oil absorption of the samples.

Thus, the sample of titanium dioxide used for viscose is close in its microstructure and particle distribution in films to the imported pigment used in leather finishes, and only differs from the latter by a lower degree of whiteness.

The lead chromate samples, while having the same structure as shown by the results of x-ray analysis, differ considerably from each other under the electron microscope.

The two imported lead chromate samples gave similar electron micrographs. Unsymmetrical elongated crystals can be seen (Fig. 5). However, the crystals in Sample 1 have a distinct internal structure (laminar, striated) while Sample 2 contains more dense crystals. The highly disperse chromate (Fig. 6) also contains predominantly elongated crystals. However, these are smaller and their internal structure is not always clear. In addition, it contains crystals typical of the ordinary chromate sample. The structure of ordinary chromate, as revealed by the electron microscope, is distinct from that of the chromates discussed above. Its crystals are finer and more symmetrical (Fig. 7). The covering power of the pigments changes with variations in the electron micrographs (Table 2). Sample 1 has the best, and Sample 4 the worst covering power.

SUMMARY

Studies of the properties and structure of samples of ferric oxide pigments, titanium dioxide and lead chromate showed that the main differences between them in relation to their use in finishes on leather are associated with the shape, uniformity and size of the particles, as revealed by the electron microscope. Structural differences between the pigments, characterizing their quality for use in leather finishes, could not be detected by chemical and x-ray analysis methods.

Received June 17, 1956

METHOD FOR THE PREPARATION OF WATER-REPELLENT, OIL-RESISTANT AND WEATHER-RESISTANT ORGANOSILICON DRYING OILS

A. P. Antykov

Various branches of our Socialist industry (the paint, chemical, electrical, electronic, machine-building, instrument construction, transformer-building, etc.) require ever-increasing amounts of water-repellent and oil-resistant coatings.

Natural drying oils (and varnishes based on them) usually give coatings which are not water-repellent, of poor or relatively satisfactory resistance to oil.

The lack of water repellence and the poor or inadequate oil resistance of natural film formers (linseed and hempseed oils, oil varnishes, etc.) are considerable disadvantages, as they lower the effectiveness and durability of protective or insulating coatings.

Among the many known [1-5] synthetic film formers used for various varnishes (phenol—formaldehyde, polyvinyl chloride, melamine, aniline—formaldehyde and other varnishes) none has outstanding water repellence in conjunction with resistance to oil and weathering, and with good mechanical properties.

The search for new water-repellent and oil-resistant coatings for the formation of water-repellent and oil-resistant films of any desired thickness, with valuable protective, mechanical, electrical and other properties is therefore a problem of urgent importance.

This paper contains a description of a method for the synthesis of water-repellent, oil-resistant and weather-resistant film formers suitable for the production of water-repellent and oil-resistant protective and insulating films of any thickness, with good mechanical and dielectric properties.

EXPERIMENTAL

Synthesis based on the use of natural drying oils and orthosilicate esters. In a 1.5 liter wide-necked Pyrex glass flask, containing a stirrer operated at 20-30 r.p.m., and immersed in a water bath, there was put 700 g of natural linseed drying oil (or any other drying oil), 150-250 g of tetraethyl (or tetramethyl) orthosilicate, 3.5 ml of water, and 7 g of No. 64 Drier.

If the natural oil already contains the required amount of drier, No. 64 Drier need not be used. Instead of a prepared natural drying oil made by the usual oxidation and polymerization methods, it is possible to use natural oils (sunflower, cottonseed, etc.) previously heated at 240-250° for 3 hours with 0.08-0.12% of No. 64 Drier (calculated on the metal).

The neck of the flask was firmly closed with a rubber bung and connected to a straight Liebig condenser by means of a bent glass tube. The bung contained holes for a thermometer, stirrer, and the tube leading to the condenser.

The thermometer was immersed in the liquid to a depth of 2-3 cm.

When the charge had been put into the flask, the stirrer was switched on, the flask was connected to the condenser and heated on the water bath to 95° during 20-30 minutes.

The liquid was then held at this temperature for 2-3 hours.

The heating was stopped when a sample of the organosilicon product had a viscosity of 12.9-17.6 seconds (according to the nature of the natural oil used) by the NIILK (Scientific Research Institute of Lacquers and Paints) funnel test at 20°.

TABLE 1

Synthesis Data for Organosilicon Drying Oils

Materials used, experimental conditions, yields	Experiment No.											
	1	2	3	4	5	6	7	8	9	10	11	12
Natural linseed drying oil (g)	101.5	20.2	20.0	20.0	20.0	—	20.0	30.0	30.0	101.5	30.5	40.0
Linseed oil (g)	—	—	—	—	—	20.0	—	—	—	—	—	—
Tetraethoxysilane (g)	101.5	20.2	20.0	5.0	5.0	14.1	—	—	—	—	—	—
Tetramethoxysilane (g)	—	—	—	—	—	—	20.0	—	—	—	—	—
Liquid Silicone No.2(g)	—	—	—	—	—	—	—	30.0	—	—	—	10
No.3(g)	—	—	—	—	—	—	—	—	30.0	—	—	—
No.4(g)	—	—	—	—	—	—	—	—	—	101.5	—	—
No.9(g)	—	—	—	—	—	—	—	—	—	—	30.5	—
Water (g)	—	0.2	7.0	0.1	0.2	—	0.2	—	—	—	—	—
Heating temperature (°C)	95	95	95	95	95	95	95	20	20	20	20	120
Heating time (min)	45	45	45	150	45	45	45	45	45	45	45	90
Yield of drying oil (as % of raw material)	90.2	86.5	87.4	89.5	86.7	99.8	81.9	100.0	100.0	100.0	100.0	96.7
Precipitate of silica (g)	—	0.10	0.40	—	—	—	—	—	—	—	—	—

During the heating, water vapor and any excess of tetraethyl (or other) orthosilicate was distilled off through the condenser and collected in a receiver (beaker) for return condensate.

When the required viscosity was obtained, the heating was stopped, and the organosilicon oil was removed and analyzed for viscosity, acid number, saponification number, iodine number, and drying time in film form at 20°.

A good organosilicon drying oil prepared by this method should have the following properties (depending on the original oils used): viscosity 12.9-17.6 seconds at 20° by the NIILK test, acid number 6.5-15.0, saponification number 180-240, ester number 174-225, iodine number 120-160, film drying time at 20° 12-30 hours.

The organosilicon drying oils are colorless or slightly brownish liquids, transparent to light and quite colorless in films.

The liquid organosilicon drying oils have the odor of the natural oils used, or of the solvent used as thinner (turpentine, kerosene, white spirit, etc.).

The films made from the organosilicon drying oils are quite odorless.

The organosilicon drying oils made by the method described have good physical and mechanical properties (good water repellence, mechanical strength and elasticity, oil resistance, weather resistance, heat resistance).

This version of the method for the synthesis of organosilicon drying oils has the following characteristics: a) the unsaturation of the oils used is increased considerably, so that vegetable oils which normally yield slow-drying and poor-quality films can be used for the synthesis of high-quality organosilicon drying oils; b) the method is simple and free of fire hazards; c) the materials are readily available and cheap (ethyl silicate and relatively plentiful vegetable oils such as cottonseed, sunflower and similar oils).

Data on the synthesis and properties of organosilicon drying oils are given in Tables 1-4.

Synthesis based on the use of natural drying oils (or varnishes) and silicone liquids. In a 1.5 liter wide-necked Pyrex glass flask, containing a stirrer operated at 20-30 r.p.m., there was put 800 g of natural linseed drying oil (or any other drying oil, either pure or in the form of No. 302, No. 1154, No. 460, etc. varnishes) and 200 g of liquid Silicone No. 2 (or No. 3, GKZh-94).

The flask containing these components was connected to a straight Liebig condenser and heated up to 120° during 30-40 minutes with the stirrer switched on.

TABLE 2

Synthesis Data of Organosilicon Drying Oils

Materials used, experimental conditions, yields of drying oils and gelatinous polymers	Experiment No.											
	13	14	15	16	17	18	19	20	21	22	23	24
Natural linseed drying oil (g)	40.0	40.0	—	—	—	—	—	—	—	—	—	—
Sunflower drying oil (g)	—	—	—	—	—	103.0	—	—	—	—	—	—
Cottonseed oil heated for 3 hours at 240° with 0.11% of Drier No. 64 (g)	—	—	—	—	—	—	—	—	—	—	—	70
Castor oil (g)	—	—	40.0	—	—	—	—	—	—	—	—	—
Tung oil (g)	—	—	—	40.0	—	—	—	—	—	—	—	—
Varnish No. 302 (g)	—	—	—	—	40.0	—	—	—	—	—	—	—
Varnish No. 1154 (g)	—	—	—	—	—	—	40.0	—	—	—	—	—
Varnish No. 460 (g)	—	—	—	—	—	—	—	40.0	—	—	—	—
Synthine (g)	—	—	—	—	—	—	—	—	40.0	40.0	—	—
Tetraethoxysilane (g)	—	—	—	—	—	44	—	—	12.0	—	20.0	30
Tetramethoxysilane (g)	—	—	—	—	—	—	—	—	—	12.0	—	—
Liquid Silicone No. 2 (g)	—	—	10.0	10.0	10.0	—	—	10.0	—	—	—	—
Liquid Silicone No. 3 (g)	10.0	—	—	—	—	—	—	—	—	—	—	—
Liquid Silicone No. 4 (g)	—	—	—	—	—	—	10.0	—	—	—	—	—
Liquid Silicone No. 9 (g)	—	10.0	—	—	—	—	—	—	—	—	—	—
Water (g)	—	—	—	—	—	—	—	—	—	—	7.0	0.40
Heating temperature (°C)	120	120	120	120	120	95	85	20	85	85	85	95
Heating time (min)	90	90	90	60	60	150	45	45	45	45	30	190
Yield of drying oil (as % of raw material)	96.7	64.1	—	89.3	80.1	84.0	—	95.3	—	—	—	81.7
Precipitate of gelatinous polymers (g)	—	12.9	43.6	—	—	—	46.1	—	44.8	43.3	—	—
Precipitate of silica (g)	—	—	—	—	—	—	—	—	—	—	5.6	—

The mixture was heated at this temperature for 1.5 hours. The heating was completed when a sample had a viscosity of 6.5-9.5 seconds by the NIILK funnel test at 20°.

Copolymerized organosilicon drying oil was formed during the heating. The weight of the mixture changed very little during the heating, and the yield of the organosilicon drying oil was 96-98%.

The product was taken out and analyzed for viscosity, film drying time, acid number, saponification number, and iodine number.

A good organosilicon drying oil prepared by this version of the method should have the following properties: viscosity 6.5-9.5 seconds by the NIILK funnel test at 20°, acid number 3-7, saponification number 148-180, iodine number 65-90, drying time at 100°, 2.5-6.5 hours.

The organosilicon drying oils so made are colorless or brownish transparent liquids with a mixed odor of the natural drying oil and the liquid silicone used. The films are odorless.

If the organosilicon drying oils are made from polyalkylsiloxane liquid Silicone No. 2 and natural drying oil, the process can be much simplified if the films are to be dried at 100° and over.

In such cases the drying oils can be made by simple mixing of 80% (by weight) of natural drying oil and 20% of liquid Silicone No. 2 in a mechanical mixer for 30 minutes at 20°. The copolymer formation then takes place during the drying (at 100°).

TABLE 3

Physicochemical Properties of Organosilicon Drying Oils

Experiment No. in Tables 1 and 2 and raw material	Properties of organosilicon drying oils											
	density at 20° (in g/ml)	viscosity by NIILK funnel test at 20° (sec)	acid number	saponification number	ester number	iodine number		actual increase of iodine number	refractive index at 20°	molecular weight found	molecular weight found	
						theoretical (for natural drying oil used)	actual (Hübl)				found	calculated
6	0.942	4.6	14.74	190.0	175.26	106.7	154.0	+47.3	1.460	472.0	136.700	126.792
Pure linseed oil	0.936	7.0	3.12	183.2	179.08	—	181.4	—	1.491	876 *	270.700	269.487
1	0.941	4 2	27.90	218.5	190.60	69.0	141.0	+72.0	1.458	476.0	137.700	126.792
3	0.943	4.8	16.94	231.0	214.06	71.7	153.6	+81.9	1.465	414.0	121.500	107.786
4	0.945	17.6	6.40	187.9	181.5	117.5	127.8	+10.3	1.493	1910.0	587.0	—
21	—	—	149.5	365.5	210.0	—	1.9	—	—	—	—	—
Synthine	—	—	179.3	369.0	189.7	—	7.0	—	—	—	—	—
Natural linseed drying oil	0.938	9.2	2.70	179.4	176.7	—	126.4	—	1.495	1018 *	278.6	—
12	0.934	6.5	4.30	149.3	145.0	104.8	69.0	—35.8	—	—	—	—
13	0.937	6.9	3.55	149.4	145.85	104.8	70.1	—34.7	—	—	—	—
14	0.953	8.1	5.10	148.5	143.4	104.8	69.4	—35.4	—	—	—	—
18	0.944	14.8	11.70	206.3	194.6	61.0	99.4	+38.4	—	—	—	—
24	0.934	12.9	9.40	203.1	193.7	53.8	89.7	+35.9	—	—	—	—

* By the method of Drinberg and Chervinskaya [6].

TABLE 4

Properties of Organosilicon Drying Oils in Films

Experiment No. in Tables 1 and 2	Film drying time (hours) at temperature (°C)			Film elasticity on NIILK scale after drying (mm)	Impact strength, Dupont (cm)	Hardness, pendulum test	Water absorption after 24 hr in water (in mg/100 cm²)	Heat resistance after 48 hours aging at 120°		Notes
	20°	100°	170°					elasticity on NIILK scale (mm)	impact strength, Dupont (cm)	
1	14	10	0.5	1	50	0.26	0.0	1	50	After drying at 100°
3	16	1.5	1.0	1	30	0.18	4.0	3	35	After drying at 20°, film turbid
3	—	1.5	—	1	50	0.23	0.0	1	40	After drying at 100°, film clear
4	14	0.75	0.40	1	50	0.22	0.0	1	50	After drying at 20°, film clear and glossy
4	—	0.75	—	1	50	0.28	0.0	1	50	After drying at 100°
8	28	3.5	2.5	3	15	0.16	1.7	5	25	After drying at 170°
9	48	4.5	3.0	3	15	0.16	2.3	5	25	
10	Does not dry	Does not dry	6.5	3	15	0.17	1.6	5	25	
11	» »	6.5	4.5	3	15	0.16	2.0	5	25	
12	24	2.0	1.0	1	50	0.21	0.0	1	50	After drying at 20°, film clear and glossy
13	24	2.5	1.5	1	50	0.22	0.0	1	50	
14	24	2.5	1.5	1	50	0.22	0.0	1	50	
16	18	2.0	1.0	1	50	0.20	0.0	1	50	
17	20	1.5	0.75	1	50	0.27	0.0	1	50	
19	Does not dry	0.6	4.5	1	50	0.20	4.7	1	35	
20	6	1.0	0.5	1	35	0.21	0.5	3	20	Black, glossy film, properties after drying at 20°
Natural linseed drying oil	24	2.0	1.0	1	50	0.21	31.8	1	50	Control sample
18	28	6.0	3.0	1	50	0.20	5.4	1	50	
24	30	8.0	3.5	1	50	0.18	6.2	1	50	

Liquid Silicone No. 9 reacts with natural drying oil to give up to 36% of solid polymers in the form of a bulky gelatinous precipitate; this is a characteristic feature of the reaction of liquid Silicone No. 9 with natural drying oil and greatly reduces the yield of the valuable organosilicon drying oil.

Copolymers of liquid Silicone No. 3 give films which do not dry at all at 20°; the films dry in 4.5-6.5 hours only at 100° and over.

Liquid Silicone No. 4 does not form copolymers with natural drying oil at 20° and onlyyields films with difficulty after prolonged drying at 100-170°.

Liquid Silicones No. 2 and No. 3 give fairly good copolymeric organosilicon drying oils with tung oil or with No. 302 varnish.

This version of the method for the synthesis of organosilicon drying oils has the following characteristics: the procedure is simple, the films formed have good physical and mechanical properties, are water-repellent, oil-resistant, weather-resistant and fairly heat-resistant.

If an excess of silicone liquid (on the average, above 20%) is used, the physical and mechanical properties of the films deteriorate sharply; the films become brittle, especially on heating, and their adhesion becomes worse.

With 15-20% (by weight) of silicone liquids, the organosilicon copolymer drying oils have good physical, mechanical, insulating and other properties.

The organosilicon drying oils contain 1-6% of silicon (depending on the relative proportions of natural oil and organosilicon compound).

After 6 months of exposure under atmospheric conditions, films of the organosilicon drying oils had high elasticity (1 mm on the NIILK scale), high impact strength (50 cm by the Dupont test), and very low water absorption (1-2 mg/ 100 cm^2).

The properties of the organosilicon drying oils made by this version of the method are given in Tables 3 and 4 (experiments 8-20).

The acid numbers and saponification numbers were determined by the usual well-known methods [7]. Iodine numbers were determined by the Hübl method [7], which has been repeatedly tested in practice.

SUMMARY

1. Natural drying oils or heated vegetable oils can react with fully substituted orthosilicate esters and with polyalkyl (or aryl) siloxane liquids to give organosilicon drying oils.

2. The reaction of orthosilicate esters with unsaturated fatty acids (or their glycerides) increases the unsaturation of the latter (see Tables 1 and 3), so that high-quality organosilicon drying oils can be produced from oils which usually dry with difficulty in films (sunflower and cottonseed oils, etc.).

3. When liquid polyalkylsiloxanes react with unsaturated fatty acids (or their glycerides), the unsaturation of the latter decreases considerably (Tables 1, 2 and 3).

4. Organosilicon drying oils made by the methods described are of practical interest (both as coatings of various types and for impregnation of insulating and other materials), owing to their water repellence, oil resistance, adequate heat resistance and good insulating properties.

LITERATURE CITED

[1] K. A. Andrianov, "Method for Production of Synthetic Resins," Author's Certif. 71115.*

[2] K. A. Andrianov and O. I. Gribanova, J. Appl. Chem. 19, 6, 10-14 (1946).

[3] B. N. Dolgov, Progr. Chem. 1, 626-648 (1932).

[4] V. V. Korshak, Progr. Chem. 21, 121-174 (1952).

[5] Zbl., II, 3952 (1936).

* In Russian.

[6] A. Ya. Drinberg and N. S. Chervinskaya, J. Appl. Chem. 27, 10, 1307-1308 (1954).*

[7] V. S. Kiselev and R. M. Erastova, Practical Manual of Film-Former Technology (Goskhimizdat, 1940) pp. 26-30.**

Received (for the second time) May 15, 1957

*Original Russian pagination. See C. B. Translation.
** In Russian.

INVESTIGATION OF BITUMINOUS LIPTOBIOLITHS FROM TKIBULI FOR PREPARATION OF AN OIL VARNISH

P. N. Dzhaparidze, L. A. Drakin and L. R. Tvaradze

Laboratory of Coal Tar Chemicals of the Institute of Metals and Mining of the Academy of Sciences, Georgian SSR

Although liptobioliths are widely distributed in nature, large deposits are relatively rare. In the Soviet Union, liptobiolith deposits are found in the Far East – Upper Suifun rhabdopissites – and in the Caucasus –Tkibuli bituminous liptobioliths.

Tkibuli bituminous liptobioliths are found with the humus coals of the Tkibuli coal deposits, forming separate seams 0.90-2.50 meters thick.

Run-of-mine Tkibuli liptobioliths constitute a high-ash, low-grade fuel for which no uses have as yet been found.

Recent investigations [1] have shown that Tkibuli bituminous liptobioliths are excellent raw material for the production of synthetic liquid and gaseous fuel. The considerable contents of bituminous metamorphosed formations in Tkibuli bituminous liptobioliths, and the possibility of their isolation in fairly pure form (by simple gravitational beneficiation followed by elastic crushing of the concentrate) suggest other and more rational uses for this peculiar form of solid fuel [2]. One such use is the production of liptobiolith oil varnish. The present paper deals with a study of this problem.

EXPERIMENTAL

Preparation and qualitative characteristics of liptobioliths. For the preparation of liptobiolith oil varnish, Tkibuli bituminous liptobioliths were first crushed to 6 mm particles and beneficiated to sp. gr. 1.25. The yield of the concentrate was about 15%. The results of proximate analysis of run-of-mine liptobioliths and the concentrates are given in Table 1.

TABLE 1

Proximate Analysis of Run-of-Mine Liptobioliths and Concentrates

Products	W	A	V_g	S_{total}
Run-of-mine liptobiolith	2.29	39.26	64.43	0.92
Liptobiolith concentrate	1.62	10.78	69.14	0.83
Intermediate product	2.20	44.04	63.80	0.90

For removal of humus coal impurity, the concentrate was treated for a short time in a ball mill, when the more brittle humus coal was abraded and easily separated by sifting through a screen of 1 mm mesh.

The liptobiolith concentrate so obtained consisted of two kinds of bituminous formations (Figs. 1 and 2), the analyses of which are given in Table 2.

TABLE 2

Analyses of Bituminous Formations

Types of bituminous formations	Proximate analysis (%)				Ultimate analysis (%)			
	W	A	V_g	S_{total}	C_g	H_g	N_g	$(O+S)_g$
Bituminous rods and bodies	0.85	9.17	77.69	0.77	80.92	9.43	1.22	8.43
Dense uniform bituminous formations	1.12	11.53	77.11	0.91	79.61	8.73	1.44	10.22

Destructive distillation of liptobioliths. The bituminous formation isolated from run-of-mine Tkibuli liptobioliths are highly metamorphosed and are insoluble in organic solvents under normal conditions. To convert them into a soluble form and to establish the optimum conditions for their solubility, they were subjected to a process of thermal degradation, such as is used in the production of copal varnishes [3]. The same process was used for the production of liptobiolith oil varnish.

Fig. 1. Bituminous bodies.

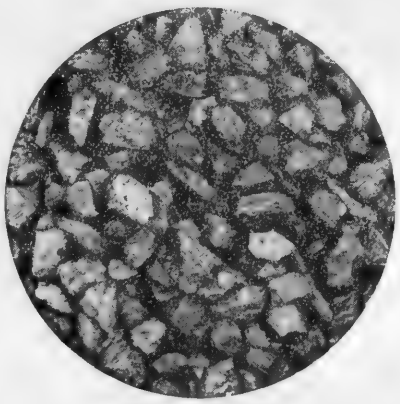

Fig. 2. Dense uniform bituminous formations.

A glass retort 250 cc in capacity was used for the thermal degradation; 50 g of the bituminous formations 2-3 mm in size was put into this. The retort was fitted with a thermometer and connected to a receiver for the liquid products. The retort was heated by means of a heater provided with a rheostat and ammeter. The heating rate was 10-12° per minute.

The bituminous formations began to melt at 360°, with evolution of liquid and gaseous products.

For determination of the optimum conditions for the conversion of the bituminous formations into a soluble form, they were heated to different temperatures and then dissolved in benzene in a Soxhlet apparatus. The effects of heat-treatment temperature on the solubility of the bituminous formations are plotted in Fig. 3.

Figure 3 shows that the solubility of the bituminous formations increases with the temperature of heat treatment up to 395-400°, and then decreases; the increase of solubility is accompanied by a decrease in the amount of insoluble residue, which reaches a minimum at 395-400°, corresponding to the temperature of maximum solubility of the bituminous formations, and then begins to increase with further increase of temperature. The yield of liquid products (primary tar) increases continuously with temperature and only reaches a maximum at 500-550°. At the maximum solubility of the bituminous formation the yield of liquid degradation products was usually 25-30%.

To give a more detailed picture of the solubility of degraded liptobiolith, the solubilities of the bituminous formations in various solvents, after heat treatment at 390-400°, are given in Table 3.

Preparation of liptobiolith oil varnish. For preparation of liptobiolith oil varnish, the bituminous formations were heated up to the so-called "miscibility point" [4], which is the temperature at which the best combination between the liptobiolith and the varnish oil occurs. This temperature generally corresponds to a decrease

of gas evolution, when the retort with the melt is free from vapor–gas mixture for a short time.

TABLE 3

Solubility of Degraded Liptobiolith in Various Solvents

Solvent	Amount of liptobiolith dissolved (%)
Ethyl alcohol	0
Acetone	12
Benzene	38
Dichloroethane	33
White spirit	25
Turpentine	50

A very interesting feature is that the miscibility point of Tkibuli liptobiolith lies within the range of its optimum degradation temperature, corresponding to the best solubility of the liptobiolith in benzene and other solvents.

Linseed oil, preheated to 200°, was put into a retort containing liptobiolith heated to the miscibility point; the temperature of the mixture was then raised again to the solubility temperature and a drop of the mixture was put onto a glass plate to test for clarity. The heating was then stopped; lead–manganese resinate drier was added at 200°, and a solvent – turpentine or white spirit – at 140-150°. When cool, the varnish was filtered and diluted with solvent to the required consistency.

The residue on the filtrate was washed with solvent, which was later used for dilution of the varnish.

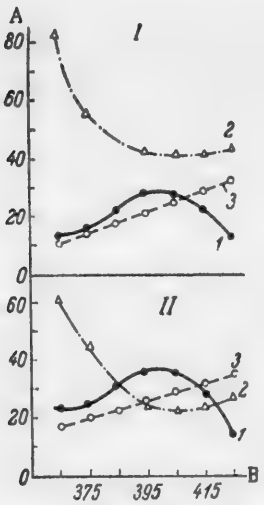

Fig. 3. Effects of heat treatment on bituminous formations. A) Solubility and yield (%); B) temperature (in ° C). I) Dense uniform bituminous formations; II) bituminous bodies. 1) Soubility in benzene; 2) yield of solid residue; 3) yield of liquid products.

The balance for the cooking of the liptobiolith varnish is given in Table 4. It is seen that the yield of varnish base is 72.4%, and that (apart from losses) the varnish base contains all the oil drier, solvent, and about 28% of the liptobiolith. The rest of the liptobiolith goes into the liquid products of thermal degradation (tar) and the solid oil-insoluble residue.

The varnish gives strong, drying films, with a pleasant brown color, high adhesion, luster and elasticity.

The tar and solid residue formed as by products during the cooking of the varnish are also very valuable and may be used in industry.

The analytical data for the tar, given in Table 5, show that the tar has low density and molecular weight, a low phenol content, and a high content of low-boiling fractions. Thus, even these incomplete data suggest that the tar may be an excellent raw material for the production of various kinds of synthetic liquid fuel.

The solid residue, with its relatively low ash content (33.11%) and high calorific power (5595 cal/kg), can be an excellent fuel for power generation; it may be burned either as dust or in the form of briquets.

The briquets, made by hot pressing withoug binder, had high mechanical strength and weathering resistance.

Analyses of the solid residue and of the briquets made from it are given in Table 6.

In view of the possibility of higher concentration of the liptobioliths, with regard both to the mineral impurities and to the organic content, it is likely that the cooking balance for the varnish can be improved appreciably. This is confirmed by our results for the cooking of a varnish based on the bituminous bodies only, which are the purest bituminous formations (Fig. 1, Table 7). It is seen that when the varnish is made with the bituminous

bodies only, the yield of varnish base increases considerably (to 83.14%),* with decreased yields of liquid products (tar) and solid residue. The characteristics of the varnish and tar do not differ from those of the varnish and tar obtained from an average sample of liptobiolith concentrate. The solid residue contains much more ash (69.50%) and has a lower calorific power (2418 cal / kg).

TABLE 4

Varnish Cooking Balance

Used			Obtained		
Substances	Amounts		Substances	Amounts	
	in g	in %		in g	in %
Liptobiolith	50	37.31	Varnish base	97.0	72.40
Varnish oil	50	37.31	Liptobiolith residue	20.3	15.14
Drier	4	2.99	Tar	15.7	11.71
Solvent	30	22.39	Gas and losses.	1.0	0.75
Total	134.0	100.00	Total.	134.0	100.00

TABLE 5

Analytical Data for Tar

Density	Molecular weight	Group composition (%)			Fractional composition (%)			
		bases	carboxylic acids	phenols	to 180°	180-225°	225-325°	residue > 325° and losses
0.9000	192	0.84	0.70	5.00	15.1	11.9	34.6	38.4

TABLE 6

Substance	Proximate analysis (%)			Ultimate analysis (%)				Calorific power Q (in cal / / kg)	Crushing strength of briquets (in kg/ cm^2)
	W	A	V_g	C_g	H_g	N_g	$(O+S)_g$		
Solid residue after filtration.	1.18	33.11	44.47	77.56	7.73	1.68	12.85	5595	–
Briquet from residue. .	0.60	35.76	37.35	75.13	7.23	1.92	15.77	5270	290

TABLE 7

Varnish Cooking Balance

Used			Obtained		
Substance	Amounts		Substance	Amounts	
	in g	in %		in g	in %
Bituminous bodies	50	37.31	Varnish base.	111.4	83.14
Varnish oil	50	37.31	Residue	7.5	5.60
Drier	4	2.99	Crude tar.	11.6	8.66
Solvent.	30	22.39	Gas and losses.	3.5	2.60
Total	134	100.00	Total	134.0	100.00

*If we ignore losses of oil and solvent, the varnish base contains 54.8 % of the bituminous bodies.

SUMMARY

The results of the investigation suggest new ways of utilization of Tkibuli bituminous liptobioliths. It is shown that they can be used for the production of liptobiolith oil varnish, synthetic liquid fuels, and high-quality fuel briquets.

LITERATURE CITED

[1] P. N. Dzhaparidze, L. A. Drakin and O. A. Loladze, Trans. Inst. Metals and Mining, Acad. Sci. Georgian SSR 3, 47 (1950).*

[2] P. N. Dzhaparidze and L. A. Drakin, J. Appl. Chem. 27, 3, 341 (1954).**

[3] A. Ya. Drinberg, Technology of Film Formers (Goskhimizdat, 1948) p. 383. *

[4] V. S. Kiselev, Practical Manual of Film-Former Technology (Goskhimizdat, 1948) p. 251.*

Received May 14, 1956

---

*In Russian

**Original Russian pagination. See C. B. Translation.

CAUSES OF THE GUMMING OF DIESEL FUELS DURING STORAGE

S. R. Sergienko and P. N. Galich

When Diesel fuels are stored for any length of time, gummy products are generally formed in them, lowering their quality and creating a number of difficulties in the use of these gummed fuels. As normal and interrupted operation of fleets of trucks in a large country cannot be maintained without the existence of reserve stores of engine fuel, the question of gumming of engine fuels during prolonged storage becomes not only of great scientific interest, but is of serious significance as a purely economic problem, in relation to the production and storage costs of fuel. It is therefore not surprising that many research workers and practical technologists both in this country and abroad have been greatly concerned with studies of the causes and sources of gum formation in both synthetic and natural hydrocarbon mixtures of various composition (various petroleum fractions and different kinds of motor fuels and oils). One of the main difficulties met in investigations of gumming processes during the storage of fuels is that fuels are usually stored at relatively low temperatures (10-30°) and gumming is very slow in these conditions. Of course, the process can be artificially accelerated by increase of temperature, and this is usually done under laboratory conditions, but the results obtained are quite different, as at high temperatures the oxidation of hydrocarbons mainly yields oxidation products of low molecular weight, whereas slow oxidation of hydrocarbons at low temperatures leads to the formation of compounds of higher molecular weight owing to the occurrence of condensation processes. Very little information is available on the nature of the processes of gum formation at low temperatures under conditions of normal storage of Diesel fuels, while interest in them is very great, especially at the present time, when the relative proportion of Diesel fuel in the total consumption of motor fuel is greatly increasing.

We studied the processes of accumulation of gummy substances during prolonged storage of Diesel fuels and of individual classes of hydrocarbons contained in these fuels, in order to determine the influence of the chemical nature of a fuel on its tendency to gumming.

EXPERIMENTAL

The principal materials chosen for the work were three samples of Diesel fuel of different origins and therefore of different hydrocarbon composition[1, 2]: 1) Balakhany (Baku winter) oil, GOST 4749-49, 2) Surakhany (Baku summer) oil, GOST 4749-49, and 3) synthetic oil, GOST 4749-49.

The group composition and properties of these Diesel fuels are given in Table 1. Individual groups of hydrocarbons – aromatic, normal paraffins, and a mixture of cycloparaffins and branched paraffins – were isolated from the winter Diesel fuel (BW) by chromatographic separation on silica gel and reaction with carbamide [3].

The sample of BW fuel was first degummed by a method described earlier [1].

The properties and elementary composition of the groups of hydrocarbons isolated from BW fuel are given in Table 2.

Previously degummed samples of the Diesel fuels (BW, BS, NZ) and of the groups of hydrocarbons isolated from BW were stored for a long time in glass vessels. Data on the storage times are given in Table 3. All the samples were stored under the same conditions, at the window of the laboratory.

After storage, all the samples were studied in detail; the group and elementary compositions and the principal properties were determined.

TABLE 1

Properties of the Original Diesel Fuel Samples

Name of sample	Boiling range (°)	Density d_4^{20}	Molecular weight	Iodine number	Acid number	Chemical group composition (wt. %)				
						Paraffinic hydrocarbons	Naphthenic hydrocarbons	Aromatic hydrocarbons	Unsaturated hydrocarbons	Tar
Baku winter (BW)	200-365	0.8484	211	0.9	Traces	54.5	16.2	27.8	0.7	0.82
Baku summer (BS)	230-400	0.8430	226	0.4	0.4	59.9	22.0	17.5	0.3	0.32
Synthetic (NZ)	193-328	0.8326	182	3.2	0.1	54.8	27.8	14.1	2.5	0.78

TABLE 2

Composition and Properties of Groups of Hydrocarbons Isolated from Degummed BW Diesel Fuel

Hydrocarbon group	Properties			Elementary composition (%)		
	b.p. (°C)	d_4^{20}	n_D^{20}	C	H	S
n-Paraffinic	45-180/3 mm	0.7973	1.4434	84.84	15.12	0
Cyclo- and isoparaffins.	40-198/3 mm	0.8249	1.4555	85.84	14.23	0
Aromatics	50-198/3 mm	0.9555	1.5386	89.65	10.20	0.15

The determinations of functional groups (peroxide, acid and hydroxyl numbers, and the saponification numbers) were carried out by potentiometric titration [4].

TABLE 3

Sample	Storage time (years)
BW fuel.	5
BS fuel	5
NZ fuel.	5
BW fuel.	2
Aromatics from BW fuel . . .	2
Cyclo- and isoparaffins from BW fuel.	2

After the general characteristics (Table 4) of the stored samples had been determined, the samples were separated into the principal constituents: carboids, asphaltenes, tars and hydrocarbons.

The composition and properties of Diesel fuel samples (BW, BS, NZ) kept for five years in glass vessels at the laboratory window are given in Table 5.

It is seen that the samples form the following sequence in order of the amounts of oxidative condensation products formed during storage: NZ (5.8%) > > BW (4.9%) > BS (4%).

The composition and properties of the gums change regularly in the same sequence: the acid and hydroxyl numbers, the saponification numbers, the oxygen content, and the C/H ratio all increase.

The asphaltenes of all these fuel samples have higher molecular weights, higher oxygen, sulfur and carbon contents, and higher C/H ratios then the corresponding tars.

The fact that NZ fuel had the highest content of highly condensed products – tars and asphaltenes (especially the latter) – can be attributed to its hydrocarbon group composition (the presence of unsaturated hydrocarbons (2.7%), a high content of cycloparaffins (27.8%) and a low content of aromatics (14.1%)).

Gurvich [5] obtained qualitatively similar results for kerosene containing unsaturated compounds, after 3 months of storage in sunlight with access of air.

The gums isolated from our samples of the different fuels also differed appreciably in external appearance. The gums from NZ fuel were viscous, almost liquid yellowish substances, whereas the gums from BW and BS fuels were viscous, almost solid substances, dark brown in color.

It follows from the data in Table 5 and Fig. 2 that gum formation in BW fuel is particularly rapid during the first 2 years of storage, and it slows down appreciably later (during the first two years 2.6% of tars and asphaltenes was formed, and after 5 years the total was 4.9%).

TABLE 4

Characteristics of Fuel Samples and their Constituent Hydrocarbon Groups after Prolonged Storage

Sample	Peroxide number	Acid number	Saponification number	Total tars and asphaltenes (%)	Storage time (years)
BW fuel	Traces	0.8	7.6	4.9	5
BS fuel	Traces	0.7	5.0	4.0	5
NZ fuel	Traces	1.6	6.8	5.8	5
BW fuel	Traces	1.9	3.8	2.6	2
Aromatics of BW fuel	Traces	3.9	9.7	6.2	2
Cyclo- and isoparaffins of BW fuel	38.5	1.8	8.4	0	2

This indicates that the tars and asphaltenes formed in fuels during storage begin to inhibit further formation of tar after a definite critical concentration has been reached.

The retardation of oxidative processes of gum formation in fuels with accumulation of tars under conditions of static storage can be explained to some extent by the mechanism of the process itself.

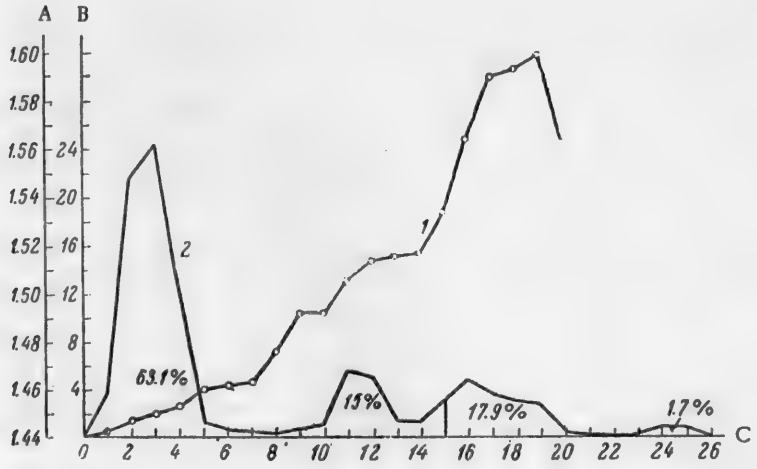

Fig. 1. Change of the hydrocarbon composition of BW fuel after two years of storage.
A) Refractive index n_D^{25} (1); B) yield, % (2); C) fraction numbers.*

When Diesel fuel samples were kept for a long time in glass vessels, a black band of tarry deposits was formed in all cases at the fuel–air boundary around the inner wall of the vessel. Some of the products of oxidative condensation dissolved in the fuel, coloring it deeply, while the products of highest molecular weight were deposited in the form of a black band on the walls of the vessel. This band is therefore important evidence that the processes of gum formation during storage take place at the fuel–air interface. It is clear, therefore, that gum formation in the fuel should be less with smaller and more constant fuel–air interface (i.e., liquid surface), and with less replenishment of the gas phase over the liquid fuel, i.e., of the atmosphere. This must be taken into consideration in practical problems relating to the prolonged storage of Diesel fuels.

Direct interaction between atmospheric oxygen and the hydrocarbon surface leads to rapid accumulation of oxygen-containing organic compounds (peroxides and their decomposition products) in the upper layer of the

*Captions to Figs. 1 and 2 as in original.

TABLE 5

Composition and Properties of Diesel Fuels after Storage

Composition of Diesel fuel samples		Weight		Acid number	Saponification number	Hydroxyl number	Molecular weight	Elementary composition				C/H
		g	%					C	H	S	O (by difference)	
NZ after 5 years	Residue insoluble in benzene	2.56	1.8	—	—	—	—	—	—	—	—	—
	Asphaltenes	2.14	1.5	—	—	—	441.4	71.25	7.55	—	21.2	9.4
	Tars	4.06	2.5	37.0	109.0	79.3	315.8	76.71	9.75	—	13.54	7.8
	Hydrocarbons and losses	131.3	94.2									
BW after 5 years	Residue insoluble in benzene	1.1	0.8	—	—	—	—	—	—	—	—	—
	Asphaltenes	0.76	0.6	—	—	—	—	71.59	6.53	1.21	20.67	10.9
	Tars	4.65	3.5	28.8	99.7	65.5	321 4	77.32	9.18	1.07	12.43	8.3
	Hydrocarbons and losses	127.1	95.1									
BS after 5 years	Residue insoluble in benzene	1.00	0.5	—	—	—	—	—	—	—	—	—
	Asphaltenes	1.2	0.6	—	—	—	—	76.90	7.37	1.65	14.08	10.4
	Tars	6.0	2.9	27.0	98.2	80.4	317.3	78.72	8.9	1.07	11.31	8.8
	Hydrocarbons and losses	196.8	96.0									
BW after 2 years	Residue insoluble in benzene	0.59	0.3	—	—	—	—	—	—	—	—	—
	Asphaltenes	0.87	0.4	—	—	—	418.4	73.21	7.19	1.80	17.80	10.2
	Tars	3.85	1.9	6.1	26.4	44.0	306.6	77.16	8.88	1.64	12.32	8.7
	Hydrocarbons and losses	194.69	97.36									

fuel; these compounds are the primary source of the tars. The rate of this first stage of tar formation, which greatly depends on such factors as the temperature, oxygen concentration, and the degree of contact between oxygen and the fuel, gradually decreases with increasing concentration of tars and asphaltenes in the upper layer of fuel (in contact with the air), and this leads to a decrease in the gumming rate. Qualitatively, the course of gumming of BW Diesel fuel during prolonged storage at room temperature (16-25°) resembles a process which takes place at higher temperatures (liquid-phase oxidation at 150°) [2], but differs from it in its rate (being slow); this is to be expected in view of the considerable differences of temperature and the degree of contact between oxygen and the fuel. To determine the role of individual groups of hydrocarbons in tar formation in fuels during storage, a study was made of the composition and properties of the aromatic and cycloparaffin–isoparaffin fractions isolated from BW Diesel fuel and then stored for 2 years under the same conditions as the BW fuel itself. The data in Table 6 show a fairly clear difference in the behavior of the different classes of hydrocarbons during storage. The cycloparaffin–isoparaffin fraction was quite free from tars and asphaltenes after two years of storage, contained a considerable amount of peroxides (peroxide number 38.5), and had low acid number (1.8) and saponification number (8.4).

TABLE 6

Composition and Properties of Hydrocarbons Separated from BW Fuel and Stored for 2 Years

Group composition of hydrocarbons samples after storage	Weight		Acid number	Saponification number	Hydroxyl number	Molecular weight	Elementary composition (%)				C/H
	g	%					C	H	S	O (by difference)	
Aromatic hydrocarbons from BW sample											
Residue insoluble in benzene	0.1	0.2	–	–	–	–	–	–	–	–	–
Asphaltenes	0.8	1.6	–	–	–	440.0	77.0	7.58	2.12	13.30	10.15
Tars	2.2	4.4	–	–	–	316.2	77.3	8.15	1.20	13.35	9.44
Hydrocarbons and losses	46.9	93.8	–	–	–	–	–	–	–	–	–
Cyclo- and isopraffins from BW sample											
Tars and asphaltenes	–	–	–	–	–	–	–	–	–	–	–
Hydrocarbons	50.0	100.0	–	–	–	–	–	–	–	–	–

After the same storage period the aromatic fraction contained 6.2% of tars and asphaltenes, peroxides were absent, while the contents of acids (acid number 3.9) and esters (saponification number 9.7) differed little from the corresponding values for the cyclo- and isoparaffin fraction. The sample of degummed BW fuel from which these hydrocarbon fractions were isolated occupies an intermediate position between these two fractions. In it was formed 2.6% of tars and asphaltenes, peroxides were absent, the acid number was 1.9 and the saponification number was 3.8. These results show the oxidation of the cyclo- and isoparaffin fraction has a lower induction period at low temperatures, and therefore at the end of two years of storage only the first stage of the gumming process was completed (the maximum concentration of peroxides was reached), and the second stage – decomposition of peroxides with formation of acid and neutral products – began; condensation of these products with formation of tars and asphaltenes constitutes the third stage of the process. The last stage of oxidation – tar formation – had not started at the end of 2 years. The aromatic fraction has a much shorter induction period under the same conditions, and the critical concentration of peroxides at which they begin to decompose and the second stage begins is evidently lower; therefore after two years this fraction did not contain peroxides, and considerable amounts of tars and asphaltenes were formed; however, the sources of the latter were far from exhausted, as shown by the relatively high contents of acids (acid number 3.9) and esters (saponification number 9.7) in the oxidation products. The sample of the original BW fuel not only passed through the stage of peroxide accumulation, like the aromatic fraction, but was close to completion of the whole gumming process. This is shown by the absence of peroxides and the low contents of oxygen-containing acids and esters, despite the fact that its tar content was less than half

that of the tar content in the aromatic fraction. These data clearly reveal the role of aromatics as the main source of gumming in Diesel fuel. However, this only applies to fuels with considerable contents of aromatics (25% and over) in absence of unsaturated hydrocarbons. Confirmation of this view is provided by data on changes of the group composition of BW Diesel fuel after prolonged storage (2 and 5 years).

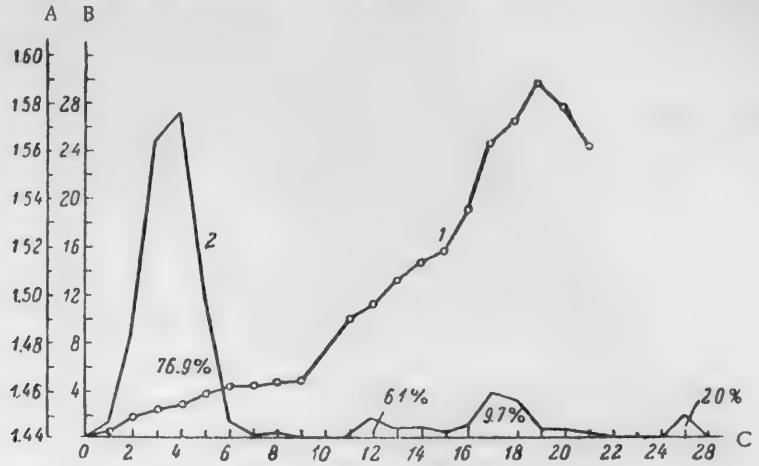

Fig. 2. Change of the group composition of BW fuel after two years of storage.

A) Refractive index n_D^{22} (1); B) yield, % (2); C) fraction numbers.*

The group hydrocarbon composition of these samples was determined by adsorption chromatography [6, 7]; the results are plotted in Figs. 1 and 2.

These results show that prolonged storage results in an appreciable decrease of the aromatic content.

SUMMARY

1. Tar formation in Diesel fuels of various group compositions, and in the main groups of hydrocarbons present in Diesel fuels, during prolonged storage (2-5 years) at room temperature in presence of air was studied; it was found that under these conditions the greatest tendency to gumming is found in aromatic hydrocarbons isolated from direct-distillation Diesel fuel; this fraction contained 6.2% of tars and asphaltenes after two years of storage.

2. In contrast to the aromatic hydrocarbons, cyclo- and isoparaffins isolated from the same direct-distillation Diesel fuel have a longer induction period of oxidation when stored at low temperatures; therefore after two years of storage they contained no tars, but had a high content of peroxides.

3. Investigations of the hydrocarbon group composition and of the contents of oxygen compounds in Diesel fuel after prolonged storage showed that aromatic hydrocarbons are the main source of gums in direct-distillation Diesel fuels containing considerable amounts of aromatics and free from unsaturated hydrocarbons.

4. It is shown that when Diesel fuels are stored for a long time at room temperature the process of gumming, which is initially rapid, gradually slows down after a definite critical concentration of tar is reached. Self-retardation of the gumming processes is caused by the oxidation products, primarily the tars, at a definite stage of oxidation.

LITERATURE CITED

[1] S. R. Sergienko, I. O. Delona and B. E. Davydov, Proc. All-Union Conference on the Chemistry and Processing of Petroleum (Azerbaidhzan SSR Press, 1953) p. 80.**

[2] S. R. Sergienko and P. N. Galich, J. Appl. Chem. 29, 12, 1717 (1956).***

[3] L. M. Rozenberg and I. S. Genekh, Proc. Acad. Sci. USSR 84, 523-526 (1952).

[4] S. R. Sergienko, N. A. Izmailov, L. L. Spivak and P. N. Galich, J. Appl. Chem. 28, 10, 315-322 (1955).***

* Captions to Figs. 1 and 2 as in original.

** In Russian.

*** Original Russian pagination. See C. B. Translation.

[5] L. G. Gurvich, Scientific Principles of Petroleum Processing (ONTI, 1924) p. 38.*

[6] S. R. Sergienko and A. A. Mikhnovskaya, Proc. Acad. Sci. USSR 91, 1, 103-106 (1953).

[7] S. R. Sergienko and A. A. Mikhnovskaya, Trans. Commission on Analytical Chemistry (Izd. AN SSSR, Moscow, 1955) pp. 162-170.*

Received March 2, 1957

* In Russian.

INFLUENCE OF HEXAMETHYLENETETRAMINE ON THE CONVERSION OF POLYVINYL CHLORIDE INTO A SPACE POLYMER

G. S. Petrov and V. F. Prosvirkina

The Moscow Scientific Research Institute of Plastics

Some linear macromolecules have the characteristic property of forming three-dimensional compounds (space polymers) under certain conditions. The conversion of linear into space polymers has been studied in a number of compounds. Korshak and his associates studied the formation of a space structure in polyamides [1] and polyvinyl alcohol [2]. A whole series of papers by Drinberg et al. deals with studies of the conversion of various linear into space polymers [3-5], including the conversion of polyvinyl chloride in film form [6]. Berlin and Denker studied the conversion of chlorinated polyvinyl chloride into the space polymer by the action of heat in presence of metal oxides [7, 8].

The present paper deals with the solid-phase conversion of polyvinyl chloride into a space polymer under the action of hexamethylenetetramine. The necessity for this investigation arose in relation to the problem of compatibility of polyvinyl chloride with phenol–formaldehyde resins in molding materials "hardened" by means of hexamethylenetetramine.

EXPERIMENTAL

The material used was PB-4 polyvinyl chloride resin made by emulsion polymerization with the use of benzoyl peroxide catalyst. The resin conformed to the specifications of GOST 3119-46, and had the following characteristics: white color, moisture 0.034%, ash 0.1%, iron 0.004%, absolute viscosity 63 centipoises.

TABLE 1

Effect of Hexamethylenetetramine on Variations of the Content of Acetone-Soluble Fraction in Polyvinyl Chloride During Rolling

Hexamethylenetetramine (%)	Acetone-soluble fraction (%)
0	26.4
0.48	25.2
1.99	23.7
4.8	21.8
11.5	18.3

Molded cylindrical specimens 4 mm high and 10 mm in diameter were used. Powdered mixtures of polyvinyl chloride with different amounts of hexamethylenetetramine were molded in a laboratory hand press at 140° under 134.5 kg/ cm^2 pressure for 15 minutes and allowed to cool in the press.

Two methods were used for preparation of the molding mixtures: 1) the components were mixed in a porcelain mortar (we refer to these as "nonrolled mixtures," and 2) the components were mixed in a mortar and then rolled for 20 minutes at 130° ("rolled mixtures").

Mixtures of polyvinyl chloride with hexamethylenetetramine, like polyvinyl chloride alone, formed into sheets when rolled, but darkened rapidly and became less flexible. The sheets were ground in a "Perplex" mill.

The powdered mixtures were extracted in Soxhlet extractors to determine the variations of the content of acetone-soluble fraction in polyvinyl chloride rolled with different amounts of hexamethylenetetramine. The results are given in Table 1; it is seen that the amount of acetone-soluble fraction in polyvinyl chloride decreased with increasing hexamethylenetetramine content. The conversion of polyvinyl chloride into the space polymer

was estimated from variations of the swelling and solubility of samples in cyclohexanone, and also by the thermomechanical method described by Kargin et al. [9-11]. This method can be used for studying changes in the physical and mechanical properties of a polymer as shown by variations of deformation produced by unilateral compression over a wide temperature range.

An instrument* operating on the principle of the Kargin balance, but designed to record larger deformations, was used. This was achieved by the use of the IZV-1 optical length-measuring instrument for measurement of the deformation. The applied load was 0.71 kg/cm^2.

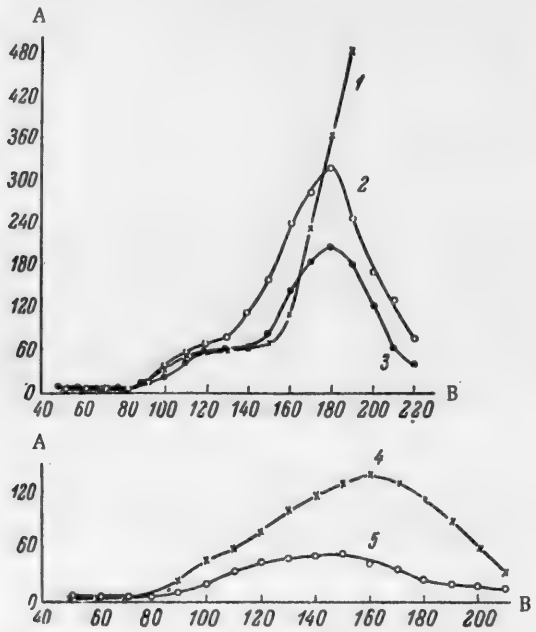

Fig. 1. Deformation—temperature curves for rolled mixtures of polyvinyl chloride and hexamethylenetetramine.
A) Deformation; B) temperature (in °C). Contents of hexamethylenetetramine (in %): 1) original polyvinyl chloride; 2) 0.48; 3) 1.99; 4) 4.8; 5) 11.5.

Figs. 1 and 2 give a series of thermomechanical curves representing the variations of deformation with temperature for rolled and nonrolled mixtures of polyvinyl chloride with different amounts of hexamethylenetetramine (apart from hexamethylenetetramine, diphenylamine and diphenylurea were used in the nonrolled mixtures).

Curve 1, Fig. 2, represents the original polyvinyl chloride. The second-order transition temperature ("glass temperature") T_g in this case is 80°. The elastic and flow regions are clearly seen. In the flow region, the deformation continued to increase over the entire temperature range of the experiment (from 20 to 210-220°). These deformations could be measured with the new instrument, but they extended far beyond the limits of the graph. Curve 1 in Fig. 1 refers to polyvinyl chloride, again without additions, but rolled at 130° for 20 minutes. This curve was almost the same as the curve for the original, nonrolled polyvinyl chloride. The other curves in Figs. 1 and 2, corresponding to mixtures of polyvinyl chloride with hexamethylenetetramine, diphenylamine and diphenylurea, differed from the curves for the original polyvinyl chloride. For example, the curves in Figs. 1 and 2 (with the exception of Curve 5 of Fig. 1, and Curves 4 and 5 of Fig. 2, corresponding to 11.8 and 17.7% of hexamethylenetetramine) had clearly defined maxima in the flow region. Flow of the polymer ceased on further increase of temperature, and the magnitude of the maximum deformation began to decrease. Flow was inhibited by other processes leading to formation of cross links between the polymer chains.

It has been pointed out by Kargin and Shteding [11, 12] and by Tager et al. [13] that the appearance of a maximum on the thermomechanical curve is the consequence of formation of reactive groups, their interaction, and formation of cross links to give a spatial network. The temperature corresponding to the maximum on the deformation curve is termed the "temperature of intensive structurization" by Tager.

It follows from Figs. 1 and 2 that as the hexamethylenetetramine content of the polymer increased, the magnitude of the maximum deformations decreased and the maxima on the curves were displaced toward lower temperatures. In Tager's terminology [13], the temperature of intensive structurization decreased.

All this indicated an increase in the number of cross links in the polymer. When this number was large enough, the maximum on the curve almost disappeared; the whole course of the curve and the magnitude of the maximum deformation indicated complete loss of fluidity (Curve 5 on Fig. 1 and Curves 4 and 5 of Fig. 2).

* The instrument was constructed by L. A. Igonin in the Moscow Scientific Research Institute of Plastics.

Comparison of the thermomechanical curves for rolled (Fig. 1) and nonrolled (Fig. 2) mixtures leads to the conclusion that the same amount of hexamethylenetetramine resulted in the formation of a denser network in rolled than in nonrolled mixtures.

We studied the influence of temperature on the formation of a three-dimensional structure in polyvinyl chloride under the influence of hexamethylenetetramine, diphenylamine and diphenylurea. In these experiments specimens made from nonrolled mixtures were heated for 3 hours in an oven at 130, 150 and 170°.

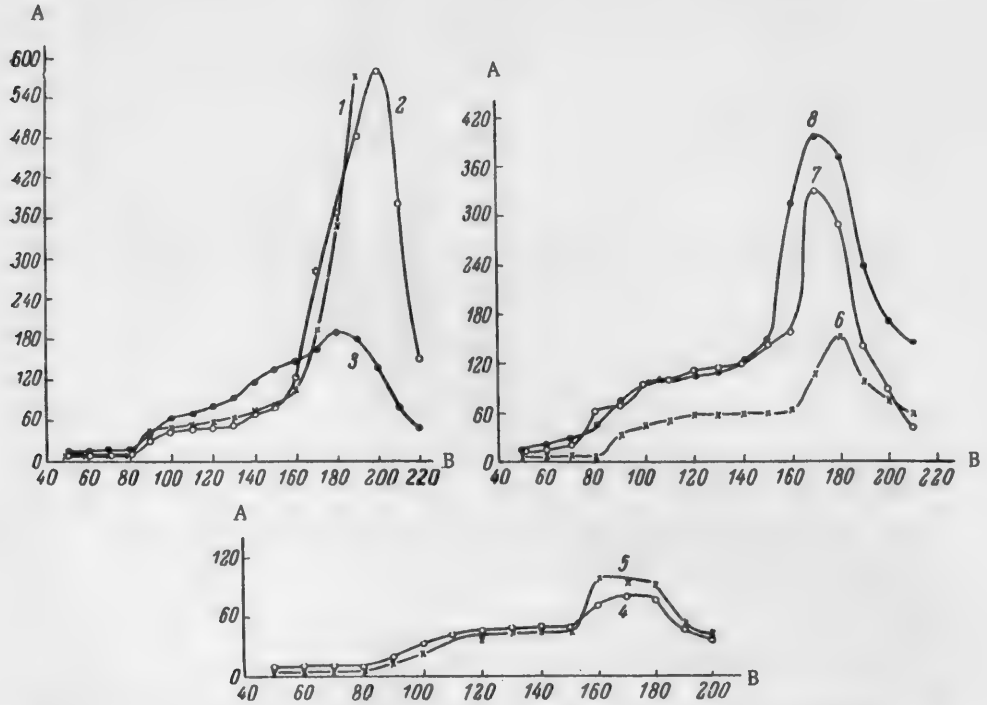

Fig. 2. Deformation—temperature curves for nonrolled mixtures of polyvinyl chloride with hexamethylenetetramine, diphenylamine and diphenylurea.
A) Deformation; B) temperature (in °C).
Contents of hexamethylenetetramine (in %): 1) original polyvinyl chloride; 2) 0.48; 3) 1.99; 4) 11.5; 5) 17.7.
Additions of 4.8% of: 6) hexamethylenetetramine; 7) diphenylamine; 8) diphenylurea.

Specimens made from rolled mixtures lost their homogeneity after being heated; the original particles from which they were compounded were clearly seen all over their surface. These specimens rapidly disintegrated in the solvent. Therefore they were not used in the subsequent experiments.

The specimens were found to lose weight when heated (Table 2). It is seen that the greatest weight loss occurred at 170°.

The percentage loss of weight increased with increasing hexamethylenetetramine content, approaching a maximum at 4.8% content. Specimens containing 4.8% of diphenylamine also showed a high weight loss. Specimens containing hexamethylenetetramine and diphenylamine liberated large amounts of gas containing hydrogen chloride when heated (especially at 170°). All these specimens decreased by 2-2.5 mm in diameter, without change of shape, when heated in the oven, and also after the thermomechanical tests. The specimens heated in the oven were used for thermomechanical tests and for determination of swelling and solubility during 120 hours in cyclohexanone at room temperature. Data on the swelling and solubility of unheated and heated specimens in cyclohexanone are presented in Table 3. Because of the considerable solubility of unheated specimens containing from 0 to 1.99% of hexamethylenetetramine and 4.8% of diphenylamine and diphenylurea, weight increases caused by swelling could not be detected. It follows from the data in Table 3 that the solubility in cyclohexanone decreased and the swelling increased with increasing hexamethylenetetramine contents and with increase of the pre-

heating temperature. For example, the solubility in cyclohexanone of specimens heated at 170 and 150°, containing 4.8% and over of hexamethylenetetramine or diphenylamine, is zero, apart from the specimens containing diphenylamine and heated at 150° (the solubility of these was not zero, but also very low). The swelling of these specimens was also very slight, indicating the formation of a dense spatial network in the polymer.

TABLE 2

Effects of Hexamethylenetetramine, Diphenylamine and Diphenylurea on the Weight Loss of Polyvinyl Chloride on Heating

Contents of additives (%)		Weight loss (%) when heated at (°C)		
		130	150	170
Hexamethylene-tetramine	0	0.26	0.39	2.73
	0.3	0.36	0.59	5.9
	0.48	0.38	0.53	5.64
	1.99	0.4	1.39	16.7
	4.8	0.46	3.3	30.1
	11.5	0.91	5.5	33.7
	17.7	0.87	5.4	33.1
Diphenylamine, 4.8		0.58	1.63	17.8
Diphenylurea, 4.8		0.35	1.08	10.0

TABLE 3

Effects of Hexamethylenetetramine, Diphenylamine, Diphenylurea, and of the Heating Temperature on the Swelling and Solubility of Polyvinyl Chloride in Cyclohexanone at 20°

Contents of additives (%)		Unheated specimens		Heating temperature (°C)					
				130		150		170	
		swelling	solubility	swelling	solubility	swelling	solubility	swelling	solubility
		%		%		%		%	
Hexamethylene-tetramine	0		87.1	9.8	71.0	29.2	60.7	89.1	41.9
	0.29	—	72.5	25.9	50.4	45.7	34.5	81.7	21.5
	0.48	—	69.2	25.1	42.6	39.9	30.7	83.4	17.3
	1.99	—	66.9	47.8	27.3	52.7	17.7	27.9	8.3
	4.8	10.4	44.5	47.5	9.2	26.0	0	0.2	0
	11.5	37.0	25.3	26.1	5.6	9.6	0	3.6	0
	17.7	34.8	27.5	27.6	5.9	11.9	0	3.8	0
Diphenylamine 4.8		—	85.7	18.7	30.3	30.3	0.71	1.8	0
Diphenylurea, 4.8		—	88.7	13.9	47.8	64.9	37.4	78.5	11.8

The thermomechanical curves for specimens heated at different temperatures are given in Fig. 3. It is seen that the density of the spatial network increased both with increasing hexamethylenetetramine content and with increase of the heating temperature, and the space polymer was formed through the whole bulk of the specimens; this influenced the course of the curves, and the magnitude of the maximum deformation decreased. For specimens of polyvinyl chloride without additives, heated at 130 and 150°, the deformation continued to increase over the entire temperature range (Curves 1 and 3 in Figs. 3, a and 3, b). The deformation curves for similar specimens, but heated at 170° (Fig. 3, c) indicate extensive degradation of the polymer and retention of flow properties in a definite temperature range. The action of diphenylamine and diphenylurea is only effective with heating temperature of 170°, and is very slight at 130°

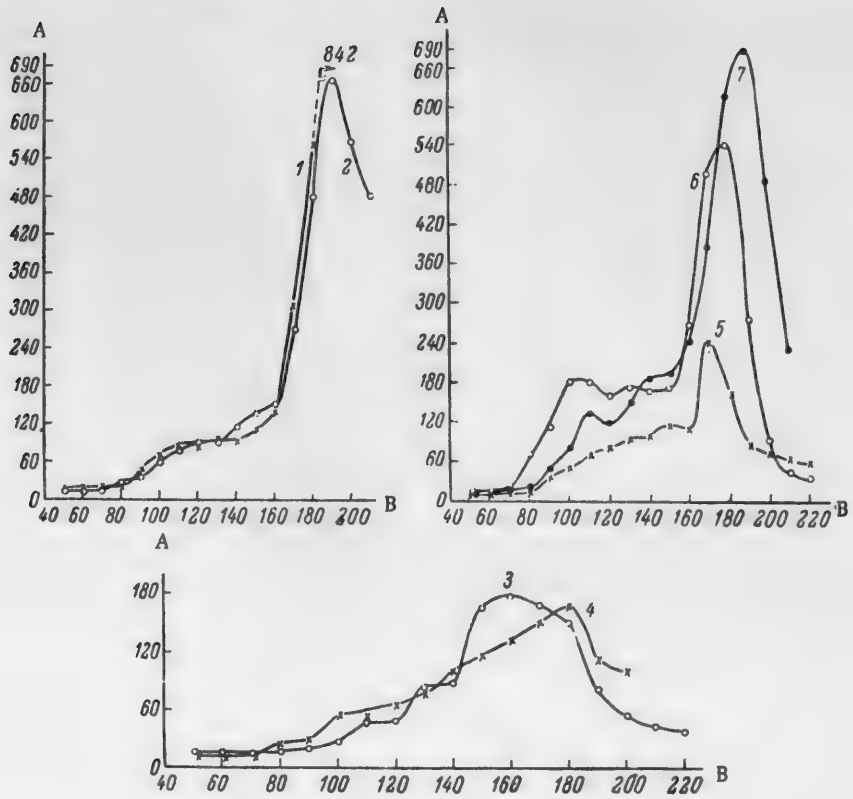

Fig. 3a

Fig. 3. Deformation–temperature curves for oven-heated specimens of polyvinyl chloride containing additions of hexamethylenetetramine, diphenylamine and diphenylurea.

A) Deformation; B) temperature.

Heating temperatures (in °C): a) 130; b) 150; c) 170.

Contents of hexamethylenetetramine (in %): 1) original polyvinyl chloride; 2) 0.48, 3) 11.5; 4) 17.7.

Additions of 4.8% of: 5) hexamethylenetetramine; 6) diphenylamine; 7) diphenylurea.

It follows from a comparison of the thermomechanical curves for unheated specimens (Fig. 2) and for specimens heated at 130 and 150° (Fig. 3, a and 3, b), and from the solubility data, that the curves for specimens heated at 150°, and especially at 130°, show considerably larger maximum deformations than the curves for unheated specimens containing the same amounts of additives. According to the data in Table 3, specimens preheated at 150 and 130° had lower contents of soluble polymer than the unheated specimens.

This discrepancy can be explained as follows: during the thermomechanical tests the specimens were deformed as well as being heated gradually from 20 to 220°. As has been pointed out by Slonimsky, Kargin and Golubenkova [14], deformation causes displacement of the interacting groups and increases the probability of collisions between them; i.e., it accelerates the reaction. When specimens which had not been preheated were subjected to the thermomechanical tests, denser spatial networks were formed throughout the bulk of the specimens, as under these conditions there was time for the necessary regrouping of the molecules to occur. When the specimens were heated in the oven, they were at once subjected to high temperatures and the cross linking was so rapid that there was not time for the necessary molecular regrouping; in this case the density of the spatial network was inadequate, and a space polymer was formed only in isolated regions of the specimens; namely, on the surface and in the center (when such a specimen was placed in the solvent, the outer shell and a black central core remained undissolved). Because of this, the maximum deformations of these specimens were greater, as Figs. 2 and 3 show. The structure during the preheating remained "fixed." When the specimens were heated at 170°, and in

some cases at 150°, there was time for more complete interaction of the reactive groups, probably owing to an increase of their reactivity at these temperatures.

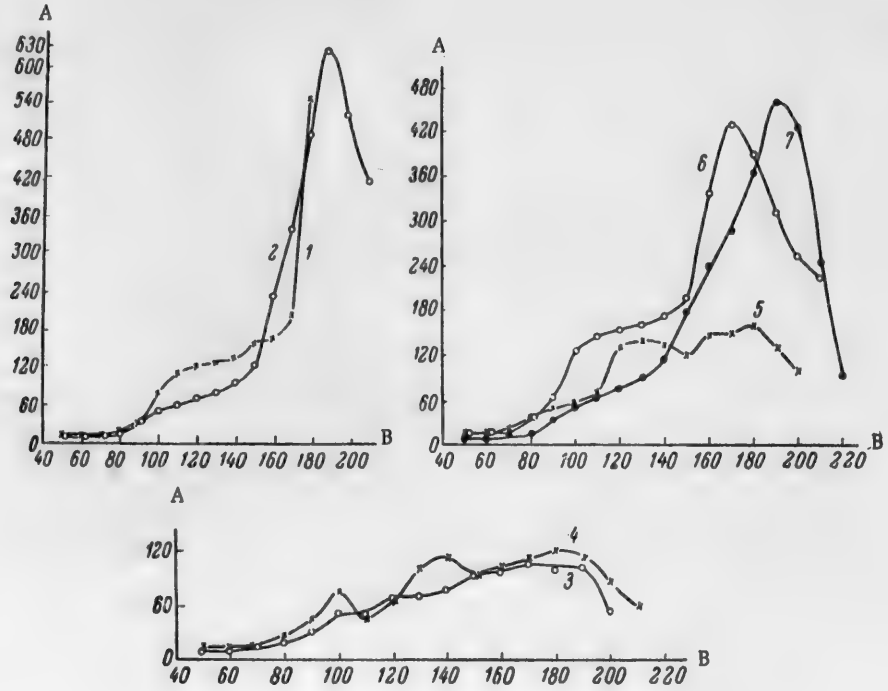

Fig. 3b.

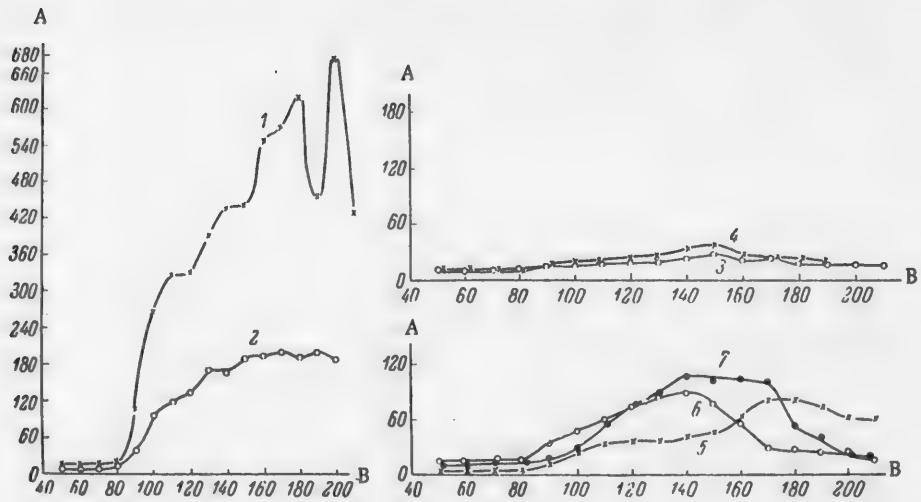

Fig. 3c.

DISCUSSION OF RESULTS

It follows from the data on the weight loss of the specimens, their solubility in cyclohexanone, and the results of the thermomechanical tests, that the greatest loss of weight on heating occurred in the specimens which had the densest spatial polymer network formed uniformly throughout their bulk.

Therefore the conversion of polyvinyl chloride into a space polymer occurred simultaneously with a degradation process, accompanied by evolution of gaseous and even liquid products. The most rapid formation of a

spatial network in the polymer, observed during the thermomechanical tests, took place at temperatures above 150°, i.e., in the flow region. Kargin and Shteding [12] advanced the hypothesis that flow of polymers is a general condition under which chemical reactions of macromolecules take place more easily. Increase of the preheating temperature and of the hexamethylenetetramine content favored the formation of a spatial network, but temperature increase alone was not sufficient for the formation of a stable spatial network, distributed uniformly throughout the polymer, as was the case in presence of hexamethylenetetramine, diphenylamine, and to some extent of diphenylurea. The formation of cross-linked polyvinyl chloride on heating was most rapid in presence of hexamethylenetetramine. The optimum content can be taken to be 4.8%. Although increase of the hexamethylenetetramine content to 11.5 and 17.7% resulted in some decrease of the percentage solubility and maximum deformation, degradation of the polymer was more prominent.

SUMMARY

1. Hexamethylenetetramine accelerates the formation of a spatial network in polyvinyl chloride on heating.

2. The amount of space polymer formed and the density of the spatial network increase with increase of temperature and hexamethylenetetramine content; 4.8% may be taken as the optimum.

3. Diphenylamine and (to some extent) diphenylurea, like hexamethylenetetramine, accelerate the conversion of polyvinyl chloride into a space polymer, but to a lesser extent than the latter.

4. The action of high temperatures (up to 170°) on polyvinyl chloride in absence of the above-named reagents results in only a slight degree of cross linking, with irregular distribution of the space polymer in the solid phase.

LITERATURE CITED

[1] V. V. Korshak and S. R. Rafikov, J. Gen. Chem. 14, 979 (1944); Proc. Acad. Sci. USSR 56, 597 (1947).

[2] V. V. Korshak and V. A. Zamyatina, Bull. Acad. Sci. USSR, Div. Chem. Sci. 106 (1946).

[3] A. Ya. Drinberg, Sh. N. Golant and L. I. Goldfarb, J. Appl. Chem. 24, 10, 1078 (1951); 11, 1181 (1951).

[4] A. Ya. Drinberg and N. S. Demchenko, J. Appl. Chem. 25, 1, 57 (1952).*

[5] A. Ya. Drinberg and A. D. Yakovlev, J. Appl. Chem. 26, 5, 532 (1953).*

[6] A. Ya. Drinberg and A. M. Bocharova, J. Appl. Chem. 26, 10, 1056 (1953).*

[7] A. A. Berlin and I. I. Denker, J. Appl. Chem. 24, 3, 308 (1951).*

[8] I. I. Denker and A. A. Berlin, J. Appl. Chem. 24, 12, 1311 (1951).*

[9] V. A. Kargin and T. A. Sogolova, J. Phys. Chem. 23, 5, 530 (1949).

[10] V. A. Kargin and Yu. M. Malinsky, Proc. Acad. Sci. USSR 72, 4 (1950).

[11] V. A. Kargin and M. N. Shteding, J. Chem. Ind. 2, 74 (1955).

[12] V. A. Kargin and M. N. Shteding, J. Chem. Ind. 3, 137 (1955).

[13] A. A. Tager et al., J. Chem. Ind. 4, 209 (1955).

[14] G. L. Slonimsky, V. A. Kargin and L. I. Golubenkova, Proc. Acad. Sci. USSR 93, 2, 311 (1953).

Received April 17, 1956

*Original Russian pagination. See C. B. Translation.

THE "LIMITING" DEGREE OF POLYMERIZATION OF CELLULOSE

V. I. Sharkov, I. I. Korolkov and E. N. Garmanova

It is known that the hydrolysis of cellulose under the action of dilute mineral acids on heating is not uniform. A small proportion (2-15%) is usually hydrolyzed 20-40 times as rapidly as the remaining, difficultly hydrolyzable portion. Investigations of the degree of polymerization of cellulose in the course of hydrolysis show that its value decreases rapidly during removal of the easily hydrolyzable portion, and reaches a certain limit, characteristic of the difficultly soluble residue.

On further hydrolysis of this residue its degree of polymerization remains almost constant for a given sample, but varies for celluloses of different origin [1-8]. For example, the "limiting" degree of polymerization of cotton cellulose is close to 150, that of mercerized cotton cellulose is 50-60, and of viscose rayon, about 30. The limiting degree of polymerization does not remain constant in all cellulose samples as hydrolysis proceeds. For example, it gradually decreases in wood cellulose, while in cotton cellulose it remains almost constant over a wide range. This effect, characteristic of heterogeneous hydrolysis of cellulose, is not observed in homogeneous hydrolysis.

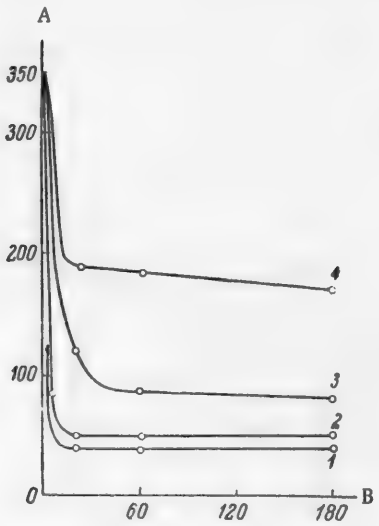

Variation of the degree of polymerization of the difficultly hydrolyzable residue of ground cellulose after hydrolysis and alcoholysis.
A) Degree of polymerization;
B) reaction time (minutes).
Medium: 1) methanol; 2) water; 3) ethanol; 4) propanol.

Studies of the difficultly soluble cellulose residue by the fractionation method showed that this residue contains cellulose macromolecules varying considerably in degree of polymerization.

For example, according to our results [9], the difficultly hydrolyzable residue of cotton cellulose, of average degree of polymerization 146, contained fractions of degree of polymerization between 233 and 16. After mercerization and subsequent hydrolysis, the same cellulose had average degree of polymerization 37, with fractions from 64 to 4.

Some investigators consider that the explanation for the "limiting" hydrolyzability of cellulose is the fact that cellulose consists of alternating amorphous and densely packed or crystalline regions. Owing to their different permeabilities to the catalyst, these two forms of cellulose are hydrolyzed at different rates. The amorphous or loose portion of the cellulose is hydrolyzed more rapidly, and the dense portion, more slowly. Therefore partial hydrolysis breaks cellulose down into small densely packed regions containing relatively short residues of the original cellulose chains. By this theory, the "limiting" degree of polymerization of cellulose should correspond to the average size of its closely packed or crystalline regions.

This explanation involves the assumption that cellulose has a two-phase structure, with relatively well-defined boundaries between the dense and loose forms.

In our opinion, this explanation is not very likely. It is difficult to imagine the existence of any well-defined boundaries in a system with a continuously changing structure. A more likely hypothesis is that of a gradual transition from loose to dense regions, with the formation of a system of capillaries with diameters varying along their length. With such a structure, the dimensions of the densely packed regions and, accordingly, the "limiting" degree of polymerization of cellulose should depend on the depth to which the hydrolyzing medium penetrates into it.

TABLE 1

"Limiting" Degree of Polymerization of Alcoholyzed and Hydrolyzed Samples of Ground Cellulose

Reaction	Time (min)	Amount dissolved (as % of weight taken)	Degree of polymerization (d.p.) of cellulose
—	—	—	350
Hydrolysis	5	—	85
	20	6.3	50
	60	13.0	49
	180	19.8	47
Methanolysis	20	27.8	36
	60	44.1	39
	180	59.0	39
Ethanolysis	20	24.0	120
	60	53.6	87
	180	63.2	80
Propanolysis	20	10.6	187
	60	24.5	190
	180	43.7	170
Butanolysis	20	4.8	189
	60	7.7	188
	180	15.6	185

TABLE 2

Effect of the Nature of the Reaction on the "Limiting" Degree of Polymerization of Different Cellulose Samples

Reaction	Reaction time (min)	Amount dissolved (as % of weight taken)	Limiting degree of polymerization (d.p.)
Cotton cellulose (d.p. =1090)			
Hydrolysis	180	5.0	150
Methanolysis		9.5	160
Ethanolysis		9.1	170
Propanolysis		8.3	180—200
Butanolysis		3.4	380—430
Wool cellulose (d.p. =860)			
Hydrolysis	180	4.3	149
Methanolysis	20	6.4	200
Butanolysis	180	5.7	480
Viscose rayon (d.p. =450)			
Hydrolysis	180	17.4	27
Butanolysis	180	8.7	185

This view is supported by the work of Assaf, Haas and Purves [10] who showed that the reaction of thallation of cellulose by thallous ethylate dissolved in different solvents, such as a series of homologous alcohols, depends on the size of the solvent molecules.

To test our hypothesis, we carried out a series of experiments on the alcoholysis of various cellulose samples in anhydrous monohydric alcohols. In the light of the above considerations it was to be expected that the "limiting" degree of polymerization of cellulose should decrease with decreasing size of the oxonium ions of the reagents acting as catalysts in the alcoholysis reaction.

The materials used were samples of cotton and wood cellulose, viscose rayon, and cotton cellulose previously ground in a ball colloid mill, with degree of polymerization 350 as determined by the Staudinger method. The alcoholysis was performed in the following anhydrous alcohols: methyl, ethyl, propyl, and butyl, containing 10% of sulfuric acid as catalyst. The reaction mixtures in 1 : 40 ratio were heated for various times in copper autoclaves contained in a boiling water bath.

At the end of the reaction the autoclave was rapidly cooled in cold water and opened; the solution was separated from the undissolved residue of cellulose. This was thoroughly washed with water on a funnel to remove acid, and dried to constant weight. The amount of cellulose which reacted was found from the weight loss of the sample.

The degree of polymerization of the cellulose residue was determined from the viscosity of a cuprammonium solution by Staudinger's method.

The results are given in Table 1 and 2 and plotted in the Figure.

These results show that the degree of polymerization of alcoholyzed celluloses, as of hydrolyzed cellulose, falls rapidly at first and then reaches a limiting value. However, the "limiting" degree of polymerization of the alcoholyzed samples differed according to the composition of the solvent used. Thus, the value for ground cotton cellulose after hydrolysis was 47, after methanolysis 39, after ethanolysis 80, after propanolysis 170, and after butanolysis 185. Analogous results were obtained for other cellulose samples.

It must be noted that the values given for the degree of polymerization correspond to roughly equal proportions of cellulose dissolved, and are therefore comparable to some extent.

The results show that the "limiting" degree of polymerization of cellulose depends on the nature of the solvent and its penetrating power. This is demonstrated particularly clearly by comparison of butanolysis with hydrolysis. For example, the "limiting" degree of polymerization of cotton cellulose is 150 in hydrolysis and 400 in butanolysis; of wood cellulose, 149 in hydrolysis and 480 in butanolysis, etc. A significant fact is that the limiting values for different cellulose samples are in the same ratio both in hydrolysis and alcoholysis, indicating the existence of corresponding multicapillary systems in the cellulose. In comparison of the cellulose residues after hydrolysis and alcoholysis it must be taken into account that in the former case, in addition to hydrolysis of the regions of the macromolecules easily accessible to the catalyst, partial recrystallization also occurs, and the size of the densely packed regions therefore increases. This is probably why the limiting hydrolyzability of cellulose is greater than the limiting hydrolyzability of methanolyzed cellulose (see figure).

These results confirm the view that cellulose does not contain sharply defined amorphous and crystalline regions and that cellulose contains a fine multicapillary structure, with varying accessibility to the catalyst. As this structure is created when the cellulose fiber is formed, it seems likely that fibers formed under different conditions may have different "limiting" degrees of polymerization, and in some cases this effect may become reversible.

To test this, we prepared a series of cellulose samples regenerated from viscose.

These samples were then hydrolyzed in boiling 10% sulfuric acid for three hours. The degree of polymerization of the difficultly hydrolyzable cellulose residues was determined. The results of these determinations and details of the cellulose samples used are given in Table 3.

TABLE 3

Determination of the Degree of Polymerization of Cellulose Samples

Sample No.	Details of sample	Degree of polymerization (d.p.) after partial hydrolysis
1	Viscose rayon	27.0
2	Viscose rayon, mercerized at 20° and washed with water	36.5
3	Same but mercerized at 0°	37.4
4	Cellulose regenerated at 15° with sulfuric acid from dilute viscose	44
5	Same regenerated at 100°	45

These data show that the "limiting" degree of polymerization of regenerated cellulose varies according to the conditions (whether the viscose is coagulated with or without tension). The lowest value was found for viscose rayon, i.e., cellulose regenerated under tension. When viscose was coagulated in a beaker (Sample 4), the value rose from 27 to 44. This shows that the average size of the densely packed regions is greater in cellulose regenerated without tension than in cellulose which was stretched at the moment of coagulation.

Another interesting fact is that when viscose rayon is mercerized, its internal structure is changed, giving an increase of the "limiting" degree of polymerization of the cellulose. This may be regarded as confirmation of the view advanced above, that the internal structure of cellulose may undergo reversible changes with corresponding variations of its "limiting" degree of polymerization.

It is known [8-11] that the hydrolyzability of viscose rayon decreases after mercerization, i.e., its content of the difficultly hydrolyzable component increases. The data in Table 3 show that the decrease of the content of the easily hydrolyzable component in viscose fibers is accompanied by an increase of the average length of the densely packed regions.

In this connection it was of interest to determine, by the alcoholysis method [12], the contents of the easily hydrolyzable component in the regenerated celluloses listed in Table 3.

The results are given in Table 4.

TABLE 4

Content of the Easily Hydrolyzable Component in Celluloses

Details of samples	Solubility of cellulose (%) in ethanolysis during (minutes)		
	20	60	180
Viscose rayon	8.0	20.8	43.1
Viscose rayon, mercerized at 20° and washed with water	8.2	17.7	23.6
Cellulose gel obtained from viscose by natural coagulation on standing	4.9	9-11	19-19.5

These results show that formation of viscose fibers in a spinning bath is associated with the formation of a large amount of the easily hydrolyzable (amorphous) fraction in the cellulose. Free swelling of such fibers, followed by drying, causes considerable structural changes, with disappearance of a part of the amorphous fraction, increase of the content of the densely packed regions, and increase of their size.

SUMMARY

1. It is shown that the "limiting" degree of polymerization of cellulose depends on the composition of the reaction medium and the microstructure of the sample. This effect is explained in terms of differences of the permeability of the cellulose to the catalyst.

2. It was found that the "limiting" degree of polymerization of hydrate cellulose decreases during stretching in the course of coagulation of viscose. The content of the easily hydrolyzable (amorphous) fraction in the cellulose increases at the same time.

3. When viscose fibers swell, the difficultly hydrolyzable regions increase, while the content of the easily hydrolyzable component decreases.

LITERATURE CITED

[1] L. Jörgenson, Acta Chem. Scand. 4, 1, 185 (1950).

[2] W. Roseveare, Ind. Eng. Chem. 44, 1 (1952).

[3] R. Nickerson, Ind. Eng. Chem. 33, 1022 (1941).

[4] F. Bauer and E. Pacsu, Text. Res. J. 22, 385 (1952).

[5] H. Staudinger and M. Sorkin, Ber. 70, 1565 (1937).

[6] A. af Ekenstam, Svensk Paperstidn. 45, 81 (1942).

[7] V. V. Nizovkin, D. M. Khai and A. P. Krupnova, J. Hydrol. Ind. 5 (1948).

[8] V. I. Sharkov, O. A. Dobush and G. D. Paramonova, Coll. Trans. All-Union Sci. Res. Inst of Hydrolysis and Sulfite Alcohol Ind. 3, 31 (1950).*

* In Russian.

[9] V. I. Sharkov, Trans. Inst. Forestry, Acad. Sci. Latvian SSR 8 (1955).

[10] A. Assaf, R. Haas and C. Purves, J. Am. Chem. Soc. 66, 59 (1944).

[11] V. I. Sharkov and Z. N. Martyshchenko, J. Appl. Chem. 26, 8, 881 (1955).*

Received August 20, 1956

*Original Russian pagination. See C. B. translation.

PREPARATION OF AMINOCARBANILIDES*

V. N. Klyuev, A. A. Spryskov and S. N. Solodushenkov

The Ivanovo Institute of Chemical Technology

Earlier [1] we prepared a series of amino- and nitrocarbanilides in order to extend the range of possible intermediates for the production of azo dyes of a high degree of fastness.

The present communication describes the synthesis of 12 new amino carbanilides by reduction of the nitrocarbanilides the preparation of which was described previously [1].

The literature on the reduction of nitrocarbanilides is very scanty. Vittenet [2], and Fleischer and Nemes [3], reduced 4,4'-dinitrocarbanilide and 4,4'-dinitro-2,2'-dimethylcarbanilide with tin and hydrochloric acid. Mention is made in a Swiss patent [4] of the possible preparation of 4,4'-diamino-2,2',5,5'-tetraalkoxycarbanilides by reduction of the corresponding dinitrocarbanilides, but the reduction method is not described. A German patent [5] describes the reduction of 4,4'-dinitro-3,3'-disulfocarbanilide with iron filings to give the corresponding amine. Reduction is facilitated in this case by the presence of sulfo groups, which make the compound soluble in water.

No information is available in the literature on the reduction of nitrocarbanilides not containing sulfo groups, with iron.

We reduced nitrocarbanilides with iron in presence of electrolytes, with zinc dust in hydrochloric acid, and with zinc dust in presence of ammonium chloride. The last method is generally used for preparation of arylhydroxylamines, but is has also been used [6] for preparation of diamines of the benzene series. Arylhydroxylamines with NH_2 and NHAc substituents in the para position relative to the hydroxylamino group are not described in the literature. Apparently they decompose readily into water and quinonediimine, while the latter, or its derivatives, is reduced further to the diamine or acyl diamine. The reduction of dinitrocarbanilides by zinc dust with ammonium chloride takes place in conditions which virtually exclude the possibility of saponification of the carbamide group and chlorination of the molecule.

EXPERIMENTAL

Synthesis of 4,4'-diamino-2,2',5,5'-tetramethylcarbanilide. 7 g of the 4,4'-dinitro-2,2',5,5'-teramethylcarbanilide prepared earlier [1] was added to 35 ml of alcohol with 60 ml of water. The mixture was heated on the water bath, 15 ml of concentrated hydrochloric acid was added, followed by additions of 12 g of zinc dust in small portions during 2 hours, and the liquid was then filtered. The diamine hydrochloride was salted out of the cooled solution by addition of common salt and purified by heating with charcoal in water. Ammonia was added to the solution of the hydrochloride to isolate 4,4'-diamino-2,2',5,5'-tetramethylcarbanilide; the latter was recrystallized from alcohol in the form of colorless crystals which did not melt at 315°, the yield being 2.8 g (48.5% of the theoretical). The diamine is soluble in dilute hydrochloric acid, in hot methanol or ethanol, and in glacial acetic acid. It is sparingly soluble in acetone and insoluble in water, benzene, toluene and ether.

0.1292 g subst.: 22.3 ml N_2 (25°, 749 mm). Found %: N 19.49. $C_{17}H_{22}N_4O$. Calculated %: N 18.78.
0.2025 g subst.: 13.24 ml 0.1 N $NaNO_2$. Found %: equiv. 152.8. $C_{17}H_{18}N_2O(NH_2)_2$. Calculated %: equiv. 149.2.

The hydrochloride separates on cooling after addition of concentrated hydrochloric acid to the solution; it forms colorless rods which do not melt at 315°.

* Communication III in the series on the synthesis and uses of carbanilide derivatives.

0.2064 g subst.: 11.04 ml 0.1 N NaOH. Found: equiv. 187.0. $C_{17}H_{22}N_4O \cdot 2HCl$. Calculated: equiv. 185.7.

Synthesis of 4,4'-diamino-2,2'-dichlorocarbanilide. 45 g of iron filings, 100 ml of water, and 7 ml of 80% acetic acid was stirred together for 1 hour at 90-95°. 11.1 g of 4,4'-dinitro-2,2'-dichlorocarbanilide was added in small portions during 3 hours to the etched filings, followed by 100 ml of water, and the reduction was continued at the same temperature for 5.5 hours. After neutralization with sodium carbonate, the solid was filtered off and the diamine extracted from it with boiling methanol. Part of the alcohol was distilled off; the cooled solution deposited the 5.8 g of the diamine (yield 63% of the theoretical). The diamine was purified in 2% hydrochloric acid with charcoal. The cooled filtrate deposited colorless leaflets of 4,4'-diamino-2,2'-dichlorocarbanilide hydrochloride, which did not melt when heated to 315°.

0.1733 g subst.: 9.16 ml 0.1 N NaOH. Found: equiv. 189.2. $C_{13}H_{12}ON_4Cl_2 \cdot 2HCl$. Calculated: equiv. 192.0.

The free base was isolated by addition of ammonia, and crystallized from water in the form of small colorless needles which melt at 287° with sublimation.

4,4'-Diamino-2,2'-dichlorocarbanilide is sparingly soluble in boiling water, rather more soluble in boiling methanol or ethanol, soluble in hot acetone and in glacial acetic acid and insoluble in benzene and toluene.

0.1530 g subst.: 24.20 ml N_2 (25°, 750 mm). Found %: N 17.89. $C_{13}H_{12}ON_4Cl_2$. Calculated %: N 18.02.
0.1967 g subst.: 12.60 ml 0.1 N $NaNO_2$. Found: equiv. 156.1. $C_{13}H_8ON_2Cl_2(NH_2)_2$. Calculated: equiv. 155.5.

Synthesis of 4,4'-diamino-2,2',5,5'-tetrachlorocarbanilide. A mixture of 35 g of iron filings, 50 ml of water, and 4 ml of 80% acetic acid was stirred on a heated water bath for 0.5 hour; 5 g of the nitro compound and 100 ml of alcohol was then added. The reduction was continued for 16 hours in the boiling mixture with stirring. The liquid was neutralized with sodium carbonate, the iron oxides were filtered off, and the filtrate cooled to precipitate the diamine. Part of the diamine remained with the iron oxides, and was extracted with hot pyridine. The diamine separated out of the pyridine on cooling, in the form of a white precipitate which did not melt when heated to 315°. Yield 2.6 g (61% of the theoretical).

0.1096 g subst.: 13.45 ml N_2 (19°, 760 mm). Found %: N 14.35. $C_{13}H_{10}N_4OCl_4$. Calculated %: N 14.75.

A simpler method of isolating the diamine is to boil the nitro compound (10 g) with crystalline sodium sulfide (100 g) under reflux for 1-1.5 hours. The mixture was cooled and treated with 700 ml of water; the diamine which separated out was filtered off, washed, and treated with hot dilute hydrochloric acid to remove the 2,5-dichloro-1,4-phenylenediamine formed as the result of hydrolysis at the carbamide group. The hydrochloric acid extract was cooled and neutralized with ammonia to deposit white crystals of 2,5-dichloro-1,4-phenylenediamine of m.p. 161°. The 4,4'-diamino-2,2',5,5'-terachlorocarbanilide, which is very sparingly soluble in dilute hydrochloric acid and very slowly hydrolyzed by it, was obtained as a grayish precipitate in 5 g yield (58% of the theoretical). Longer heating increases the yield of 2,5-dichloro-1,4-phenylenediamine.

4,4'-Diamino-2,2',5,5'-tetrachlorocarbanilide is soluble in hot glacial acetic acid, hot methanol and ethanol, and pyridine. After recrystallization from alcohol it forms small colorless crystals which do not melt when heated to 315° and darken somewhat in air.

0.1240 g subst.: 16.76 ml N_2 (18.5°, 731 mm). Found %: N 15.22. $C_{13}H_{10}N_4OCl_4$. Calculated %: N 14.75.
0.2193 g subst.: 11.17 ml 0.1 N $NaNO_2$. Found: equiv. 196.3. $C_{13}H_6N_2OCl_4(NH_2)_2$. Calculated: equiv. 190.0.

Synthesis of 4,4'-diamino-2,2'-dimethyl-5,5'-dichlorocarbanilide. A mixture of 10 g of 4,4'-dinitro-2,2'--dimethyl-5,5'-dichlorocarbanilide, 75 ml of methyl alcohol, 75 ml of water, and 15 ml of concentrated hydrochloric acid was heated under reflux on the water bath. 12 g of zinc dust was added by portions to the boiling liquid during 1 hour, and the reduction was continued for 2.5 hours until the mixture became pale. The alcohol was then distilled off, excess zinc dust was filtered off, and concentrated hydrochloric acid was added to the filtrate; 4,4'-diamino-2,2'-dimethyl-5,5'-dichlorocarbanilide was precipitated slowly as the hydrochloride in 6.5 g yield (63.5% of the theoretical). Crystallization from water in presence of charcoal gave colorless crystals which did not melt when heated to 315°.

0.3991 g subst.: 19.78 ml 0.1 N NaOH. Found: equiv. 201.8. $C_{15}H_{16}N_4OCl_2 \cdot 2HCl$. Calculated: equiv. 206.0.

The base, isolated by addition of ammonia, dissolves on warming in methanol, ethanol and butanol. It is soluble in acetone, pyridine and 80% acetic acid; it is almost insoluble in benzene. It crystallizes from 3 : 1 pyridine—water mixture in the form of small colorless needles which do not melt when heated to 315°.

0.0821 g subst.: 12.15 ml N_2 (25°, 732 mm). Found %: N 16.32. $C_{15}H_{16}N_4OCl_2$. Calculated %: N 16.52.
0.3064 g subst.: 18.33 ml 0.1 N $NaNO_2$. Found: equiv. 167.2. $C_{15}H_{12}N_2OCl_2(NH_2)_2$. Calculated: equiv. 169.6.

Synthesis of 4,4'-diamino-2,2'-dimethoxycarbanilide. Iron filings were used for the reduction of 4,4'-dinitro--2,2'-dimethoxycarbanilide, as described above for 4,4'-dinitro-2,2'dichlorocarbanilide. The reduction was complete after 8-9 hours; the hot mixture was made alkaline with sodium carbonate and filtered. A white precipitate of 4,4'-diamino-2,2'-dimethoxycarbanilide, m.p. 187°, was deposited from the cooled filtrate. A further quantity of the diamine may be extracted from the iron oxides by boiling water, the total yield being 50-60% of the theoretical.

The diamine is soluble in water, but the solution darkens rapidly in air unless a little hydrosulfite is added. It is more soluble in methanol, ethanol, glacial or dilute acetic acid, and readily soluble in dilute hydrochloric acid; it is almost insoluble in benzene and in toluene.

4,4'-Diamino-2,2'-dimethoxycarbanilide crystallizes from water in the form of small colorless needles, m.p. 192°.

0.1466 g subst.: 24.2 ml N_2 (26°, 741 mm). Found %: N 18.41. $C_{15}H_{18}O_3N_4$. Calculated %: N 18.54.
0.2125 g subst.: 14.12 ml 0.1 N $NaNO_2$. Found: equiv. 150.5. $C_{15}H_{14}O_3N_2(NH_2)_2$. Calculated: equiv. 151.1.

The hydrochloride is precipitated from a solution of a diamine in hydrochloric acid (by the action of excess concentrated hydrochloric acid) in the form of colorless crystals which melt at 279° with decomposition.

0.2142 g subst.: 11.46 ml 0.1 N NaOH. Found: equiv. 186.8. $C_{15}H_{18}O_3N_4 \cdot 2HCl$. Calculated: equiv. 187.5.

Synthesis of 4,4'-diamino-2,2',5,5'-tetramethoxycarbanilide. 4,4'-Dinitro-2,2',5,5'-tetramethoxycarbanilide was reduced by means of iron filings in presence of ferrous acetate by the action of heat for 4.5 hours on the boiling water bath. The reaction mixture was neutralized with sodium carbonate, the iron oxides were filtered off and boiled with methyl alcohol to extract the amine. The gray precipitate of the diamine which formed in the cooled alcohol was dissolved in dilute hydrochloric acid and warmed with charcoal. On addition of ammonia, a white precipitate of the diamine, which darkened somewhat in air, was formed in 45-50% yield. After recrystallization from benzene, 4,4'-diamino-2,2',5,5'-tetramethoxycarbanilide was obtained in the form of long colorless needles, melting at 236° with decomposition.

The diamine is very slightly soluble in boiling water, soluble in hot methanol and ethanol, in cold acetone, 80% acetic acid, and slightly soluble in boiling benzene and toluene.

0.1072 g subst.: 15.01 ml N_2 (24.5°, 732 mm). Found %: N 15.47. $C_{17}H_{22}N_4O_5$. Calculated %: N 15.46.
0.3246 g subst.: 18.01 ml 0.1 N $NaNO_2$. Found: equiv. 180.1. $C_{17}H_{18}N_2O_5(NH_2)_2$. Calculated: equiv. 181.2.

The hydrochloride was isolated in the form of thin colorless needles which did not melt at 315°, by addition of an equal volume of concentrated hydrochloric acid to a solution of the diamine in hydrochloric acid.

0.2491 g subst.: 11.58 ml 0.1 N NaOH. Found: equiv. 215.1. $C_{17}H_{22}N_4O_5 \cdot 2HCl$. Calculated: equiv. 217.6.

Synthesis of 4,4'-diamino-2,2'-diethoxy-5,5'-dimethylcarbanilide. 4,4'-Dinitro-2,2'-diethoxy-5,5'dimethylcarbanilide was reduced with zinc dust in aqueous alcohol on a boiling water bath for 5 hours. The diamine was isolated as the hydrochloride, which crystallizes from water in the form of small pink needles, melting at 289° with decomposition.

0.1958 g subst: 9.23 ml 0.1 N NaOH. Found: equiv. 212.2. $C_{19}H_{26}O_3N_4 \cdot 2HCl$. Calculated: equiv. 215.6.

The diamine was isolated from the hydrochloride and crystallized from 50% alcohol in the form of fine needles with m.p. 184°. It is readily soluble in methanol and in ethanol, and more so in acetic acid; it is sparingly soluble in boiling water, and insoluble in ether, benzene and toluene.

0.0948 g subst.: 13.35 ml N_2 (25°, 743 mm). Found %: N 15.77. $C_{19}H_{26}O_3N_4$. Calculated %: N 15.63.
0.1944 g subst.: 10.73 ml 0.1 N $NaNO_2$. Found: equiv. 181.2. $C_{19}H_{22}O_3N_2(NH_2)_2$. Calculated: equiv. 179.2.

Synthesis of 4,4'-diamino-2,2',5,5'-tetraethoxycarbanilide. 4,4'-Dinitro-2,2',5,5'-teraethoxycarbanilide was reduced with zinc dust in aqueous alcohol in presence of ammonium chloride on the water bath for 3 hours until the mixture became light gray in color. The diamine was extracted in acetone from the solid phase. The acetone solution was evaporated; a dark precipitate formed, which was dissolved in dilute hydrochloric acid and

purified by means of charcoal. Ammonia was added to isolate the base in the form of a white precipitate, darkening in air, the yield being about 50% of the theoretical. 4,4'-diamino-2,2',5,5'-tetraethoxycarbanilide crystallizes from alcohol in the form of colorless needles, m.p. 199°. It is soluble on boiling in methanol and ethanol, in 80% acetic acid and acetone; it is sparingly soluble in boiling benzene and toluene and insoluble in water.

0.1304 g subst.: 15.86 ml N_2 (23.5°, 743.5 mm). Found %: N 13.69. $C_{21}H_{30}O_5N_4$. Calculated %: N 13.39.
0.3182 g subst.: 14.96 ml 0.1 N $NaNO_2$. Found: equiv. 212.7. $C_{21}H_{26}O_5N_2(NH_2)_2$. Calculated: equiv. 209.2.

The hydrochloride is readily soluble in water; it is precipitated from solution in the form of small colorless needles, which do not melt at 315°, by addition of an equal volume of concentrated hydrochloric acid.

0.3706 g subst.: 15.03 ml 0.1 N NaOH. Found: equiv. 246.6. $C_{21}H_{30}O_5N_4 \cdot 2HCl$. Calculated: equiv. 245.7.

Synthesis of 4,4'-diamino-2,2'-dimethoxy-5,5'-dimethylcarbanilide. 4,4'-Dinitro-2,2'-dimethoxy-5,5'-dimethylcarbanilide was reduced with iron filings in presence of ferrous acetate at 90-93° for 10-12 hours. 4,4'-Diamino-2,2'-dimethoxy-5,5'-dimethylcarbanilide was extracted from the solid phase in boiling acetone in approximately 50% yield, and crystallized from 50% methyl alcohol in the form of colorless needles, melting at 230° with decomposition. It is insoluble in benzene, toluene, ether and carbon tetrachloride. It is readily soluble in acetic acid, methanol, ethanol, acetone and pyridine, and is almost insoluble in water.

0.1209 g subst.: 18.4 ml N_2 (19.5°, 740 mm). Found %: N 17.27. $C_{17}H_{22}O_3N_4$. Calculated %: N 16.97.
0.2476 g subst.: 14.78 ml 0.1 N $NaNO_2$. Found: equiv. 167.5. $C_{17}H_{18}O_3N_2(NH_2)_2$. Calculated: equiv. 165.1.

The diamine was dissolved in dilute hydrochloric acid. Excess of the concentrated acid was added to precipitate the hydrochloride in the form of colorless rhombic crystals melting at 277° with decomposition.

0.2260 g subst.: 11.13 ml 0.1 N NaOH. Found: equiv. 203.0. $C_{17}H_{22}O_3N_4 \cdot 2HCl$. Calculated: equiv. 201.6.

Synthesis of 4,4'-diamino-2,2'-dimethoxy-5,5'-dichlorocarbanilide. 4,4'-Dinitro-2,2'-dimethoxy-5,5'-dichlorocarbanilide was dissolved in a mixture of alcohol and water and added at once to iron filings previously treated with acetic acid. The reduction was continued for 7.5-8 hours on the water bath. After neutralization with sodium carbonate, the solid phase was filtered off, and the amine was extracted from it in boiling acetone. After evaporation of some of the solvent, the solution was cooled; a white precipitate of 4,4'-diamino-2,2'-dimethoxy-5,5'-dichlorocarbanilide was formed in approximately 70% yield.

The diamine is soluble in acetone, hot 80% acetic acid, hot methanol and ethanol, and dilute hydrochloric acid. It is insoluble in water, benzene, toluene and carbon tetrachloride. It crystallizes from methanol in the form of small colorless needles of m.p. 254-256° (the capillary was immersed in the apparatus heated to 2-3° below the melting point).

0.1068 g subst.: 14.16 ml N_2 (24°, 746.5 mm). Found %: N 15.08. $C_{15}H_{16}O_3N_4Cl_2$. Calculated %: N 15.09.
0.2105 g subst.: 11.37 ml 0.1 N $NaNO_2$. Found: equiv. 186.8. $C_{15}H_{12}O_3N_2Cl_2(NH_2)_2$. Calculated: equiv. 185.6.

When concentrated hydrochloric acid is added to a solution of the diamine in dilute hydrochloric acid, the hydrochloride is precipitated in the form of colorless needles of m.p. 293° (the capillary was immersed in the apparatus heated to 2-3° below the melting point).

0.2570 g subst.: 11.40 ml 0.1 N NaOH. Found: equiv. 225.4. $C_{15}H_{16}O_3N_4Cl_2 \cdot 2HCl$. Calculated: equiv. 222.1.

Synthesis of 4-amino-2,2'-dimethoxycarbanilide. 4-Nitro-2,2'-dimethoxycarbanilide was reduced with iron filings previously treated with acetic acid, on a boiling water bath for 5-5.5 hours. After neutralization with alkali the solid phase was filtered off; the filtrate on cooling deposited 4-amino-2,2'-dimethoxycarbanilide, m.p. 160--162°, the yield being 20-25% of the theoretical. To prevent darkening of the filtrate in air, 0.2-0.3 g of hydrosulfite was added to the reduction mixture before filtration. A further quantity of the amine may be extracted from the residue of iron oxides by repeated treatment with boiling water or alcohol.

4-Amino-2,2'-dimethoxycarbanilide is soluble in hot methanol and ethanol, dilute acetic acid, and hot dilute hydrochloric acid; it is sparingly soluble in hot water and in boiling toluene, and is insoluble in benzene. It crystallizes from ethanol in the form of colorless needles, m.p. 166°.

0.1433 g subst.: 19.07 ml N_2 (23°, 743 mm). Found %: N 14.99. $C_{15}H_{17}O_3N_3$. Calculated %: N 14.64.

The hydrochloride crystallizes from water and melts at 209°.

0.2598 g subst.: 7.9 ml 0.1 N NaOH. Found: equiv. 329.5 $C_{15}H_{17}O_3N_3 \cdot HCl$. Calculated: equiv. 323.6.

Synthesis of 4-amino-2,2',4'-trimethoxy-5'-methylcarbanilide. 4-Nitro-2,2',4'-trimethoxy-5'-methylcarbanilide was reduced with iron filings as described for 4-nitro-2,2'-dimethoxycarbanilide. The amine was extracted from the solid phase in boiling methanol, and was obtained in 82% yield in the form of crystals of a faint violet color, melting at 174.5° with decomposition.

4-Amino-2,2',4'-trimethoxy-5'-methylcarbanilide is soluble in hot water and in methanol, ethanol, acetic acid, and acetone. It is sparingly soluble in benzene and in toluene. It crystallizes from water in the form of colorless needles, m.p. 175°.

0.1129 g subst.: 12.95 ml N_2 (24°, 742 mm). Found %: N 12.87. $C_{17}H_{21}O_4N_3$. Calculated %: N 12.68.
0.4044 g subst.: 12.40 ml 0.1 N $NaNO_2$. Found: equiv. 326.3. $C_{17}H_{19}O_4N_2(NH_2)$. Calculated: equiv. 331.3.

The hydrochloride is precipitated from water in the form of colorless needles, melting at 200° with decomposition.

0.0916 g subst.: 9.12 ml N_2 (25°, 740 mm). Found %: N 11.10. $C_{17}H_{22}O_4N_3Cl$. Calculated %: N 11.42.
0.4892 g subst.: 13.46 ml 0.1 N NaOH. Found: equiv. 363.6. $C_{17}H_{21}O_4N_3 \cdot HCl$. Calculated: equiv. 367.8.

In conclusion it must be mentioned once again that in the melting-point determinations the capillary was often introduced into the heated apparatus, as described previously [1].

LITERATURE CITED

[1] A. A. Spryskov, S. N. Solodushenkov and V. N. Klyuev, J. Appl. Chem. 30, 7, 1065 (1957);* 30, 9, 1361 (1957).*

[2] H. Vittenet, Bull. Soc. Chim., [3], 31, 150, 660 (1899).

[3] A. Fleischer, G. Nemes, Ber. 10, 1295 (1877).

[4] J. R. Geigy A. G., Swiss Patent 240993 (1946); Ch. A. 43, 6426 (1949).

[5] Bayer and Co., German Patent 140613 (1900); Frdl. 6, 1292.

[6] V. F. Borodkin and S. I. Burmistrov, J. Gen. Chem. 17, 64 (1947); S. I. Burmistrov and N. A. Zuikova, J. Gen. Chem. 20, 1856 (1950).*

Received April 17, 1956

*Original Russian pagination. See C. B. Translation.

GLYCEROL – DIPHENIC ACID POLYESTERS

A. I. Kogan and M. M. Kitaigorodsky

The Odessa Institute of Electrical Communications

Glycol terephthalate polyesters have considerably higher elasticity and flexibility than glycol phthalate polyesters. We showed earlier [1] that the same relationship holds for glycerol polyesters, i.e.,films made from glycerol terephthalate resin are considerably more elastic than films from glycerol phthalate resin. It was therefore of interest to find whether this rule applies to other dibasic acids. According to the literature [2],the tendency to fiber formation increases in the series of hexamethylene glycol–diphenic acid polyesters from the 3,3'-diphenic to the 4,4'-diphenic acid polyester. The object of the present investigation was the comparative evaluation of the properties of the glycerol polyesters of these acids. The glycerol–2,2'-diphenic acid polyesters have already been prepared and studied by Drinberg, Snedze and Nechaeva [3]. They were investigated during the course of the present work in order to obtain data for comparison with the polyesters of 3,3'- and 4,4'-diphenic acids.

The acids required for preparation of the polyesters were synthesized. 2,2'-Diphenic acid was made from anthranilic acid.

Anthranilic acid was converted, by diazotization and a number of subsequent operations, into the methyl ester of m-iodobenzoic acid. 2,2'-Diphenic acid was prepared from this ester by Ullmann's method (in 49.6% yield calculated on the anthranilic acid, m.p. 224°).

4,4'-Diphenic acid was prepared by an analogous method from p-toluidine. The yield of acid was 9.6%. The purity of the acid, determined by titration of a sample dissolved in pyridine, was 99.2%.

3,3'-Diphenic acid was also synthesized by Ullmann's method [4]. The methyl ester of m-iodobenzoic acid required for the reaction was made by two methods: 1) from methyl benzoate by nitration [5], reduction (with hydrogen sulfide in ammoniacal solution), diazotization, and treatment with hydrogen iodide; 2) direct iodination of benzoic acid, by the method of Tronov and Novikov [6]. In the former case the yield of 3,3'-diphenic acid was 8.4%, m.p. 344°; in the latter, the yield was 24.2%, m.p. 342°. The conversion of methyl m-iodobenzoate into the dimethyl ester of 3,3'-diphenic acid is a more sluggish reaction than the formation of the dimethyl ester of 2,2'-diphenic acid. The degree of subdivision of the copper is of decisive significance.

To avoid increase of particle size during the reduction of copper oxide by hydrogen, the copper was distributed over an aluminum oxide support. Powdered anhydrous aluminum oxide (pure) was introduced into copper nitrate solution in the proportion necessary to give equal weights of copper and alumina in the final product. The suspension of alumina in copper nitrate solution was heated to boiling, and a boiling solution of sodium carbonate was added in slight excess. The precipitate of basic copper carbonate, mixed with aluminum oxide, was filtered off by suction, dried, and heated to convert the carbonate into oxide. The mixture of copper oxide and alumina was washed repeatedly with hot water to remove soluble salts completely, dried, and reduced with hydrogen at a dark red heat.

It is known that the preparation of polyesters from 2,2'-diphenic acid and glycerol does not present any special difficulties [3]. The 2,2'-diphenic acid was mixed with glycerol (pure) in 1 : 1 and 1 : 2 molar ratios and heated at 225-240° for 15 minutes. The mixture was cooled and the resin formed was investigated. The following were determined: acid number (by titration of a weighed sample of the resin dissolved in pyridine, with aqueous alkali), anhydride groups [7], saponification number, hydroxyl groups [8], and molecular weight by the Rast method [9].

For preparation and investigation of the polyester films, the resins were dissolved in double their weight of a mixture of equal volumes of toluene and n-butanol. The solutions were applied to glass and aluminum plates. After evaporation of the solvent the films were hardened at 150-160° until they ceased to peel off at that temperature. It was found that at the hardening temperature, after peeling ceased, the films were soft, i.e., pressure left indentations in them.

The films were tested for hardness by the pendulum method [10], elasticity on the NIILK (Scientific Research Institute for Lacquers and Paints) scale [11], and impact strength [12]. The dielectric constant and dielectric loss angle were determined by means of a Q-meter at 50 kc [13], and the breakdown voltage was determined by means of a transformer apparatus [14]. The results are summarized in the table.

A resin containing fatty acids from sunflower oil in addition to 2,2'-diphenic acid was prepared by the same method and studied as described above. These results are given in the same table.

In attempts to prepare polyesters from 3,3'- and 4,4'-diphenic acids and glycerol by analogous methods, the same difficulty was met as in the preparation of glycerol terephthalate polyesters [1], namely: when a mixture of the acid was heated with glycerol, even if the latter was present in excess (up to 5 moles of glycerol per 1 mole of acid), the reaction mixture tended to pass into the final state long before it became homogeneous. Therefore glycerol was used in large excess (from 25 to 60 moles per 1 mole of acid), and served as solvent for the polyester formed. To isolate the resin from the solution in glycerol, the reaction mixture was poured into a 6 to 7-fold amount of water. The resin was filtered out of the emulsion on a Buchner funnel. The resins containing 4,4'-diphenic acid were filtered off easily. Resins containing 3,3'-diphenic acid were filtered off easily only if the reaction mixture was poured into water immediately after it became completely homogeneous. If the heating of the reaction mixture at 240-250° was continued for 30-40 minutes, the emulsion formed when it was poured into water did not give a clear filtrate when drawn through a double filter. In one instance (Table, Experiment 4) the filtration was continued to the end despite the inhomogeneity of the filtrate. The amount of 3,3'-diphenic acid recovered from the filtrate was 15% of the amount taken for the synthesis.

In the other cases the resins were removed completely from the emulsions by salting out. The amount of 3,3'-diphenic acid in the decanted liquid was determined (by saponification with alkali followed by addition of hydrochloric acid to liberate the acid). From 11 to 16% of the 3,3'-diphenic acid taken was found in different experiments.

The resins were dried in air and investigated as described above. Solutions in volatile solvents (lacquers) were prepared at the same time. However, because of the incomplete solubility of these polyesters in toluene—butanol mixture, the solvent used was dioxane in 1 : 2 ratio of resin to solvent. The lacquers were made into films, data for which are given in the Table.

It must be noted that if, in the preparation of the polyester, the heating with excess glycerol is stopped as soon as the reaction mixture becomes homogeneous, the precipitate formed on addition of water is easy to filter off. However, it is not a resin, but shows signs of a crystalline structure and does not form films from solutions in dioxane, even after prolonged heating at 200°.

For preparation of a polyester containing fatty acids, a mixture of 3,3'-diphenic acid with fatty acids from sunflower oil in 3:1 weight ratio was heated with excess glycerol. At 250° the mixture became homogeneous, but not completely, as a part of the fatty acids formed an infusible rubberlike lump on the surface. After precipitation of the resin with water, the lump was separated mechanically from the emulsion and investigated. It was saponified with alcoholic alkali, and the soap solution was decomposed by hydrochloric acid after evaporation of the alcohol. Fatty acids were extracted in benzene from the acid mixture formed. 22.5% of the fatty acids and 7% of the 3,3'-diphenic acid taken for the synthesis were found. After separation of the rubberlike mass, the resin was salted out of the emulsion. Data on this resin are given in the table (Experiment 7).

Polyesters containing 4,4'-diphenic acid (Table, Experiments 8 and 9) were prepared by similar methods, with the difference that, after addition of water to separate the resin out of the solution of the polyester in glycerol, salting out was not necessary; the resin was easily separated by filtration on a Buchner funnel. The amount of 4,4'-diphenic acid remaining in the filtrate in the form of soluble esters was determined; it was found to be 4% of the amount taken.

The same effect was observed in the preparation of polyesters of 4,4'-diphenic acid containing sunflower oil fatty acids as for the resins based on 3,3'-diphenic acid: part of the fatty acids and other resin components

Properties of Glycerol–Diphenic Acid Polyesters

Experiment No.	Acid portion of polyester	Acid-glycerol ratio in synthesis (molar)	Acid number	Anhydride groups (%)	Saponification number	Hydroxyl groups (%)	Molecular weight	Results of tests on films				Notes
								hardness (pendulum test)	dielectric constant	tan of loss angle	breakdown voltage (kv/mm)	
1	2,2'-Diphenic acid	1 : 2	97.7	0.56	281.7	14 74	469	0.87	5.4	0.006	8	—
2	2,2'-Diphenic acid	1 : 1	218.8	0.47	350.1	8.73	280	0.87	4.3	0.004	16	—
3	2,2'-Diphenic acid 75%+ sunflower oil fatty acids 25%	1.3 : 1	125.8	0.20	331.8	4.00	430.1	0.90	3.35	0.007	30	—
4	3,3'-Diphenic acid	1 : 60	133.7	3.43	272.7	12.12	194	0.84	3.52	0.014	20	Heated for 30 minutes at 250° after mixture became homogeneous. Resin precipitated with water.
5	3,3'-Diphenic acid	1 : 25	37.9	0.65	277.4	12.93	245	0.87	4.8	0.015	28	Heated for 45 minutes at 250° after mixture became homogeneous . Resin precipitated with water and salted out.
6	3,3'-Diphenic acid	1 : 25	213.1	—	341.8	6.56	273	—	—	—	—	Heating stopped when 250° reached. Resin precipitated with water.
7	3,3'-Diphenic acid 85%+ sunflower oil fatty acids 15%	1: 25	96.9	6.9	271.1	12.56	227	0.94	4.4	0.014	20	Heated for 45 minutes at 250°. Resin precipitated with water and salted out.
8	4,4'-Diphenic acid	1 : 60	106.5	—*	246.0	9.60	—*	0.80	4.6	0.017	40	Heated for 30 minutes at 250°. Resin precipitated with water.
9	4,4'-Diphenic acid 90%+ sunflower oil fatty acids 10%	1 : 60	88.0	0.94	235.7	7.93	277	0.83	4.95	0.023	36	Heated for 20 minutes at 250°. Resin precipitated with water.

*Not determined, owing to incomplete solubility of the resin in acetone and camphor.

formed an infusible rubberlike mass, which was separated mechanically from the main mass of the polyester, present in the form of an aqueous emulsion.

The data in the Table show that films of all the polyesters have high hardness. However, further investigations showed that their elasticity is quite inadequate. None of the films satisfied the minimum requirements. In determinations of elasticity by bend tests over standard rods by the NIILK method [11], all the films showed cracks when bent over the rod 20 mm in diameter. In impact-strength tests [12], the films crack and peel when a 2 kg striker falls from a height of 1 cm.

Of the electrical insulating properties of these films, the progressive increases of the breakdown voltage and tan loss angle along the series of 2,2'-diphenic, 3,3'-diphenic, and 4,4'-diphenic acid polyesters are noteworthy. In tests on the effects of frequency variations between 50 and 24 kc on the values of the dielectric constant and tan loss angle for films made from certain of the resins (Table, Experiments 3 and 7) it was found that the dielectric constant remains almost unchanged, while the tan loss angle increases by a factor of 2.5-3.

SUMMARY

1. Solutions of glycerol polyesters of 2,2'-, 3,3'- and 4,4'-diphenic acids, after evaporation of the solvent, form films of high hardness but inadequate elasticity (the films are brittle). There were no significant differences in properties between films of polyesters based on the different diphenic acids.

2. Investigations of the dielectric properties of the polyesters showed that the tan loss angle and specific breakdown voltage increase along the series from 2,2'-diphenic to 4,4'-diphenic acid polyesters.

LITERATURE CITED

[1] A. I. Kogan and M. M. Kitaigorodsky, J. Appl. Chem. 29, 628 (1956)*

[2] Z. A. Rogovin, Progr. Chem. 23, 300 (1954).

[3] A. Ya. Drinberg, A. A. Snedze and L. P. Nechaeva, Trans. Leningrad Technol. Inst. 14, 93 (State Chem. Press, Leningrad-Moscow, 1947).**

[4] F. Ullmann, Ann. der Chemie 332, 70 (1904).

[5] Organic Synthesis, Collective Vol. 1 (Russian translation) (IL, 1949) p. 260.

[6] B. V. Tronov and A. N. Novikov, Report on the Scientific Work of the Members of the Mendeleev All-Union Chemical Society, 3, 9 (1953).**

[7] A. I. Kogan, J. Appl. Chem. 21, 677 (1948).

[8] K. A. Andrianov and D. Kardashev, Practical Work on Synthetic Resins and Plastics, 2nd edn. (State Chem. Press, Moscow-Leningrad, 1946) p. 140.**

[9] H. Meyer, Analysis and Structure Determination of Organic Substances (Russian Translation) (Ukrainian State Sci.-Tech. Press, 1935) p. 226.

[10] S. V. Yakubovich, Tests of Lacquer and Paint Materials and Coatings (State Chem. Press, Moscow-Leningrad, 1952) p. 247.**

[11] ibid, p. 253.

[12] ibid, p. 274.

[13] N.P. Bogoroditsky, V. V. Pasynkov and B. M. Tareev, Electrical Engineering Materials (State Power Press, Leningrad-Moscow, 1950) p. 113.**

[14] S. V. Yakubovich, Tests of Lacquer and Paint Materials and Coatings (State Chem. Press, Moscow-Leningrad, 1952) p. 406.**

Received May 25, 1956

*Original Russian pagination. See C. B. Translation.
**In Russian.

BRIEF COMMUNICATIONS

REACTION OF CALCIUM SULFATE WITH ALUMINATES AT 1200°

T. A. Ragozina

Budnikov and Sologubova [1] demonstrated the beneficial effect of additions of calcium sulfate to the raw mix on the activity of aluminous belite cement made in the 1000-1300° range. From the results of petrographic and x-ray analyses these authors concluded that $CaSO_4$ acts as a mineralizer which favors the formation of monocalcium aluminate and prevents the formation of gehlenite.

In a study of the processes of mineral formation during the firing of $nSiO_2 \cdot mAl_2O_3 \cdot 2n+m\,CaO$ mixtures, we found that the temperature, degree of saturation, and presence of calcium fluoride have a considerable influence on the formation of gehlenite and various aluminates [2]. It was found that gehlenite formation is favored by increase of temperature (above 1200°) and decrease of the degree of saturation. The presence of CaF_2 (2%) in mixtures with not less than 100% saturation prevents formation of gehlenite and tricalcium aluminate. The smallest amount of gehlenite is formed at 1200°, at high saturations (108%), in presence of calcium fluoride, but much $5CaO \cdot 3Al_2O_3$ is formed in these conditions. Small amounts of monocalcium aluminate are formed at 1200° when the saturation of the mixture is 94-100%.

The quantitative mineral composition of the fired mixtures was determined by means of the method of chemical analysis developed by the author, based on differential solution of the minerals in normal acetic acid [3]. In this method $2CaO \cdot SiO_2$ and $3CaO \cdot Al_2O_3$ are completely dissolved, while gehlenite and $CaO \cdot Al_2O_3$ remain in the insoluble residue. $5CaO \cdot 3Al_2O_3$ also remains undissolved in the main mass.

This method was used for analysis of sulfate–alumina–belite cement made from a mixture containing 10% gypsum; it was found that $CaSO_4$ reacts during the heating with monocalcium aluminate, and scarcely any gehlenite or tricalcium aluminate is formed. This conclusion was based on the almost complete dissolution of SiO_2 in acetic acid, slight dissolution of alumina, and the presence of most of the $CaSO_4$ in the insoluble residue.

For a more detailed study of the reaction between calcium sulfate and aluminates, mixtures of tricalcium aluminate with gypsum, and monocalcium aluminate with gypsum, were fired at 1200°. Mixtures of $CaCO_3$, Al_2O_3 and gypsum, and hydrosulfoaluminate and gypsum separately, were also fired in order to determine the thermal stability of $CaSO_4$ and the solubility of anhydrite fired at high temperatures. The samples were fired in platinum crucibles in a Silit furnace for 2 and 6 hours. The furnace was cooled to 700°, the crucibles were removed and placed in a desiccator containing soda lime and calcium chloride. The fired mixtures were then analyzed chemically and petrographically.

First, it was found that the fired calcium sulfate contains no free lime. Therefore it does not decompose at 1200° in absence of a reducing medium and aluminate impurities. Its refractive index is in the range 1.615--1.576, which is characteristic for anhydrite [4]. The solubilities of the high-temperature anhydrite at room temperature were: in water, 0.700 g, in saturated lime solution 0.376 g, and in normal acetic acid 1.16 g $CaSO_4$ per liter.

Because of the low solubility of the anhydrite in lime solution, the method of Gudovich [5] for determination of free and bound $CaSO_4$ cannot be used. We therefore used normal acetic acid, which quantitatively separates tricalcium and monocalcium aluminates, dissolves anhydrite fairly well, and completely dissolves hydrosulfoaluminate. This last fact is very important, because hydrosulfoaluminate may be formed during the analysis from

Results of Chemical Analyses of the Fired Mixtures (in %)

Experiment No	Composition of original mixtures	Firing time (hours)	Free CaO (%)	Acetic acid extract			Insoluble residue			Total	Calculated mineral composition			
				Al_2O_3	CaO	SO_3	Al_2O_3	CaO	SO_3		$nCA \cdot CaSO_4$ in %	$nCA \cdot CaSO_4$ CA : $CaSO_4$	C_3A	CA	free $CaSO_4$
1	$CA \cdot CaSO_4$	6	none	6.0	18.4	17.4	32.5	19.1	5.8	99.2	50.5	3 : 1	7.0*	8.2**	28.1
2	$3CA \cdot 2CaSO_4$	2	none	9.0	15.5	14.8	32.7	21.9	5.3	98.5	58.2	3 : 1	—	19.5	21.2
3	$2CA \cdot CaSO_4$	2	none	8.0	11 5	10.2	37.6	25.6	6.5	99.4	65.2	3 : 1	—	19.9	13.8
4	$CaCO_3 \cdot Al_2O_3 + 10\%\ CaSO_4$	6	none	3.0	4 0	0.7	53.1	33.7	5.0	99.5	30.3	3 : 1	4.0	64.2	0.6
5	$C_3A \cdot 3CaSO_4$	6	15.6	1.6	37 4	27.4	14.2	12.7	7.0	100.3	33.9	1.6 : 1	4.2	—	46.6
6	$3C_3A \cdot 2CaSO_4$	2	28.2	5 4	40.5	9.7	22.6	16.3	5.5	100.0	50.4	3.2 : 1	6.2	—	15.1
7	$2C_3A \cdot CaSO_4$	2	29.2	5.2	40.0	6.3	24.6	17.7	6.1	99.9	52.3	3 2 : 1	8.7	—	9.8
8	$C_3A + 10\%\ CaSO_4$	2	25.0	19.6	50.0	2.8	14.3	9.9	3.1	99.7	44.3	3.6 : 1	29.5	—	1.0
9	$3CaCO_3 \cdot Al_2O_3 \cdot 3CaSO_4$	6	13.8	1.7	35.6	27.1	17.5	13.2	5.2	100.3	35.9	2.6 : 1	4.5	—	46.1
10	$3CaO \cdot Al_2O_3 \cdot 3CaSO_4 \cdot 30H_2O$	6	16.7	10.6	45.5	31.5	5.4	4.6	2.4	100.0	35.1	1.8 : 1	2.2	—	41.9

* C_3A is the result of formation of hydrosulfoaluminate during the analysis.

** The actual CA content in the product was 20.4%.

free $CaSO_4$ and aluminates; however, this will be found in the acetic acid extract, and the $CaSO_4$ which reacted during the firing will remain in the insoluble residue.

The results of chemical analyses of the fired mixtures are given in the Table; the compositions of the acetic acid extracts, insoluble residues, free lime contents, and calculated mineral compositions are given.

The results show that in no case did calcium sulfate dissociate, and the large amounts of free lime found (Experiments 5-10) were formed as the result of decomposition of tricalcium aluminate. This is confirmed by the constant contents of SO_3 in the mixtures before and after firing, a negative microscopic reaction in Astreeva's test [6] for C_3A,* and the small amount of alumina in the acetic acid extract. Thus, a mixture of $C_3A - 3CaSO_4$, containing 41.7% C_3A and 58.3% $CaSO_4$, should dissolve completely in acetic acid (Experiment 5), but after the firing the extract contained only 1.6% Al_2O_3, which corresponds to 4.2% C_3A. The remaining 37.5% of tricalcium aluminate decomposed, with liberation of 15.6% CaO, corresponding to two equivalents of lime. Consequently, in presence of $CaSO_4$ tricalcium aluminate decomposes at 1200° into monocalcium aluminate and lime according to the reaction

$$3CaO \cdot Al_2O_3 \longrightarrow CaO \cdot Al_2O_3 + 2CaO.$$

In this reaction calcium sulfate does not act as a catalyst, but interacts with $CaO \cdot Al_2O_3$; this is shown by the presence of SO_3 in the insoluble residue, which appears as a single phase under the microscope, and consists of weakly birefringent, almost isotropic six-sided plates of refractive index 1.567-1.561. No grains of ahydrite or $CaO \cdot Al_2O_3$ were found. The results of the microscopic and chemical analyses indicate that the insoluble residue is the compound 1.6 $CA \cdot CaSO_4$. To find whether the composition of the compound is constant, mixtures containing different amounts of C_3A and gypsum were fired. Analysis showed that more undecomposed C_3A remains with decrease of the amount of gypsum in the original mixture, and the composition

* The following abbreviations are used: $C_3A = 3CaO \cdot Al_2O_3$ and $CA = CaO \cdot Al_2O_3$.

of the compound $nCA \cdot CaSO_4$ alters, the coefficient n increasing to 3.6. Therefore the product of the reaction of calcium aluminate with $CaSO_4$ does not have a definite chemical composition.

When mixtures containing monocalcium aluminates and gypsum are fired, free lime is not liberated, and calcium sulfate reacts with the aluminate, as proved by the presence of insoluble $CaSO_4$. The residue after treatment with acetic acid contains $CaO \cdot Al_2O_3$ in addition to the reaction product; this is confirmed by petrographic analysis. The presence of free calcium aluminate interferes with determination of the coefficient n in the formula $nCA \cdot CaSO_4$. In the subsequent calculation it was assumed that $n = 3$.

Calculations of the mineral composition of the fired mixtures were based on: 1) complete solubility of $CaO \cdot C_3A$, hydrosulfoaluminate, and anhydrite in normal acetic acid at room temperature; 2) insolubility of CA; and 3) partial solubility of the compound $nCA \cdot CaSO_4$ formed. Hence the insoluble residue should contain CA and $nCA \cdot CaSO_4$. The determinations of the composition of all the insoluble residues showed that the equivalent proportions of the oxides correspond to CA and $CaSO_4$. The only exception was the composition of the insoluble residue in Experiment 1, where 5.2% of excess alumina remained after combination of the lime in the sulfate and monocalcium aluminate.

This gives a high $CaO-Al_2O_3$ ratio in the acetic acid extract, giving 7.0% C_3A in the calculation of the mineral composition. The presence of tricalcium aluminate in the fired mixture consisting of $CaO \cdot Al_2O_3$ and $CaSO_4$ is doubtful, and was not confirmed by Astreeva's microscopic reaction. Therefore the high $CaO-Al_2O_3$ ratio in the extract and the excess Al_2O_3 in the insoluble residue must be attributed to the formation of hydrosulfoaluminate which could have been formed during the analysis by the reaction

$$3(CaO \cdot Al_2O_3) + 3CaSO_4 + nH_2O \longrightarrow 3CaO \cdot Al_2O_3 \cdot 3CaSO_4aq + 2Al_2O_3aq.$$

The hydrosulfoaluminate dissolves in acetic acid, while the hydrated alumina remains in the insoluble residue. Calculation shows that 5.2% Al_2O_3 is equivalent to 7.0% C_3A. Consequently, the fired product does not contain tricalcium aluminate, and its monocalcium aluminate content is not 8.2% but 12.2% more (7.0% C_3A + 5.2% Al_2O_3), i.e., 20.4%.

The $CaO-Al_2O_3$ ratio in the acetic acid extracts after subtraction of free lime and lime in the form of $CaSO_4$ varies from 1 to 3, indicating that not only tricalcium aluminate but also the compound $nCA \cdot CaSO_4$ is dissolved. Therefore the C_3A and CA contents are calculated from the CaO and Al_2O_3 contents. The monoaluminate is calculated as $nCA \cdot CaSO_4$ from the insoluble residue in accordance with the value of the coefficient n. In mixtures containing monocalcium aluminate in the insoluble residue it was assumed that $n = 3$.

The calculation showed that the amount of free lime found exactly corresponds to the amount of tricalcium aluminate which decomposed to the monoaluminate. Thus, a mixture consisting of tricalcium aluminate and 10% gypsum contained 25% free lime after firing. This corresponds to 60.3% C_3A, which decomposed with formation of 35.3% CA. Of this amount, 22.2% of monocalcium aluminate remained in the insoluble residue, and 13.1% was dissolved in acetic acid as $3.6\ CA \cdot CaSO_4$. The solution contained 19.6% Al_2O_3; subtraction of the alumina contained in 13.1% CA from this gives 11.2% Al_2O_3, which corresponds to 29.5% C_3A. The amounts of alumina and lime found in the acetic acid extract, after subtraction of the free lime and the lime combined as the sulfate, are equivalent to the calculated amounts of C_3A and CA. This confirms the calculation and the conclusion concerning the nature of the decomposition of tricalcium aluminate with liberation of two molecules of CaO. The reaction takes this course irrespective of the amount of $CaSO_4$, but if there is a deficiency of calcium sulfate a large proportion of C_3A remains undecomposed, as is confirmed by petrographic analysis. At 1200° sulfoaluminate also decomposes with liberation of lime and anhydrite and formation of $1.8\ CA \cdot CaSO_4$ (Experiment 10).

These experiments show that when mixtures of calcium aluminate with $CaSO_4$ are heated, 66-72% CA and 89-92% C_3A react. From 20 to 50% of the calcium sulfate, depending on the amount present in the mixture, is consumed in the reaction (Experiments 1-3, 5-7). In Experiment 8, 90% $CaSO_4$ and 66% C_3A reacted, as the original mixture contained considerably less calcium sulfate.

In lime–alumina mixtures containing gypsum the lime is combined in monocalcium aluminate which reacts with $CaSO_4$, while the excess CaO remains in the free state. Thus, in Experiment 9, 13.8% of free lime remained, while the insoluble residue contained 8.8% $CaSO_4$, 17.5% Al_2O_3 and 9.6% CaO, i.e., the molecular ratio of alumina to lime was 1 : 1.

After all the fired mixtures had been stained with "Bright Blue Z" by Astreeva's method, microscopic examina-

tion revealed only individual light blue and blue-green grains and very occasional pale blue edges in the aggregates. The mixture in Experiment 8 was an exception; its coloration after firing and staining was very intense. Brightly colored light blue and blue-green grains were seen in considerable numbers under the microscope, predominantly in aggregates. Chemical analysis showed 29.5% C_3A in this mixture.

The results of the investigation of the reaction between calcium sulfate and calcium aluminates at high temperatures are of interest for interpretation of the processes of mineral formation which take place in the burning of cement mixes.

SUMMARY

1. Tricalcium aluminate reacts with calcium sulfate at 1200° with liberation of two molecules of lime and formation of the compound n CA · $CaSO_4$.

2. Tricalcium aluminate is not formed when lime–alumina mixtures containing calcium sulfate are fired; the lime is combined in the form of monocalcium aluminate, and excess of lime remains free.

This suggests that introduction of gypsum to the raw mix would yield cements containing aluminates with less lime and silicates with more lime than are formed under normal conditions.

LITERATURE CITED

[1] P. P. Budnikov and O. M. Sologubova, Proc. Acad. Sci. USSR 85, 5 (1952).

[2] T. A. Ragozina, Proc. Acad. Sci. Uzbek SSR 1 (1956).

[3] T. A. Ragozina, Proc. Acad. Sci. Uzbek SSR 11 (1954).

[4] A. N. Winchell, Microscopic Characters of Artificial Inorganic Solid Substances or Artificial Minerals (Russian translation) (State Chem. Tech. Press, Leningrad, 1933) p. 72.

[5] L. A. Gudovich, Trans. State Inst. for Planning and Research in the Cement Industry 13 (1952).*

[6] O. M. Astreeva and L. Ya. Lopatnikova, Advances in the Petrography of Cement Clinker (Industrial Construction Press, Moscow, 1951).*

Received February 20, 1956

* In Russian.

GERMANIUM IN COKE OVEN WASTES

N. P. Diev and V. I. Davydov

Because of the wide distribution of germanium in the earth's crust and of its occurrence in a great variety of sources – mixed copper and zinc sulfide ores, iron ores, coal, petroleum, etc. [1, 2], there are dozens of different methods and processes for the production of this metal [3].

The concentration of germanium in different rocks and ores is from 10^{-4} to 10^{-3}%, and rarely 10^{-2}%. This low content of germanium in the raw materials makes its production very complex. One possible way of solving the problem is by beneficiation of the raw materials by different processes, or by the use of processes in which different germanium-containing materials are used in the production of germanium. For example, in the production of germanium from copper, zinc, or iron ores, fuels containing somewhat higher amounts of the metal are used; natural germanium-containing precipitants or sorbents are used for separation of germanium from solutions, etc. It was shown by Kostrikin [4] that one possible source of germanium is coke oven wastes. These wastes consist of mixtures of coke fines carried over into the gas mains, and coal tar.

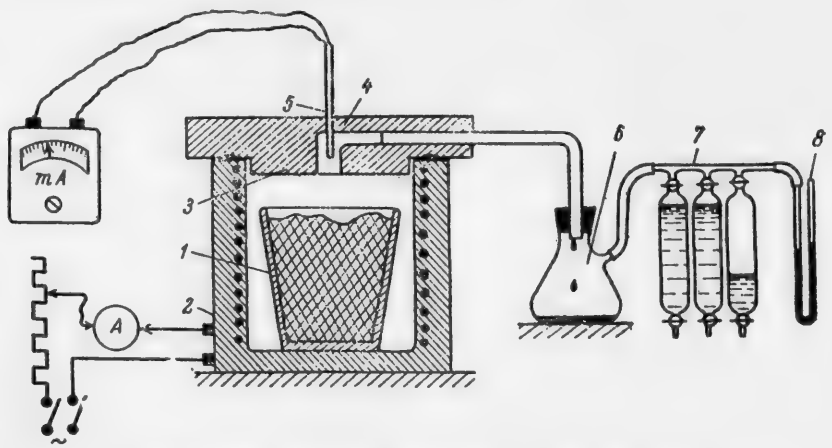

Apparatus for fractional distillation of coke oven wastes.
Explanations are given in the text.

Kostrikin attempted to enrich with germanium the ash formed by combustion of the coke oven wastes in a muffle furnace at 700-750° with adequate access of air. He did not succeed in obtaining any appreciable degree of concentration. It follows from the data given below that a considerable amount of the germanium enters the gas phase during combustion of coke oven wastes.

The purpose of the present investigation was to determine which fraction obtained in the distillation of coke oven wastes has the highest germanium content.

The apparatus used for the fractional distillation of the wastes is illustrated in the Figure. A sample weighing about 200 g was put into the graphite crucible 1 contained in the furnace 2. The furnace was closed with an asbestos plug 3 set in a special cement.* The plug had a channel 4 for removal of the distillates; the end of a

* Composition of the cement: 3 parts of fine corundum powder, 2 parts of raw clay, 1 part of borax, and enough water to give a paste.

Chromel–Alumel thermocouple was inserted in this channel for determination of the temperature of the distillates. The distillates were collected in the receiver 6, connected to a system of gas-sampling burets 7 and manometer 8. The system was isolated from the external air. Leakage of air into the system was prevented by a slight positive pressure (1-2 mm water column) set up within the system. Excess pressure, especially at the start of the distillation as the result of expansion of the air in the system, was released by means of the gas-sampling burets.

Air cooling of the receiver was sufficient to condense the distillates.

Wastes from the Magnitogorsk Coke Oven Works, with a low germanium content (of the order of 10^{-4}%) were used in the experiments. According to Kostrikin [4], these wastes have moderate germanium content. Wastes obtained by the coking of Donets, Karaganda and Kizel coals have the highest germanium contents; wastes from the coking of Kuznetsk coals have the lowest. The results of the experiments are summarized in the Table.

Temperature range of fraction (°C)	Yield of fraction		Color and nature of fraction	Germanium content*	
	in g	in %		in g	in %
20—200	21.2	10.6	Pale liquid distillate	$1.357 \cdot 10^{-4}$	$6.4 \cdot 10^{-4}$
200—300	17.05	8.5	Mixture of thick black and colorless liquid distillates	$8.89 \cdot 10^{-4}$	$5.2 \cdot 10^{-3}$
300—400	4.25	2.13	Mixture of brown and colorless liquid distillates	$1.11 \cdot 10^{-4}$	$2.5 \cdot 10^{-3}$
400—600	28.5	14.23	Mixture of thick black liquid and a dark brown thick paste	$9.4 \cdot 10^{-6}$	$3.2 \cdot 10^{-5}$
>600	123	61.5	Residue – coke fines coalesced into a single lump	$7.36 \cdot 10^{-4}$	$6 \cdot 10^{-4}$

The loss of distillates owing to leaks in the system was 6 g (3% of the total amount taken).

The experiments showed that the distillates between 200 and 400° are appreciably richer in germanium. The germanium probably volatilizes in the form of organic Ge compounds, as at temperatures up to 300° only its halides are volatile, and their presence in the wastes is unlikely. As already stated, wastes of moderate germanium content were used in the experiments. Concentration of wastes richer in germanium by distillation should probably yield fractions containing some hundredths or even tenths of one per cent of the metal. Extraction of Ge from such concentrated fractions presents no difficulties. More detailed study of the form in which germanium is present in the wastes is required.

Investigations of the distillation products of Cheremkhovo coal [5] showed that primary tar of the 185-325° fraction contains 25.8% phenolic groups and 13.8% monocyclic aromatic hydrocarbons. There may be a connection between germanium and these groups.

If this hypothesis is correct, these fractions could be used as reagents in the flotation process for the concentration of germanium in certain sources [6], and in analytical chemistry and technology.

SUMMARY

Distillation of coke oven wastes resulted in distribution of germanium between the fractions, with appreciable concentration of the metal in the fractions collected in the 200-400° range.

LITERATURE CITED

[1] A. E. Fersman, Geochemistry, 1, IV (1933).

[2] V. M. Goldshmidt, Collected Papers on the Geochemistry of Rare Elements (GONTI, Moscow-Leningrad, 1938).**

[3] D. G. Kochergina, "Production of Ge and Ga in the Capitalist Countries" Central Inst. Inf. Bull. 13 (66), 13-26 (1956).

* The chemical analysis was performed by M. S. Marekha in the Analytical Laboratory of the Urals Branch of the Academy of Sciences USSR.

** In Russian.

[4] V. M. Kostrikin, J. Appl. Chem. 12, 10, 1449 (1939).

[5] N. I. Popova, D. Kh. Kurban-Galeeva and M. V. Shorokhova, Trans. Eastern Siberian Branch, Acad. Sci. USSR, Chem. Ser. 3 (1955).

[6] I. P. Ratledge, J. N. Ong and J. H. Boyce, Mining Engineering, 7, 4, 379 (1955).

Received December 31, 1956

THERMODYNAMICS OF THE INTERACTION OF FUSED $CaCl_2$ WITH ALKALI METAL CHLORIDE MELTS

M. V. Smirnov, S. F. Palguev, L. A. Lyapina and Yu. N. Krasnov

It was shown in one of our previous papers that the e.m.f. isotherms of glavanic cells with electrodes reversible with respect to Ca^{++} and Cl^- ions in fused mixtures of the chlorides of sodium, potassium and calcium deviate very considerably from ideality when the mole fraction of calcium present exceeds 5×10^{-2} (16.5 wt.% $CaCl_2$). This is evidently associated with a change of the ionic state of calcium in the transition from fused $CaCl_2$ to its mixtures with melts of alkali metal chlorides. Definite conclusions concerning the interaction between the components of such mixtures can be drawn from the results of studies of their thermodynamic properties.

If we measure the e.m.f. of a cell with electrodes reversible with respect to Ca^{++} and Cl^-, in fused calcium chloride and in a mixed chloride melt of a given composition, the difference gives the isobaric potential change ΔZ when the salts are mixed. If the e.m.f.–temperature relationship is known, the heat (ΔH) and entropy (ΔS) of mixing can be calculated.

Reversible cells with calcium electrodes are unobtainable in practice because the free metal reduces $CaCl_2$ to the subchloride in melts [1, 2]. Instead of the metal, calcium oxide–carbon electrodes can be used. It has been shown that, in accordance with the electrode reaction: $CaO + \frac{1}{2} C - 2e \rightleftharpoons Ca^{++}(melt) + \frac{1}{2} CO_2$, the potential of this electrode is determined by the activity of the Ca^{++} ions in the melt, as shown by the thermodynamic equation

$$E = E^\circ + \frac{RT}{2F} \ln a_{Ca^{++}(melt)}.$$

However, these electrodes are also unsuitable for measurements in pure fused calcium chloride, as they disintegrated fairly rapidly in it owing to formation of the oxychloride. Nevertheless, we succeeded in determining the e.m.f. of the cell $CaO + C \mid CaCl_2(melt) \mid Cl_2, C$ at 800°. Its value was about 1.6 v, which gives for the reaction $CaO(S) + \frac{1}{2} C(S) + Cl_2(g) = CaCl_2(l) + \frac{1}{2} CO_2(g)$ the value $\Delta Z = -73.8$ kcal / mole of $CaCl_2$.

From data available in the literature [3], we can calculate the variation of ΔZ with temperature for this reaction:

$$\Delta Z_1 = (-78.7 + 4.3 \cdot 10^{-3} T) \pm 1.8 \text{ kcal / mole } CaCl_2$$

At 800°, $\Delta Z_1 = -74.1$ kcal / mole. Thus there is good agreement between the calculated and experimental values. The equation therefore describes quite satisfactorily the thermodynamics of the chlorination reaction when calcium chloride is formed in the liquid state. It now remains to find the thermodynamic parameters for this reaction for the case when melts dilute with respect to $CaCl_2$, which behave as ideal solutions, are formed. This would make it possible to determine the thermodynamics of the reactions of fused calcium chloride with melts of alkali metal chlorides.

EXPERIMENTAL

It has been established that a fused equimolar mixture of sodium and potassium chlorides, containing less than 16.5% $CaCl_2$ by weight, behaves like an ideal solution. We studied the thermodynamics of the chlorination reaction in the formation of a melt containing 0.60 wt.% $CaCl_2$ (mole fraction of calcium $1.78 \cdot 10^{-3}$). The measurements involved the determination of the temperature–e.m.f. relationship for the cell:

$$CaO + C \mid \text{melt: } 0.60\%CaCl_2 + 99.40\%(NaCl + KCl) \mid Cl_2, C.$$

The experimental procedure was similar to that used by us in determinations of the equilibrium potentials of calcium oxide–carbon electrodes. The difference was that the temperature and not the concentration was varied. The temperature was kept constant within ± 2.5° until the e.m.f. became constant (for several hours) within 1 mv. To minimize the errors due to possible differences in the behavior of individual electrodes, the measurements were performed with different electrodes, in which the molar ratio of oxide to carbon was varied over a wide range (from the required stoichiometric ratio to a tenfold excess of carbon).

RESULTS AND DISCUSSION

The results of e.m.f. determinations in the 800-900° range may be represented by the linear equation:

$$\epsilon = (1.8245 + 1.99 \cdot 10^{-4}T) \pm 0.0045 \text{ v.}$$

Hence the change of isobaric potential in the chlorination reaction, in the formation of $0.60\%CaCl_2$ solution in a fused equimolar mixture of NaCl and KCl is

$$\Delta Z_2 = (-84.153 - 9.179\,T) \pm 208 \text{ kcal/ mole } CaCl_2.$$

Therefore the transition from pure fused calcium chloride to its dilute (0.60 wt. %) solution in a fused mixture of sodium and potassium chlorides is accompanied by a change of isobaric potential equal to:

$$\Delta Z_{mixing} = \Delta Z_2 - \Delta Z_1 = (-5.5 - 13.5 \cdot 10^{-3}\,T) \pm 2 \text{ kcal / mole } CaCl_2.$$

It is seen that mixing of the salts results in liberation of heat

$$(\Delta H_{mixing} = -5.5 \text{ kcal / mole } CaCl_2)$$ and increase of entropy

$$(\Delta S_{mixing} = 13.5 \text{ kcal / degree mole } CaCl_2).$$

The entropy of fusion of binary salts of univalent metals (NaCl, KCl, TlCl, AgCl etc.) which dissociate to give two ions in the fused state is closed to 6 cal / degree · mole. If we assume [4] that the formation of 1 gram-ion during the fusion of the salt produces an entropy increase of $\frac{3}{2}$ R (3 kcal / degree · g-ion), and the entropy of fusion is 6.45 kcal / degree · mole $CaCl_2$ [3], it follows that $CaCl_2$ in the melt is mainly dissociated into $CaCl^+$ and Cl^- ions. This is in agreement with the results obtained in determinations of the transference numbers of ions in pure fused lead chloride, first carried out by Karpachev and Palguev [5], and later confirmed by Delimarsky, Turov and Gitman [6] and others [7]. It was found that even at a temperature 180° above the melting point of the salt the transference number of the anion is about four times the transference number of the cation. It is probable that zinc chloride in the liquid state is not dissociated into simple ions, but contains the $PbCl^+$ ion, which has low mobility (the entropy of fusion of $PbCl_2$ is 7.31 kcal / degree · mole).

The possible existence of $CaCl^+$ cations in fused calcium chloride has been considered by others. For example, Markov and Delimarsky [8, 9] account for certain properties (electrical conductivity, transference numbers of the ions, solubilities of metals in melts) of fused chlorides of beryllium, magnesium and the alkaline-earth metals by their stepwise dissociation in the fused state.

$$MeCl_2 \rightleftharpoons MeCl^+ + Cl^- \rightleftharpoons Me^{++} + 2Cl^-.$$

The transition from pure fused calcium chloride to its mixtures with alkali metal chloride melts is essentially a replacement of a part of the Ca^{++} ions by Na^+ and K^+ ions. Since the charge on a calcium ion is twice as large, this results in a change of the short-range order in the melt. The remaining calcium ions bind the chloride ions more firmly than do the ions of alkali metals (especially K^+).

Experiments show that at low concentrations the melts behave like ideal solutions, further dilution of which does not produce any ionic rearrangements, but is merely accompanied by random distribution of calcium ions. The experimental e.m.f. isotherms begin to deviate from the ideal curves when the concentration of calcium ions in the melt approaches a value corresponding to the composition $CaCl_2 + 2MeCl$(Me = Na, K).

In dilute melts calcium is evidently present largely in the form of complex $CaCl_4^{--}$ anions, as is the case in chloride melts containing $MgCl_2$ [10]. The number of simple Cl^- anions in the melt decreases with increasing $CaCl_2$ concentration. They would ultimately vanish entirely if the $CaCl_4^{--}$ ions were sufficiently stable. However,

the $CaCl_4^{--}$ ions begin to decompose under the influence of the cation even before the Cl^- ions have disappeared from the melt. It seems that in the region of high concentrations, where the melts deviate from ideality, chloride ions are detached consecutively from the complex calcium groups in the melt.

$$CaCl_4^{--} \rightarrow CaCl_3^- \rightarrow CaCl_2 \rightarrow CaCl^+.$$

Therefore there are certain grounds for the belief that our value for the heat of mixing of liquid calcium chloride with an equimolar mixture of sodium and potassium chlorides corresponds to the process

$$CaCl^+ + 3Cl^- \rightarrow CaCl_4^{--} \quad -5.5 \text{ kcal.}$$

Lantratov and Alabyshev [11], and subsequently Markov, Delimarsky and Panchenko [12] have published the results of their investigations of the thermodynamic properties of binary melts of lead chloride with alkali metal chlorides, carried out by the e.m.f. method. It should be noted that their melts had relatively high mole fractions of lead ions, at which deviations from ideality were observed in the case of calcium. Nevertheless, the results of these investigations show convincingly that when the fused salts are mixed definite interaction occurs between lead chloride and the alkali metal chloride. This interaction is more pronounced with increasing radius of the alkali metal ion. Similar results were obtained by Markov, Delimarsky and Panchenko [13] for binary melts of magnesium chloride and alkali metal chlorides.

LITERATURE CITED

[1] O. Ehrlich, L. Gentsch. Naturwissenschaften 40, 460 (1953).

[2] G. Wehmer, Z. anorg. allg. Chem. 276, 72 (1954).

[3] O. Kubaschewski and E. Evans, Metallurgical Thermochemistry (Russian translation) (IL, 1954), pp. 252, 298.

[4] G. Sutra, Compt. rend. 234, 1283 (1952).

[5] S. V. Karpachev and S. F. Palguev, J. Phys. Chem. 23, 942 (1949).

[6] Yu. K. Delimarsky, P. P. Turov and E. B. Gitman, Ukrain. Chem. J. 21, 314 (1955).

[7] F. R. Duke and R. W. Laity, J. Am. Chem. Soc. 76, 4046 (1954); J. Phys. Chem. 59, 549 (1955).

[8] B. F. Markov and Yu. K. Delimarsky, Ukrain. Chem. J. 19, 255 (1953).

[9] Yu. K. Delimarsky, Papers on the Chemistry of Solutions and Complex Compounds (Acad. Sci. Ukrainian SSR Press, Kiev, 1954) p. 29*

[10] H. Flood and S. Urnes, Z. Elektroch. 59, 834 (1955).

[11] M. F. Lantratov and A. F. Alabyshev, J. Appl. Chem. 26, 263 (1953).**

[12] B. F. Markov, Yu. K. Delimarsky and I. D. Panchenko, J. Phys. Chem. 28, 1987 (1954).

[13] B. F. Markov, Yu. K. Delimarsky and I. D. Panchenko, J. Phys. Chem. 29, 51 (1955).

Received March 26, 1956

---

*In Russian.

**Original Russian pagination. See C. B. Translation.

THE PREPARATION OF PURE SILICA

O. N. Nikitina

Institute of Silicate Chemistry, Academy of Sciences USSR

In the development of a method for the spectroscopic determination of small amounts of Fe, Co, Ni, Mn, Cr, Ti, V, Al, Ca and Mg in quartz, sand and other high-silica materials, it became necessary to prepare synthetic standards, owing to the lack of samples with chemical composition known reliably from analytical data [1]. Specimens of the purest native rock crystal or quartz could not be used as the pure material for preparation of standards, as they contained iron, calcium, aluminum, magnesium, titanium and sodium. Pure reactive silica (analytical-reagent grade) was also unsuitable, as it contains these elements in even greater amounts, and, moreover, has a much lower bulk density (about two fifths) than native rock crystal, quartz, or sand.

We obtained the purest silica by hydrolysis of silicon tetrachloride (tetrachlorosilane) [2]. Because of the method used for its preparation, silicon tetrachloride could not contain admixtures of elements the chlorides of which have relatively low volatility (calcium, magnesium and some others), whereas other silicon compounds are usually contaminated with these elements. Technical silicon tetrachloride may contain aluminum, titanium and iron, which form relatively volatile chlorides (b.p. of $AlCl_3$ 182.7°, $FeCl_3$ 315° and $TiCl_4$ 136.4°). Silicon tetrachloride was purified by fractional distillation. The distillation system was dried by means of concentrated sulfuric acid. The distillation of $SiCl_4$ was carried out twice. The fraction boiling at 57.6° was used for the preparation of silica.

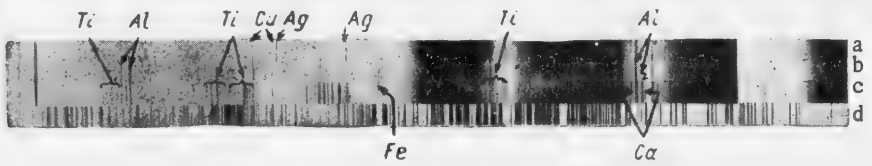

Regions of spectra: a) SiO_2 from $SiCl_4$; b) quartz; c) silicic acid (analytical grade); d) iron.

The silicon tetrachloride was hydrolyzed in ice-cooled platinum vessels. Water redistilled from a silver still was used. $SiCl_4$ was added cautiously dropwise with continuous stirring with a quartz rod until a gelatinous mass of silicic acid was formed. The gel was slowly heated on a hot plate until evolution of hydrochloric acid fumes ceased. The dried silica powder was placed in a cold muffle furnace, which was gradually heated to 1100°, and kept at 1100° for 2 hours. This gave a partially sintered powder which was ground in an agate mortar. The density of this silica was the same as the density of the specimens to be analyzed; its purity, as the figure shows, is higher than other pure specimens of silica. The spectra of specimens of quartz, silicic acid (analytical grade), and silica obtained by hydrolysis of $SiCl_4$ were photographed in the conditions used for analysis of sand and quartz samples [1].

The pure silica obtained by hydrolysis of distilled silicon tetrachloride was used for the preparation of spectroscopic standards.

The melting points of finely ground crystalline quartz and pure silica were compared. The quartz and silica powders were heated to 1700° in Galakhov's microfurnace* [3] in an atmosphere of argon, and held at that tem-

*I take this opportunity to thank F. Ya. Galakhov and S. F. Konovalova, who kindly agreed to compare the melting points of quartz and pure silica.

perature for 20 minutes. Comparison of the sinters showed that the pure silica had melted to a greater extent than the quartz. By repetition of this experiment it was established with adequate certainty that pure silica melts somewhat more readily than crystalline quartz.

The purity of the silica made by hydrolysis of silicon tetrachloride and its somewhat lower melting point than that of quartz suggest that this form of silica may be used as a material for the production of special pure crucibles and other ware used in the fusion of particularly pure materials such as silicon or germanium.

LITERATURE CITED

[1] O. N. Nikitina, Bull. Acad. Sci. USSR, Phys. Ser. 19, 2, 199 (1955).

[2] R. C. Hughes, J. Optical Soc. America 33, 1, 49 (1943).

[3] F. Ya. Galakhov, Factory Labs. 2, 254 (1951).

Received May 12, 1957

THE DYNAMIC ACTIVITY OF ADSORBENTS*

I. V. Lyubinov and N. I. Smirnov

Chair of Technology of Fundamental Organic Synthesis and Synthetic Rubber, the Lensoviet Technological Institute, Leningrad

We showed earlier [1] that the usual methods of calculation, based on determination of mass-transfer coefficients, are inconvenient for adsorption processes. Direct determinations of the dynamic activity of sorbents in relation to the adsorption conditions are of much more value. In Dubinin's well-known work [2] it is concluded, on the basis of very extensive experimental data, that dynamic activity depends on the nature of the gas and sorbent, the geometrical configuration of the layer, diameter of the sorbent grains, velocity of the air–gas mixture, and concentration of the gas in the air. On the assumption that the nature of the gas and sorbent is uniquely determined by the magnitude of the static activity in each system at the corresponding gas concentration and temperature, it is logical to assume (in the notation used in the previous communication [1]) that

$$a_g = f(a_s, w, \nu, c, d, h, d_3). \tag{1}$$

Function (1) may be expressed in criterial form either as

$$\frac{a_g}{a_s} = f(Re, C, \Gamma_1, \Gamma_2), \tag{2}$$

or as

$$\frac{a_s - a_g}{a_g} = f(Re, C, \Gamma_1, \Gamma_2). \tag{3}$$

The form (3) is preferable, as it can then be represented in terms of the usual relationship

$$\frac{a_s - a_g}{a_g} = aRe^x C^y \Gamma_1^z \Gamma_2^u, \tag{3a}$$

whereas for use of Expression (2) it is necessary to find a relationship of the type:

$$\frac{a_g}{a_s} = e^{aRe^x C^y \Gamma_1^z \Gamma_2^u}. \tag{2a}$$

We used the experimental data presented in the previous paper [1] to obtain (3a) in explicit form, on the assumption that $\frac{a_s - a_g}{a_g} = A$. The results of a series of experiments on the sorption of water vapor from air by silica gel with 2.15 mm grains, with constant layer height and apparatus diameter, made it possible to establish a direct relationship between values of A and Re, since the concentration of water vapor in the air entering the adsorption system remained practically constant. This relationship is shown graphically in Fig. 1. For comparison, the same diagram contains plots of the A–Re relationship for the systems benzene–silica gel and benzene–activated

* Communication IV.

charcoal, from our data, and ethylene–activated charcoal, from the data of Regak and Smirnov [3]. The experimental data cover the range of Re between 13 and 900.

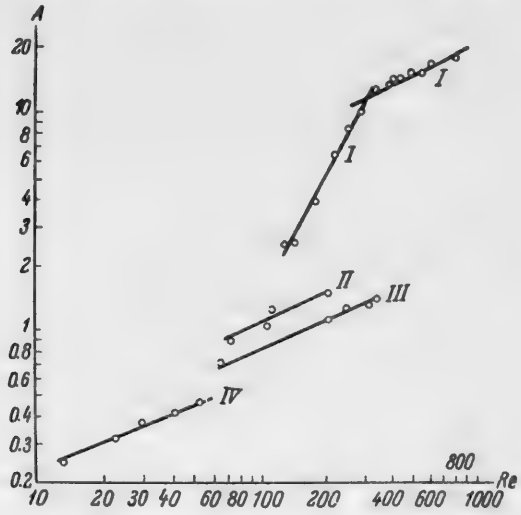

Fig. 1. Variation of the ratio A with Reynolds number (Re).
Systems: I) water vapor–silica gel (C = 2.2%), II) benzene–silica gel (C = 7.4%), III) benzene–activated charcoal (C = 8.2%), IV) ethylene–silica gel (C = 12.5%).

A number of very important conclusions can be drawn from the data in Fig. 1. First, it is clear that there is a well-defined connection between values of A and Re. Two regions determine the nature of this connection: the region of low gas concentrations and low Reynolds numbers, and the region of high concentrations. In the region of high concentrations the nature of the relationship is exactly the same for all the systems (the lines all have the same slope). This confirms our hypothesis that the values of the static activity completely and uniquely determine all the characteristics of the gas and sorbent. The same should be true in the region of low concentrations. Unfortunately, we could not prove this experimentally, as even with a small increase of the gas concentration the break between the two regions is shifted strongly in the direction of very low Reynolds numbers, which we could not achieve consistently.

The graphical relationship of Fig. 1 can be very easily obtained in analytical form. For the region of low concentrations it has the form

$$A = aRe^{1.75} \qquad (4)$$

and for the region of high concentrations

$$A = bRe^{0.5}. \qquad (5)$$

The coefficients a and b in these equations are evidently functions of C, Γ_1 and Γ_2. The region of high concentrations is the more important, and therefore we shall first consider the values of b. If the values of b are determined from the data of each experiment by means of Equation (5), it is seen that for a series of experiments performed at almost equal concentrations and equal values of Γ_1 and Γ_2 they retain a very high degree of constancy. Therefore we can take the average values of b for each series and compare them, as is done in Table 1.

TABLE 1

Comparison of Average Values of b for Different Systems

Systems	Concentration of the sorbed component in the gas (vol.%)	Γ_1	Γ_2	b
Water vapor-silica gel	2.4	0.174	0.139	0.658
	2.3	0.172	0.161	0.661
	2.2	0.330	0.139	0.665
Benzene-silica gel	7.4	0.264	0.091	0.099
	8.2	0.167	0.100	0.077
Benzene-activated charcoal	8·4	0.267	0.100	0.080
Carbon tetrachloride-activated charcoal	13.3	0.137	0.107	0.038

It is quite clear from the data in Table 1 that b does not depend either on Γ_1 or on Γ_2, but depends only on

the concentration of the substance in the gas. If the data in Table 1 are plotted as a b−C curve in logarithmic coordinates (Fig. 2), it is seen that the plot is a definite straight line, described by the equation

$$b = 0.0016\, C^{-1.6}. \tag{6}$$

From Equation (5) and (6) we have

$$A = 0.0016\, Re^{0.5} C^{-1.6}. \tag{7}$$

This is the final and complete equation for determination of dynamic activity in the region of high concentrations.

TABLE 2

Comparison of Average Values of a for the System Water Vapor−Silica Gel

Concentration of the sorbed component in the gas (vol.%)	Γ_1	Γ_2	a
2.0	0.174	0.139	0.00046
2.3	0.172	0.161	0.00048
2.2	0.333	0.161	0.00152

TABLE 3

Average Values of a_1 for Different Systems

System	Concentration of the sorbed component in the gas (vol.%)	a_1
Water vapor−silica gel	2.2	0.0100
Benzene−silica gel . . .	7.9	0.0099
Carbon tetrachloride−−activated charcoal	12.3	0.0104

It was considerably more difficult to establish the relationship between the criteria in the region of low concentrations, as only one curve for the sorption of water vapor by silica gel, and individual points for other systems were available. The suitability of these points, which corresponded to the lowest Reynolds numbers, was determined by the fact that the relationships given by them showed large deviations from Equation (7). As in the previous instance, the average values of a were first compared for the system water vapor−silica gel (Table 2).

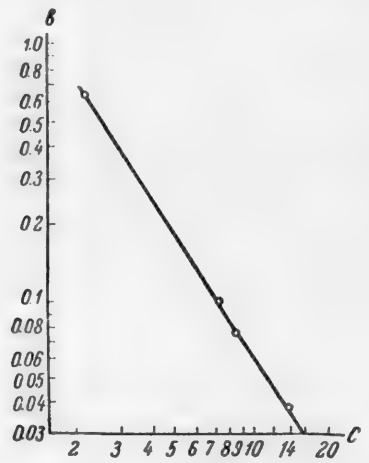

Fig. 2. Variation of the coefficient b with the concentration C.

It is clear from Table 2 that in the region of low concentrations the criterion Γ_2 again has no influence on the dynamic activity, but the influence of Γ_1 is very pronounced. By the same procedure as before it is easy to show that

$$a = a_1 \Gamma_1^{1.75}. \tag{8}$$

We now determine the average values of a_1 for different systems in order to establish the effect of concentration on it. It is easy to find the average values of a_1, as variations between different experiments in a given series are negligible. The results are tabulated in Table 3.

The data in Table 3 show convincingly that the dynamic activity is independent of the concentration in the region of low concentrations. By combining Equations (4) and (7), with the use of the value of a_1 from Table 3 for the low-concentration region, we finally obtained the complete equation:

$$A = 0.01\ Re^{1.75} \Gamma^{1.75}. \tag{9}$$

From equations for both regions it is possible to determine the critical value of the criterial complex for the transition from one region to the other. At the transition point Equations (7) and (9) are evidently both valid. Therefore we can write

$$0.0016\, Re^{0.5} C^{-1.6} = 0.01\, Re^{1.75} \Gamma_1^{1.75}.$$

Hence

$$Re^{1.25} C^{1.6} \Gamma_1^{1.75} = \frac{0.0016}{0.01} = 0.16$$

or

$$Re C^{1.28} \Gamma_1^{1.4} = 0.351. \quad (10)$$

All cases of adsorption for which the value of the power term in the left-hand side of Equation (10) is less than 0.351 belong to the first region, which we describe as the region of low concentrations, and Equation (9) should be used for calculations in these cases. All other cases belong to the region of high concentrations, and Equation (7) is used for calculations for them.

TABLE 4

Verification of Equations (7) and (9) for the System Isobutylene—Activated Charcoal

Re	Γ_1	$Re C^{1.28} \Gamma_1^{1.4}$	A experiment	A calculated	Deviation (%)
26.62	0.1646	below 0.351	0.171	0.133	—22.2
39.60	0.1646		0.209	0.189	— 9.5
40.93	0.1667		0.186	0.194	+ 4.3
49.63	0.1646		0.242	0.212	—12.4
64.23	0.1646	above	0.231	0.241	+ 4.3
66.44	0.1646	0.351	0.262	0.245	— 6.5
106.1	0.1667		0.290	0.309	+ 6.6
122.9	0.1667		0.310	0.333	+ 7.4
141.1	0.1646		0.321	0.357	+11.2

The accuracy of Equations (7) and (9) is very high. This is shown by the fact that our experimental values of A obtained for the sorption of water vapor from air by silica and alumina gels, for the sorption of benzene vapor from air by silica gel and activated charcoal, and for the sorption of carbon tetrachloride vapor from air by activated charcoal, do not differ from the values calculated by means of these equations by more than ± 5% in the great majority of cases. It was very important to test these equations for data obtained by other workers. As an example, we used the data of Regak and Smirnov [3] on the sorption of isobutylene from its mixtures with nitrogen, containing 16 vol.% of the hydrocarbon, by activated charcoal. The results are given in Table 4.

It is seen that our equations are confirmed quite satisfactorily by these data.

SUMMARY

1. It was confirmed experimentally that the value of the static activity in adsorption with respect to the substance being adsorbed characterizes completely and uniquely the nature and the structural features of the sorbate and sorbent.

2. On this basis, the laws governing the dynamic activity of sorbents, which are the same for all sorbent—sorbate systems, have been determined. These laws are expressed in the form of criterial equations.

3. It is shown that there are two regions of the relationship between the dynamic activity and the hydrodynamic, concentrational, and geometrical factors of the adsorption process. The critical value of the criterial complex for the transition from one region to the other has been determined. It is shown that in the first region, which we term the region of low concentrations, the dynamic activity does not depend on the concentration, and that in the second region, which we term the region of high concentrations, the dynamic activity does not depend on geometrical factors. It is shown that in both regions the dynamic activity is independent of the particle size of the sorbent, at least in the range of grain diameter — apparatus diameter ratios between 0.04 and 0.16.

LITERATURE CITED

[1] I. V. Lyubimov and N. I. Smirnov, J. Appl. Chem. 30, 9, 1408 (1957).*

[2] M. M. Dubinin, Physicochemical Principles of Sorption Technology (ONTI, 1935).**

[3] N. Ya. Regak and N. I. Smirnov, J. Appl. Chem. 28, 433 (1955).*

Received April 12, 1957

*Original Russian pagination. See C. B. Translation.

** In Russian.

PHASE DIAGRAM OF THE SYSTEM $Na_3AlF_6 - Li_3AlF_6 - Al_2O_3$

V. P. Mashovets and V. I. Petrov

All-Union Aluminum–Magnesium Institute

Because of the difficulties in the production of alumina by electrolysis of cryolite–alumina melts, mainly due to the high melting point of the electrolyte, numerous attempts have been made to find additives which would lower the melting point and improve the other technological properties of the melt. Many additives (the fluorides of calcium and magnesium, sodium chloride, etc.) have been tested in industry over a period of several decades, but none proved very effective.

The addition of lithium fluoride, which should lower the melting point, decrease the density, and increase the conductivity of the electrolyte, is a very attractive proposition. The availability of considerable amounts of lithium raw materials, and the successes achieved in the technological processing of these materials, open up prospects of the utilization of lithium fluoride in the production of aluminum.

Pushin and Baskov [1], and later Fedotyev and Timofeev [2] found lithium cryolite, Li_3AlF_6, with m.p. 800° [1] and 790° [2] in the system $LiF - AlF_3$; the mleting points given for LiF by these authors are 870° [1] and 860° [2], whereas others [3-7] found that lithium fluoride melts at 845 ± 5°.

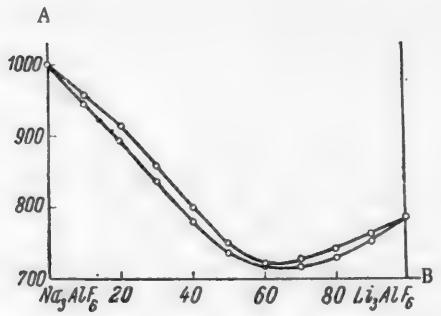

Fig. 1. The system $Na_3AlF_6 - Li_3AlF_6$, after Drossbach [8].
A) Temperature (in °C), B) composition (wt.%).

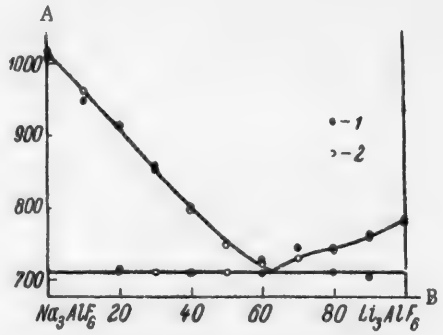

Fig. 2. The system $Na_3AlF_6 - Li_3AlF_6$ from our data.
A) Temperature (in °C), B) composition (wt.%).
1) By Kumakov's pyrometer, 2) from cooling curves.

Drossbach [8] carried out a detailed electrochemical study of the system $Na_3AlF_6 - Li_3AlF_6 - Al_2O_3$, but he investigated the phase diagram of the system mainly by the visual method. Moreover, the diagram obtained by Drossbach for the binary system $Na_3AlF_6 - Al_2O_3$ differed appreciably from Lundina's diagram [2]; we consider that the latter is the more reliable, as it is in good agreement with the results of many other investigations [9, 10]. We therefore repeated the investigation of the ternary system.

We used, both the usual cooling-curve method, and the thermogram method with the use of Kumakov's pyrometer with a differential platinum/platinum–rhodium thermocouple. Native coarsely-crystalline cryolite, sublimed aluminum fluoride, and chemically pure lithium fluoride and aluminum oxide were used. The fusion was performed in platinum crucibles with closely fitting lids, to prevent interaction of the melts with atmospheric moisture.

Drossbach found m.p. 998 and 875° respectively for pure sodium and lithium cryolites; our values are 1012 ± 4° and 782 ± 3°. The system $Na_3AlF_6 - Li_3AlF_6$, according to Drossbach (Fig. 1) forms a continuous series of solid solution with minimum crystallization temperature 720-723°. According to our data, this system has a simple eutectic corresponding to 62 wt. % Li_3AlF_6 and 710° (Fig. 2). The solidus temperature is very indistinct on the cooling curves, but it can be determined very distinctly by means of Kurnakov's pyrometer with good reproducibility over the whole composition range. The liquidus curves in the two graphs agree closely, except in the region near the eutectic point. Optical crystallographic investigations revealed the presence of a eutectic consisting of two anisotropic phases, sodium and lithium cryolites, in all the specimens. The structure of the eutectic is in the form of close parallel lines. Specimens from the hypoeutectic region also contain cubic crystals of sodium cryolite. Cryolithionite ($Na_3Li_3Al_2F_{12}$, corresponding to 43.5 wt.% Li_3AlF_6), which is known as a mineral, does not appear in the phase diagram. It is evidently decomposed completely below the eutectic temperature.

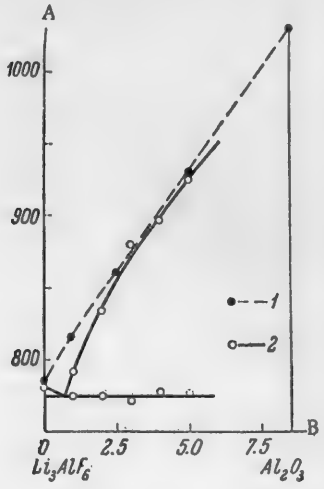

Fig. 3. The system $Li_3AlF_6 - Al_2O_3$.
A) Temperature (in °C),
B) composition (wt. %).
1) After Drossbach [8],
2) our data.

The points tested by us in the system $Na_3AlF_6 - Al_2O_3$ were in excellent agreement with Kostyukov's diagram [10] in the hypoeutectic region, and with Lundina's diagram [9] in the hypereutectic region. These two diagrams are, however, similar. The eutectic corresponds to 15wt.% Al_2O_3 and 935°; the solubility of Al_2O_3 at 1000° is 16.5wt.%.

The system $Li_3AlF_6 - Al_2O_3$ was represented by Drossbach as a linear branch of primary crystallization. The end of crystallization could not be detected visually. According to our data, this is a system with a eutectic (Fig. 3). The eutectic temperature 775 ± 3° is determined quite definitely, but the eutectic composition, 0.7 wt.% Al_2O_3, is found only from the point of intersection of the hypereutectic branch of the liquidus with the solidus line. The solubility of alumina in lithium cryolite at 950° (the temperature used in industrial electrolysis) reaches 6 wt.%.

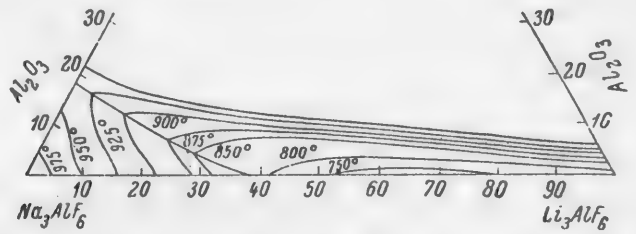

Fig. 4. The system $Na_3AlF_6 - Li_3AlF_6 - Al_2O_3$, after Drossbach [8].

The diagram for the ternary system $Na_3AlF_6 - Li_3AlF_6 - Al_2O_3$, according to Drossbach (Fig. 4), is divided into two fields by the eutectic line originating from the binary eutectic sodium cryolite–alumina, and reaching the side of the two cryolites at a point corresponding to 40 wt.% Li_3AlF_6. This last point has no justification, as Drossbach denied the eutectic character of the system of the two cryolites.

We studied, within the field of the ternary diagram, five sections with the weight ratios Na_3AlF_6 : Li_3AlF_6 9 : 1, 8 : 2, 7 : 3, 6 : 4 and 5 : 5, containing up to 12-18 wt. % Al_2O_3. The region richer in lithium cryolite was not investigated as the nature of the diagram is obvious. The ternary diagram (Fig. 5) is divided into three fields of primary crystallization by three eutectic lines, originating from the three binary eutectics and meeting at the ternary eutectic point. The latter is so close to the eutectic for the two cryolites that its exact position could not be determined. Similarly, the line which limits the field of primary crystallization of lithium cryolite is so close to the side for the two cryolites that it almost coincides with this side of the triangle on the scale used in the diagram. However, the eutectic nature of all the binary systems leaves no doubt about the nature of the ternary diagram.

It follows from Fig. 5 that partial substitution of lithium cryolite for sodium cryolite considerably lowers the melting point of the electrolyte, but at the same time decreases the solubility of alumina. Nevertheless, regions suitable for practical electrolysis can be found in the ternary system. For example, an electrolyte containing 68 wt.% Na_3AlF_6, 25% Li_3AlF_6 and up to 7% Al_2O_3 can be used for electrolysis at about 880°, i.e., about 80° below the temperature used at present. Of course, as the solubility of alumina is so low, the amount of it put in the cell at a time must be decreased, i.e., the bath needs more frequent adjustment than is the current practice. An increase of the amount of electrolyte in the cell is also desirable.

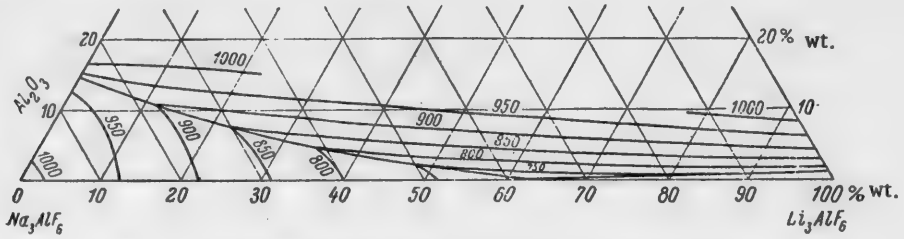

Fig. 5. The system Na_3AlF_6–Li_3AlF_6–Al_2O_3, from our data.

SUMMARY

1. The system Na_3AlF_6–Li_3AlF_6 has a simple eutectic corresponding to 710° and 62 wt.% of lithium cryolite. In the system Li_3AlF_6–Al_2O_3 the eutectic is at 775° and 0.7 wt.% Al_2O_3.

2. The diagram for the system Na_3AlF_6–Li_3AlF_6–Al_2O_3 has three fields of primary crystallization; the ternary eutectic is very close to the binary eutectic for the two cryolites.

3. Although the solubility of alumina is lower in mixtures of the two cryolites, there are nevertheless regions in the ternary system which are suitable for industrial electrolysis at a lower temperature (of the order of 880°).

LITERATURE CITED

[1] N. A. Pushin and A. V. Baskov, J. Russ. Phys.-Chem. Soc. 45, 82 (1913); Z. anorg. Ch. 81, 347 (1913).

[2] P. P. Fedotyev and R. Timofeev, Z. anorg. Ch. 206, 263 (1932); Metallurgist 7, 60 (1933).

[3] H. Wartenberg and H. Schulz, Z. Elektroch. 27, 568 (1921).

[4] F. M. Jaeger, Z. anorg. allg. Ch. 101, 177 (1927).

[5] I. I. Kitaigorodsky, T. A. Popova and O. K. Botvinkin, Bull. Inst. Phys. Chem. Analysis 6, 135 (1933).

[6] E. Thilo and H. A. Lehman, Z. anorg. and allg. Ch. 258, 332 (1949).

[7] A. V. Novoselova, Yu. P. Simonov, and E. I. Yarembash, J. Phys. Chem. 26, 1245 (1952).

[8] P. Drossbach, Z. Elektroch. 42, 65 (1936).

[9] V. P. Mashovets, The Electrometallurgy of Aluminum (ONTI, 1938).*

[10] G. A. Abramov, M. M. Vetyukov, I. P. Gupalo, A. A. Kostyukov and L. N. Lozhkin, Theoretical Principles of the Electrometallurgy of Aluminum (Metallurgy Press, 1953).*

Received April 19, 1957

* In Russian.

EQUATION FOR CALCULATION OF FLOODING VELOCITIES IN PACKED COLUMNS

V. V. Kafarov and Yu. I. Dytnersky

It was shown in previous publications [1, 4] that the most efficient conditions for mass transfer in packed columns arise at flooding velocities.

Several equations have been proposed for determination of the flooding velocities in packed columns, for gas–liquid [3], vapor–liquid [4, 5], and liquid–liquid [6, 7] systems.

It has been shown [2] that the equations for the limiting flow rates in different systems are of the same form, and only the numerical values of the coefficients vary. However, no general equation for flooding velocities in packed columns has been derived. It is true that some attempts were made [8, 9] to derive such an equation for gas–liquid and liquid–liquid systems, but the expressions obtained are cumbersome and inconvenient to use.

By the generalization of extensive numerical data obtained by a number of investigators [3-6, 8-25] and of our own data, we have been able to derive a single equation for calculation of flooding velocities in packed columns, for gas–liquid, vapor–liquid, and liquid–liquid systems.

At flooding velocities in packed columns free turbulence develops, characterized by instability of the interphase boundaries, with eddies of one phase penetrating into eddies of the other; it is therefore not possible to determine which of the phases in the packing is continuous and which disperse. Therefore in calculations of flooding velocities it is sufficient to determine the linear velocity of one of the phases, and it is then possible to determine the linear velocity of the other from the ratio of the flow rates of the two phases.

The figure shows the dependence of limiting flow rates in packed columns on different physical properties of the phases and the characteristics of the packing, for different systems. The abscissa axis gives values of the term:

$$x = \left(\frac{L}{G}\right)^{\frac{1}{4}} \left(\frac{\gamma_1}{\Delta\gamma}\right)^{\frac{1}{8}}, \tag{1}$$

and the ordinate axis, the values of the term:

$$y = \frac{W_1^2 \sigma}{g F_s^3} \frac{\gamma_1}{\Delta\gamma} \left(\frac{\mu}{\mu_w}\right)^{0.16} \left(\frac{S_{cd}}{S_{ca} + S_{da}}\right)^{0.2}, \tag{2}$$

where W_1 is the linear velocity of the light phase (in m/second); γ_1 is the density of the light phase in kg/m^3 (the density of the gas or vapor in gas–liquid or vapor–liquid systems); γ_h is the density of the heavy phase in kg/m^3 (the density of the liquid phase in gas–liquid or vapor–liquid systems); Δ_γ is the difference of the densities of the heavy and light phases (in kg/m^3); μ is the viscosity of the liquid in gas–liquid and vapor–liquid systems, and the viscosity of the liquid which constitutes the continuous phase in the full section of the column for liquid–liquid systems (in centipoises); μ_w is the viscosity of water at 20° (in centipoises); S_{cd} is the surface tension at the interface between the continuous and disperse phases (in dynes/cm); S_{ca} and S_{da} are the surface tensions at the interfaces between the continuous phase and air, and the disperse phase and air, respectively (in dynes/cm); σ is the specific surface of the packing (in m^2/m^3); g is the acceleration due to gravity (9.81 m/sec^2);

L is the flow rate of the heavy phase: gravimetric (in kg/ m^2 · hour) for gas–liquid and vapor–liquid systems, and volumetric (in m^3/m^2 · hour) for liquid–liquid systems; G is the corresponding rate for the light phase; e is the base of natural logarithms.

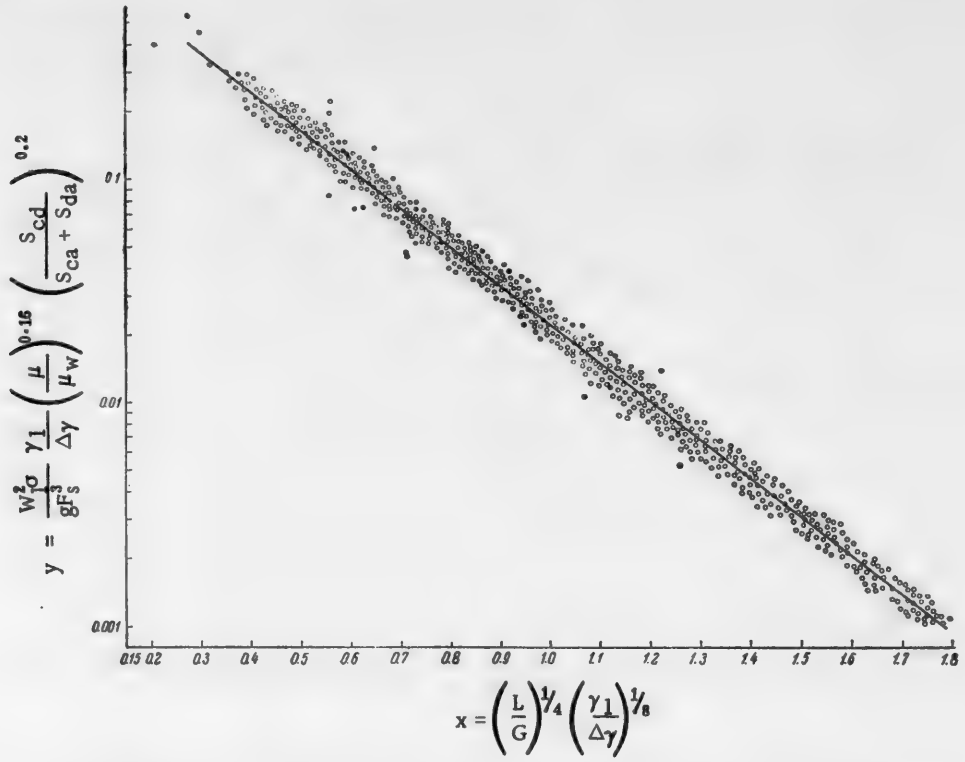
$y = \frac{w_0^2 \sigma}{g F_s^3} \frac{\gamma_1}{\Delta\gamma} \left(\frac{\mu}{\mu_w}\right)^{0.16} \left(\frac{S_{cd}}{S_{ca} + S_{da}}\right)^{0.2}$
0.1
0.01
0.001
0.15 0.2 0.3 0.4 0.5 0.6 0.7 0.8 0.9 1.0 1.1 1.2 1.3 1.4 1.5 1.6 1.7 1.8
$x = \left(\frac{L}{G}\right)^{1/4} \left(\frac{\gamma_1}{\Delta\gamma}\right)^{1/8}$

Limiting flow rates in packed columns for different physical phases and packing characteristics.

Experimental data obtained by the author and data taken from the literature for gas–liquid [3, 10-12, 14, 19-23], vapor–liquid [4, 13,* 15, 16], and liquid–liquid [5, 6, 8, 9, 17, 18, 24-26] systems are plotted in the graph. It is seen that the experimental data for different systems and different packings fit fairly satisfactorily around a straight line, the average percentage deviation being ± 12.5%.

The straight line can be represented by the equation:

$$y = 1.2\, e^{-4x}. \tag{3}$$

If it is taken into account that in the experimental data used $\frac{L}{G}$ varied in the range 0.05 – 260, μ = 0.3 – 113 centipoises, γ_l = 0.08 – 1000 kg/ m^3, γ_h = 1000 – 1580 kg/ m^3, S = 8.9 – 71 dynes/ cm, while the various packings included rings from 5 × 5 to 80 × 80 mm, saddles between 8 and 25 mm, balls and lumps of various sizes, etc., it may be assumed that the equation is reasonably reliable.

Therefore Equation (3) may be used for calculation of flooding velocities in packed columns for any system and any type of packing, and can be regarded as universal in this sense.

For gas–liquid and vapor liquid systems:

$$\frac{S_{cd}}{S_{ca} + S_{da}} = 1,$$

while $\Delta\gamma = \gamma_s - \gamma_l \approx \gamma_s$

* The data from paper [13] are taken for the maximum column efficiency.

and the terms (1) and (2) become:

$$x = \left(\frac{L}{G}\right)^{\frac{1}{4}} \left(\frac{\gamma_1}{\gamma_s}\right)^{\frac{1}{8}} \tag{4}$$

and

$$y = \frac{W_1^2 \sigma}{g F_s^3} \frac{\gamma_1}{\gamma_s} \left(\frac{\mu}{\mu_w}\right)^{0.16}. \tag{5}$$

Specimen calculation. Calculate the diameter of an extraction column for the system benzene–phenolic water. The packing consists of Raschig rings 12 × 12 × 2 mm, σ = 420 m^2/m^3, F_s = 0.58 m^2/m^2. The phenolic water rate L = 6 m^3/hour. The benzene rate G = 3 m^3/hour (the disperse phase). γ_l = 880 kg/m^3, γ_h = 1000 kg/m^3, μ = 1 centipoise, $\frac{S_{cd}}{S_{ca} + S_{da}} = \frac{35}{72.8 + 30} = 0.34$.

The value of y is found from Equation (3).

$$y = 1.2 \cdot 2.71^{-4\left(\frac{6}{3}\right)^{1/4}\left(\frac{880}{120}\right)^{1/8}} = 0.0027.$$

Then the limiting linear velocity of the light phase (benzene) is

$$W_1 = \sqrt{\frac{ygF_c^3\Delta\gamma}{\sigma\gamma_1}\left(\frac{\mu_w}{\mu}\right)^{0.16}\left(\frac{S_{ca}+S_{da}}{S_{cd}}\right)^{0.2}} =$$

$$= \sqrt{\frac{0.0027 \cdot 9.8 \cdot 0.58^3 \cdot 120 \cdot 1}{420 \cdot 880 \cdot 0.34^{0.2}}} = 0.00133 \text{ m/sec.}$$

Since the linear velocity of the continuous phase in the full section of the column is used for determination of packed column diameters, it is ultimately necessary to determine the velocity of the continuous phase calculated for the full section of the column.

For $\frac{L}{G} = \frac{6}{3}$ and the linear velocity W_l of the disperse light phase found above, we find the linear velocity of the continuous phase (W_c).

$$W_c = W_1 \frac{L}{G} = 0.00133 \cdot 2 = 0.00266 \text{ m/sec.}$$

The amount and the linear velocity of the phenolic water being known, we can find the diameter of the packed extraction column operating at flooding velocities.

$$d = \sqrt{\frac{4 \cdot L}{3600\pi \cdot W_c}} = \sqrt{\frac{4 \cdot 6}{3600 \cdot 3.14 \cdot 0.00266}} = 0.89 \text{ m.}$$

LITERATURE CITED

[1] V. V. Kafarov, Processes and Equipment in Chemical Technology, Collected Papers (Goskhimizdat, 1953).*

[2] V. V. Kafarov, J. Chem. Ind. 5 (1953).

[3] W. A. Bain and O. A. Hougen, Trans. Am. Inst. Chem. Eng. 40, 29 (1944).

[4] V. V. Kafarov and L. P. Blyakhman, J. Appl. Chem. 24, 12, 1274 (1951).**

[5] A. N. Planovsky and V. V. Kafarov, J. Chem. Ind. 4 (1946).

* In Russian.

** Original Russian pagination. See C. B. translation.

[6] J. W. Grawford and C. R. Wilke, Chem. Eng. Progr. 47, 423 (1951).

[7] V. V. Kafarov and M. A. Planovskaya, J. Appl. Chem. 24, 624 (1951).*

[8] S. Fujita, T. Kikuzawa and S. Watanabe, Chem Eng. 17, 6, 230 (1953).

[9] E. H. Hoffing and F. J. Lockhart. Chem. Eng. Progr. 50, 2, 94 (1954).

[10] N. M. Zhavoronkov, Hydraulic Principles of the Scrubber Process and Heat Transfer in Scrubbers (Soviet Science, 1944).**

[11] T. K. Sherwood, G. H. Shipley and F. A. Holloway, Ind. Eng. Ch. 30, 765 (1938).

[12] T. K. Sherwood and R. L. Pigford. Absorption and Extraction (1952).

[13] E. Kirschbaum and A. David, Chem. Eng. Techn. 25, 10, 592 (1953).

[14] I. C. Elgin and F. B. Weiss, Ind. Eng. Ch. 31, 435 (1939).

[15] V. V. Kafarov and B. G. Lukyanov, J. Chem. Ind. 4, 11 (1950).

[16] A. C. Heinlein, R. E. Manning and M. R. Cannon, Chem. Eng. Progr. 47, 7, 344 (1951).

[17] J. H. Ballard and E. L. Piret, Ind, Eng. Ch. 42, 6, 1088 (1950).

[18] R. R. Breckenfeld and C. R. Wilke, Chem. Eng. Progr. 46, 187 (1950).

[19] A. M. White, Trans. Am. Inst. Chem. Eng. 31, 390 (1935).

[20] E. M. Schoenborn and W. J. Dougherty, Trans. Am. Inst. Chem. Eng. 40, 51 (1944).

[21] S. Uchida and S. Fujita, J. Soc. Chem. Ind. Japan, 39, 885 (1936).

[22] T. S. Baker, T. H. Chilton and H. C. Vernon, Trans. Am. Inst. Chem. Eng. 31, 296 (1935).

[23] V. V. Kafarov, A. G. Kasatkin and N. A. Prishedko, J. Chem. Ind. 6, 171 (1949).

[24] F. H. Blanding and I. C. Elgin, Trans. Am. Inst. Chem. Eng. 38, 305 (1942).

[25] S. B. Row, I. H. Koffolt and I. R. Withrow, Trans. Am. Inst. Chem. Eng. 37, 559 (1941).

[26] A. P. Colburn, Trans. Eng. Am. Chem. Eng. 38, 336 (1942).

Received May 25, 1956

---

*In Russian.

**Original Russian pagination. See C. B. Translation.

THROWING POWER IN ELECTROFORMING

A. M. Ginberg and Yu. A. Klyachko

In available publications on the throwing power of electrolytes, including copper electrolytes, the relationship between throwing power and the time of electrolysis or the thickness of the deposited layer is not considered. The probable reason is that all the investigations in this field have been carried out in relation to galvanic coatings, the thickness of which does not usually exceed a few hundredths of a millimeter.

Nevertheless, it is generally known that in the electrolytic refining of copper the uniformity of the coatings formed on the copper cathodes depends on the time of electrolysis (they become progressively thicker at the edges while the middle of the cathode is covered considerably more slowly). It has been observed that this effect is much more pronounced in prolonged electrolysis. It is especially prominent at high current densities.

The progressive increase in the irregularity of the coating during prolonged electrolysis is caused by distortion of the initial configuration of the cathode, and the subsequent influence of this distortion on the distribution of the current over the coated surface.

As a result, the distribution of the copper deteriorates progressively with duration of the process.

The literature does not contain any quantitative evaluation of this effect, which is highly important in electroforming. To obtain some idea of the effect of the time of electrolysis on throwing power in rapidly-acting acid copper electrolytes, we measured the thickness of the copper layer at various points of the cathode at intervals. The cathodes were polished rectangular plates 100 × 100 × 1 mm. The electrolysis was carried out in a standard works cell used for high-speed electrodeposition, 1000 × 800 × 800 mm in size, fitted with a special heater, devices for air agitation and continuous filtration, and a special instrument for automatic regulation of current density.

The anodes were pairs of rectangular copper plates 100 × 100 × 10 mm, placed parallel and on each side of the cathodes 100 mm from the latter. Copper was deposited from an electrolyte of the following composition (in g/liter): $CuSO_4$ – 250, H_2SO_4 – 70, ethyl alcohol – 10.

The electrolyte temperature was 38°. The cathode current density was 20 amps/dm^2. The electrolyte was vigorously agitated by means of air and continuously filtered during the electrolysis. The cathodes were coated for 1, 10 and 20 hours. The reverse sides of the cathodes were coated with a layer of special insulating material to prevent deposition of copper on them. Two cathodes connected by their insulated sides, thus forming a single separable cathode, were simultaneously placed in the cell. This allowed relatively accurate measurements of the thickness of the copper deposits to be made.

A horizontal optimeter was used for all the measurements before and after the deposition, the accuracy being 1 μ. Spherical heads were used for the measurements. Each cathode was measured at 49 points. Because of the overgrowth at the edges of the specimens, which interfered with the measurements, the extreme points were measured at a distance of 2 mm from the edges. All the points measured were arranged symmetrically over the cathode, 16 mm apart.

Investigation of the thickeness of the copper layer at different points showed that the initially flat surface of the cathode became curved as the result of nonuniform deposition.

To determine the nature of the curvature, several sections were taken in horizontal and vertical directions.

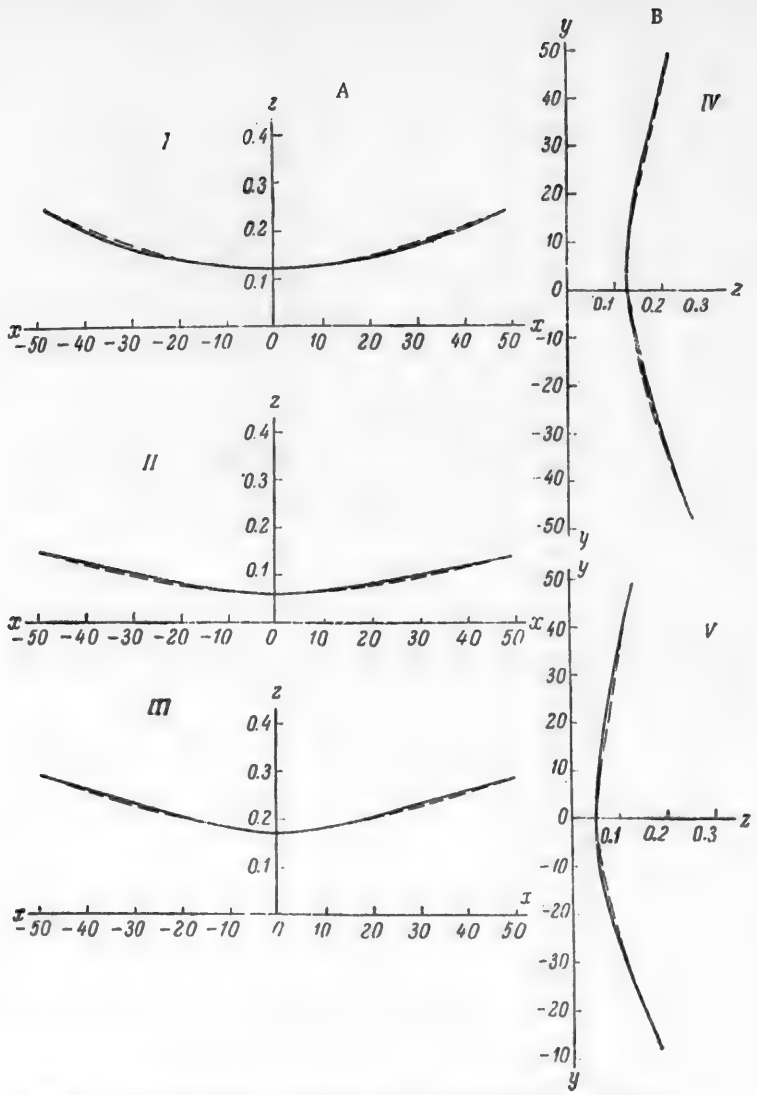

Fig. 1. Curves for the horizontal (A) and vertical (B) sections of the cathode after deposition of copper for 1 hour (the dash lines here and in Figs. 2 and 3 represent calculated hyperbolas).

A: I) top, II) middle, III) bottom; B: IV) edge section, V) middle (this applied to all the figures). 1 : 1 scale along x and y axes, 100 : 1 along the z axis.

The most typical of the curves obtained along the horizontal sections are shown as continuous lines in Figs. 1, 2 and 3. In these figures the distances from the median line of the cathode to each of the points (in mm) are taken along the x axis, and the thicknesses of the copper deposits (in mm) are taken along the y axis.

Examination of Figs. 1, 2 and 3 suggests that these curves are hyperbolas. To test this, hyperbolas were plotted from the equation:

$$\frac{z^2}{A^2} - \frac{x^2}{B^2} = 1.$$

in Figs. 1, 2 and 3 together with the experimental curves.

The values of A and B were so chosen that the hyperbolas were as close as possible to the experimental curves. Comparison of the experimental and the calculated curves shows that the deviations do not exceed 10%. This confirms that the experimental curves are hyperbolas.

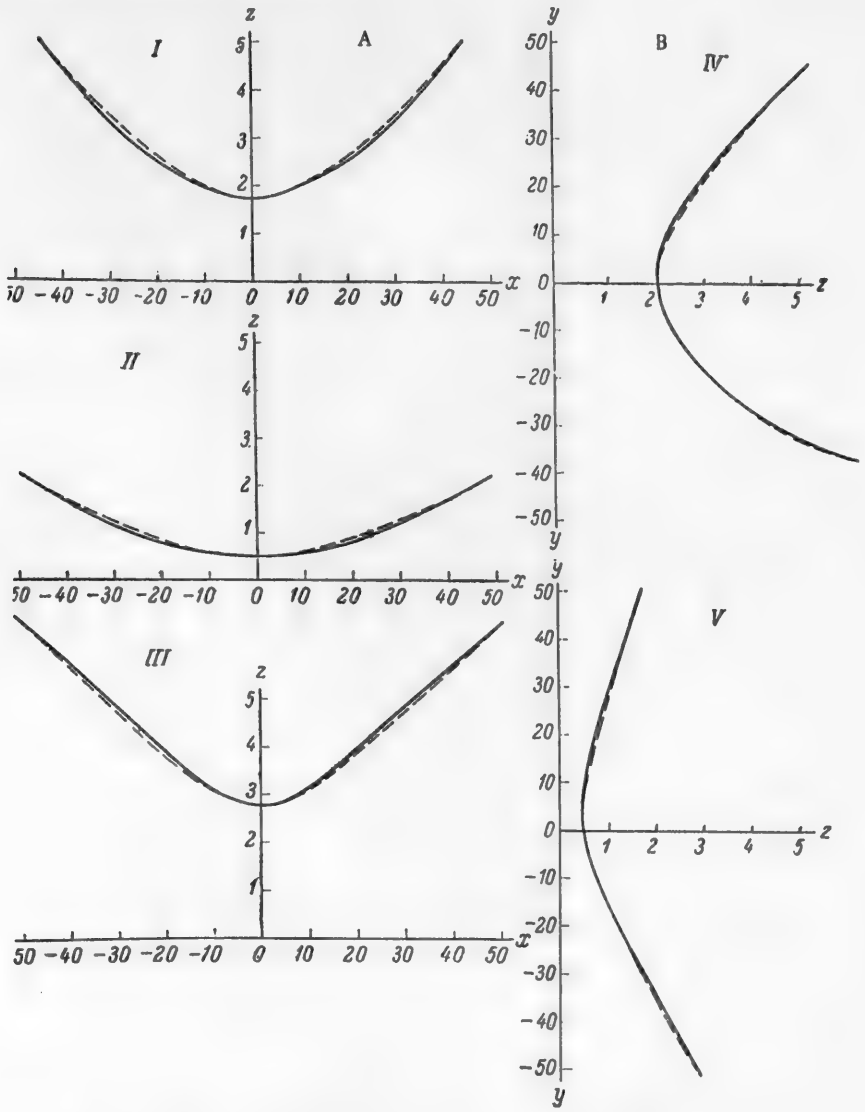

Fig. 2. Curves for the horizontal (A) and vertical (B) sections of the cathode after deposition of copper for 10 hours.

1 : 1 scale along x and y axes, 10 : 1 along the z axis.

The curves for the horizontal sections are symmetrical about the median line of the cathode. This is not so for the curves for the vertical sections. This suggests that the curves for the vertical sections consist of branches of different hyperbolas.

The curves obtained for the vertical sections are indicated in Figs. 1, 2 and 3 by continuous lines. The distances from the median line of the cathode to the points are taken along the y axis (in mm), and the thickness of the copper layer is taken along the z axis. Branches of hyperbolas calculated from the equation

$$\frac{z^2}{A^2} - \frac{y^2}{B^2} = 1.$$

are also plotted in the same coordinates.

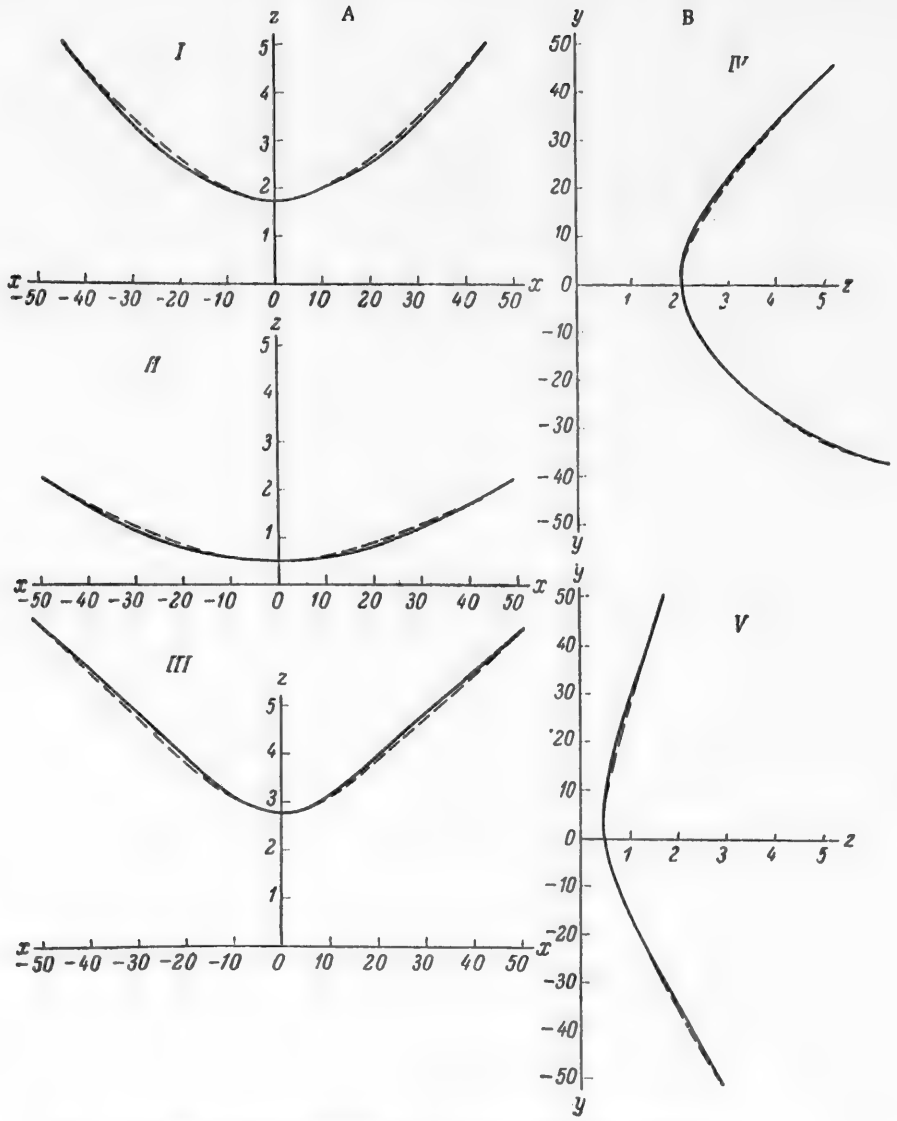

Fig. 3. Curves for the horizontal (A) and vertical (B) sections of the cathode after deposition of copper for 20 hours.

1 : 1 scale along x and y axes, 10 : 1 along the z axis.

The deviations betweeen the calculated hyperbolas and the curves based on the measurements do not exceed 10% in this case.

We now consider the nature of the variations of the hyperbolas with the time of deposition. To do this, we compare the ratio $\frac{A}{B}$ for the hyperbolas, which is to some extent a measure of the curvature.

Values of the ratio $\frac{A}{B}$ for different deposition time are given in the Table. It is seen that the ratio $\frac{A}{B}$ increases with deposition time, indicating increasing curvature of the hyperbolas.

The different values of $\frac{A}{B}$ for hyperbolas in the upper, middle and lower horizontal sections of the cathode

show that their curvatures differ. The hyperbola for the bottom edge has the greatest curvature. The curvature diminishes toward the middle section, and the hyperbola in the middle section of the cathode has the least curvature. The curvature increases in the upper part of the cathode, but less so than in the lower part.

Values of the Ratio $\frac{A}{B}$ for Different Deposition Times

Hyperbola	Deposition time (hours).	Ratio A/B
Upper for horizontal section	1	0.00374
Middle for horizontal section		0.0024
Lower for horizontal section		0.0043
Upper for horizontal section	10	0.0044
Middle for horizontal section		0.00241
Lower for horizontal section		0.0566
Upper for horizontal section	20	0.106
Middle for horizontal section		0.0429
Lower for horizontal section		0.127

SUMMARY

1. When copper is deposited in electroforming on flat surfaces, the configuration of the surfaces is distorted, and the flat surfaces become curved.

Sections of the curved surface formed are hyperbolas; curves for the vertical sections consist of branches of different hyperbolas. These hyperbolas are usually less curved at the top than at the bottom.

2. The curvature of the hyperbolas increases with increasing time of deposition.

Received July 21, 1956

CORROSION OF STEEL IN THE ATMOSPHERE OF A STEEL MILL*

A. V. Shreider and A. I. Sokolikov

Moscow Steel Institute

The equipment of the different departments of steel mills is damaged by atmospheric corrosion in very different ways. Mobile structures and other constructions often present peculiarities of structure preventing their protection by surface coatings. Because of this the destruction of steel assembly parts and beams by corrosion is often so intense that replacements must be made annually and sometimes even biannually.

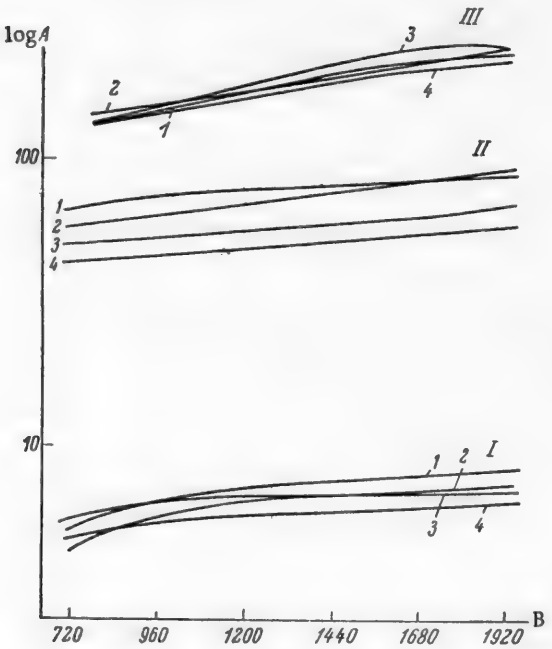

Kinetics of corrosive destruction of steel samples: (1) – Steel 40; (2) – Steel 30 KhGSA; (3) – Armco iron; (4) – Steel NL-2, in the atmosphere of I) open hearth plant; II) plant's yard; III) etching shop of the rolling mill.
A) Loss of weight (in g/m^2); B) time (in hours).

Examination of various installations at the "Sickle and Hammer" plant in Moscow allowed us to distinguish three areas of the plant, divided according to the intensity and the character of the damage observed: 1) Areas where scale is being removed by acid treatment; in these areas the air contains:

0.0003-0.0026 mg/l of H_2SO_4
0.00003-0.00010 mg/l of HNO_3
0.00002-0.00004 mg/l of HCl

and the relative humidity is 80-95%. 2) Open hearth plant, characterized by higher temperature and low relative humidity of the air. 3) Plant's yard, characterized by strong variations of air humidity, and by pollution with dirt, smoke, soot, and acid and sulfurous exhaust products from the etching, open hearth, rolling mill and other departments.

The most intense corrosion takes place in all the areas of acid etching and the least intense corrosion in the open hearth plant.

Intermediate attack occurs in the open yard of the mill.

Four different steels: Steel 30 KhGSA (0.30 C, 0.95 Mn, 0.95 Si, 0.033 S, 0.030 P, 0.83 Cr, 0.25 Ni); Steel 40 (0.39 C, 0.56 Mn, 0.25 Si, 0.038 S, 0.040 P, 0.28 Cr, 0.23 Ni); Steel NL-2 (0.18 C, 0.61 Mn, 0.33 Si, 0.025 S 0.017 P, 0.67 Cr, 0.46 Ni, 0.46 Cu); Armco Iron (0.033 C, 0.050 Mn, 0.027 S, 0.011 P, 0.013 Ni, 0.18 Cu), were submitted to the action of the plant's atmosphere in the following areas: above the descaling bath, near the open

* In this work we have used the results of investigations on polluted atmospheres, pursued over the period 1952-1956 by M. K. Kharakhin and V. A. Khrustalev (F. F. Erisman Moscow Scientific Research Institute of Sanitation and Hygiene), by A. A. Vasilyev, Ts. P. Kruglikova and Efimova (Moscow Municipal Sanitation-Epidemological Station) and by A. P. Flerovsky, medical doctor of industrial sanitation at the "Sickle and Hammer" plant.

hearth furnaces, on the roof of the plant away from the ventilation and exhaust chimneys. The particular effects of the aggressive components of the plant atmosphere were also studied in the laboratory; samples of the different steels were kept at 18-22°C in desiccators with atmospheres of different relative humidity (60, 75 and 90%) containing different concentrations of HCl (0.0019, 0.035 and 0.360 mg/l) and SO_2 (0.02 mg/l). Ordinary city air (containing in mg/l : 0.6 CO_2, 0.011-0.054 CO, 0.00030-0.00038 NO_2, 0.00016 dust and 0.000024 soot) to which SO_2 (0.02 mg/l) and HCl (0.01 mg/l) were added in proportions corresponding to maximum tolerance of the plant atmosphere (according to sanitary norms [1]) was used as the base atmosphere of the experiments. The intensity of the corrosion was judged by visual examination and the gravimetric method; the aggressiveness of the corrosive medium was measured with the element whose use for industrial and laboratory investigation was suggested by Tomashov and others [2].

The results obtained at the plant are represented in the figure.

The low corrosion rate in the atmosphere of the open-hearth plant can be explained by the particular conditions of temperature and relative humidity in the building. At the place where the samples were exposed during the season when the building was not heated, (April 15 – October 15) the temperature varied from 28°C to 50°C and the humidity (due to artificial humidification of the air supplied to places of work) varied from 71% to 86%. The humidification of the air supplied by ventilation is accompanied by the extraction of SO_2, soot and dust from the air forced into the building; analysis of the air performed during the summer proved this point; the results of the analysis showed that the concentration of SO_2 did not exceed $1 \cdot 10^{-6}$ mg/l. It must be noted that the air intake for ventilation purposes is sufficiently removed from the exhaust of the open-hearth combustion products. During the season when the building is heated the temperature near the furnace varies from 15 to 35°C; artificial humidification is not performed and the air near the furnaces during the fall and winter has a very low humidity (γ = 44-68%). During winter and fall the concentration of SO_2 in the atmosphere of the building (0.0003-0.0010 mg/l) was three times lower than that of the plant's yard (0.0005-0.0040 mg/l). This situation can be explained by the fact that in winter, when air is not supplied by ventilation, SO_2 is partially eliminated by the condensation of the humidity carried by the gas, during filtering of the air sucked in through cracks, pores, etc. (because of the exhaust ventilation).

Effect of Relative Humidity of SO_2 and HCl and of the Type of Steel on the Loss of Weight Due to Corrosion Over a Period of 160 Hours (average results)

Characteristics of the atmosphere	Weight loss (in g/ m^2) due to the corrosion of different steels			
	Steel 40	Steel 30	KhGSA	Steel NL-2
Humidity 60%.	1.25	1.80	0.77	0.92
Humidity 60%+ 0.02 mg/l SO_2 . .	1.09	1.42	0.86	0.91
Humidity 60%+ 0.36 mg/l HCl . .	275.11	358.22	357.90	299.78
Humidity 75%.	1.41	2.16	0.89	1.20
Humidity 75%+ 0.02 mg/l SO_2 . .	18.54	19.81	12.48	12.03
Humidity 77.5%+ 0.035 mg/l HCl	463.12	534.98	540.13	469.90
Humidity 90%.	9.02	8.80	7.51	5.22
Humidity 90%+ 0.02 mg/l SO_2	216.02	230.10	193.88	167.91
Humidity 89.5%+ 0.0019 mg/l HCl	67.74	77.03	69.32	93.59

The relatively high corrosion rate of the samples in the atmosphere of the plant's yard is due to the high humidity of the air during the fall and to the high concentration of SO_2 in the air; thus during 24 hours 750 kg of sulfur, in the form of SO_2, resulting from the combustion of black oil with a high sulfur content ($\geq$ 0.5% S), is eliminated by only one open-hearth plant. Soot and dust deposited on the metal surfaces facilitate the condensation of humidity and its retention on the surface of the structures; this increases the electroconductivity of the surface layer and consequently the aggressiveness of the corrosion attack. This situation is due to the fact that

the dust present in the air of the plant's yard (up to 0.05 mg/l) contains 0.5-3% chlorides and 12-40% sulfates.

The character of the corrosion curves in the atmosphere of the etching shop indicates that the corrosion products are not protective. The hygroscopic corrosion products formed absorb water easily and slide off the surface, which leads to strong corrosion in this atmosphere. The results of the experiments performed in the desiccator (see table) show that the addition of HCl renders the atmosphere much more aggressive than the addition of SO_2 (at the same concentration and for the same degree of humidity of the air). This difference is explained by the fact that chlorides are not only much more active but are also much more hygroscopic than the sulfates and the sulfites.

The samples corroded in the atmosphere of the open-hearth plant look very much like the samples maintained in air containing 0.02 mg/l of SO_2 whose humidity is $\gamma = 75\%$ or like the samples exposed to the atmosphere of the plant's yard where the humidity is $\gamma = 90\%$ and the SO_2 content is 0.02 mg/l, or like the samples kept in the etching shop where the humidity $\gamma = 89.5\%$ and the HCl concentration 0.0019 mg/l.

Electrochemical measurements made during the summer period (June – July) showed that the current intensity of corrosion elements in the atmosphere of the etching shop, the plant's yard and the open hearth plant are in the ratio of 8 : 4 : 1. The ratio obtained in the case of the measurement of weight loss was 30 : 10 : 1; this difference can be explained by the difference in the humidity of the open-hearth plant and the yard during the summer (when the electrochemical measurements were made) and the fall (when the samples were exposed).

The copper-containing steel NL-2 and Armco iron manifest higher resistance to atmospheric corrosion only when the atmosphere is not too corrosive (see table and figure). Under these conditions the current intensity has the minimum value necessary for the micro-electrochemical passivation [3]. In strongly aggressive media (desiccators containing air and HCl, the atmosphere of the etching shop) copper-containing steels do not manifest resistance to corrosion because the aggressive agents present in the corrosive media, prevent the passivation of the anodic areas, and the contact deposition of copper can only facilitate the cathodic depolarization by oxygen and sulfur dioxide [4].

LITERATURE CITED

[1] B. M. Zlobinsky, Foundations of Safety Technique [in Russian] (Metallurgy Press, Moscow 1956).

[2] N. D. Tomashov, A. A. Lokotilov and K. G. Berukshtis, ZL 3 (1956).

[3] N. D. Tomashov, G. P. Sinelnikov and M. A. Vedeneeva, J. Phys. Chem. USSR 23, 3, 289 (1949).

[4] I. L. Rosenfeld, Proc. Acad. Sci. USSR 111, 1, 136 (1956).

Received July 30, 1956

ELECTRICALLY CALIBRATED ICE CALORIMETER

M. V. Kniga and K. P. Mishchenko

Institute of Chemistry, Academy of Sciences, Estonian SSSR

An isothermal ice calorimeter has been constructed for measurement of heat effects in the interaction between shale samples and solvents [1]. It was taken into consideration that the interaction to be studied is relatively slow and that the heat effects are small.

A schematic diagram of the calorimeter is given in Fig. 1.

The calorimetric vessel consists of a thick-walled glass test tube A, closed by a ground-glass stopper B. This test tube is sealed into a cylindrical glass vessel D, with a glass tube E, bent upward, sealed to its lower end. A graduated capillary H, with a special funnel J attached, is fitted into the ground-glass joint F of the side tube E; the funnel is used for addition of mercury.

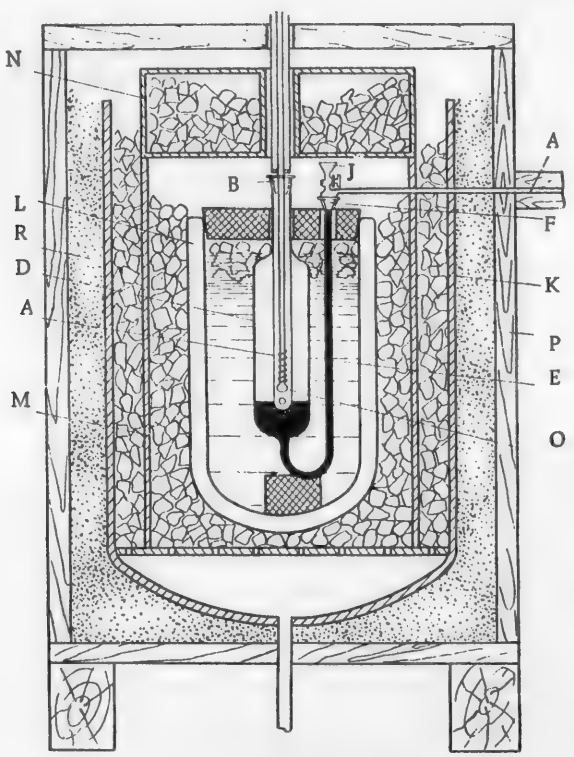

Fig. 1. Ice calorimeter.
Explanation in text.

The calorimeter is insulated internally and externally. It is insulated internally by means of a layer of chemically pure water and ice which forms in the glass vessel D. External insulation is effected by means of the outer

jacket L (a Dewar flask) filled with ice-cold water and ice made artificially from distilled water, and external insulating stainless steel shells M and K. The shells M and K are also filled with ice. The lid N of the shell M is filled with ice and is provided with an opening for the heater O. The space R is filled with sawdust; the whole calorimeter is inserted in a wooden box P covered with felt.

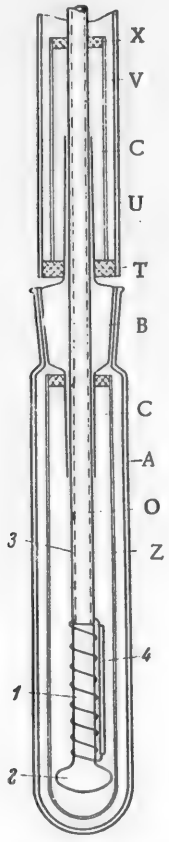

Fig. 2. Reaction tube of calorimetric vessel. Explanations in text.

Preliminary experiments showed that a number of modifications had to be made in the original external insulation in order to eliminate the influence of the surrounding temperature on the temperature within the apparatus. The calorimetric vessel was placed inside a wide Dewar flask L (Fig. 1), and the wooden box P was covered with felt.

The reaction tube (Fig. 2) of the ice calorimeter was also modified in a number of ways, namely: the reaction tube A was closed by means of a ground-glass stopper B (Fig. 2) containing directing tubes C for the heater O. A rubber bung T was fitted onto the upper tube C, and inside a glass tube U. Inside this tube the heater O passed through the tubes C of the glass stopper B, and a glass tube V, packed with cotton wool, was placed around the heater and held in position by means of the cork X. The portion of the tube projecting above the calorimeter was also insulated and surrounded by the lid N (Fig. 1) containing ice. A thin-walled tube Z, of almost the same length as the reaction tube A of the calorimetric vessel, was fitted around the lower tube C (Fig. 2). This design gave satisfactory results in experiments with volatile organic solvents. It was possible to record heat effects of the order 1-2 calories, to an accuracy of ± 2.5 - 3%. The capillary was calibrated by Neumann's method [2]

The shale samples were put in thin-walled spherical glass bulbs. The experiments were performed as follows. The solvent was weighed in the thin-walled tube Z, and into it were put the bulb with the shale and the heater O, inserted through the glass stopper B and the tubes C (first variant). The whole system was placed in a jar with ice, put into a refrigerator for 1 hour, and then inserted into the reaction tube A of the calorimetric vessel. Methyl alcohol was poured in the space between the tubes A and Z (Fig. 2) to serve as a heat transfer medium. The system was left at rest to reach thermal equilibrium. The experiment was then performed. In a second variant, we introduced the bulb containing the shale and the solvent directly into the reaction tube A. This is a better method with regard to contact with the ice, but it is possible to damage the apparatus when the bulb is broken, and the cleaning of the reaction tube to remove shale is a lengthy operation. Therefore the second variant was used only when the experimental technique was being developed. The first variant involves less risk of damage to the apparatus and requires less time for preparation of the experiment. The experiment was commenced with observations of the position of the mercury in the capillary at 5-minute intervals. The position of the mercury in the capillary was observed with the aid of a telescope device. When the course of the mercury became uniform (6-7 readings are sufficient for this), the bulb (which was attached to the end of the heater) was broken by impact against the bottom of the tube, and the heater was carefully raised to a definite height. The duration of the principal period was 60-140 minutes, and of the final period, 45-55 minutes. Shale samples weighing between 1 and 2.5 g, and 20 cc of solvent, were taken for each experiment. The heat-transfer correction was calculated for each experiment [3].

For calculation of the results, the capillary was calibrated in calories/division by an electrical method with the aid of a heater (of the Fischer type [4], specially designed for our purpose (Fig. 2)).

The heater was made from Constantan wire 0.2 mm in diameter, the specific resistance being 16.2 ohms/m. A glass rod 1 was made, with a flattened disk at the end (Fig. 2). A glass tube 3 was sealed to the other end of the glass rod 1. Two holes 0.5 mm in diameter were made in the tube 3, and copper wires were passed through them. Constantan wire was wound around the lower end of the heater; one end was attached to the copper wire passing

through the hole in the glass tube, and the other was sealed to the glass close to the disk 2, passed through the capillary 4, and then connected to the second copper wire.

LITERATURE CITED

[1] M. V. Kniga "Study of the Energy of Interaction of Kukersit Shale with Certain Solvents" (Dissertation, Leningrad State University, 1954);* M. V. Kniga and K. P. Mishchenko, Bituminous Shales, Chemistry and Technology, 3 (Estonian State Press, Tallinn, 1957).*

[2] A. N. Georgievsky, Calibration of Capillaries (1915).*

[3] M. M. Popov, Thermometry and Calorimetry (Izd. MGU, 1954).*

[4] U. Fischer, Z. anorg. Ch. 78, 41 (1912).

Received April 8, 1957

* In Russian.

EFFECT OF RANEY NICKEL ON HYDROCARBONS UNDER CONDITIONS OF PROLONGED CONTACT

A. A. Balandin and S. E. Raik

Chair of Organic Catalysis, Moscow State University

It is known that many reactions in organic chemistry, occurring at relatively high temperatures (400° and over) are accompanied by formation of various amounts of carbon owing to decomposition of the molecules into their constituents, both in presence and in absence of catalysts. The carbon formed very often covers the catalyst surface, thereby lowering its activity. In practice, such deposition makes it necessary to regenerate the catalyst at intervals by oxidation of the carbon by oxygen or air; if metallic catalysts are used, this is followed by reduction with hydrogen at high temperatures. It was therefore desirable to study the conditions of carbon formation, and its influence on catalysis.

Systematic investigations of this question were carried out by Balandin, Kotelkov and Patrikeev [1-7], by Rubinshtein [8], and by Hofmann [9, 10]. These investigations dealt with the behavior of isopropyl [3, 4, 5], n-butyl [5] and isoamyl [8] alcohols during dehydrogenation and dehydration; of cyclohexane [1], ethylbenzene [7] and benzene [9] during dehydrogenation; and the conversion of carbon monoxide with formation of carbon and carbon dioxide [10].

The catalysts used in these investigations were metals: iron [1, 7, 9, 10], aluminum [4], and copper [4, 7]; alloys: Nichrome, nickeline, manganin, Constantan, and iron–chromium–aluminum alloy [1, 4, 6], and the oxides of iron, chromium, zinc and beryllium [8]. The metals also include nickel on aluminum oxide [2], and platinum and palladium deposited by a special method on wire spirals of Nichrome and other alloys [1, 4, 5]. All these investigations were performed in flow systems.

TABLE 1

Physical Constants of the Hydrocarbons Tested

Hydrocarbon	Boiling point at 748 mm		d_4^{20}		n_D^{20}	
	experimental	literature data	experimental	literature data	experimental	literature data
n-Heptane	98	98.4 [12]	0.6833	0.6836 [12]	1.3880	1.3877 [12]
Hexene-1	64	64 [13]	0.6766	0.6734 (d_0^{20}) [13]	1.3908	1.3870 [13]
Benzene	80	80	0.8780	0.8781 [14]	1.5505	1.5007 [15]
Cycloheptane . . .	118	118 [16]	0.8098	0.8099 [16]	1.4445	1.4440 [16]
Ethylcycloheptane	103	103 [17]	0.7667	0.7669 [17]	1.4210	1.4201 [17]

These investigations showed that: a) all the catalysts tested, except copper, induce the decomposition of alcohols, hydrocarbons and carbon monoxide with liberation of carbon; the decomposition of hydrocarbons is obviously always accompanied by evolution of hydrogen; b) this decomposition occurs at 400° and higher; c) carbonization of the catalysts initially does not decrease but rather increases catalyst activity until the catalyst is al-

most completely covered with carbon. This effect is explained very satisfactorily by the dendrite theory of carbon formation, which was put forward and experimentally verified by the authors [1, 11].

In the present investigation we studied the behavior of certain hydrocarbons in relation to Raney nickel catalyst, which has recently been used extensively at the lower temperatures employed in reactions taking place in the vapor phase in the presence of nickel catalysts. As decomposition was not observed in flow systems at temperatures below 350°, the experiments were performed in a closed apparatus, where it is possible to create conditions for more prolonged contact between the reacting molecules and the catalyst, but under atmospheric pressure.

For studies of the qualitative aspects of the problem, we selected one representative of each principal class of hydrocarbons, namely: n-heptane, hexene-1, benzene, cycloheptane and ethylcyclopentane; and one temperature, 220°.

Benzene ("pure thiophene-free"), and "standard" n-heptane were used as supplied; hexene-1, cyclopheptane and ethylcyclopentane were synthesized by us. The properties of all the compounds tested are given in Table 1.

TABLE 2

Experimental Results

Hydrocarbon	Experiment No.	Amount of hydrocarbon taken (g)	Gas	Catalyst*	Reaction time (min.)	Amount of gas formed		Hydrogen absorbed at start of reaction (ml)	Hydrocarbons in gas formed (% as CH_4)
						in ml	% of complete decomposition		
n-Heptane	I	3.6402	H_2	Ni	480	277	4.25	—	—
	II	3.6595	N_2	Ni	240	202	3.07	—	17.4
	III	3.6692	H_2	—	75	31	0.47	—	—
	IV	3.6352	N_2	—	120	25	0.39	—	—
Hexene-1	I	2.9431	H_2	Ni	300	35	0.75	485	20.3
	II	2.9335	N_2	Ni	170	143	3.01	—	—
	III	3.0042	H_2	—	95	19	0.41	9	—
	IV	3.0411	N_2	—	110	22	0.46	—	—
Benzene		2.8470	N_2	Ni	160	46.2	1.89	—	—
Cycloheptane	I	3.5623	H_2	Ni	480	232.3	4.07	—	7.5
	II	3.5334	N_2	Ni	375	152.1	2.69	—	15.3
	III	3.5711	H_2	—	300	72	1.27	—	—
	IV	3.5717	N_2	—	180	59.9	1.05	—	—
Ethylcyclopentane	I	3.5959	H_2	Ni	375	199	3.46	68	9.5
	II	3.5625	N_2	Ni	480	3.05	5.32	—	14.0
	III	3.5863	H_2	—	115	41	0.72	6	—
	IV	3.5672	N_2	—	140	44	0.75	—	—

* A dash indicates absence of catalyst.

EXPERIMENTAL

A metal apparatus (brass and stainless steel) 1800 ml in capacity was used for the experiments. The inner walls of the apparatus were electrocoated with nickel. The apparatus was airtight, and the temperature could be maintained to within ±1°. The reactor was heated by means of a specially made electric heater of the crucible furnace type. The catalyst was made from aluminum–nickel alloy (30% nickel, 70% aluminum) by treatment with caustic soda; it was obtained in the form of irregular lumps which were placed in special nests made out of nickel wire. These nests with the catalyst were inserted in the reactor before the experiments, and kept in ether between experiments. A weighed sample of the substance under test, contained in a sealed bulb for which a special nest is provided in the apparatus, was previously introduced into the reactor and the bulb was broken at the start of the experiment with the aid of a special device. A measuring buret was attached to the reactor for supply of

the gas in presence of which the reaction was carried out, and for measurement of the gas evolved.

As the decomposition of hydrocarbons always takes place in presence of hydrogen because of its liberation in the reaction, all the experiments were repeated in presence of a more inert gas – nitrogen. To confirm that the catalyst plays the principal role in the decomposition of hydrocarbons, all the experiments were repeated under the same conditions, but without catalyst. The amounts of hydrocarbons taken were so calculated that the volume of the vapor under the experimental conditions was 1500 ml. As the volume of the vessel was 1800 ml, the ratio of the volume of the vapor of the substance to the volume of the gas present was 5 in all the experiments. At the end of each experiment a sample of the gas was taken and analyzed for hydrogen and hydrocarbons by simultaneous combustion in the VTI apparatus.

The results of the experiments are summarized in Table 2 and plotted in the figure.

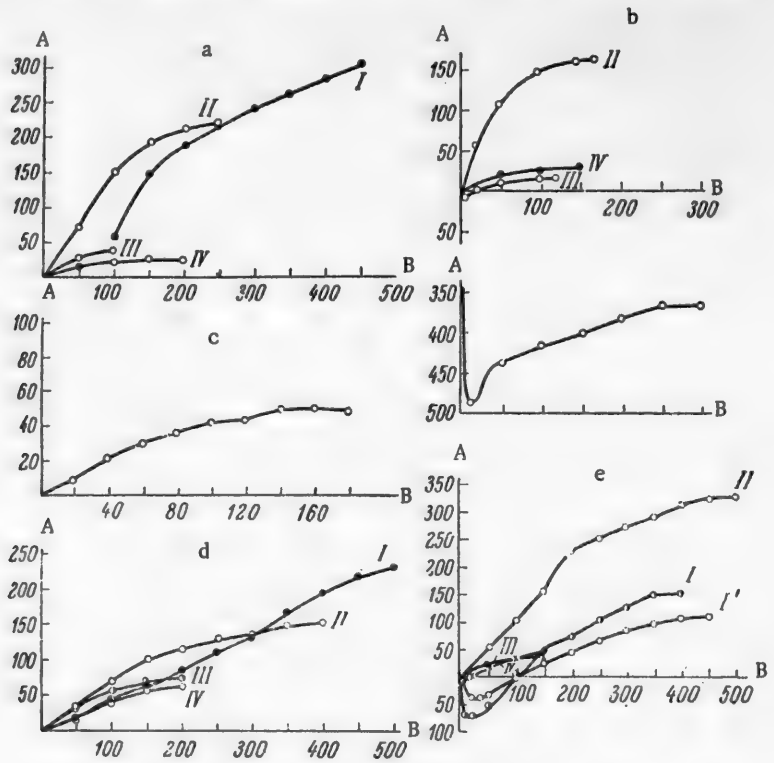

Decomposition of hydrocarbons in conditions of prolonged contact.
A) Amount of gas liberated (in ml); B) contact time (minutes).
I, II, III, IV) numbers of experiments.
Hydrocarbons: a) n-heptane; b) hexene-1; c) benzene; d) cycloheptane; e) ethylcyclopentane.

In addition to cycloheptane, it was decided to test another member of the polymethylene hydrocarbons, ethylcyclopentane; this, unlike cycloheptane, has conjugate bonds in the ring.

As very little gas was evolved in the experiments with benzene in presence of the catalyst, and as its hydrogenation in presence of hydrogen was highly probable, it was used in only one experiment, in presence of nitrogen.

DISCUSSION OF RESULTS

It follows from the graphs that the decomposition depends on the nature of the original substances (compare the data in Table 2, and Curves I-II and III-IV in all the graphs). It is also seen that decomposition also took place in absence of catalyst in all the experiments, although to a much smaller extent (see Curves III and IV). The explanation is that the nickel-coated walls of the vessel also have a certain catalytic effect on the decomposition. The results showed that whenever the reaction was carried out in presence of hydrogen and the hydro-

carbons used were capable of adding hydrogen, such as hexene and ethylcyclopentane, hydrogen was absorbed for hydrogenation of the molecules at the start of the experiment, but after some time evolution of hydrogen owing to decomposition began to predominate. For example, in the case of ethylcyclopentane 68 ml of hydrogen was absorbed at the start of the reaction; this is ~7% of the amount of hydrogen required for hydrogenation of all the ethylcyclopentane taken. In the case of hexene-1, 485 ml of hydrogen was absorbed at the start of the reaction, or about 60% of the hydrogen required for saturation of all the hexene taken (see Table 2, Column 9). In the graphs the absorption of hydrogen at the start of the reaction is also indicated by the fact that the points on the curves lie below the abscissa axis (Curves I and III in Figs. b and e).

The contents of gaseous hydrocarbons were calculated as methane. The amount of hydrogen was calculated from the formula:

$$y = \frac{2}{3}(c - 2x),$$

where y is the volume of H_2; x is the volume of CO_2; c is the contraction.

This amount was less in all the determinations, than the amount of hydrogen taken for the analysis. This shows that the gases contained other gaseous hydrocarbons, of higher molecular weight than methane.

It was noticed in the experiments with hexene that after the catalyst had been used for 40 hours with ethylcyclopentane and n-heptane its activity fell (see Fig. e, Curve I'). Attempts at regeneration of the catalyst by a current of air followed by hydrogen at 300° did not have any significant influence on the catalyst, but its activity remained constant throughout the operating time, about 60 hours, with all the other hydrocarbons.

The fact that the activity of the catalyst does not decrease after a definite time and in some cases even increases during the reaction (see Curve I in Figs. a and e, and Curve II in Fig. e) suggests that carbon is deposited in the form of dendrites on the catalyst.

SUMMARY

1. In a study of the effect of Raney nickel catalyst on hydrocarbons (n-heptane, hexene-1, benzene, cycloheptane and ethylcyclopentane) at 220° during prolonged contact under atmospheric pressure it was found that all these hydrocarbons decompose under these conditions to give carbon and hydrogen, both in presence of nitrogen and in presence of hydrogen.

2. The decomposition reaction is accompanied by partial splitting of the molecules with formation of gaseous hydrocarbons.

3. Benzene, unlike the hydrocarbons of the other classes tested, has a low tendency to decomposition.

LITERATURE CITED

[1] A. A. Balandin and N. Z. Kotelkov, J. Appl. Chem. 15, 139 (1942).

[2] A. A. Balandin, M. I. Marushkin and M. M. Afanasyeva, Bull. Acad. Sci. USSR 1, 93 (1941).

[3] N. Z. Kotelkov, J. Appl. Chem. 25, 337 (1952).*

[4] N. Z. Kotelkov, J. Appl. Chem. 26, 209 (1953).*

[5] N. Z. Kotelkov, J. Appl. Chem. 27, 1019 (1954).*

[6] N. Z. Kotelkov, J. Appl. Chem. 27, 1221 (1954).*

[7] A. A. Balandin and V. V. Patrikeev, Proc. Acad. Sci. USSR 34, 96 (1942).

[8] A. M. Rubinshtein and E. P. Gracheva, J. Phys. Chem. 8, 725 (1936).

[9] U. Hofmann, Ber. 61, 2183 (1928).

[10] U. Hofmann, Ber. 61, 1180 (1928).

[11] A. A. Balandin and V. V. Patrikeev, Proc. Acad. Sci. USSR 40, 171 (1943).

[12] C. P. Smyth, W. N. Stoops, J. Am. Ch. Soc. 50, 1886 (1928).

*Original Russian pagination. See C. B. Translation.

[13] N. Kizhner, J. Russ. Phys.-Chem. Soc. 45, 980 (1913).

[14] H. Prunert, Z. anorg. Ch. 169, 257 (1927).

[15] K. Brand and K. W. Kranz, J. pr. Ch. (2) 115, 156 (1927).

[16] N. A. Rozanov, J. Russ. Phys.-Chem. Soc. 48, 318 (1916).

[17] G. Chavanne and P. Becker, Bl. Soc. chim. Belg. 36, 595 (1927).

Received November 29, 1956

SYNTHESIS OF LEPIDINE BASES FROM ACETANILIDES AND OXO COMPOUNDS*

B. I. Ardashev and B. A. Tertov

In view of the lack of economic methods for the production of lepidine bases used in the manufacture of dyes and sensitizers and of interest in relation to the synthesis of alkaloids, their preparation from available raw materials is of practical significance.

The Beyer reaction [1, 2] for the synthesis of lepidine from aniline, methylal and acetone in 3-4% yield is unsuitable for the industrial synthesis of lepidine bases.

The American chemist Mikeska [3] improved the Beyer reaction and obtained lepidine in 4.3% yield [3]. Other methods for the preparation of lepidine are difficult to carry out owing to their complexity or to the unavailability of the starting materials [4].

A method for the preparation of lepidine from acetanilide, paraform or formalin, and acetone in presence of ferric chloride has been developed in the Organic Chemistry Laboratory of the Rostov State University; the yield is 18% calculated on acetanilide. The reaction mechanism is [5]:

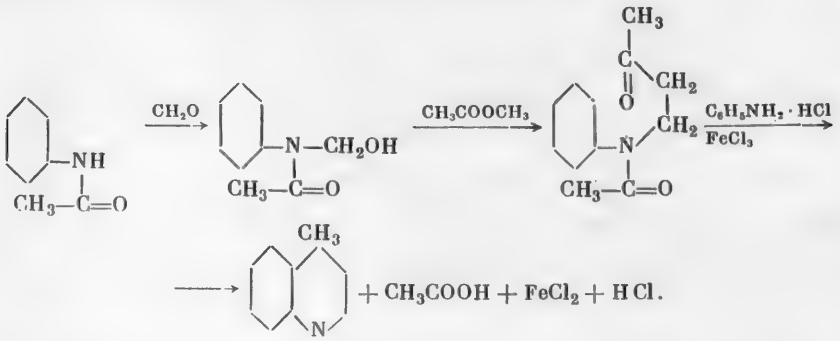

However, this method [5] is only suitable for the preparation of lepidine bases in small quantities, about 5 g, because of the hydrolysis which occurs simultaneously with cyclization. By our method it is possible to prepare lepidine bases in considerable quantities.

Synthesis of a mixture of formaldehyde acetals. 200 g of anhydrous calcium chloride was added to a mixture of 200 ml of technical formalin (d = 1.00), 300 ml of 25% alcohol, and 20 ml of concentrated hydrochloric acid (d = 1.19). The mixture was shaken, with cooling at intervals, until the calcium chloride was dissolved, and then left at room temperature for 24 hours. The upper layer was then separated off, washed quickly with a little water, neutralized with 5% caustic soda solution, dried over potash, and distilled from the start of boiling to 90°. The yield was 80%. As technical formalin contains 8-10% methyl alcohol, the mixture formed contained dimethylformal, methylethylformal and diethylformal.

Synthesis of lepidine. 300 ml of 95% alcohol, 200 ml of acetone, 250 g of $FeCl_3 \cdot 6HCl$, 50 g of zinc chloride, and 140 ml of concentrated hydrochloric acid were put into a 5-liter round-bottomed flask fitted with a reflux condenser, two burets with taps, a stirrer and a thermometer.

* Communication XIV in the series on quinoline derivatives.

The reaction mixture was heated to 75°, and then the following were added from the burets during 2.5 hours, at 5-minute intervals, with continuous stirring: 1) 30 ml lots of a solution of acetanilide (200 g of acetanilide in a mixture of 40 ml of aniline, 275 ml of acetone, and 384 ml of alcohol; 2) 6 ml lots of the mixture of formaldehyde acetals (total 180 ml). When paraform was used, a solution of 50 g of paraform was made in alcohol (total volume 300 ml), 1 ml of concentrated hydrochloric acid was added, and the solution was added from the buret in the same manner as the mixture of formaldehyde acetals. Zinc chloride was not used in this instance.

After the end of the addition of the acetanilide and acetals, the reaction mixture was heated for 30 minutes. The solvent was distilled off up to 100-105° (the temperature of the mixture); the mixture was made alkaline with 40% caustic soda, the bases were distilled in steam and extracted in benzene. The benzene layer was shaken with 200 ml of 15% hydrochloric acid; the acid extract was made alkaline, and the bases were extracted in ether. The ether was distilled off, most of the unreacted aniline was distilled off over a column of 6-7 theoretical plates, the bases were dissolved in a fivefold volume of ether, and the ether extract was dried with potash.

To a solution of crude lepidine in 300 ml of ether, 30 g of powdered phthalic anhydride was added with stirring during 20-30 minutes. The phthalamic acids were extracted in 5-7% alkali, and the ether layer was separated off and dried over potash. After this a further 10 g of phthalic anhydride was dissolved in the ether solution of lepidine. After 10-12 hours a further quantity of phthalamic acids separated out and was extracted in alkali. The ether extract was dried by potash, the ether was driven off, and the lepidine was distilled at 258-263°. The yield was 36-40 g. The refractive index was 1.6180. The picrate and other derivatives of the lepidine so prepared had melting points coinciding with literature data.

The spent solvent (fraction up to 80-83°) was used as solvent for the acetanilide in the subsequent synthesis.

Synthesis of 4,6-dimethylquinoline. 100 g of acetyl-para-toluidine (by synthesis analogous to that of lepidine) 31 g (29.4%) of 6-methyllepidine (4,6-dimethylquinoline) with b.p. 272-277°. The picrate melted at 236°. The refractive index was 1.608.

LITERATURE CITED

[1] C. Beyer, J. pr. Chimie 121, 33, 293 (1886).

[2] A. Pictet, K. Misner, Ber. 45, 1880(1912).

[3] L. A. Mikeska, J. Am. Chem. Soc. 42, 2396 (1928).

[4] Organic Syntheses, 4, 294 (Russian translation) (IL, Moscow, 1953).

[5] V. I. Ardashev and B. A. Tertov, J. Gen. Chem. 24, 316 (1954).*

[6] B. A. Porai-Koshits, Author's Certif. 47297, June 30, 1936.

Received February 1, 1957

*Original Russian pagination. See C. B. Translation.

THE ANALYSIS OF PHTHALIC ANHYDRIDE

E. E. Shkolman and N. M. Voroshilova

The Central Laboratory of the Chelyabinsk Lacquer and Paint Works

By the method for the determination of phthalic anhydride laid down in the State Standard for phthalic anhydride now in force [1], the amount of phthalic anhydride is calculated on the assumption that the esterification of phthalic anhydride with anhydrous methyl alcohol is 99.4% complete.

The correction in the calculation formula given in the GOST is based on the work of Lukashevich [2].

However, in analyses of distilled phthalic anhydride, with the use of thoroughly dehydrated methyl alcohol, the phthalic acid content was often found to be greater than the total acidity, and sometimes over 100%, which gave reason to doubt Lukashevich's assertion [2] that the methylation of phthalic anhydride is only 99.4% complete.

It should be noted that it is not stated in Lukashevich's paper what method was used for the dehydration of the methyl alcohol used, and what the degree of dehydration was; if water was present in the alcohol some of the phthalic anhydride might be converted into phthalic acid during the methylation, which might have given a low yield of the ester. Neither are details of the phthalic anhydride used given in Lukashevich's paper.

The purpose of the present work was to test Lukashevich's conclusion that the methylation of phthalic anhydride is only 99.4% complete, and also to check the suitability of the GOST formula, allowing for incomplete esterification, for calculation of the phthalic anhydride content.

EXPERIMENTAL

The phthalic anhydride and methyl alcohol used for the work had the following characteristics: phthalic anhydride – distilled grade 1, color white, total acidity as phthalic anhydride 100%, phthalic acid content 0.011%, m.p. 130.8°, completely soluble in caustic soda solution; methyl alcohol – conforming to GOST 2222-54, d_{20}^{20} = = 0.793.

Small admixtures of water in methyl alcohol may escape detection in density determinations. Therefore our methyl alcohol with d_{20}^{20} = 0.793 was dehydrated by means of magnesium methylate and then distilled [3].

If the alcohol contained larger amounts of water, it was dehydrated by means of metallic sodium [3], distilled, treated with magnesium methylate, and distilled again.

The percentage esterification of phthalic anhydride with methyl alcohol was calculated by means of the formula

$$C = \frac{2(A - B) \cdot 100}{A - m}, \qquad (1)$$

where C is the degree of esterification of the phthalic anhydride (in wt.% of the amount of anhydride), B is the acidity of the phthalic anhydride after esterification, expressed in the same way as the total acidity, m is the amount of phthalic acid found in the phthalic anhydride (in wt.%). For determination of the acidities A and B, two weighed samples of about 1.2 g phthalic anhydride each, weighed to the nearest 0.0002 g, were taken. One was dissolved, with warming, in 80 ml of freshly boiled distilled water. The solution was cooled without access of carbon dioxide and titrated with 0.5 N caustic soda solution, previously treated with barium chloride to remove carbonates. The second sample was dissolved in 20 ml of anhydrous methyl alcohol, warmed for an hour to gentle

boiling in a small flask under reflux, cooled, diluted with 50 ml of freshly boiled distilled water (cold), and titrated with the same sodium hydroxide solution.

TABLE 1

Effect of Reaction Time on the Degree of Esterification of Phthalic Anhydride (A = = 99.99%; m = 0.011%)

Time (min)	B, acidity after esterification (wt.%)	C, degree of esterification (%)
10	52.56	94.89
17	50.30	99.41
17	50.14	99.73
30	50.01	99.99
30	49.99	100.03
60	50.01	99.99
60	50.0	100.00
120	49.99	100.03
120	50.03	99.95
240	50.02	99.97
240	50.01	99.99

In both cases the titration was carried out in presence of 1% solution of phenolphthalein in alcohol until a faint color appeared.

The values of A and B were calculated from the formulas:

$$A = \frac{v \cdot T\ 100}{g}, \qquad (2)$$

$$B = \frac{v_1 \cdot T\ 100}{g_1}, \qquad (3)$$

where v and v_1 are the volumes of 0.5 N caustic soda solutions (in ml) used in the titration of the first and second sample; g and g_1 are the weights of the first and second sample of phthalic anhydride (in g); T is the titer of the alkali in terms of phthalic anhydride.

Table 1 contains the results of experiments on the effect of the duration of the reaction on the degree of esterification of the phthalic anhydride; the anhydrous alcohol was prepared as described above.

The discrepancies between the results of the individual experiments in Table 1 are caused mainly by titration errors; an error of 0.01 ml in the buret-reading can give an error of $\frac{0.01 \cdot 0.037 \cdot 100}{1.2} = \pm 0.03\%$ for B, and $\pm$ 0.06% for C.

It follows from the data in Table 1 that the esterification of phthalic anhydride proceeds not to 99.4%, as is stated by Lukashevich [2], but is 100% complete, with 30-60 minutes reaction time. Evidently Lukashevich used methyl alcohol containing a certain amount of water, so that some of the phthalic anhydride was converted into phthalic acid.

TABLE 2

Results of Esterification of Phthalic Anhydride with Alcohol Containing Various Amounts of Water (time, 60 minutes)

Characteristics of methyl alcohol		B, acidity after esterification (wt.%)	C, degree of esterification (%)
Moisture content (%)	d_{20}^{20}		
Dehydrated	–	50.01	99.99
0.118	0.79291	50.18	99.55
0.244	0.79323	50.29	99.43
0.619	0.79439	50.57	98.89

Table 2 contains the results obtained in esterification of phthalic anhydride (A = 100%; m = 0.011%) with alcohol containing different amounts of moisture, in 60 minutes.

Dehydrated alcohol with definite amounts of added distilled water was used.

The data in Table 2 show that the degree of esterification of phthalic anhydride decreases with increasing amounts of water in the alcohol, owing to conversion of part of the anhydride into phthalic acid. At a strictly definite water content (0.244%) the GOST formula gives satisfactory results.

However, in practice it is inconvenient first to make dehydrated alcohol, and then to add the necessary amount of water to it. Therefore freshly dehydrated methyl alcohol should be used, so that it is possible to calculate the phthalic anhydride content without the use of a correction for incomplete esterification.

In this connection a series of samples of phthalic anhydride was analyzed, the phthalic anhydride content x (in %) being calculated by means of two formulas:

$$x = \left(\frac{v}{g} - \frac{v_1}{g_1}\right) \cdot 0.07450 \cdot 100, \quad (4)$$

$$x' = \left(\frac{v}{g} - \frac{v_1}{g_1}\right) \cdot 0.07406 \cdot 100, \quad (5)$$

where v and v_1, and g and g_1 are as in Formulas (2) and (3); 0.07450 is the amount of phthalic anhydride (in g) corresponding to 1 ml of 0.5 N caustic soda solution on the assumption that the esterification reaction is 99.4% complete; 0.07406 is the equivalent value on the assumption that the esterification is 100% complete.

Formula (4) corresponds to the formula in GOST 7119-54. The method used for the determination conformed exactly to the GOST specification [1] as described above, while the methyl alcohol used for the analysis was dehydrated by treatment with magnesium methylate. The results of these determinations are given in Table 3.

It follows from Table 3 that when methyl alcohol dehydrated by means of magnesium methylate was used, the phthalic anhydride content calculated by Formula (4) was higher than the total acidity, and over 100%. This is impossible, and this result is merely the consequence of the use of the high factor 0.0745 rather than 0.07406 which corresponds to 100% esterification of phthalic anhydride.

TABLE 3

Phthalic Anhydride Contents of Different Samples

Sample No.	Acidity (wt. %)		Phthalic anhydride content x (wt. %).	
	total, A	after esterification, B	by Formula (4)	by Formula (5)
1	99.98	50.02	100.52	99.92
	99.99	50.01	100.56	99.96
2	99.93	50.02	100.42	99.82
3	99 98	50.03	100.51	99.90
4	99.96	50.02	100.48	99.98
	99.99	50.03	100.52	99.92

High results were also obtained in calculations of the phthalic anhydride contents by Formula (4) in analyses of the first sample of phthalic anhydride (Table 3) with the use of methyl alcohol before dehydration, but conforming to GOST 2222-54 (d_{20}^{20} = 0.79281 ≈ 0.793); in this case B was 50.15% and the phthalic anhydride content was 100.30%.

The phthalic anhydride content as calculated by Formula (5) was 99.70%, as compared with the 99.94% found when the same sample of alcohol was used, but after dehydration (Table 3).

It is seen that more accurate and consistent results in the analysis of phthalic anhydride can be obtained only if thoroughly dehydrated methyl alcohol is used; Formula (5) should be used for calculation of the phthalic anhydride content.

The completeness of dehydration of the methyl alcohol should be tested against a standard sample of phthalic anhydride; the calculation should be based, in the first instance, on the acidity of the sample after esterification (b should be 50%, or somewhat higher if the phthalic anhydride contains acid).

SUMMARY

1. The esterification of phthalic anhydride with anhydrous methyl alcohol proceeds to 100% completion.

2. For analysis of phthalic anhydride it is recommended to use methyl alcohol dehydrated by means of

magnesium methylate; the phthalic anhydride content should be calculated by means of a formula in which it is assumed that the esterification of phthalic anhydride goes to completion.

LITERATURE CITED

[1] GOST 7119-54, Phthalic Anhydride.*

[2] V. O. Lukashevich, J. Chem. Ind. 11-12, 1086 (1931).

[3] P. I. Voskresensky, Laboratory Techniques (Goskhimizdat, 1941) p. 180.*

Received May 29, 1956

*

THE SYNTHESIS OF TOLUENE*

I. L. Kotlyarevsky and A. S. Zanina

Toluene, one of the most important organic intermediates, is at present made mainly by pyrolysis of suitable kerosene fractions. A method was recently developed in our laboratory for the synthesis of aromatic hydrocarbons of predetermined structure by aromatization of divinylacetylene hydrocarbons. This method can be used for synthesis of hydrocarbons of the general formula, where R can be hydrogen or hydrocarbon radicals. After the successful synthesis of p-xylene and phenanthrene [1] by this method, it was desired to study the aromatization of isopropenylvinylacetylene (I) (2-methylhexadiene-1,5-yne-3) and the products obtained by incomplete hydrogenation of it, in order to develop a method for the synthesis of toluene.

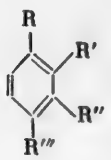

Acetone is formed as a by-product in the synthesis of phenol from benzene and propylene, and vinylacetylene is an intermediate in the production of chloroprene; therefore the starting materials for our synthesis of toluene are readily available, and it may prove economic to synthesize toluene with vinylacetylene and acetone as the starting materials, especially in view of the ever-increasing demand for kerosene.

Our process for the synthesis of toluene is represented by the following reaction sequence:

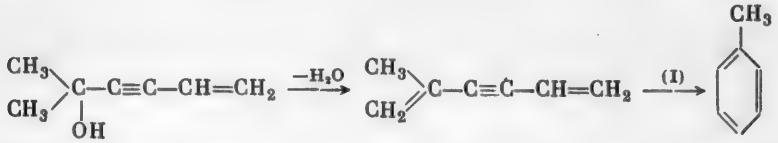

The synthesis of dimethylvinylethynylcarbinol has been achieved on the industrial scale, while its dehydration is a well-known reaction.

The aromatization of vinylisopropenylacetylene was effected over Cr_2O_3/Al_2O_3 (20 : 80) and $MgO/Cr_2O_3/Al_2O_3$ (2 : 18 : 80) catalysts; the first gave toluene in 28.2% yield (400°, 0.2 kg/liter catalyst hour), and the second, 11% (450°). To increase the yield in aromatization, we introduced a stage of intermediate hydrogenation, 1, 2, or 3 molecules of hydrogen being introduced into the vinylisopropenylacetylene molecule. As the hydrogenation of divinylacetylene compounds over Raney nickel does not proceed selectively, partial hydrogenation of 2-methyldivinylacetylene does not yield individual compounds, but mixtures consisting mainly of the following compounds are obtained in each case:

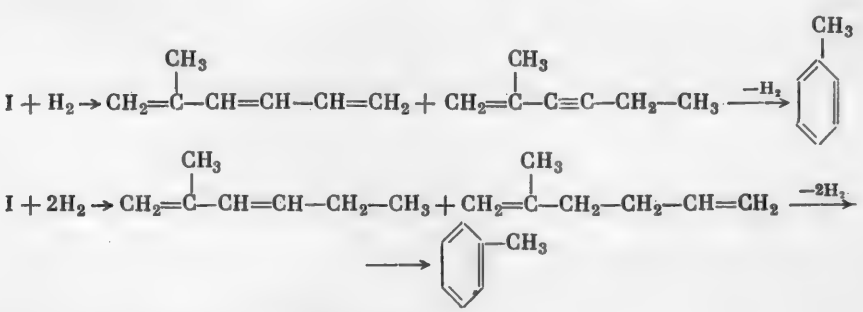

* Communication IV in the series on unsaturated hydrocarbons.

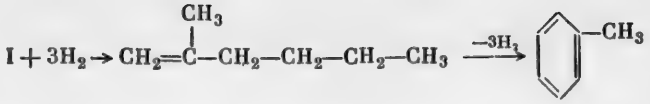

Thus, in studying the aromatization of the products of partial hydrogenation of vinylisopropenylacetylene, we are investigating not the aromatization of individual hydrocarbons, but merely the over-all effect of the introduction of 1, 2, or 3 molecules of hydrogen into the molecule.

It was found that, in presence of $MgO/Cr_2O_3/Al_2O_3$ (2 : 18 : 80) catalyst, under optimum conditions, the yields of toluene from the hydrogenation products of vinylisopropenylacetylene after addition of 1, 2 and 3 molecules of hydrogen respectively, were 38.2, 43 and 51.5%; in presence of Cr_2O_3/Al_2O_3 (20: 80) catalyst the yields were 28.7 and 27% (with 1 and 2 molecules of hydrogen).

The temperature required for aromatization increases with increasing saturation of the isopropenylvinylacetylene molecule with hydrogen. Thus, whereas the best temperature for the aromatization of isopropenylvinylacetylene is 450°, after hydrogenation with 1 molecule of hydrogen aromatization of the product proceeds best at 450°; with 2 molecules of hydrogen, at 500°, and with 3 molecules, at 550°.

EXPERIMENTAL

Vinylisopropenylacetylene was prepared by dehydration of dimethylvinylethynylcarbinol by means of 50% sulfuric acid (4 hours at 40-60°); the yield was 80%, b.p. 30° at 12 mm.

TABLE 1

Aromatization of Isopropenylvinylacetylene and Its Hydrogenation Products over Cr_2O_3/Al_2O_3 (20 : 80) Catalyst in a Current of Hydrogen (experiments 1-5) and Nitrogen (experiments 6-9)

Experiment No.	Starting substance	Temperature (°C)	Amount of starting substance passed (g)	Feed rate of starting substance (g/hour)	Amount of catalizate (g)	Formolite reaction	Total yield of toluene (%)
1	Isopropenylvinylacetylene (I)	370	10	10	4.5	Strong	26.5 *
2		400	40		20.2	Strong	28.2 **
3		450	40		18.7	Strong	21.9 ***
4		500	10		1.2	Very strong	— ****
5	I, hydrogenated with 1 molecule of hydrogen	450	10	6.3	3.33	Very strong	28.7 *****
6		500	15	5	5.6	Moderate	15
7		550	15	5	3.3	Very strong	13
8	I, hydrogenated with 2 molecules of hydrogen	450	15	6.65	7	Weak	—
9		550	15	6	40	Very strong	20

The aromatization was carried out in presence of Cr_2O_3/Al_2O_3 (20: 80) and $MgO/Cr_2O_3/Al_2O_3$ (2 : 18 : 80) catalysts, made by impregnation of pieces of commercial alumina with the calculated amount of aqueous chromic anhydride solution or of an aqueous solution of chromic anhydride and magnesium chromate, followed by evapora-

* Distillation of 3.4 g of catalyzate gave 2 g of a mixture of toluene with the starting material, b.p. 97-108° (89.5% toluene).

** Distillation of the catalyzate yielded 12.1 g of a toluene fraction, b.p. 105-110° (93.4% toluene).

*** Distillation of the catalyzate gave 10.25 g of a fraction boiling at 97-110° (85.6% toluene).

**** The catalyzate was not investigated because of the low yield.

***** 3.33 g of a toluene fraction was obtained; b.p. 99-114° (86% toluene).

tion, drying of the pieces at 105° in a drying oven, and heating at 300-500° in the catalytic furnace in a stream of air. Hydrogen or nitrogen was blown through the tube containing 50 ml of catalyst before the aromatization, and the substance was introduced in a current of one of these gases. The catalyzate was collected in a receiver, and the amount of gas liberated in the reaction was measured in a gas holder.

The partial hydrogenation of isopropenylvinylacetylene was carried out over Raney nickel, either under normal pressure in a hydrogenation vessel, or, to accelerate the reaction, in an autoclave under moderately high pressure (20-30 atm.).

For preliminary evaluation, the catalyzate was tested qualitatively for aromatic hydrocarbons by the formolite reaction.

TABLE 2

Aromatization of Isopropenylvinylacetylene Hydrogenation Products over $MgO/Cr_2O_3/Al_2O_3$ (2 : 18 : 80) Catalyst in a Current of Nitrogen

Experiment No.	Starting substance	Temperature (°C)	Amount of starting substance passed (g)	Feed rate of starting substance (g/hr)	Amount of catalyzate (g)	Formolite reaction	Total yield of toluene (%)
10	Isopropenylvinylacetylene (I)	450	13.5	10	4.3	Moderate	11
11	I, hydrogenated with 1 molecule of hydrogen	450	10	4	4.25	Very strong	88.2 *
12		500	10	4	5.38		— **
13		550	10	5	2.2		— **
14	I, hydrogenated with 2 molecules of hydrogen	450	30	10	17.23	Strong	35.8 ***
15		500	20	6.06	9.9	Very strong	43 ****
16	I, hydrogenated with 3 molecules of hydrogen	450	15	10	9.38	Strong	8.7
		500	10	4.2	6.15		39.1
		550	10	6	5.8	Very strong	50 *****

For quantitative analysis of the catalyzate the fraction containing toluene and the unreacted substance was distilled off, and the amount of the latter was found from the amount of hydrogen required for exhaustive hydrogenation of this fraction over Raney nickel at room temperature and atmospheric pressure. The toluene obtained in the best experiments was oxidized by 20% nitric acid to benzoic acid. The higher catalyzate fractions were not investigated, as the yields were low. The catalyst was regenerated after each experiment by the passage of a current of air for 2 hours at 500°. The results of the experiments are summarized in Tables 1 and 2. When the feed rate of the starting substance was 5 g/hour the yield of toluene was 51.5%, b.p. 107-110°, n_D^{20} 1.4961.

SUMMARY

A new method for the synthesis of toluene from acetone and acetylene by aromatization of divinylacetylene hydrocarbons has been studied; it was found that the highest yields of toluene (51.5%) are obtained by aromatization of isopropenylvinylacetylene, partially hydrogenated to absorb up to 3 molecules of hydrogen per molecule (550°, 0.1 liter/liter of catalyst · hour), in presence of $MgO/Cr_2O_3/Al_2O_3$ (2 : 18 : 80).

* 4.05 liters of gas formed, instead of 2.4 liters as calculated.

** The catalyzate was not studied further because of the low yield.

*** 5.1 liters of gas formed (calculated, 13.8 liters). When the feed rate was reduced to 5 g/hour, the yield of toluene was 35%.

**** 9.7 liters of gas formed (calculated, 9.2 liters). No significant changes produced by 1.5-fold decrease of increase of the contact time.

***** 5.1 g of toluene with b.p. 107-111° obtained and 5.1 liters of gas liberated (calculated, 4.6 liters).

LITERATURE CITED

[1] I. L. Kotlyarevsky, A. S. Zanina and V. G. Lipovich, J. Appl. Chem. 30, 2, 321 (1957).*

Received February 20, 1956

*Original Russian pagination. See C. B. Translation.

BOOK REVIEW

W. Hübner and A. Schiltknecht. Die Praxis der anodischen Oxydation des Aluminiums. Düsseldorf, 1956, 355pp.

The practice of anodic oxidation of aluminum. Aluminum and its alloys with copper, magnesium, manganese, silicon and other elements are widely used in the automobile, chemical and aircraft industries, in architecture, and in the production of a range of extensively used goods.

The natural oxide film which forms on aluminum and which protects the metal against further attack is often inadequate. It is therefore necessary in technology to form artificial oxide films with better protective properties on the surface of aluminum or its alloys. The artificial oxide films are mainly made electrolytically, by anodic oxidation of aluminum in various electrolytes. The technology of anodic oxidation of aluminum is a delicate electrochemical process which naturally involves certain difficulties. A good book containing practical advice and guidance on the subject is the best aid the chemical engineer could have. That is why the publication of the new and very useful book by Hübner and Schiltknecht "The Practice of Anodic Oxidation of Aluminum" is timely and most satisfactory.

Unfortunately there is no book on the anodizing of aluminum in the Russian language.

This is not the first book in German on the electrolytic oxidation of aluminum, but is has one important distinction, which is pointed out by the authors in their preface – it is written for practical men and is based on practice. In it the authors summarize their experience of many years (in Switzerland) on the design and equipment of units for the anodic oxidation of aluminum, and on operation of the process.

The book contains detailed descriptions of technological processes, formulations, analytical methods and data on layout of plant for the anodic oxidation of aluminum; some of these have not been published before or are scattered through the journals and the specialist literature. This is a great merit of the book.

The book is pleasant to read; it is well presented, printed on excellent paper, and profusely illustrated. The 255 illustrations include numerous excellent photographs which clarify and augment the text; this is very helpful for production workers in the anodizing field.

The book consists of seven chapters, most of which contain several extensive sections (Chapters III, V, VI, and VII).

The first chapter is a short introduction of six pages.

The second chapter – the Course of the Process – gives an outline of the technological process of aluminum anodizing (mechanical and chemical preparation of the surface, anodic oxidation, coloration of the surface, compression of the coating, final finishing of the surface).

The third chapter – Chemical Section. Oxidation Methods – comprises about one third of the total bulk of the book (pp. 12-105). The six sections of this chapter contain the basic data on the oxidation of aluminum and its alloys – chemical methods of surface oxidation, anodic oxidation (electrolyte composition, temperature, duration of exposure in the bath, electrolysis conditions, description of the process, analysis, specimen calculations), chemical surface brightening (alkaline and acid baths), electrolytic polishing, coloration of the oxide layer on aluminum, compression of the coating.

The short fourth chapter deals with the Selection of Materials for anodic oxidation.

The fifth chapter is important in content and if of considerable length (113 pages).

It deals with Anodizing Plant, and covers in great detail a number of important questions of great interest to chemical engineers and planners in the field of anodic oxidation of aluminum and its alloys. This chapter contains sections on the layout of the building for the anodizing plant and its various sections (polishing, suspension of the articles to be treated, anodizing, assembly, packing and dispatch), the necessary equipment and its grouping (arrangement and dimensions of the baths for pickling, electropolishing and anodizing; their layout; electricity supply; heating and cooling of the solutions; ventilation; illumination); water supply (demineralization); neutralization and disposal of effluents.

The sixth chapter – Mechanical Preparation of Articles for Anodic Oxidation – contains a description of the equipment for grinding and polishing of the aluminum surfaces before anodizing.

A separate chapter, the seventh, deals with Suspension of Articles. Successful anodizing depends to a considerable extent on adequate conductivity of all the current-carrying devices.

A bibliography of the most important literature (81 references) is given at the end of the book.

Use of the book is facilitated by a detailed contents list (five pages) and a subject index.

A defect of the book, in our opinion, is the almost entire lack of information on the theoretical principles of the anodic oxidation process. It is true that the authors point out in the preface that the theoretical aspects are deliberately given little space in the book, as extensive special literature on the question is available. Nevertheless, it would seem to be very appropriate and necessary to include a special section on the physicochemical principles of the anodizing of aluminum in a book of this type.

On the whole, Hübner and Schiltknecht's book is a valuable contribution to the literature on the anodic oxidation of aluminum, and it should be translated into Russian. The translation will be welcome and will find a place in every technical library.

Chemical engineers and planners will find much necessary and useful information in it. The book can also be used by students specializing in electrochemistry and electrometallurgy.

I. Ya. Volkind

JOURNAL OF

ANALYTICAL CHEMISTRY

OF THE USSR

in complete English translation

The top Russian journal in this field, dealing with all phases of analysis, organic and inorganic, including metallurgy, petroleum, spectrochemistry. Sample articles: A simple rational design for the elementary cell of a countercurrent distribution apparatus; a potentiometric method of determining saponification numbers in solutions of petroleum resins; potassium tetraborate as a primary standard in acidimetry. Translation began with the 1952 volume. Annual subscription, 6 issues, approximately 900 pages, $80.00.

CONSULTANTS BUREAU, INC.
227 W. 17th St., NEW YORK 11, N. Y.

JOURNAL OF GENERAL CHEMISTRY OF THE USSR

(Obshchei Khimii.)

in complete English translation

The most important Russian chemical journal, with broad coverage of all aspects of investigation, from the purely theoretical and experimental, to the most practical, including industrial applications, covers: Organic and inorganic research, pharmacology, petroleum, textiles, biology, medicine, dyes, and fuels, etc.

SAMPLE ARTICLES: Some problems pertaining to the reaction kinetics of the reductive alkylation of hexamethylenediamine; reaction of organomagnesium compounds with mixed organosilicon acetals; preparation of aliphatic alcohols from petroleum hydrocarbons; organophosphorus insecticides, some derivatives of methylthiophosphonic and methyldithiophosphonic acids; new method for synthesis of quinolines by rearrangement of acylated arylamines.

Annual subscription, 12 issues, approx. 3600 pp: $90.00 in the U.S. and Canada; $95.00 elsewhere. (Special price for libraries of non-profit academic institutions: $30.00 in the U.S. and Canada; $35.00 elsewhere.)

Tables of Contents on request.

C/b CONSULTANTS BUREAU, INC.
227 W. 17th St., NEW YORK 11, N. Y.